Sources and Ocean-Atmosphere Processes Controlling the Distributions of Dimethylsulfide and Isoprene over the Northern Indian Ocean

A thesis submitted in partial fulfilment of
the requirements for the degree of

Doctor of Philosophy

by

Mansi Gupta

(Roll No. 20330012)

Under the guidance of

Prof. Lokesh Kumar Sahu

Professor

Space and Atmospheric Sciences Division (SPA-SC)

Physical Research Laboratory, Ahmedabad, India.

Discipline of Physics

Indian Institute of Technology, Gandhinagar

2025

Dedicated to

Papa, Momma

&

Gabbu

Declaration

I declare here that this thesis report represents my own ideas in my own words, and where others' ideas have been included, I have adequately cited and referenced appropriate citations from original sources. I also declare that I have followed all principles of academic honesty and integrity and have not misrepresented or fabricated or falsified any idea/fact/source/data in my submission. I understand that any violation of the above can cause disciplinary action by the Institute and can also evoke penal action from the sources that have thus not been properly cited or from whom proper permission has not been taken when needed.

Date: 19|01|2026

(Signature)
Mansi Gupta
(Roll No. 20330012)

Certificate

I hereby certify that **Ms. Mansi Gupta** (Roll no: 20330012) conducted the research presented in the thesis titled **"Sources and Ocean-Atmosphere Processes Controlling the Distributions of Dimethylsulfide and Isoprene over the Northern Indian Ocean"** under my supervision. I confirm that this work has not been submitted elsewhere for any other degree. Having thoroughly examined this dissertation, I believe it meets the necessary standards in terms of scope and quality for the award of the Doctor of Philosophy degree.

Date: 22-01-2026

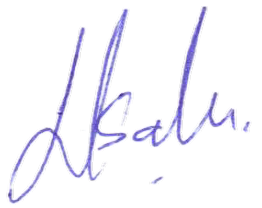

(Signature)
Prof. Lokesh Kumar Sahu
Professor
Space and Atmospheric Sciences Division,
Physical Research Laboratory,
Ahmedabad, India.
(Thesis Supervisor)

Acknowledgements

The accomplishment of this thesis would not have been possible without the support and encouragement of numerous individuals. I wish to extend my heartfelt gratitude to each one of them.

First and foremost, I would extend my sincerest gratitude to my supervisor, Prof. Lokesh Kumar Sahu, for his unwavering support, guidance, and mentorship throughout the entire journey of completing my thesis. His knowledge and valuable perspectives have played a crucial role in influencing the focus and depth of my research. I am grateful for his conviction in my abilities and continuous encouragement to explore challenging ideas, which have served as a source of encouragement and inspiration throughout this journey.

I am deeply thankful to Dr. Arvind Singh, Dr. A.K. Sudheer, Mr. T.K. Sunil Kumar, Dr. S. Venkataramani, and Dr. Nidhi Tripathi for their valuable assistance and contributions throughout the course of my PhD.

I extend my sincere thanks to the Doctoral Scientific Committee (DSC) members, Prof. Varun Sheel, Prof. Neeraj Rastogi, and Dr. Narendra Ojha, for the valuable feedback and insightful discussions on my research work.

I would like to express my sincere gratitude to the Director of PRL, Prof. Anil Bhardwaj; Dean, Prof. D. Pallamraju; Chair of Academic Committee, Prof. Bijaya K. Sahoo; Head of Academic Services, Dr. Bhushit Vaishnav; Head of the SPASC Division, Prof. Dibyendu Chakrabarty; Deputy Head of SPASC Division, Prof. Som Kumar Sharma; Prof. Shyam Lal and Prof. Harish Chandra for their constant support and guidance throughout my Ph.D. tenure. I also thank all the faculty members and supporting staff of SPASC division for their continued encouragement and cooperation. My heartfelt thanks go to my peers from GSDN Division, PRL, for their support and camaraderie during several demanding ship campaigns.

I take this opportunity to thank Mr. Shubham Sharma and Mr. Ram Kishore from Swan Tech, Hyderabad, and Mr. Ashok Misra from Mars Bioanalytical, for their technical assistance in the deployment of instruments

during various ship and field campaigns during my PhD.
I am also grateful for the wonderful circle of friends and colleagues I got in PRL. I extend my heartiest thanks to Nazir, Swagatika, Kimi, Garima, and Meghna di for the unconditional love, friendship, and care. I am very thankful to Mrs. Yogita Sahu for her care and support during these 5 years in PRL. I am thankful to Shreya and Aishwarya for providing an amicable atmosphere in Lobby-D. I am also grateful to Sourita Di, Meghna Di, Dharmendra, and Haritha for the wonderful company in 552. A special thanks to Haritha for proofreading my thesis. I am also grateful to my batchmates, Dharmendra, Debashis, Kamran, Guru, Arup C, Akanksha, Chandrima, Malika, Sanjay, Wafikul, Arup M, Trinesh, and Aditya, who added more joy to this journey with there quirks and were always available to help in personal and professional matters. A special thanks to Abhinav Padala for his patience, time and support, and for sharing his computational knowledge and skills, which were useful in several stages of this work.
I am deeply and eternally grateful to my parents and my brother, whose unconditional love, sacrifices, and unwavering support have shaped the person I am today. They have been my source of strength, believing in me even when I doubted myself, encouraging me through setbacks, and standing by my side through every challenge. The resilience and invaluable guidance of my parents have laid the foundation for all that I have achieved.
Every day has been a new opportunity to unlearn and learn. To everyone who has played a role, big or small, in this academic endeavour, your support has been invaluable.

Mansi Gupta

Abstract

The tropical marine boundary layer represents a dynamic region where ocean-atmosphere exchange governs the composition of reactive trace gases, chemistry-climate interactions, and marine biogeochemical cycles. Air–sea exchange of trace gases links ocean biogeochemistry to atmospheric chemistry and climate. This exchange regulates the sources and sinks of reactive species, and play a crucial role in modulating aerosol formation, cloud properties, and radiative forcing in the lower troposphere. Among the biogenic reactive trace gases in the marine atmosphere, dimethyl sulfide (DMS) and isoprene are particularly important due to their roles in the formation of non-sea-salt-sulfate and secondary organic aerosols, respectively.

This thesis presents the first comprehensive investigation of the sources and atmospheric chemistry of DMS and isoprene in diverse marine environments of the northern Indian Ocean. The northern Indian Ocean includes the basins of the Arabian Sea and the Bay of Bengal, as well as marginal seas such as the Andaman Sea and the Laccadive Sea. The diverse biogeochemical regimes across these basins are uniquely characterized by seasonally reversing monsoonal circulation, coral reef ecosystems, and continental outflows. Several modelling studies have highlighted that the northern Indian Ocean is an important source of DMS due to high biological productivity and favourable meteorological conditions. However, we still lack *in situ* measurements of DMS and other reactive trace gases over the northern Indian Ocean. Although elevated levels of isoprene have been reported over the Arabian Sea, the role of sources and processes controlling its level in the marine boundary layer (MBL) of the northern Indian Ocean is not well understood.

We conducted the first high-resolution continuous shipborne *in situ* measurements of DMS and isoprene in the MBL of the northern Indian Ocean during the post-monsoon season. The campaigns covered the open ocean and coastal regions of the Arabian Sea, Bay of Bengal, Andaman Sea,

and the coastal waters surrounding Sri Lanka and the Laccadive Sea. By integrating high-resolution atmospheric measurements with concurrent oceanographic and meteorological observations, we examined the mechanistic drivers of spatial and temporal variability of DMS and isoprene emissions, their dependence on biological and physical processes, and their implications on the atmospheric chemistry.

The atmospheric DMS mixing ratios over the Arabian Sea varied in the range of 20–709 ppt during the post-monsoon season of 2021. The measurements over the southeast (98 ± 87 ppt) and northeast (116 ± 120 ppt) coastal regions exhibited significantly higher levels than the oligotrophic central Arabian Sea (62 ± 53 ppt), driven by a combination of elevated chlorophyll-a, under high sea surface temperatures (SST) and lower salinity, and calm winds. DMS showed strong diurnal variability with elevated concentrations during early morning and evening, particularly in coastal zones. The daytime decline of DMS was attributed mainly to the OH oxidation, while the role of nighttime radical chemistry was noticeable in polluted coastal air masses. Overall, the DMS variability was found to be sensitive to the changes in meteorological and sea surface parameters, including salinity gradients associated with localized upwelling. Despite relatively low phytoplankton biomass in the post-monsoon period, estimated DMS fluxes of $\sim$11 μmol m^{-2} d^{-1} were $\sim$3 times higher than the values reported two decades ago, suggesting a possible role of changing environmental conditions in DMS emissions from the Arabian Sea.

Over the Bay of Bengal and Andaman Sea, distinct regional differences in the DMS mixing ratios were observed, with higher values in the Andaman Sea (112 ± 68 ppt) compared to west-east (77 ± 24 ppt) and east-west (103 ± 37 ppt) longitudinal transects across the Bay of Bengal. The origin of the air masses strongly influenced the DMS levels measured along the longitudinal transects over the Bay of Bengal. The higher DMS were associated with oceanic air masses with high chlorophyll exposure values, while continental outflows diluted the DMS concentration and led to lower background concentrations ($\sim$47 ppt). The diurnal and short-term DMS variability reflected the interplay of oxidation chemistry, atmospheric dilution, and downdraft events. The role of biological factors with variations in nutrient concentrations and phytoplankton composition (e.g., picophytoplankton, diatoms) influencing the regional DMS emissions was also evident. The estimated DMS fluxes (3.5 ± 1.2 μmol m^{-2} d^{-1}) over the open ocean

are consistent with climatological data but notably higher than previous estimates reported for the post-monsoon season. However, based on the extrapolations of the fluxes over the Arabian Sea and Bay of Bengal, we estimated an annual DMS flux of $\sim$1.21 Tg S yr^{-1} from the northern Indian Ocean.

The thesis also highlights the emissions from the coral reefs as an important localized source of DMS in the Andaman Sea and southern coastal regions of the Indian subcontinent. During the low tide and elevated SST conditions, DMS fluxes from coral reefs reached $\sim$0.5 μmol m^{-2} hr^{-1} in the Andaman Sea, translating to an estimated annual sulfur emission of $\sim$1.43 Gg S yr^{-1} from the coral reefs of the Andaman and Nicobar Islands. The enhanced DMS levels (>200 ppt) over the coastal regions of northeast Sri Lanka and southwest India were measured in the vicinity of coral reefs and favourable tidal conditions, emphasizing the role of reef-associated processes in modulating regional sulfur emissions. The DMS concentration shows a stronger dependence on atmospheric dilution than on the ocean productivity over the Laccadive Sea. Under the influence of terrestrial outflow, the higher OH reactivity of isoprene also influenced the DMS oxidation chemistry and diurnal variability along the coastal waters of Sri Lanka. This interaction between land outflow and ocean emissions may significantly affect the composition of secondary aerosols in coastal marine air.

In contrast to DMS, high-resolution *in situ* measurements of atmospheric isoprene mixing ratio were substantially higher over the Bay of Bengal (0.82 ± 0.15 ppb) compared to the Arabian Sea (0.44 ± 0.08 ppb), and due to regionally distinct source characteristics. Isoprene mixing ratios were higher over the west-east longitudinal transect (0.96 ± 0.07 ppb) than 0.62 ± 0.06 ppb along the east-west longitudinal transect, associated with land-influences and marine air mass. Exponential increase of isoprene with air temperature over the west-east longitudinal transect revealed dominance of terrestrial contributions in elevated isoprene. However, a decline in isoprene with increasing Chl-a along the east-west transect suggested potential microbial/chemical consumption in seawater. Coral reef emissions under disturbed surface physico-chemical conditions influenced the isoprene levels over the Andaman Sea. Significant contributions of marine isoprene observed over the Arabian Sea were attributed to photochemical production at SML, particularly in open ocean regions.

Overall, these findings presented in this highlight the complex interplay of physical, chemical, and biological drivers governing the distribution and atmospheric reactivity of marine DMS and isoprene over the northern Indian Ocean. The results emphasize the need to account for coral reef emissions, terrestrial influences, and inter-seasonal variability in regional sulfur budget estimates, as well as their impact on aerosol-cloud-climate interactions. The results highlight the importance of accounting for coral reef emissions, terrestrial influences, and sub-seasonal variability in regional sulfur budgets and their role in aerosol-cloud-climate interactions. The detailed datasets of atmospheric DMS and isoprene presented in this thesis provide valuable inputs for modelling secondary aerosols in both coastal and open ocean regions of the northern Indian Ocean.

Keywords: Dimethyl sulfide; Isoprene; Air-sea flux; Coral reefs; Terrestrial outflow; Atmospheric chemistry; Arabian Sea; Bay of Bengal; Andaman Sea; Laccadive Sea

Contents

List of Figures

List of Tables

List of Abbreviations

Abbreviations/symbols	**Full form/definition**
AVISO	Archiving, Validation and Interpretation of Satellite Oceanographic data
AVOCs	Anthropogenic Volatile Organic Compounds
AWS	Automatic Weather Station
BOBMEX	Bay of Bengal Monsoon Experiment
Br	Bromine radical
BrO	Bromine monoxide radical
BVOCs	Biogenic Volatile Organic Compounds
CCN	Cloud Condensation Nuclei
Chl–a	Chlorophyll-a
Cl	Chlorine radical
CTD	Conductivity, Temperature, and Depth
DMS	Dimethyl sulfide
DMSP	Dimethylsulfoniopropionate
DOM	Dissolved Organic Matter
EPT	Equivalent Potential Temperature
ERA	ECMWF Reanalysis 5th generation
FID	Flame Ionization Detector
FPD	Flame Photometric Detector
GBR	Great Barrier Reef
H_2SO_4	Sulfuric acid
HYSPLIT	Hybrid Single-Particle Lagrangian Integrated Trajectory model
I^-	Iodide ion

ICS	Internal Calibration System
ID	Internal Diameter
IEW	Indian Ocean Equatorial Westerlies
IGP	Indo-Gangetic Plain
INDOEX	Indian Ocean Experiment
IO	Iodine monoxide radical
MBL	Marine Boundary Layer
MBLH	Marine Boundary Layer Height
MLD	Mixed Layer Depth
MODIS	Moderate Resolution Imaging Spectroradiometer
MSA	Methanesulfonic acid
NMHCs	Non-Methane Hydrocarbons
NO_3	Nitrate radical
nss-SO_4^{2-}	Non-sea-salt sulfate
OH	Hydroxyl radical
OVOCs	Oxygenated Volatile Organic Compounds
PLOT	Porous–Layer Open Tubular
ppb	Parts per billion
ppt	Parts per trillion
PTFE	Polytetrafluoroethylene (Teflon)
SML	Sea-surface Microlayer
SO_2	Sulfur dioxide
SOA	Secondary Organic Aerosols
SST	Sea Surface Temperature
TD-GC	Thermal Desorption–Gas Chromatography
VC	Ventilation Coefficient
VHCs	Volatile Halocarbons
VOCs	Volatile Organic Compounds
VSCs	Volatile Sulfur Compounds

Chapter 1

INTRODUCTION

The Earth's atmosphere primarily composed of nitrogen (78%), oxygen (21%), argon (0.9%), and a wide array of trace gases (<0.1%), including greenhouse gases (typically in parts per million to parts per billion) and reactive trace gases (parts per billion to parts per trillion). Despite being present at very low concentrations, trace gases play key roles in tropospheric chemistry and radiative forcing. Among these, Volatile Organic Compounds (VOCs) constitute a diverse group of reactive species (e.g., DMS, NMHCs, OVOCs, etc.) that significantly influence the oxidative capacity of the atmosphere. Although present at low concentrations, VOCs undergo rapid oxidation, primarily through reactions with hydroxyl (OH) radicals, and contribute to the formation of tropospheric ozone (O_3) and secondary organic aerosols (SOAs), both of which have implications for air quality, human health, and climate (Hallquist et al., 2009; Sahu, 2012). Several VOCs are also classified as short-lived climate forcers (SLCFs) due to their short atmospheric lifetimes and direct or indirect impacts on radiative forcing. Several SLCFs can modulate the abundance of longer-lived greenhouse gases and other radiatively active species through chemical adjustments (Gupta et al., 2024).

Based on the emission sources, VOCs are classified as anthropogenic VOCs (AVOCs) and biogenic VOCs (BVOCs). AVOCs are predominantly emitted through human activities, including fossil fuel combustion, petroleum refining, biomass burning, vehicular exhaust, industrial solvent usage, and

evaporation from fuels and chemicals. On the other hand, BVOCs are released from natural sources such as terrestrial vegetation, oceans, soils, and grasslands. The ambient air concentration and composition of AVOCs have become increasingly important in densely populated urban-suburban or industrialized areas due to strong localized sources. However, BVOCs dominate the global VOC budget, accounting for an estimated 70-90% of total VOC emissions (Guenther et al., 1995, 2006).

Natural vegetation, such as forests, is the dominant contributor to BVOC emissions. The predominant terrestrial BVOCs include isoprene (~70%), monoterpenes (~11%), and sesquiterpenes (~2.4%), light alkenes like ethene (~2%) and propene (~1.7%), and oxygenated-VOCs (OVOCs) such as methanol (~6%) and acetone (~3%) (Guenther et al., 2012; Sindelarova et al., 2014). Tropical regions are the major sources of both monoterpenes and isoprene emissions for the global budget, accounting for 88% and 83%, respectively (Sindelarova et al., 2014).

In addition to terrestrial biota, oceans are a significant source of BVOCs in the remote marine atmosphere. The surface ocean produces a variety of VOCs through both abiotic and biotic production processes in seawater, and the predominance of these mechanisms and sources varies for different VOCs (**Figure 1.1**). The major production mechanisms include biological production from marine phytoplankton, seaweed, and corals, microbial degradation, and photochemical processes involving dissolved organic matter (Beale et al., 2013; Ciuraru et al., 2015; Davie-Martin et al., 2020; Gupta et al., 2024; Moore, 2008; Okuda et al., 2023; Ratte et al., 1993; Shaw et al., 2010; Yoch, 2002). And the emission rates can be modulated by physical and biological factors, including sea surface temperature (SST), solar radiation, nutrient availability, and mixed layer depth (MLD). The major oceanic VOCs include:

i. Dimethyl sulfide (CH_3SCH_3; DMS) and other sulfur trace gases including carbonyl sulfide (COS), methanethiol (CH_3SH; MeSH), and carbon disulfide (CS_2) (J. W. Dacey & Zemmelink, 2001; Gupta et al., 2025; Lawson et al., 2020a; Marandino et al., 2007, 2009; Novak et al.,

2022a; Shenoy & Kumar, 2007; Watts, 2000).

ii. Non-methane hydrocarbons (NMHCs) e.g. light (C_2-C_5) alkanes and alkenes, isoprene, monoterpenes, and toluene (Plass-Dülmer et al., 1995; Sahu et al., 2010; Shaw et al., 2010; Tripathi et al., 2020a; 2020b; Wohl et al., 2023; Yassaa et al., 2008).

iii. OVOCs, e.g., methanol, acetone, acetaldehyde, propanol, glyoxal (Beale et al., 2010, 2013; Mahajan et al., 2014; Mungall et al., 2017; S. Wang et al., 2020).

iv. Halocarbons, e.g., iodinated halocarbons (CH_3I) and bromoalkanes (e.g., CH_2Br_2, $CHBr_3$, $CHBrCl_2$, and $CHBr_2Cl$) (Carpenter et al., 2013; Chance et al., 2014; Gómez-Consarnau et al., 2021; C. E. Jones et al., 2010; MacDonald & Moore, 2007; Mahajan et al., 2019; Ooki et al., 2015; Ziska et al., 2013).

The contribution of oceans to global VOC emissions is still not adequately constrained due to the lack of observations. Globally, the most extensively studied oceanic VOC is DMS, which is the largest natural source of sulfur in the atmosphere and holds significant climatic importance (Barnes et al., 2006). DMS and other oceanic VOCs, such as isoprene and monoterpenes, contribute to photochemical reactivity and secondary aerosol formation in the marine boundary layer (MBL) (Hoffmann et al., 2016; Kilgour et al., 2024; Hu et al., 2013; Cui et al., 2019). The significance of marine isoprene emissions has also attracted considerable scientific attention in the last decade (Conte et al., 2020; Gantt et al., 2010; W. Zhang & Gu, 2022).

1.1 Dimethyl sulfide (DMS)

DMS is the most abundant biogenic volatile sulfur compound in the atmosphere and plays a crucial role in climate regulation and the global sulfur cycle (Charlson et al., 1987; Ghahreman et al., 2019; Levasseur, 2013). Oceans are the major source of DMS, contributing to ~90–95% of

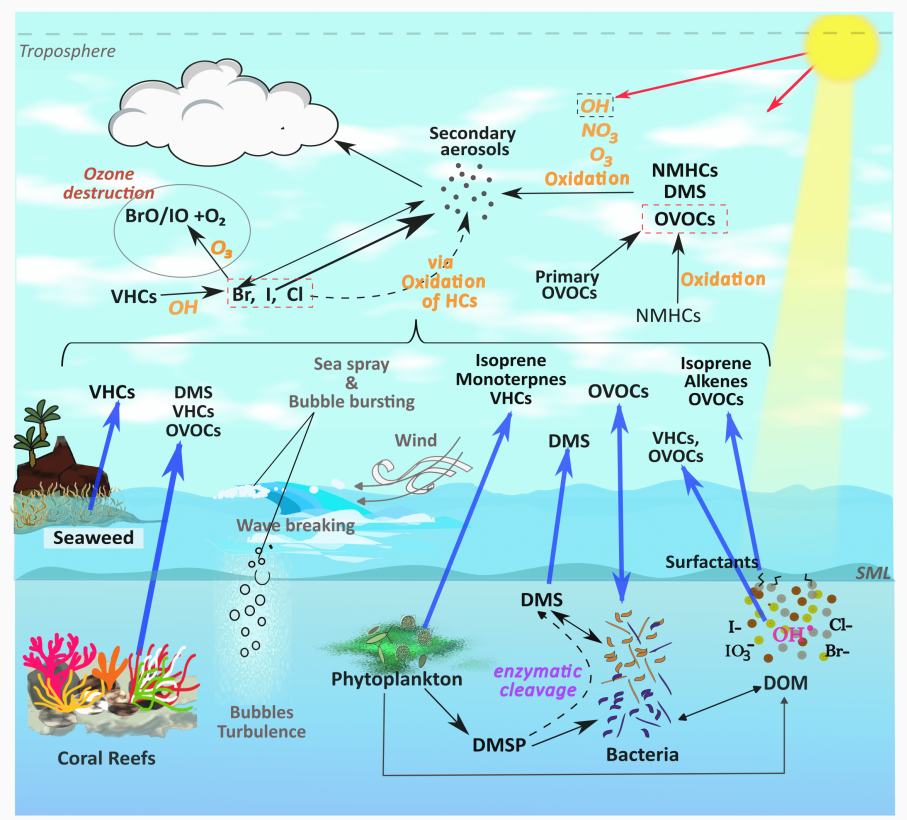

Figure 1.1: *Schematic representation of sources and atmospheric chemistry of reactive trace gases in MBL. Air–sea exchange is represented by blue arrows, photochemical processes by red arrows, and multistep indirect mechanisms by dashed arrows.*

the global source emission, and global oceanic DMS emissions account for about 70% of natural sulfur emissions in the atmosphere (Galí et al., 2018). The global DMS flux has been estimated to be 28.1 (17.6–34.4) Tg S yr^{-1} (Lana et al., 2011), which is about half the anthropogenic sulfur input to the atmosphere (Klimont et al., 2013; Hulswar et al., 2021). Emissions from tropical oceans (20 °N–20 °S) alone contribute ~48% to the global DMS budget despite covering only 33% of the global oceanic area (Simó & Dachs, 2002).

1.1.1 Climatic significance of DMS

DMS is produced mainly in seawater by phytoplankton metabolic activity and released into the atmosphere via air-sea exchange processes (Gupta et al., 2024). The oxidation of DMS can lead to the formation of non-sea-

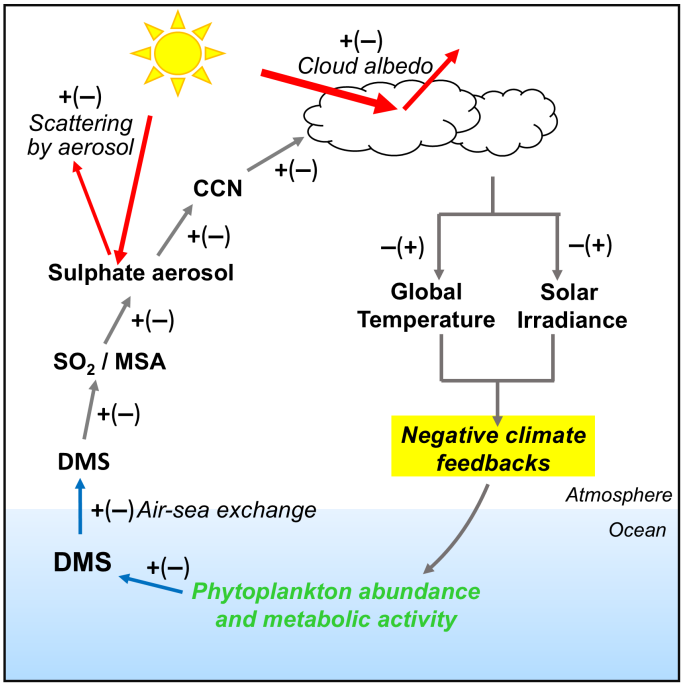

Figure 1.2: *Schematic representation of the CLAW hypothesis.*

salt sulfate (nss-SO_4^{2-}) aerosols. Nss-SO_4^{2-} aerosols are highly hygroscopic (water-attracting), making them efficient CCN because they can activate at relatively lower supersaturations compared to less hygroscopic particles. This consequently influences the cloud formation processes in the remote marine atmosphere (Mayer et al., 2020). Thus, DMS can have a significant impact on chemistry-climate interactions in the marine atmosphere.

The CLAW hypothesis by Charlson et al. (1987) proposed a negative feedback loop that connects marine phytoplankton activity to Earth's climate (Figure 1.2). Oceanic phytoplankton activity and air-sea exchange processes release DMS into the atmosphere, where it is oxidized and leads to the formation of sulfate aerosols. These aerosols act as cloud condensation nuclei (CCN). An increase in CCN leads to higher albedo clouds, reducing the solar radiation flux reaching the surface. This results in a decrease in temperature, and consequent decline in phytoplankton activity, and DMS production. Thus, the mechanism acts as a potential natural thermostat that helps regulate the Earth's climate. However, detailed scientific reviews based on several modelling and observational studies have shown that, while some aspects of the mechanism are proven, the entire feedback loop

as described originally by the CLAW hypothesis has not been convincingly demonstrated globally. Many gaps and uncertainties persist, especially in the quantification of cloud feedbacks and the extent of DMS contribution to CCN populations and activity, and cloud properties. (Ayers & Cainey, 2007; Quinn & Bates, 2011).

1.1.2 Production of oceanic DMS

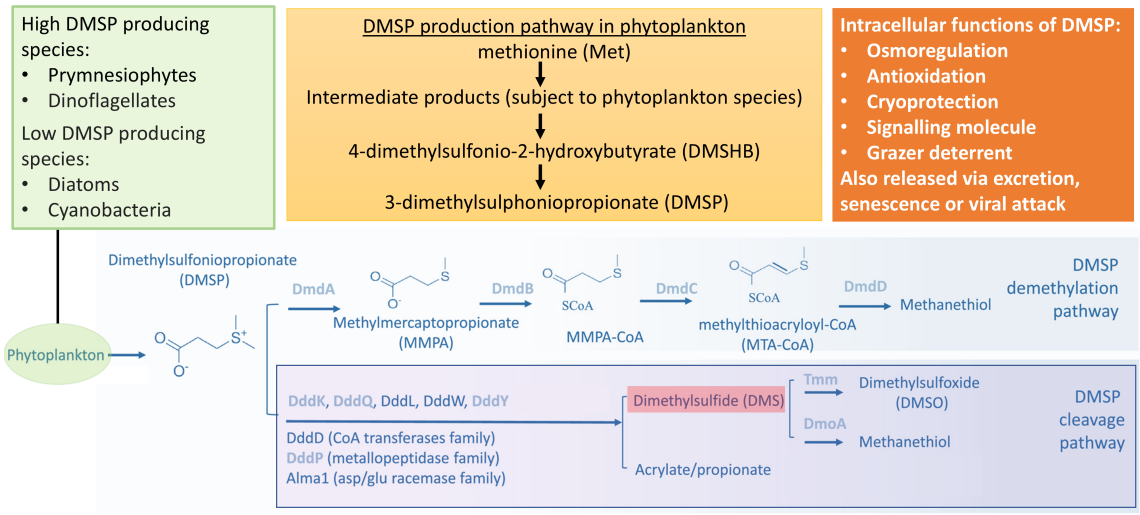

Figure 1.3: *DMSP and DMS production mechanisms in seawater. The bottom panel of the schematic is adapted from Chen & Schäfer, 2019.*

DMS is primarily produced via enzymatic cleavage of dimethylsulfoniopropionate (DMSP) in seawater (Keller et al., 1989). DMSP is a metabolite synthesized by phytoplankton and serves several crucial physiological functions, including osmoregulation, cryoprotection, antioxidant defence, and deterrence against grazers (Stefels et al., 2007). The biosynthesis of DMSP in phytoplankton begins with a sulfur-containing amino acid, methionine, and proceeds through several enzymatic steps, including methylation, transamination, and decarboxylation (Zhang et al., 2019; **Figure 1.3**). Further, DMSP can catabolize through two major pathways: the demethylation pathway and the cleavage pathway (**Figure 1.3**). The demethylation pathway results in the formation of acetaldehyde, which can be further oxidized to acetate and methanethiol. The cleavage pathway leads to the production

of DMS, facilitated by a diverse group of enzymes (DddK, DddQ, DddL, DddW, and DddY) during microbial activity (Chen & Schäfer, 2019). DMSP production levels vary widely among different phytoplankton groups (Bullock et al., 2017). Dinoflagellates and prymnesiophytes are associated with high intracellular DMSP concentrations, while most species of diatoms, cyanobacteria, and chlorophytes are low DMSP producers with intracellular concentrations < 50 mM (McParland & Levine, 2019). Its production and release are sensitive to the environmental conditions, such as UV radiation, SST, salinity, and nutrient availability (Bucciarelli & Sunda, 2003; Stefels et al., 2007). DMSP-to-DMS lyase also increases under oxidative stress, as DMS acts as an antioxidant by scavenging reactive oxygen species (ROS) (Sunda et al., 2002, 2007). Thus, the seawater DMS concentration is controlled by a complex interplay of phytoplankton species composition, biotic and abiotic stresses, and bacterial activity (Stefels et al., 2007). Since DMS is typically supersaturated in the surface ocean (Marandino et al., 2013), its sea-to-air flux is primarily governed by its concentration in surface waters and the turbulent exchange processes near the air–sea interface (Liss et al., 2014). Globally, only $\sim$10% of the dissolved DMS is released into the marine atmosphere through air-sea exchange processes, while the rest is recycled in seawater by bacterial oxidation and UV photolysis (Galí & Simó, 2015).

1.1.3 Fate of DMS in atmosphere

DMS is rapidly oxidized in the atmosphere by atmospheric radicals (e.g., hydroxyl (OH), nitrate (NO_3), and halogen (Cl, BrO, etc.), which is also the major sink mechanism of DMS in the atmosphere. OH-oxidation is the dominant loss process of DMS in the atmosphere during daytime, which results in the formation of methanesulfonic acid (MSA) and sulfur dioxide (SO_2) through temperature-dependent pathways of OH-addition and H-abstraction. While MSA is produced primarily by OH-addition, which becomes more relevant with decreasing temperature ($\sim$50-33% contribution at 285–295 K; Barnes et al., 2006), SO_2 comes from both the OH-oxidation

pathways (Boucher et al., 2003). H-abstraction is the preferred pathway at higher temperatures, with ∼70% contribution at 298 K (Novak et al., 2022b). The nighttime DMS chemistry is dominated by NO_3 radicals, which efficiently oxidize DMS to SO_2. The oxidation by NO_3 radical is more efficient under conditions of outflow of continental pollution than in pristine marine air (Osthoff et al., 2009; Stark et al., 2007).

Gas-phase oxidation of atmospheric DMS is the major source of nss-SO_4^{2-} aerosols in the remote MBL (Hoffmann et al., 2016). DMS oxidation products like sulfuric acid (SA), which is formed by further oxidation of SO_2, and MSA can undergo heterogenous nucleation by condensing on pre-existing particles to form nss-SO_4^{2-} aerosols. In low condensation sink environments, associated with lower pre-existing aerosol concentrations, SA and MSA can lead to new particle formation (NPF) by homogenous nucleation with water vapour or by clustering with ammonia and amines (Hoffmann et al., 2016; Rosati et al., 2021; Sipilä et al., 2010). About 18% of the global nss-SO_4^{2-} has been found to be associated with oceanic DMS (Gondwe et al., 2003). These particles have substantial contributions (33–55%) to CCN over remote marine regions (Sanchez et al., 2018), and hence affect atmospheric radiative properties directly and indirectly.

1.1.4 Present understanding of DMS flux from the northern Indian Ocean

DMS has been extensively studied in different parts of the world, but we still lack *in situ* measurements over the northern Indian Ocean. The previous *in situ* measurements over the Arabian Sea and Bay of Bengal have mainly focused on the distribution of DMS concentration in seawater (Hatton et al., 1999; Rao et al., 2015; Shenoy et al., 2000, 2002, 2006; Shenoy & Kumar, 2007). The estimates of DMS seawater concentrations and of air-sea fluxes using interpolated climatologies, empirical algorithms, and prognostic biogeochemical models have shown significant discrepancies (Tesdal et al., 2016). Lana et al. (2011; L11) provide one of the most comprehensive and widely tested global monthly climatology of

DMS surface seawater concentration and fluxes. The study showed large seasonal variations in DMS flux over the northern Indian Ocean, with highest values during the southwest monsoon ($\sim$335 kg S km^{-2} yr^{-1}) and the lowest in the pre-monsoon season (Tegtmeier et al., 2022). Recently, an updated global climatology of DMS seawater concentrations and fluxes has been presented by Hulswar et al. (2022; H22), taking account of the new inclusions in the DMS database in the last decade and the seasonal changes in biogeochemical and physical characteristics in distinct oceanic provinces of DMS. Interestingly, lower DMS seawater concentrations and air-sea fluxes over the northern Indian Ocean were found to be lower in H22 than estimated in L11, indicating uncertainties resulting from the lack of DMS measurements. In H22, emissions from the Arabian Sea and Bay of Bengal were identified among the few DMS hotspots globally, with flux ranging between 10–20 μmol S m^{-2} d^{-1}. However, the estimations of DMS fluxes in L11 and H22 are based on the assumption that the emissions are entirely controlled by the seawater concentrations and wind speeds. Though the production of DMS is primarily associated with biological productivity, biomass abundance (Chl-a) supports only $\sim$15% of the seawater DMS variability (Bell et al., 2021). Few studies have reported an overestimation of oceanic DMS in the Indian Ocean region through global parameterization schemes (Galí et al., 2018; Zavarsky et al., 2018b). Thus, the limited *in situ* seawater data and lack of atmospheric measurements of DMS over the northern Indian Ocean add to the uncertainties of these estimates. DMS flux depends largely on physical forcing, impacting the spatial and vertical dynamics of the mixed layer and the associated biogeochemical processes (Gupta et al., 2024). And the implication of these fluxes on the direct and indirect regional radiative forcing depends on the atmospheric levels of DMS. Therefore, a comprehensive analysis of well-resolved spatial and temporal variability of DMS concentration and its relationships with sea surface and atmospheric parameters is essential to understand the factors controlling DMS emissions (Royer et al., 2015).

1.2 Isoprene

Emission from the terrestrial biosphere is a major source of BVOCs, contributing ~760 Tg C yr^{-1} to the global atmosphere (Sindelarova et al., 2014). As estimated using the Model of Emissions of Gases and Aerosols from Nature (MEGAN), isoprene (2-methyl-1,3-butadiene, C_5H_8) contributes about 410-660 Tg C yr^{-1} to the global BVOCs (Guenther et al., 2006; Müller et al., 2008; Sindelarova et al., 2014). Therefore, most research on the production and roles of isoprene is largely confined to plants in terrestrial biomes (Sharkey et al., 2008). However, oceanic emissions can also be an important source of isoprene and several light NMHCs in the remote marine atmosphere (e.g., Meskhidze et al., 2015; Plass-Dülmer et al., 1995; Sahu et al., 2010; Shaw et al., 2010; Tripathi et al., 2020a; 2020b). Recent studies have revealed higher emission rates of isoprene and other NMHCs from marine ecosystems than previously estimated (e.g., Giorio et al., 2022; Wohl et al., 2023; Rocco, 2021).

Recent studies have revealed higher emission rates of isoprene and other NMHCs from marine ecosystems than previously thought (Giorio et al., 2022; Rocco et al., 2021; Wohl et al., 2023). The production of isoprene in seawater is driven by both biotic and abiotic processes (**Figure 1.1**). A few studies have reported isoprene production as a secondary metabolite by different phytoplankton species in the Indian Ocean and other oceanic regions (e.g., Booge et al., 2018; Hackenberg et al., 2017; Ooki et al., 2015), with higher isoprene production tendency in tropical waters than high latitudes (Dani & Loreto, 2017). The production mechanism is strongly influenced by environmental factors such as light, temperature, nutrient availability, and phytoplankton community composition (Shaw et al., 2010). The production rates of isoprene in seawater are controlled by various microbial communities, including algae and macroalgae. Cyanobacteria tend to dominate isoprene emissions in tropical and subtropical oceans, while other phytoplankton groups prevail at higher latitudes (Cui et al., 2023). In addition to this, abiotic photochemical processes at the sea surface

microlayer (SML) can also make a substantial contribution to the marine isoprene budget (e.g., Brüggemann et al., 2018; Ciuraru et al., 2015). Photosensitized reactions in the SML, enriched with organic surfactants and dissolved organic matter (e.g., humic acids), are important pathways for marine isoprene production. The primary sink for oceanic isoprene is air–sea exchange, with additional losses from microbial consumption, chemical degradation, and advective mixing (Booge et al., 2018; Conte et al., 2020). However, the processes controlling oceanic production and emissions are poorly understood, mainly due to limited field measurement data to parameterize the model simulations of global isoprene emissions (Exton et al., 2013; Hackenberg et al., 2017). The global estimates of marine isoprene emissions of ∼0.4–11.6 Tg C yr^{-1} (Arnold et al., 2009; Conte et al., 2020) are far less than the emissions from terrestrial plants. Nonetheless, modelling studies have shown that marine isoprene emissions, produced through biological and photochemical processes, are strongest from the equatorial region (15°N–15°S), contributing more than 36% to the global annual oceanic emission (Conte et al., 2020). However, the processes controlling oceanic production and emissions are poorly understood due to limited field data required to constrain global model simulations (Exton et al., 2013; Hackenberg et al., 2017).

Despite lower emission rates from the oceans, isoprene can play a key role in modulating the oxidation capacity of the remote marine atmosphere. Oxidation of isoprene in remote MBL can also lead to the formation of secondary VOCs such as methacrolein and methacrylic acid (Cui et al., 2019). Over biologically productive waters, it can significantly impact the oxidant loadings, contribute to SOA production, and modify particle size and microphysical properties (e.g., Krüger & Graßl, 2011; Meskhidze & Nenes, 2006). The marine isoprene-derived SOA can contribute >30% of the total monthly averaged submicron organic carbon fraction of the marine aerosol over the tropical oceanic regions (Gantt et al., 2009). Recently, Tripathi et al. (2024) have reported episodes of NPF over the equatorial Indian Ocean, associated with marine emissions of reactive NMHCs. Zavarsky et

al. (2018b) have observed significant positive correlations between isoprene fluxes and atmospheric aerosols in the western tropical Indian Ocean during the summer monsoon.

1.2.1 Present understanding of isoprene emission from the northern Indian Ocean

Studies of NMHCs in the marine atmosphere have been mainly focused on the Pacific and Atlantic Oceans, or smaller basins such as the Arabian Gulf, Mediterranean Sea, Gulf of Mexico, Black Sea, etc. (Arnold et al., 2009; Baker et al., 2000; Bourtsoukidis et al., 2019; Lewis et al., 1999; Liakakou et al., 2007; Mungall et al., 2017; Saito et al., 2000). The Asian continent and the islands of Southeast Asia are significant emitters of NMHCs (Li et al., 2014), which can be transported across the western North Pacific and eastern Indian Ocean. The measurements of biogenic NMHCs in air and seawater of the tropical Indian Ocean have been rarely reported (Blake et al., 1997; Gupta et al., 2024; Sahu et al., 2010; 2011; Tripathi et al., 2020a; 2020b), particularly for isoprene (**Table 1.1**). The average surface isoprene concentration of ~50 pmol/L reported in the tropical Indian Ocean with higher sea surface temperature (SST >28°C) were significantly higher than those in subtropical, sub-polar, and polar waters (Ooki et al., 2015; Zavarsky et al., 2018a). However, the model does not show agreement with the measurements over the tropical Indian Ocean (Booge et al., 2016).

A few studies have attributed high isoprene concentrations in the tropical marine atmosphere to the contributions of the transport from terrestrial sources, in addition to the oceanic emissions (Shaw et al., 2010; Tripathi, 2020a; Yokouchi et al., 1999). The biogenic emissions from coastal waters have been reported to be an important source of isoprene (0.01–2.74; 0.53±0.73 ppb) in the MBL of the Yellow Sea and the East China Sea (Li et al., 2022; Wu et al., 2021). Tripathi et al. (2020a) have reported elevated isoprene concentrations of 0.16–1.12 ppb in marine air of the oligotrophic Arabian Sea during the spring inter-monsoon season, mainly associated with blooms of *Trichodesmium* and *Thalassiosira* at high SST.

The estimated mean isoprene flux of ∼64.5 nmol m^{-2} d^{-1} in Tripathi et al. (2020a) was higher than the global annual mean flux of 41.4 nmol m^{-2} d^{-1} modeled by Conte et al. (2020). The relative disparities in the estimated values indicate the high spatial and temporal variability of marine isoprene emissions, highlighting the importance of assessing the seasonal isoprene fluxes from the northern Indian Ocean.

Table 1.1: *Summary of air-sea fluxes and concentrations of isoprene and DMS reported over the northern Indian Ocean.*

BVOC	**Region/Season**	**Concentration/flux data**	**References**
Isoprene	Tropical Indian Ocean/ Annual	50 pmol/L	Ooki et al., 2017
	AS/ pre-monsoon	0.16–1.12 ppb; 21.5–172.2 nmol m^{-2} d^{-1}	Tripathi et al., 2020a
	NIO/Annual	upto 1 kg km^{-2} yr^{-1} (28 μmol m^{-2} d^{-1})	Tegtmeier et al., 2022
DMS	Central BoB/ winter	500–800 ng/L	Yamamoto et al., 2001
	AS+BoB/ Monsoon	0.04–41.1 μmol m^{-2} d^{-1}	Shenoy et al., 2007
	AS+CIO winter	0.03–34.4 μmol m^{-2} d^{-1}	Shenoy et al., 2007
	AS+BoB (pre-monsoon and post-monsoon)	upto 13.1 μmol m^{-2} d^{-1}	Shenoy et al., 2007
	Coastal BoB/ Monsoon	5.5 $\pm$ 4 μmol S m^{-2} d^{-1}	Rao et al., 2015
	Northwest coastal AS/ Monsoon	100–800 ppt	Edtbauer et al., 2020
	NIO/ Annual	5–20 μmol m^{-2} d^{-1}	Hulswar et al., 2022
	NIO/ Annual	upto 650 kg km^{-2} yr^{-1} (∼40 nmol m^{-2} d^{-1})	Tegtmeier et al., 2022

1.3 Northern Indian Ocean

The northern Indian Ocean experiences seasonally varying wind circulation due to strong land-ocean-atmosphere coupling (**Figure 1.4**), controlling the key physical and biogeochemical properties of the surface ocean (Tegtmeier et al., 2022; Webster et al., 1999). The North Indian Ocean comprises the Bay of Bengal and Arabian Sea basins, along with marginal seas such as the Andaman Sea and the Laccadive Sea. The Arabian Sea is one of the most biologically productive oceanic regions of the world, known to possess a perennial oxygen minimum zone (Naqvi, 1991; Vidhya et al., 2022). The basin has been experiencing one of the largest warming trends over the tropical oceans (Roxy et al., 2015). The long-range atmospheric transport of airborne mineral dust and ocean upwelling provide increased nutrients to the Arabian Sea, leading to its higher biological productivity than the Bay of Bengal (Madhupratap et al., 1996; Murtugudde et al., 1999; Singh & Ramesh, 2015; Sreeush et al., 2018). Seasonally varying processes such as upwelling, wind-driven mixing, and lateral advection of upwelled coastal waters are major drivers of intense biological productivity in the open ocean Arabian Sea, particularly during the summer monsoon (Kumar et al., 2002). Relatively lesser biological production in the Bay of Bengal is primarily attributed to the limited availability of nutrients in the upper layers, arising from strong stratification and weaker winds, which inhibits vertical mixing.

However, the physical conditions in the Bay of Bengal make it more prone to extreme conditions. The SST climatology exhibits a bimodal distribution pattern in the Bay of Bengal, with a primary peak during May-June and a secondary peak in October (Sarker et al., 2020). Relatively higher SSTs (28–30°C) lead to a thermodynamically unstable atmosphere and significant tropical cyclonic (TC) activities over the Bay of Bengal. The TC conditions during pre-monsoon and post-monsoon (primary TC peak season) over the Bay of Bengal account for ∼6% of the global annual tropical storm events. Tropical cyclonic activities can modulate the trace gas fluxes and trigger

episodes of surface productivity post-cyclone (Kumari et al., 2019; Lévy et al., 2012). Additionally, eddy-driven nutrient upwelling is the main factor driving the surface biological productivity in the post-monsoon season (September–October). Thus, due to favourable biogeochemical conditions and tropical-meteorological events, the Arabian Sea and Bay of Bengal could be potentially important in BVOCs (e.g. DMS) production and air-sea exchange and play an important role in the global natural sulfur budget.

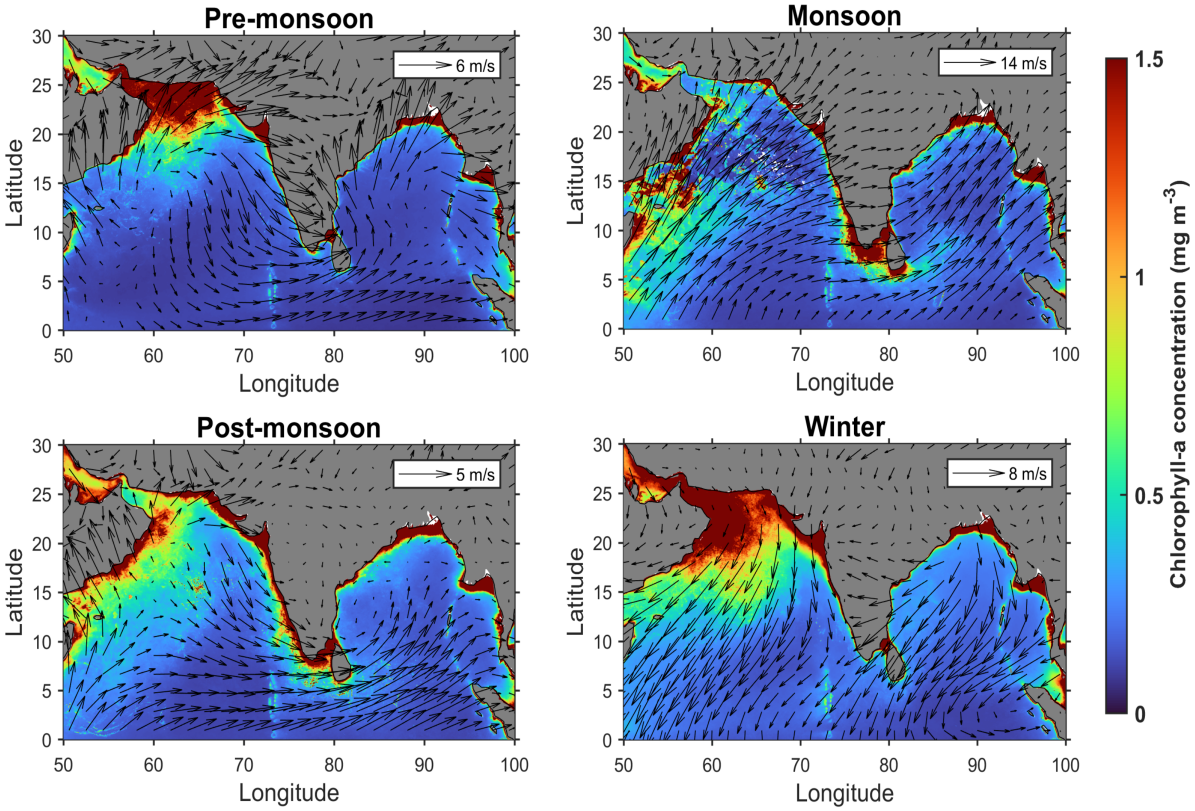

Figure 1.4: *Maps of Chl-a concentration (from MODIS-A) and wind field climatology (from NCEP/NCAR reanalysis data) for the pre-monsoon (MAM), Monsoon (JJA), Post-monsoon (SON), and Winter (DJF) seasons for the period of December 2012 to February 2022 over the northern Indian Ocean.*

1.4 Objectives

The research presented in this thesis is based on the first high time-resolution continuous shipborne measurements of atmospheric DMS and NMHCs over the northern Indian Ocean. These measurements were carried out during the following two field campaigns:

i. SK#373 over the Bay of Bengal and Andaman Sea during 26 September–14 October 2021 in the post-monsoon season.

ii. SK#374 over the Arabian Sea, the eastern and southern coastal waters of Sri Lanka, and the Laccadive Sea during 27 October–24 November 2021 in the post-monsoon season.

These unique datasets could provide valuable insights into detailed features of DMS and isoprene variability, the co-emission of DMS and other biogenic VOCs like isoprene, and the dominant factors controlling the exchange/emission rates to the atmosphere. The results from this study could be beneficial inputs for chemistry-climate interaction modelling over the northern Indian Ocean.
The central objective of the thesis is to address the knowledge gap about the sources, and physical and biogeochemical drivers of air-sea exchange processes controlling the DMS and isoprene concentrations in the marine air of the northern Indian Ocean. The specific objectives are summarized below:

i. *Investigate the spatio-temporal variations of DMS and isoprene mixing ratios in the MBL of the northern Indian Ocean using high-resolution in situ measurements.*

We have characterized the regional and short-term variability of atmospheric DMS and isoprene using shipborne measurements (resolution 24 and 30 min, respectively), conducted over the Bay of Bengal, Arabian Sea, Andaman Sea, Sri Lanka coast, and Laccadive Sea in the post-monsoon season. We have also investigated the distribution of isoprene and aromatic

hydrocarbons over the Bay of Bengal during the southwest monsoon season. The characteristics and key features of day-to-day and diurnal variability of the DMS and isoprene mixing ratios observed in these different basins of the northern Indian Ocean are discussed in detail.

ii. *Investigate the roles of atmospheric and oceanic factors in controlling the DMS and isoprene distribution.*

We have investigated the relationships of DMS mixing ratios with several hydrographic, biogeochemical, and meteorological variables under different environmental conditions. These include sea surface salinity, SST, satellite-derived Chl-a, nutrients, picophytoplankton abundance, wind speed, and ventilation coefficient. The variations of isoprene with SST, salinity, surface Chl-a, air temperature, RH, and wind conditions are examined to determine the sources and impact of these parameters on isoprene levels in the MBL.

iii. *Investigate the relationships between DMS and isoprene to characterize their major source and loss processes.*

The variations of DMS with isoprene and benzene mixing ratios in the MBL are investigated in the coastal and open ocean regimes. The distinct relationships between DMS and isoprene in different parts of the northern Indian Ocean are then used to describe the underlying processes and contributing sources, including co-emissions of isoprene and DMS, that are driving these variations over the study region.

iv. *Investigate the impact of terrestrial outflow and oceanic emission on the atmospheric chemistry of DMS over the coastal regions.*

We have investigated the changes in VOC composition, particularly the relative abundances of DMS, isoprene, and aromatics in the coastal regions. We further examined the modulation of DMS chemistry and atmospheric mixing ratios during interactions of terrestrial outflow and oceanic air masses.

v. *Estimate the air-sea fluxes of DMS over the northern Indian Ocean using both bottom-up and top-down methods.*

Air-sea fluxes of DMS are calculated using two distinct approaches, top-down and bottom-up, based on different assumptions. Given the complexities involved in direct air-sea flux measurements of DMS, the estimates obtained from different approaches provide a wider domain to compare the data and improve the understanding of the limitations and uncertainties associated with the different approaches. The DMS seawater concentration, required for the bottom-up approach, is estimated using satellite data-based global parametrizations by Galí et al. (2018). The parametrized estimates, derived using satellite and *in situ* data as input variables, are compared with previous studies to evaluate the applicability of global parametrization at regional levels.

Chapter 2

Experimental Techniques and Data Analysis

2.1 Analysis of the DMS and NMHCs concentrations

2.1.1 Instrumentation

The continuous *in situ* measurements of the mixing ratios of DMS and NMHCs were carried out using online Sulfur trace gas analyzer, C_2–C_6 and C_6–C_{12} VOC analyzers onboard the Oceanographic Research Vessel (ORV) *Sagar Kanya (SK)*. These analyzers are based on the principle of Thermal Desorption-Gas Chromatography (TD-GC), coupled with a Flame Photometric Detector (FPD) for the analysis of sulfur trace gases and with a Flame Ionization Detector (FID) for the analysis of NMHCs.

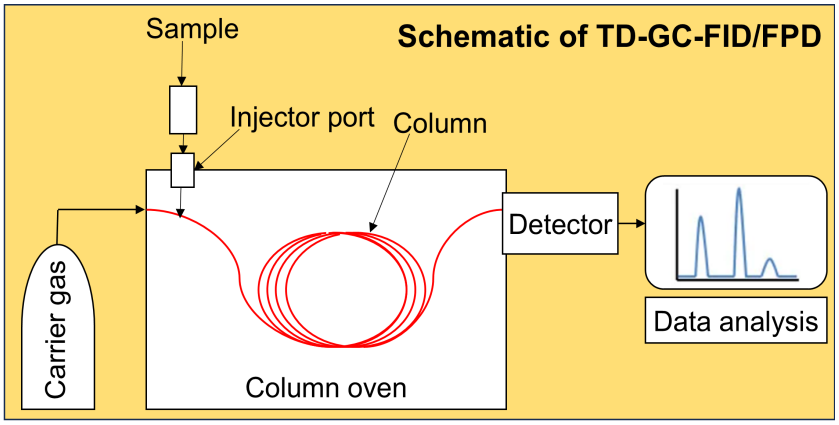

Figure 2.1: *A schematic diagram of the TD-GC system for the analysis of VOCs in the ambient atmosphere.*

Along with the online measurements, pressurized air samples were also collected in glass canisters for the offline analysis using the TD-GC-FID system at our Laboratory in PRL. A brief description of the working of TD-GC-FID/FPD systems (**Figure 2.1**) is provided below:

i. **Thermal Desorption-Gas chromatography (TD-GC)**

TD-GC is a highly sensitive analytical technique to detect and quantify atmospheric VOCs. The TD unit is primarily used for the preconcentration of VOCs as they exist at very low concentrations in the ambient atmosphere, typically in the parts per billion (ppb) to parts per trillion (ppt) levels. This method can significantly improve the detection limits and sensitivity of the analytical system. In the TD process, the air sample is drawn into the system through a cryo-trap filled with a sorbent material specifically chosen to adsorb the targeted VOCs. The material inside the trap (e.g., Tenax TA and Carbopack) is selected based on the volatility and chemical properties of the VOCs of interest. Maintaining the trap at a low temperature or cryogenic-trapping enhances the retention of highly volatile compounds, such as NMHCs and DMS, by reducing their vapor pressure and minimizing losses, and therefore, is essential for accurate quantification of the most atmospheric VOCs.

The trap is then heated under an inert gas flow, and the desorbed analytes are transferred into the GC column by a carrier gas. The column is the core component of the GC system, where the separation of the mixture takes place. In the column, the components of the mixture interact with two phases: the stationary phase, which is a chemical coating on the inner walls of the column; and the mobile phase, which is the carrier gas that transports the sample through the column. The carrier gas is selected to be chemically inert to prevent any reactions with compounds and the hydrogen flame used in detection. To optimize this separation, the column temperature is gradually increased according to a programmed temperature ramp. The tempera-

ture programming facilitates effective separation of a complex mixture containing compounds with diverse volatilities and boiling points. The compounds in the mobile phase interact with the stationary phase as they pass through the column and get separated based on the volatility and interaction with the column's stationary phase. The separated compounds elute from the column to the detector in sequence, where a signal is recorded for each compound corresponding to its retention time in the column. There are several detection methods available for VOC analysis, based on their sensitivity and selectivity towards different chemical groups. For our measurements, FPD and FID were used to efficiently detect sulfur-containing VOCs and NMHCs, respectively.

ii. **Flame Photometric detector (FPD)**

FPD is a photometric emission-based detector selectively suited for the detection of sulfur- and phosphorus-containing compounds. In this detector, the sample is introduced into a hydrogen-oxygen flame, where sulfur compounds generate chemiluminescent emissions at a characteristic wavelength of 394 nm. The emitted light is detected by a photomultiplier tube, and the signal is calibrated to quantify the concentration of target analytes.

iii. **Flame ionization detector (FID)**

The operation of FID is based on generation of ions by combustion of organic compounds in a hydrogen-air flame. These ions are collected by electrodes, producing an electrical current proportional to the carbon content of the analytes, which is amplified and recorded as a measurable signal. Due to its high sensitivity, selectivity, wide dynamic range, and stability, the FID has been widely used for quantitative analysis of various hydrocarbons.

GC-FPD has been widely used for DMS measurements in marine environment in several studies across different oceanic basins (Cooper & Saltzman, 1993; Davison & Allen, 1994; Kato et al., 2009; Park & Lee, 2008; Zhao et

al., 2022), due to its high selectivity and sensitivity in field and shipboard environments. A few previous studies have also reported better sensitivity of GC-FPD in DMS detection than GC coupled with mass spectrometer (MS) (Franchini & Steinke, 2017; Hopkins et al., 2016; Mesarchaki et al., 2014). Although modern mass spectrometry-based systems such as AP-CIMS and PTR-ToF-MS offer high-resolution, real-time measurements with excellent sensitivity, they are often more complex and difficult to stabilize on moving platforms (e.g. ships), and under the high-humidity conditions typical of the tropical marine atmosphere. In contrast, GC-FPD is a low-maintenance and robust analytical technique that has shown good agreement in DMS measurements with modern MS-based methods (Royer et al., 2014).

For NMHCs, GC-FID is considered to be the most reliable analytical technique, and has been widely applied in previous studies in the marine atmosphere, particularly for light (C_2-C_5) NMHCs (Blake et al., 2003; Goldan et al., 2004; Sahu et al., 2006; Tripathi et al., 2020a; 2020b; Williams et al., 2010). Although, PTR-ToF-MS provides high time resolution, its application to light NMHCs is limited by several factors: (i) Low proton-transfer efficiency of these compounds (except isoprene) due to lower proton affinities than that of water, resulting in poor ionization and quantification of these compounds, (ii) Isobaric interferences, which prevent differentiation of structural isomers (e.g., i-&n-butane, i-&n-pentane), and (iii) humidity-dependent sensitivity, which can affect calibration stability under marine conditions. This makes PTR-ToF-MS less reliable for measuring light NMHCs in marine environments, whereas GC-FID offers a superior separation for isomers and is relatively unaffected by humidity. Warneke et al. (2001), have reported good agreement between isoprene measurements from PTR-MS and GC-FID in clean atmosphere over the tropical rainforest. However, based on measurements in polluted coastal marine air, de Gouw et al. (2003) found an overestimation in isoprene mixing ratios for levels below 100 ppt.

2.2 Experiments onboard ship

A common sampling system was designed for all analyzers using a PTFE tube of 1/2" ID, a glass manifold, and a vacuum pump. The inlet of the PTFE tube (1/2" ID) was placed facing downward toward the water surface at the starboard side of the ship, ~5 m above the sea surface. A snippet of the onboard laboratory set-up for VOC measurements is shown in (**Figure 2.2**)

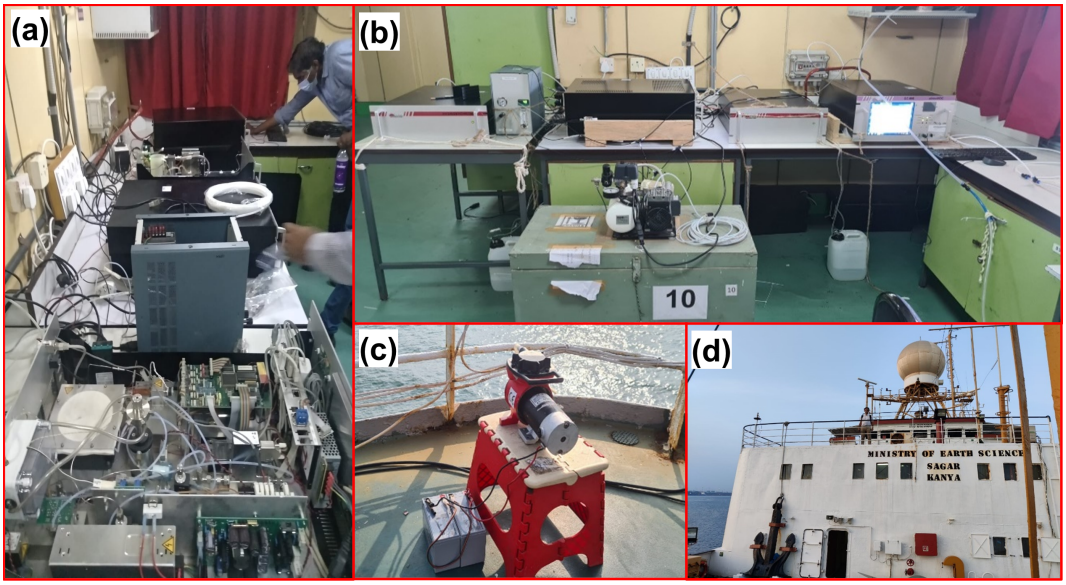

Figure 2.2: *Onboard laboratory set-up for ambient air VOC measurements during the cruise campaigns.*

2.2.1 Measurements of DMS concentration

The measurements of atmospheric DMS concentration were conducted using an online sulfur trace gas analyzer (AirmoS, Model: C51022-TRAP, Chromatotec®, Saint-Antoine, France). Detection of volatile sulfur compounds (VSCs) is based on the principle of thermal desorption-gas chromatography -flame photometric detection (TD-GC-FPD).

Ambient air was sub-sampled from a glass manifold into the analyzer through a 1/4" ID PTFE tube at a flow rate of ~80 mL min^{-1} for 6 min using a pump (KnF 65 LABOPORT® Vacuum Pump). Sulfur trace gases present in air samples were pre-concentrated on a Peltier-cooled (at +5 °C)

Tenax trap, desorbed at 180°C for 120 s, and transferred into a metallic column (MXT, 4 m × 0.53 mm, 1.5 μm film thickness, Restek Corp., USA) by a carrier gas at a flow rate of ∼4 mL min^{-1}. Zero-air generated by the Ultra High Purity Zero Air Generator (airmoPURE D 45 PSI, Model No: XXX031-D) was used as the carrier gas. The GC column temperature was set to isothermal at 35°C during analysis. Pure hydrogen gas (generated using Hydroxychrom USB 4U, Model No: XXX916) and zero-air were supplied to the FPD at 10 and 60 mL min^{-1} in the lower flame and 50 and 60 mL min^{-1} in the second flame, respectively.

2.2.2 Measurement of C_2–C_6 and C_6–C_{12} NMHCs

The mixing ratios of different C_2–C_6 NMHCs were measured using a TD-GC-FID-based online C_2–C_6 VOC analyzer (AirmoVOC C2-C6, Model: A12000, Chromatotec®, Saint-Antoine, France) at a resolution of 30 min. Ambient air was sub-sampled from the manifold at a flow rate of ∼11 mL min^{-1} for 10 min via a vacuum pump (KNF Laboport®, KNF Neuberger, Inc.). The VOCs are pre-concentrated on a Peltier-cooled (at -15 °C) adsorbent trap. The pre-concentrated sample was desorbed at 220 °C and transferred into a PLOT Alumina column (Al_2O_3/Na_2SO_4, 25 m × 0.53 mm, 10 μm film thickness) using hydrogen (H_2) as a carrier gas at a flow rate of ∼7 mL min^{-1}. The ultra-high purity H_2 gas was generated using Hydroxychrom (Model No: XXX916, Chromatotec®, Saint-Antoine, France). The GC column temperature was programmed with an initial temperature of 36 °C, increased to 38°C at a gradient of 2 °C min^{-1}, and to 202°C at 15 °C min^{-1}. H_2 and zero air (produced using airmoPURE D 45 PSI, Model No: XXX031-D) were supplied as fuel gases to the FID at 23 and 180 mL min^{-1}, respectively.

The mixing ratios of several C_6–C_{12} NMHCs were conducted using an C_6–C_{12} VOC analyzer (AirmoVOC C6-C12, Model: A23022, chromatotec®, Saint-Antoine, France). The ambient air was subsampled from the manifold into the system at a flow rate of ∼30.3 mL min^{-1} for 30 min via a vacuum

pump (KNF Laboport®, KNF Neuberger, Inc.). The sampled air is first introduced into a peltier-cooled (at -15 °C) adsorbent trap via a 1 m long stainless steel (SS) tube (0.25" ID). Sample pre-concentrated on the adsorbent trap is desorbed at 380 °C and transferred into a MXT30CE column (30 m × 0.28 mm, 1 μm film thickness, Restek Corp., USA) by H_2 gas as carrier gas (flow rate: 4mL min^{-1}) generated by Hydroxychrom hydrogen generator (Model No: XXX916, Chromatotec®, Saint-Antoine, France). The GC column temperature was programmed with an initial temperature of 38 °C, and is increased consecutively in following order: to 40 °C at a gradient of 2 °C min^{-1}, to 50 °C at 2 °C min^{-1}, to 80 °C at 10 °C min^{-1}, to 220 °C at 15 °C min^{-1}, to 230 °C at 2 °C min^{-1} and to a final temperature of 260 °C at 9 °C min^{-1}. A mixture of H_2 and zero-air (generated using airmoPURE D 45 PSI, Model No: XXX031-D, Chromatotec®, Saint-Antoine, France) fuelled the FID flame at flow rates 27 and 180 mL min^{-1}, respectively.

2.2.3 Calibration analysis

i. **Sulfur trace gas analyzer**

In Sulfur trace gas analyzer, regular calibrations were performed using a DMS permeation tube (Model No: DMS N° 20191018-G637; Chromatotec®, Saint-Antoine, France) to monitor the sensitivity and stability of the instrument. Desired DMS concentrations of standards were generated using an internal calibration system (ICS). Two primary components of the ICS are:]

(a) *Permeation oven*, where the standard gas is released from the permeation tube in the chamber. The amount of gas released is highly dependent on the oven temperature.

(b) *Dilution setup*, where the known concentrations can be generated by regulating zero-air flow.

A constant flow of zero air (101.1 mL min^{-1}) was maintained in the

permeation oven when the ICS was idle to avoid calibration errors caused by the accumulation of substances released in the oven due to system heating or pressure changes. The permeation tube releases standard gas mass at a rate of 36.6 ng min^{-1} ($\pm$10%) at a permeation oven temperature of 40 °C and is supplied with a total dilution flow of 435.5 mL min^{-1}. The concentrations of DMS in the calibration mixture exiting from the ICS were calculated using the following equations.

$$\text{Concentration } (\mu g\ m^{-3}) = \frac{\text{Permeation rate } (ng\ min^{-1})}{\text{Total dilution flow } (L\ min^{-1})} \tag{2.1}$$

$$\text{Mixing ratio (ppb)} = \frac{\text{Concentration } (\mu g\ m^{-3}) \times 24.54\ L}{62.13\ g\ mol^{-1}} \tag{2.2}$$

Where 24.45 L is the molar volume at 25 °C and 62.13 g mol^{-1} is the molar weight of DMS. The standard gas mixing ratio of 33.07 ppb ($\pm$10%) was used for the calibration (**Figure 2.3**).

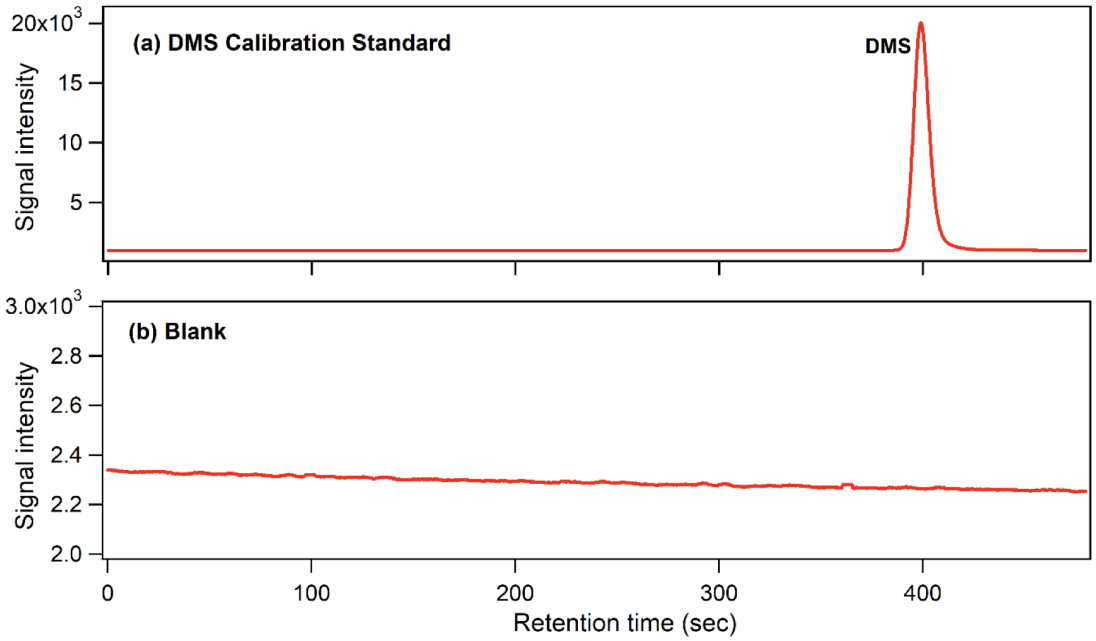

Figure 2.3: *Typical TD-GC-FPD chromatograms obtained from the analysis for (a) DMS standard gas (~33.07 ppb), and (b) blank sample.*

The following detector response function, established during the stabilization of the instrument, was used for the calculation of mass from peak area.

$$\text{Mass (ng)} = A \times \left(\frac{\text{Peak Area}}{\text{BS}}\right)^{0.6} \tag{2.3}$$

Where A (1.176) is the correction factor and BS is the base sensitivity (10000) used for the DMS concentration calculation. The precision of ~17% and detection limit of 16 ppt were calculated using the relative standard deviation (RSD) and 3-times the standard deviation (σ) of the peak areas, respectively.

ii. C_2–C_6 and C_6–C_{12} VOC analyzers

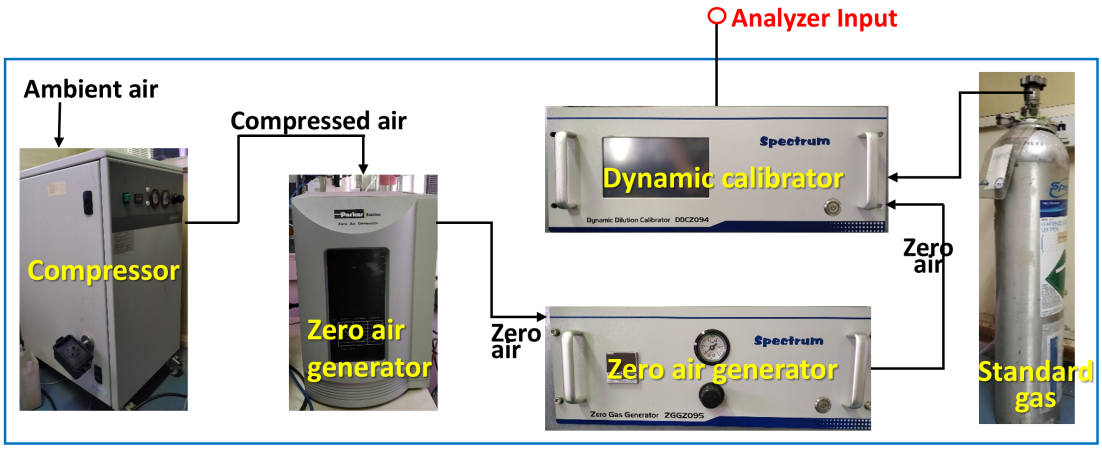

Figure 2.4: *Laboratory set-up of dynamic dilution system for multipoint calibration.*

Multi-point calibrations of the C_2–C_6 and C_6–C_{12} VOC analyzers were performed using a dynamic calibrator system (DDCZ094, Spectrum) with a standard gas mixture containing C_2–C_8 NMHCs at ~1 ppm (±5%) (Lot No.: 1341032, Linde, USA). The dynamic dilution system used dual-step generated zero-air to dilute the standard gas to the desired concentrations of 2, 4, 6, and 8 ppb (**Figure 2.4**). Blank (zero-air only) and generated standards were analyzed using TD-GC-FID-based analyzers, with five replicates for each. An example chromatogram obtained from analysis of ~4 ppb standard gas mixture in C_2–C_6 VOC analyzer is shown in **Figure 2.5**.

The chromatograms obtained were used to generate a linear calibration curve for each identified compound by establishing a best-fit line in the integrated peak area vs known concentrations from the calibration stan-

dards plot (**Figure 2.6**). These linear relationships were used to quantify the response factor of each compound, and further determine the unknown sample concentrations based on their chromatographic signal responses.

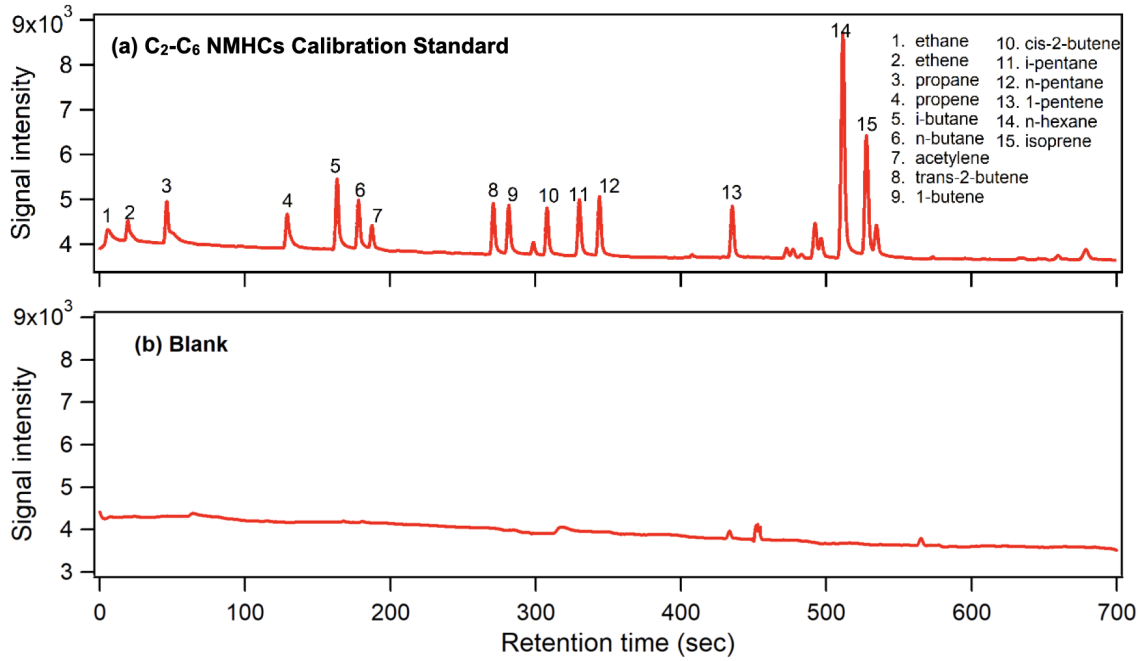

Figure 2.5: *Typical TD-GC-FID chromatograms obtained from the analysis of (a) NMHCs standard mixture (set at 4 ppb), and (b) blank sample in C_2-C_6 VOC analyzer.*

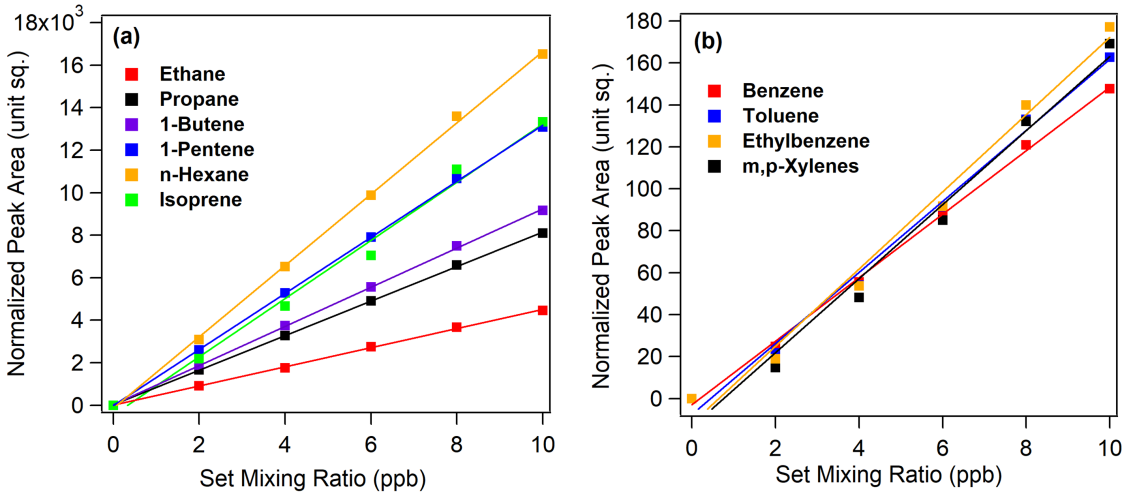

Figure 2.6: *The calibration curves for selected (a) C_2–C_6, and (b) C_6–C_{12} NMHCs.*

Based on guidelines of the International Conference on Harmonization, the

sensitivity was determined as the slope of the calibration curve, and the detection limit was determined as:

$$\mathrm{DL} = 3.3\frac{\sigma}{S} \tag{2.4}$$

where *(*σ) is the standard deviation of the y-intercept (or the blank), and *(*S) is the slope of the calibration curve. The DL of isoprene is 25 ppt and for C_2-C_6 NMHCs it varied between 20–80 ppt, and the precisions of the measurements were in the range of 2–8%. For C_6-C_{12} NMHCs, the DLs and precision was in the ranges of 5–20 ppt and 2–5%, respectively.

2.3 Auxiliary data

2.3.1 Meteorological and physicochemical data

The meteorological parameters along the cruise tracks were measured using an Automatic Weather Station (AWS) system installed onboard ORV *Sagar Kanya* during the campaigns. The weather data for the Port Blair station, Andaman Islands, India, during 6-7 October 2021 were obtained from the historical archives on 'timeanddate.com' (https://www.timeanddate.com/weather/india/port-blair/), a globally recognized website operated by Time and Date AS, Norway. The air temperature data at Colombo, Sri Lanka, was retrieved from Wunderground meteorological datasets (https://www.wunderground.com/weather/VCCC) at Colombo Ratmalana Airport station, for the period of 27-31 October 2021.

The Oceanographic parameters, such as SST and salinity, were measured using the ship's Thermosalinograph situated under the hull. The depth profiles of temperature and salinity were acquired using Sea-Bird SBE 9 CTD instrument (Sea-Bird Scientific, Bellevue, Washington) at 13 stations in Arabian Sea (SK#374) and 5 stations in Bay of Bengal of Bengal (SK#373). The nutrient $(NO_3^- + NO_2^-)$ concentrations were analyzed in the sea surface samples collected at each station using a nutrient autoanalyzer (SKALAR, The Netherlands).

2.3.2 Marine picophytoplankton data

The picophytoplankton (*Synechococcus* and *Prochlorococcus*) cell abundance was measured in the seawater samples collected at CTD stations using flow-cytometry analysis. The samples were fixed with glutaraldehyde (final concentration: 1%) for 10 min and then stored at -20 °C. Prior to laboratory analysis, the frozen samples were thawed at room temperature under dark conditions. They were then analyzed using a flow cytometer equipped with 405, 488, and 640 nm laser sources (BD FACS Aria Fusion). Each sample was run for a total of 10000 events at a flow rate of ~22 μL min^{-1}. The scatter plots of the relative red fluorescence vs the relative orange fluorescence and relative red fluorescence vs side scatter were used to identify the phytoplankton groups. Different picophytoplankton groups were classified based on their size and the position of optical signals in the scatter plots as per Marie et al. (2000). The fluorescence data were analyzed using BD FACS DIVA (Version 8.0) software.

2.3.3 Air mass back trajectory

The three-dimensional 5-day and 2-day backward air mass trajectories were calculated using the National Oceanic and Atmospheric Administration (NOAA)-HYbrid Single-Particle Lagrangian Integrated Trajectory (HYSPLIT) model (Draxler and Hess, 1998) within the R environment via the 'splitr' package (Iannone, 2024). The trajectories were computed using meteorological data from the National Center for Environmental Prediction (NCEP)-Global Data Analysis System (GDAS1; 1° × 1°), which are accessible through the NOAA Air Resources Laboratory (ARL) GDAS1 archive (https://www.ready.noaa.gov/archives.php).

Although the GDAS (1°×1°) dataset is widely used for back-trajectory analyses, including over regions with complex topography (Draxler & Hess, 1998; de Jonge et al., 2024; Krüger & Quack, 2013; Stein et al., 2015; Crawford et al., 2016; Flood et al., 2025; Sanchez-Barrero et al., 2025; Marandino et al., 2013; Sanchez et al., 2021), its coarse spatial and temporal (3hr)

resolution introduces inherent uncertainties in trajectory calculations. The inability to represent sub-grid scale wind fields, convective processes, and boundary layer dynamics limits the model's capability to resolve mesoscale features such as land-sea breezes, localized turbulence, and complex flow fields over rugged terrain, which influence the accuracy of the derived trajectory. These uncertainties can lead to positional errors in the trajectories, typically ranging from tens to a few hundred kms after 3-5 days of transport (Stohl, 1998; Harris et al., 2005). Therefore, the calculated air-mass trajectories should be interpreted as indicative of broad transport pathway rather than exact air-parcel history. However, the uncertainty is generally smaller over open ocean areas where meteorological gradients are weaker and flow fields are more homogeneous.

Along with the input data resolution, several other components contribute to the estimated total positional error of 15-30% of the distance travelled by air mass (Draxler, 2008). These components include physical error, computational (or numerical) error, measurement error, and forecast error. Physical error arises from the simplified representation of the physical processes in the atmosphere within the model. Computational error is composed of integration and resolution errors, that arise from the necessary use of discrete time stepping to integrate air parcel movement and representing continuous atmospheric variables with gridded data, respectively. Resolution error is particularly important for the vertical position due to limited vertical resolution in the input meteorological fields. Measurement and forecast errors originate from uncertainties in observations, data assimilation procedures, and the numerical weather prediction models used to generate the GDAS meteorological data fields.

2.3.4 Chl-a, SST and wind field distribution maps

The maps of mean Chl-a concentration and SST during the campaigns were generated using 8-day composite data products at a resolution of 4 km × 4 km from the Moderate Resolution Imaging Spectroradiometer (MODIS) onboard Aqua satellite (https://oceancolor.gsfc.nasa.gov/). The

8-day composite data products were preferred over the daily data to reduce the data gaps due to cloud interference. Chl-a data along the track was extracted from the campaign mean files. The near-surface (10 m ASL) wind fields were obtained from ERA-5 single-level hourly reanalysis datasets (0.25° x 0.25°) at the Copernicus Climate Change Service (C3S) Climate Data Store (https://cds.climate.copernicus.eu/).

2.3.5 Tide height data

1. The *in situ* tide gauge data at the Port Blair and Aerial Bay stations in the Andaman Islands during 1–8 October 2021 were obtained from ESSO-Indian National Centre for Ocean Information Services (INCOIS), India.

2. The hourly *in situ* tide height at Colombo station, on the west coast of Sri Lanka, for the campaign period (27 October–2 November 2021) was taken from the University of Hawaii Sea Level Center (UHSLC) tide-gauge data (Caldwell et al., 2015) accessed at: https://uhslc.soest.hawaii.edu/).

3. The simulated tidal elevation data at Trincomalee station, on the east coast of Sri Lanka, for the period of 27–29 October 2021, was obtained from the Finite Element Solution tide model developed in 2014-2016 (FES2014) and altimetry data from AVISO (Archiving, Validation and Interpretation of Satellite Oceanographic data). The model and data can be accessed at: https://www.aviso.altimetry.fr/en/data/products/auxiliary-products/global-tide-fes.html.

2.3.6 Coral data

The global distribution map of coral reefs was taken from the United Nations Environment Programme-World Conservation Monitoring Centre (UNEP-WCMC et al., 2010) at: https://www.unep-wcmc.org/en. The information about the benthic corals in the Andaman Sea and bleaching alert

data were retrieved from the NOAA-National Centers for Environmental Information (NEIC) portal (https://www.ncei.noaa.gov/). The ocean floor bathymetry maps in the Andaman Sea were made using the gridded bathymetric datasets from the General Bathymetric Chart of the Oceans (GEBCO; https://www.gebco.net/), an organization operated by the International Hydrographic Organization (IHO) and the Intergovernmental Oceanographic Commission (IOC) of UNESCO.

2.3.7 Statistical analysis

The statistical significance of regional means of DMS and isoprene was assessed using standard error (SE) (Asher et al., 2017), Welch's t-test (Kerrison et al., 2012) and non-parametric Kruskal-Wallis (K-W) ANOVA (Masdeu-Navarro et al., 2024; Vogt et al., 2008). Normality of data in each region was tested using Q-Q plots and Shapiro-Wilk test.

2.4 Air mass exposure to chlorophyll

The extent of biological exposure of an air mass to the ocean surface transport to the observation site can be determined by integrating chlorophyll concentration along the back-trajectory of the air mass (Arnold et al., 2010; Park et al., 2021). We used 2-day (48 hours) subset of the 5-day back-trajectories calculated using the HYSPLIT model (see section 2.3) along with satellite-derived Chl-a as a proxy for phytoplankton biomass (Siegel et al., 2013) to calculate the sea-surface chlorophyll exposure of air mass (E_a). The chlorophyll exposure is normalized with $e^{-\frac{t}{48}}$ to account for the decrease in the expected biological exposure due to chemical and diffusion loss processes in the MBL.

$$E_a = \frac{\sum_{t=1}^{48} \mathrm{Chl}_{a_t} \cdot e^{-\frac{t}{48}}}{n} \tag{2.5}$$

Where Chl_{at} is the mean chlorophyll-a concentration within 20 km radius around the air mass location at time t in the back-trajectory. The mean

chlorophyll values were extracted from MODIS-Aqua 8-day composite Chl-a data product at 4 km resolution and Chl-a is considered as 0 for the points falling over land. t is the backward tracking time, chosen to be limited to 48 hours as the chemical lifetime of DMS in the atmosphere is 1-2 days (Sharma et al., 1999). n is the number of points in the back-trajectory with valid Chl-a data available. n is the number-count of data points in the back-trajectory with valid Chl_{at} data available, and typically varies between 1-48. Assuming that DMS is well mixed in MBL, the chlorophyll exposure from biologically rich surface waters would be restricted to MBL. Therefore, the trajectory points with air mass height is greater than MBL height were not integrated in the analysis. Air mass height and MBL height were retrieved from HYSPLIT back-trajectory analysis and the corresponding GDAS1 meteorological data, respectively.

2.5 VC-normalized mixing ratios

The ventilation coefficient (VC) has been used to study the effect of dilution as it captures both vertical and horizontal dispersions (e.g., Sahu et al., 2022 and references therein). At a given time/location along the track, the VC_i can be calculated as the product of wind speed (ws_i) and marine boundary layer height (MBLH_i) and is used as a measure to assess the extent of dilution and dispersion of a compound in the MBL.

$$\mathrm{VC}_i = \mathrm{MBLH}_i \times \mathrm{ws}_i \tag{2.6}$$

Where ws_i is the *in situ* wind speed data and MBLH_i is ERA5 hourly re-analysis data (https://cds.climate.copernicus.eu/) over different sampling locations along the track.

Furthermore, the VC-normalized mixing ratio of DMS (DMS_{VC}) and isoprene (Iso_{VC}) accounts for the turbulence and wind-driven variability of these compounds (Sahu et al., 2020 and references therein). The VC normalized mixing ratio (X_{VC}) was used to account for the turbulence and

wind-driven variability (Sahu et al., 2020 and references therein).

$$[\mathrm{X_{VC}}]_i = [\mathrm{X}]_\mathrm{i} \times \frac{\mathrm{VC}_i}{\mathrm{VC_{mean}}} \tag{2.7}$$

Where $[\mathrm{X}]_i$ and VC_i are the measured mixing ratio of the compound (X) and VC during the sampling period (i), respectively. VC_{mean} is the average of VC_i calculated separately for each transect in the Arabian Sea and Bay of Bengal, and for the entire cruise track in the southern coastal waters of the Indian subcontinent.

2.6 Estimation of DMS concentration in surface seawater

The surface seawater DMS concentration, as a function of photosynthetic active radiation (PAR) and total DMSP (DMSPt) in seawater, can be calculated using the following empirical equation (Galí et al., 2018).

$$\log_{10}\mathrm{DMS} = -1.237 + 0.578\log_{10}(\mathrm{DMSP}_t) + 0.018\,\mathrm{PAR} \tag{2.8}$$

PAR was retrieved from MODIS monthly mean (November 2021) data, and DMSP_t concentration was calculated using the following parameterization given by Gali et al. (2015).

$$\log_{10}(\mathrm{DMS}) = -1.237 + 0.578\log_{10}(\mathrm{DMSPt}) + 0.018\,\mathrm{PAR} \tag{2.9a}$$

for $\mathrm{Z}_{eu}/\mathrm{MLD} < 1$ (i.e., mixed waters)

$$\log_{10}(\mathrm{DMSPt}) = 1.74 + 0.81\log_{10}(\mathrm{Chl}) + 0.60\log_{10}\left(\frac{Z_{eu}}{\mathrm{MLD}}\right) \tag{2.9b}$$

for $\mathrm{Z}_{eu}/\mathrm{MLD} > 1$ (i.e., stratified waters)

Where Z_{eu} is the euphotic layer depth (m), MLD is the mixed layer depth (m), Chl is the chlorophyll concentration (mg m^{-3}) in surface water, and SST is the sea surface temperature (°C).

The Chl and Z_{eu} data are derived from the MODIS-A chl-a and diffuse attenuation coefficient (K_{490nm}) products (Mueller and Lange, 1989). SST was measured continuously using a Thermosalinograph, while MLD was estimated using the CTD profiles at different stations during the campaign. MLD was taken as the isothermal depth, defined as the depth at which the difference between local temperature and the reference temperature (at 10 m depth) becomes 0.2°C (de Boyer Montégut et al., 2004).

2.7 DMS flux calculation

In this study, the air-sea fluxes of DMS were estimated using both bottom-up and top-down approaches.

2.7.1 Bottom-up approach

The bottom-up approach is based on thin film model given by Liss and Slater, (1974), assuming that the transfer across the interface is dominated by molecular diffusion,

$$F = k\,\Delta C \tag{2.10}$$

$$F = k_{\mathrm{DMS}}\,(C_w - C_a \cdot \alpha) \tag{2.11}$$

Where, C_w and C_a are the DMS concentrations in bulk water and air, respectively. k_{DMS} is the total transfer velocity of DMS and α is the Ostwald solubility coefficient.

The C_a is measured during the campaign and C_w are estimated using the parameterization schemes given by and Galí et al. (2018; G18), respectively. The details of G18 parameterization schemes are discussed in section 2.5. kDMS is estimated using parameterizations by McGillis et al. (2000) as discussed in this section.

The Ostwald solubility constant was calculated using the following SST (K) -dependent equation (Dacey et al., 1984; Saltzmann et al., 1993).

$$\ln(\alpha) = -10.1794 + 3761.33\left(\frac{1}{\mathrm{SST}}\right) \tag{2.12}$$

$$\frac{1}{k_{\mathrm{DMS}}} = \frac{1}{k_w} + \frac{\alpha}{k_a} \tag{2.13}$$

The transfer rate for water-soluble gases is dominated by the air-side resistance, whereas the water-side resistance dominates for insoluble or sparingly soluble gases (Carpenter et al., 2012). Due to its moderate solubility in seawater, the water-side resistance for DMS becomes dominant, however, at low temperatures or high wind speed conditions air-side resistance becomes important and in known to contribute 5–20% to the total resistance (Bell et al., 2017; McGillis et al., 2000).

The water-side transfer velocity of DMS can be calculated using the wind speed (u) and Schmidt number (Sc) dependent parameterization method (Wanninkhof, 1992).

$$k_w = 0.31 \times u_{10}^2 \left(\frac{\mathrm{Sc_{DMS}}}{660}\right)^{0.5} \tag{2.14}$$

In the above equation, $\mathrm{u_{10}}$ is the wind speed at 10 m above the sea surface, 660 is the Schmidt number of CO_2 in seawater at 25°C. Sc_{DMS} was calculated using the following SST (K)-dependent equation given by Saltzman et al. (1993).

$$\mathrm{Sc_{DMS}} = 2674.0 - 147.12\,T + 3.726\,T^2 - 0.038\,T^3 \tag{2.15}$$

The air-side resistance can be accounted by correcting kw with the atmospheric gradient fraction (γ_a), then the total transfer coefficient can be calculated as follows.

$$k = k_w\,(1 - \gamma_a) \tag{2.16}$$

$$\gamma_a = \left(1 + \frac{k_a}{\alpha k_w}\right) - 1 \tag{2.17}$$

$$k_a = k_{\mathrm{H_2O}} \left(\frac{M}{M_{\mathrm{H_2O}}}\right)^{-1/2} \tag{2.18}$$

$$k_{\mathrm{H_2O}} = 659 \times u_{10} \tag{2.19}$$

Where, M is the molecular weight of the gas and $\mathbf{M_{H_2O}}$ is the molecular weight of water vapor (Kondo, 1975; McGillis et al., 2000).

2.7.2 Top-down approach

The top-down approach uses nighttime built-up in MBL to estimate the air-sea fluxes of trace gases (e.g., Marandino et al., 2007; Warneke and de Gouw, 2001). In our analysis, the VC-normalized DMS mixing ratios is used to account for the relative changes in atmospheric dilution during the build-up periods. assuming a steady state condition between production, loss, and entrainment, the surface DMS flux can be determined using the following boundary layer column budget equation given by Bandy et al. (1996).

$$\mathrm{h}\dot{s}_n = \mathrm{J}_o - \mathrm{J}_h = \mathrm{J}_o - w_e\,\mathrm{s}_o \tag{2.20}$$

DMS flux at the surface,

$$\mathrm{J}_o = h\dot{s}_n + w_e\,\mathrm{s}_o \tag{2.21}$$

Where, h is MBL height, $\dot{s}_n$ is the slope of the nighttime build-up of DMSVC, and J_o and J_h are the DMS fluxes at the surface and MBL top, respectively. J_h is calculated as the product of entrainment velocity (w_e) and DMS mixing ratio (s_o) at the beginning of the night. This method works essentially under the assumption that the sea-to-air flux of DMS is spatially homogenous over the area traversed during the night under consideration.

Chapter 3

Processes controlling atmospheric DMS variability and fluxes over the Arabian Sea

Key takeaways

- Continental outflow and nighttime chemistry influence the DMS variability in the northeast coastal Arabian Sea
- Sharp enhancements in atmospheric DMS concentrations in response to changes in sea surface salinity and other physicochemical parameters
- The estimated air-sea DMS flux of $\sim$11 μmol m^{-2} d^{-1} was $\sim$3 times higher than the values reported two decades ago

3.1 Introduction

The Arabian Sea, a semi-enclosed basin in the northern Indian Ocean, is known as one of the most biologically productive oceanic regions in the world. It has a perennial oxygen minimum zone (Naqvi, 1991; Vidhya et al., 2022) and has been experiencing one of the largest warming trends among tropical oceans (Roxy et al., 2015). Seasonal changes in phytoplankton abundance/composition in the Arabian Sea are driven by nutrient supply through wind-driven coastal and open-ocean upwelling systems during the monsoon season (Sreeush et al., 2018), density-driven convective mixing in winter (Madhupratap et al., 1996), and long-range transport and

deposition of mineral dust (Banerjee & Prasanna Kumar, 2014; Tyagi et al., 2020). The seasonal and spatial patterns of dominant phytoplankton groups also show large variations (Minu et al., 2014). The phytoplankton species composition in open ocean waters of the Arabian Sea is dominated by diatoms and mixotrophic dinoflagellates in winter (Lakshmi et al., 2021), and prochlorophytes and cyanobacteria during intermonsoon season (Bemal & Anil, 2016; Gandhi et al., 2011). In coastal waters, diatoms are the dominant species year-round (Ahmed et al., 2016; Minu et al., 2014), followed by seasonally dependent abundance of dinoflagellates and cyanobacteria in the eastern Arabian Sea (Chowdhury & Biswas, 2023; Padmakumar et al., 2010; Vijayan et al., 2021), and prymnesiophytes in the northwest and western regions (Barlow et al., 1999; Fuller et al., 2006; Parab et al., 2006). Since the last decade, the northern Arabian Sea has been experiencing a radical shift in winter phytoplankton bloom composition from diatoms to dinoflagellates (Goes & Gomes, 2016; Mathew et al., 2021). Therefore, the anticipated increasing emissions of DMS from the Arabian Sea could play a significant role in the global natural sulfur budget.

Hatton et al. (1999) conducted the first study to characterize the distribution of seawater DMS in the western coastal and open ocean regions of the Arabian Sea during August-October 1994. They reported DMS concentrations of 2.5–6.4 nM, with particularly enhanced values after the summer monsoon due to a shift in the phytoplankton community from diatoms to prymnesiophytes. Shenoy et al. (2002) reported DMS surface concentrations of 0.7–8.0 nM during the winter of 1998 and 1999. Shenoy et al. also elucidated the roles of physical forcings such as wind speed and MLD and associated biological processes in DMS variability in the Arabian Sea. Shenoy and Patil (2003) reported much higher DMS concentrations (up to 15.4 nM) in the estuarine waters of the eastern Arabian Sea than in the coastal and offshore waters of Oman (Hatton et al., 1999). The elevated DMS concentrations, typically associated with the blooms of dinoflagellate *Gonyaulax polygramma*, have been reported in the coastal waters of the southeast Arabian Sea (Dias et al., 2023). These previous studies have

mainly focused on the distributions of seawater DMS concentrations, but there is a lack of DMS measurements in the marine air of the Arabian Sea.

In addition to the DMS concentration in seawater, physical and dynamic processes in the lower atmosphere significantly influence the exchange and levels of DMS in the MBL (Gupta et al., 2024). Moreover, though the production of DMS is primarily associated with biological productivity, biomass abundance (Chl-a) supports only ∼15% of the seawater DMS variability (Bell et al., 2021). The seawater DMS concentration is determined largely by the physical factors that drive the spatial and vertical dynamics and associated biogeochemical processes. Therefore, it is important to understand the well-resolved spatial and temporal variability of DMS and its relationships with sea surface and atmospheric parameters to comprehend the factors controlling DMS emissions (Royer et al., 2015). Edtbauer et al. (2020) is the only study that reports atmospheric DMS measurements (100–300 ppt) over the northwest coastal regions of the Arabian Sea during the summer monsoon. The measurements of seawater DMS concentrations and estimates of air-sea fluxes using interpolated climatologies, empirical algorithms, and prognostic biogeochemical models have shown significant discrepancies (Tesdal et al., 2016). Lana et al. (2011; L11) have provided one of the most comprehensive and widely tested global monthly climatologies of surface seawater DMS concentration and flux data. The study (L11) also reveals a large seasonal variability of DMS flux over the Arabian Sea, with the highest value of ∼29 μmol DMS m^{-2} d^{-1} during the summer monsoon and the lowest during the pre-monsoon period (Tegtmeier et al., 2022). Hulswar et al. (2022; H22) have reported an updated global climatology of surface seawater DMS concentration and flux by taking into account the new inclusions in the DMS database over the past decade. An interesting finding of this updated climatology is that the DMS seawater concentrations and air-sea fluxes are less than those estimated in the previous climatology over the northern Indian Ocean (Lana et al., 2011), indicating uncertainties resulting from the lack of DMS measurements. Nonetheless, according to

both L11 and H22 climatologies, the Arabian Sea was found to be among the DMS hotspot regions with fluxes up to 30 μmol DMS m^{-2} d^{-1}. The interpolation of limited *in situ* data with poor spatial and temporal coverage is the biggest source of uncertainty in model estimates of DMS flux over the northern Indian Ocean (Tegtmeier et al., 2022). The basin-scale estimations of DMS emission can be improved by spatiotemporally resolved measurements of DMS variability and its relationships with key biological and physical variables (Royer et al., 2015).

In this chapter, we have analyzed the shipborne measurements of atmospheric DMS concentration conducted over the Arabian Sea to understand the role of emissions and dominant oceanic and meteorological factors controlling its variability. The high time-resolved continuous data were analyzed to characterize the diurnal and day-to-day variability features observed in the DMS concentrations. We have investigated the influences of local atmospheric chemistry and transport of different air masses along different transects covering coastal and open ocean regions. The supporting meteorological and several sea surface variables have been used to determine the direct or indirect links between the atmospheric DMS concentration and air-sea exchange processes. To the best of our knowledge, this study presents the first measurement of atmospheric DMS in the eastern coastal and open ocean regions of the Arabian Sea.

3.2 Ship campaign

A shipborne experimental campaign onboard ORV *Sagar Kanya* (SK#374) in the Arabian Sea was conducted during 3–23 November 2021. The Arabian Sea is the western basin of the northern Indian Ocean, which lies approximately between latitudes of 0–25°N and longitudes of 50–80°E with a surface area of ~3.8×106 km^2. It is bordered by the Arabian Peninsula in the north, the Western Ghats (forested hills) of India in the east, the deserts of Africa in the west, and the Southern Ocean in the south. The cruise started from Kochi port (9.57°N; 76.16°E), India on 3 November 2021

and sailed southwest towards the equatorial Indian Ocean until 4°N-68°E. And then proceeded northward between 4-18°N along 68°E in the open ocean waters of the central Arabian Sea, and finally moved east/southeast and reached Goa port (15.41°N, 73.80°E), India on 23 November 2021.

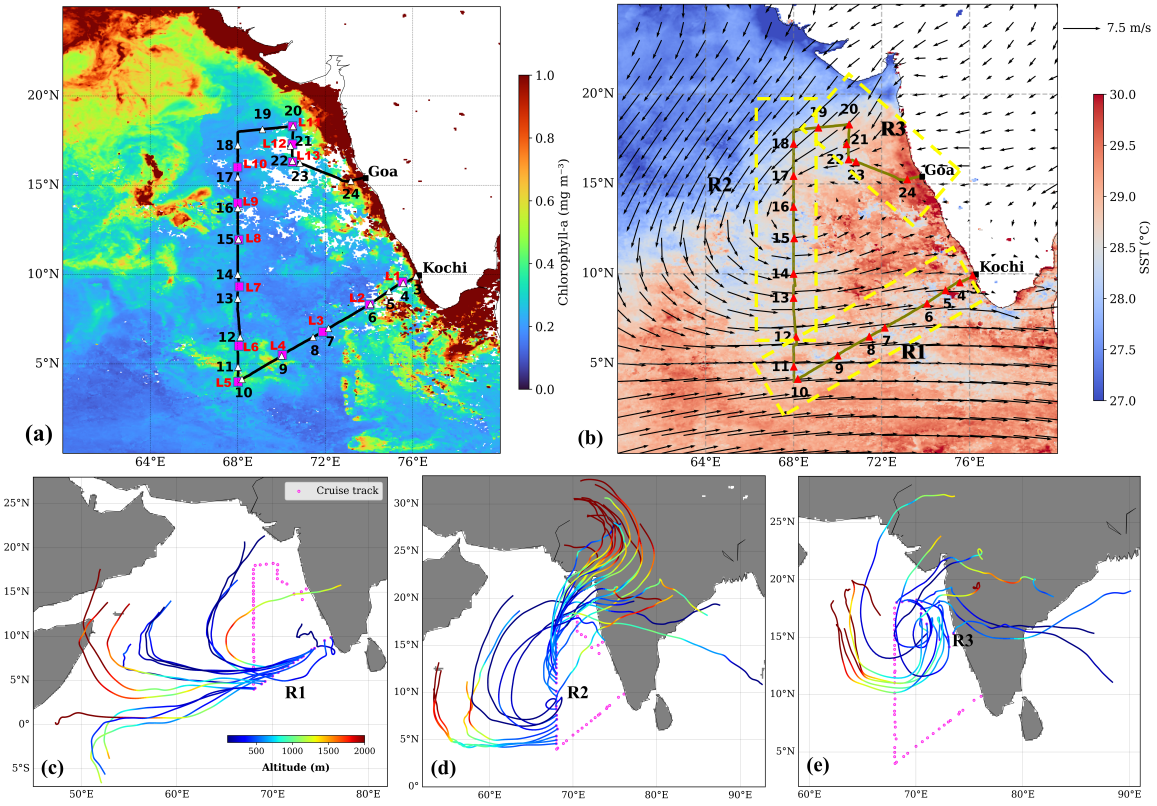

Figure 3.1: *Composite maps of (a) Chl-a (mg m-3) and (b) SST (°C), retrieved from the MODIS-Aqua for the cruise period (1-24 November 2021). The campaign average near-surface wind vector field (m s^{-1}) overlaid on the SST map was obtained from the ERA-5 reanalysis data. The numbers along the cruise track represent the reference date (day of November 2021 at 00 hr; triangles). The oceanographic sampling locations are shown in (a) (pink squares; annotated in red). The bottom panels (c-e) are the 5-day backward air mass trajectories over the R1, R2, and R3 regions, respectively.*

Overall, the cruise track covered the northern coastal, and southeast and central open ocean regions of the Arabian Sea. As shown in **Figure 3.1b**, the data measured during the campaign are divided into three different regions of R1 (3–11 November), R2 (12–18 November), and R3 (19–23 November), representing the southeast, central, and coastal Arabian Sea,

respectively. These regions can be characterized by distinct hydrographic and biogeochemical features, marked by noticeable differences in biological productivity and anthropogenic/terrestrial influences (**Figure 3.1**).

3.3 Results and Discussion

3.3.1 Environmental and hydrographic conditions during the campaign

The satellite-derived SST and Chl-a distributions exhibit significant spatial variability, with northwest-to-southeast increasing and decreasing trends, respectively (**Figure 3.1a,b**). During the campaign period, daily *in situ* measurements of SST, salinity, and wind speed varied in the ranges of 28.5–29.5°C, 34.5–36.5, and 3–11 m s^{-1}, respectively. However, with some short-term variations, the SST data shows a north-south increasing latitudinal trend (**Figure 3.1b**) and average values of 29.38±0.18, 29.04±0.15, 28.90±0.46 °C in the R1, R2, and R3 regions, respectively (**Table 3.1**).

Table 3.1: *Region and campaign mean (±standard deviation) of DMS mixing ratio, meteorological and hydrographic parameters over the Arabian Sea during 4–23 November 2021.*

Parameters	**R1**	**R2**	**R3**	**All data**
DMS (ppt)[†]	99±87 [4]	62±53 [3]	116±120 [7]	91±87 [3]
Wind speed (m s^{-1})	7.61±2.57	6.99±2.5	3.92±1.87	6.76±2.88
SST (°C)	29.38±0.18	29.04±0.15	28.90±0.46	29.13±0.34
Salinity	35.64±0.67	36.32±0.07	34.96±0.37	35.71±0.67
Solar flux (W/m^2)	183±267	144±225	141±207	158±239
Pressure (mb)	1008.4±1.3	1007.3±1.6	1007.6±2.7	1007.6±2.0
Air temperature(°C)	27.29±0.91	27.35±0.37	27.65±0.91	27.24±0.92
Relative humidity(%)	76.67±5.36	74.04±4.95	79.32±5.25	77.38±5.84
Chl-a (mg m^{-3})	0.46±0.53	0.21±0.03	0.37±0.21	0.35±0.39

[†]Standard error [SE]

The distribution of Chl-a concentration shows significant spatial heterogeneity, with highly enhanced concentrations (>1 mg m^{-3}) in western coastal waters of India and around Maldives islands (0–5°N, 73°E), indicating higher abundance in phytoplankton biomass than in the open ocean waters of the central Arabian Sea. The coastal primary productivity is mainly influenced by the input of nutrients from terrestrial sources. In the open ocean waters, the Chl-a data shows higher concentrations in region R1 (9–11 November) than in the central Arabian Sea region R2 (12–15 November). Transects also covered concentrated patches of Chl-a in the coastal waters of R1 (southeast Arabian Sea) and R3 (northeast Arabian Sea). The regions with elevated Chl-a concentrations (>1 mg m^{-3}) in offshore waters of the southern Arabian Sea (4–10°N) coincide with the colder SST patches. The high Chl-a in the northwest Arabian Sea is driven by winter convective mixing (Keerthi et al., 2017). As the post-monsoon season transitions to winter (northeast monsoon), weaker surface wind circulation changes to strong northeast trade winds over the Arabian Sea. The transport of cold and dry air masses from the northern continental regions causes evaporative cooling (Thoppil et al., 2022), leading to higher salinity in the surface waters of the northeast Arabian Sea during early November. The denser surface water sinks and brings the nutrient-rich subsurface water to the surface, triggering intense blooms of diatoms and dinoflagellates (Garrison et al., 2000; Gomes et al., 2016), which proliferate towards the open ocean Arabian Sea as winter progresses. During early winter, picophytoplankton (*Prochlorococcus* and *Synechococcus*) contribute significantly to the plankton biomass and productivity in the oligotrophic waters of the central Arabian Sea (Garrison et al., 2000). As shown in **Figure 3.1a** and **b**, the high SST and low Chl-a values at lower latitudes (0–10°N) were associated with warm and stratified surface ocean conditions, which resulted in reduced nutrient supply into the euphotic zone and hence lesser productivity (Kumar et al., 2000).

The Arabian Sea is known for high surface salinity (>35) due to the negligible freshwater inputs and higher evaporation exceeding annual mean

precipitation (Rao and Sivakumar, 2003). The *in situ* measurements of salinity in R1 (~32.2-36.4) and R3 (34.7-36.5) showed more pronounced variations than in the central Arabian Sea (35.7–36.4), despite large latitudinal coverage of R2 (**Figure 3.1b**). The salinity sharply decreased during the transition from the open ocean to coastal waters due to riverine freshwater input. However, the lower salinity in the open ocean at lower latitudes (5–8°N) could be due to the advection of low salinity waters from the eastern tropical Indian Ocean (Zhu et al., 2022). The wind speed data showed large variations (0.5–15.5 m s^{-1}) across the different regions. Episodes of strong winds (>10 m s^{-1}) during 6-12 November were associated with scattered rainstorms. The wind flow was predominantly from the NW, north, and east/SW directions during the measurements along the R1, R2, and R3 transects, respectively. As shown in **Figure 3.1b**, the prevailing stronger westerly winds over the southern Arabian Sea (5–10° N) were part of the Indian Ocean Equatorial Westerlies (IEW) (Hastenrath et al., 1993). The campaign means of air temperature (T_a) and relative humidity (RH) were 27.2±0.9°C and 77.4±5.8%, respectively. Levels of T_a and RH showed local time dependence with more pronounced diurnal variations over coastal regions than over the open ocean. However, some periods of short-scale rapid fluctuations in Ta and RH were also noted, particularly during the strong winds. During 13-17 November over R2, the analysis of back-trajectories indicates the transport of continental air masses originated from the Indo-Gangetic plain (IGP) (**Figure 3.1d**). The transport of maritime air masses from the productive western Arabian Sea prevailed during 5-12 November over parts of R1 and R2.

3.3.2 Time series variation of atmospheric DMS concentration

The time series of DMS mixing ratio shows large variations in the ranges of 22–415, 20–382, and 30–709 ppt over the R1, R2, and R3 regions, respectively (**Figure 3.2a**). The difference in mean DMS observed over R1, R2, and R3 were statistically significant (χ^2= 90.08, K-W p<0.0001

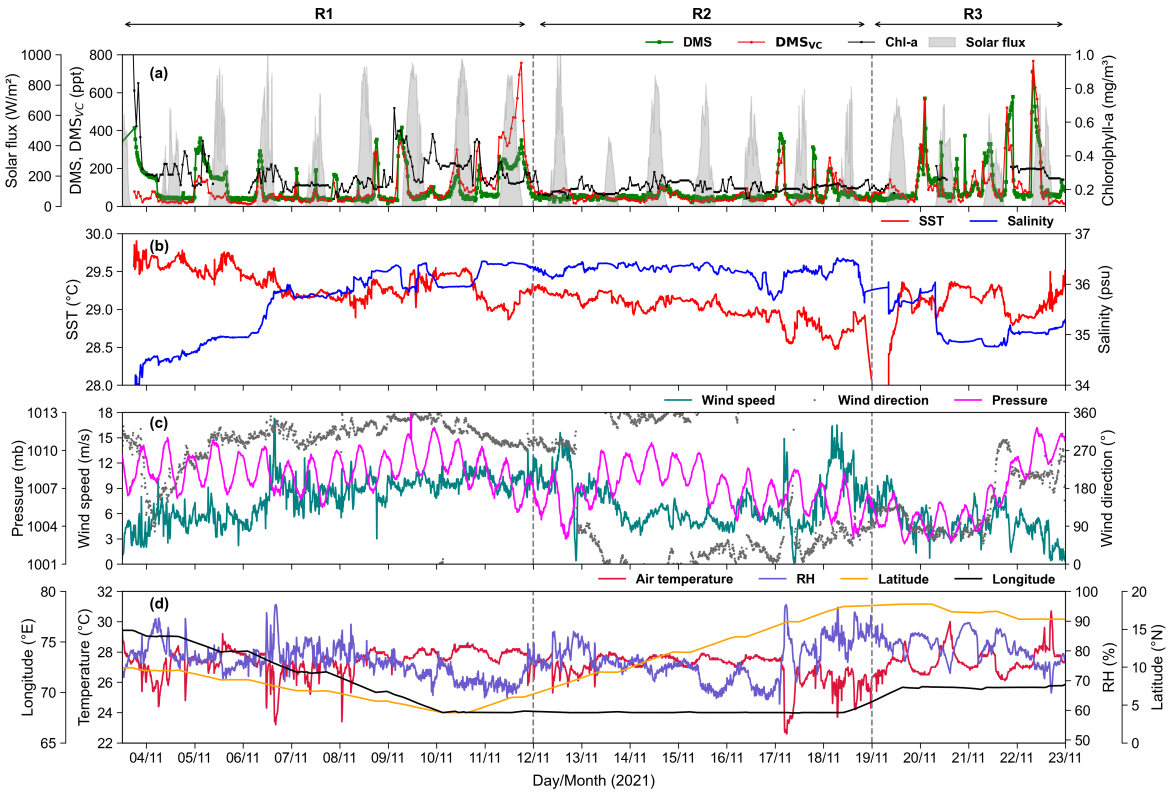

Figure 3.2: *Time series variations of (a) DMS mixing ratio, DMS_{VC}, solar flux, and MODIS-A Chl-a concentration, (b) SST and salinity, and (c, d) several meteorological parameters along the ship track. The dashed vertical lines separate the track into three transects of R1, R2, and R3, as discussed in section 2.1.*

[α=0.05]). Measurements over R1 and R3 show higher DMS levels and large diurnal and day-to-day variations than over R2. The background values of DMS, calculated as the 5th percentile (Apte et al., 2017), were almost the same over central (R2; ~34.2 ppt) and southeast (R1; ~33.6 ppt) Arabian Sea. However, a slightly higher background concentration of ~38.6 ppt was estimated for the northeast coastal region (R3). The DMS mixing ratios are higher in regions with higher satellite-derived concentrations of Chl-a in surface seawater of R1 (0.14–1.2 mg m^{-3}) and R3 (0.18–0.34 mg m^{-3}) than in R2 (0.15–0.31 mg m^{-3}). A strong positive correlation between the daily mean DMS mixing ratio and log_2-transformed Chl-a concentration (Pearson's r = 0.72; (**Figure 3.3**) indicates the significant role of phytoplankton biomass among factors driving oceanic DMS emissions to the atmosphere. The relationship between DMS and Chl-a over the Arabian

Sea is parametrized as function: DMS = 52 $\times \log_2(\text{Chl}_a)$ + 189.

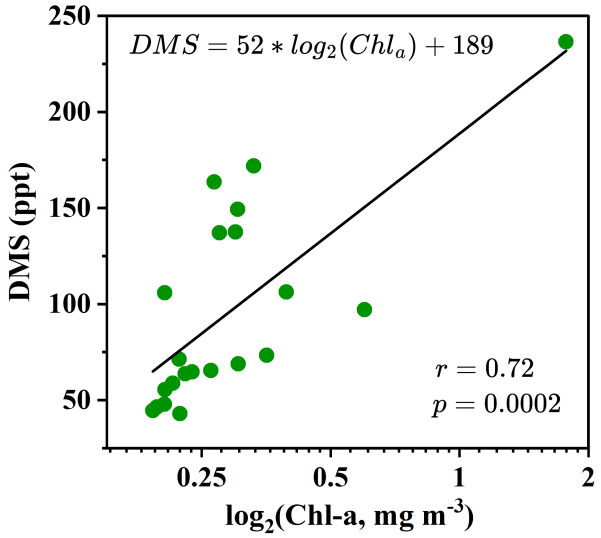

Figure 3.3: *Linear regression fit between daily means of in situ DMS mixing ratio and log_2-transformed satellite-derived Chl-a concentration in the Arabian Sea observed during 3-23 November 2021.*

Regardless of the time of day, in many instances, the measurements of elevated DMS peaks were typically associated with lower salinities or sudden changes in salinity levels. The impact of salinity fluctuations is particularly evident during 17-18 November, when sharp nighttime DMS peaks coincided with sudden dips in salinity in otherwise steady salinity in R2. On 11 November, a broad DMS peak (345 ppt) with a simultaneous increase in salinity (0.6) and decrease in SST (0.5°C) reflects the influence of the upwelling of DMS-rich sub-surface waters. The subsurface waters are more saline than surface waters in the central Arabian Sea (Hareesh Kumar & Mathew, 1997). Thus, a localized drop in SST accompanied by an increase in salinity may indicate vertical mixing in the surface layer and upwelling of deeper surface as well as sub-surface waters that are nutrient-rich, cooler, and therefore more productive. Upwelling enhances the surface concentration of DMS by bringing the nutrient-rich waters to the surface and promoting phytoplankton growth, and by exposing the sub-surface DMS pool to the surface for the sea-air exchange (e.g., Zindler et al., 2012). The amplified release of DMSP due to thermal and osmotic

stresses on the phytoplankton could also be an important factor for the higher DMS concentrations (Kettles et al., 2014; Speeckaert et al., 2019). The DMS levels were significantly higher (250 ppt) in the afternoon of 11 November compared to the preceding 3 days (~50 ppt) with similar solar flux, indicating increased DMS emissions during upwelling events. Similar occurrences of elevated DMS concentrations associated with SST and salinity fluctuations have been attributed to upwelling systems over the western coastal Arabian Sea (Warneke & de Gouw, 2001) and subpolar coastal waters (Herr et al., 2019). However, the DMS mixing ratio and salinity do not show any direct correlation, as DMS peaks were measured over both low- and high-saline surface waters (Figure 3.2). This could mainly be attributed to heterogeneity in biogeochemical properties like phytoplankton abundance and taxonomy, resulting in variability in DMS source strength along the ship track.

The wind speed is an important parameter controlling the air-sea exchange and transport processes in the MBL (Wanninkhof et al., 2009). However, except for a few cases mostly in central Arabian Sea, the relative changes in DMS mixing ratios do not show any direct relation with the wind speed within or among the different biogeochemical regions. The wind speeds in the central Arabian Sea (R2) were low to moderate (5-10 m s^{-1}). The sharp enhancements of DMS during 17-18 November were associated with rapid fluctuation in meteorological parameters and a drop in salinity. In contrast to R2, multiple DMS peaks over the northeast coastal region (R3) were associated with light winds (<6 m s^{-1}). However, this region also experienced higher T_a (27–31°C), partly cloudy conditions, lower salinity, higher SST, and elevated Chl-a concentrations. Stagnant wind conditions during the elevated DMS levels with frequent peaks/spikes in R3 could be attributed to less efficient dispersion of DMS and stronger source concentrations, leading to sustained higher levels despite the chemical loss processes. Interestingly, DMS peaks were more pronounced in SW maritime winds than in the east and NE continental winds. Therefore, in addition to local air-sea fluxes, the transport of marine air masses originating from

nearby coastal waters could have contributed to the elevated levels of DMS in R3 due to the prevailing low-pressure system. Nonetheless, the direct impact of wind speed-induced regulation of DMS exchange is not seen in the observed atmospheric DMS levels along the R1 and R3 regions. Apart from the role of horizontal advection of DMS enriched air masses, another crucial factor could be the small-scale changes in physical and biogeochemical properties in oceanic mixed layer determining the DMS source strength. Marandino et al. (2009) and Yang et al. (2011) have also reported a lack of noticeable wind speed dependence of DMS fluxes in the tropical Pacific and Southern Ocean (45-60° S), respectively, concluding the complex relationship of DMS transfer with wind speed that could be controlled by oceanic physical properties such as SST.

DMS_{VC} has been used to account for turbulence and wind-driven variability (Sahu et al., 2022 and references therein). Except for a few instances, the time series variability of DMS_{VC} does not show significant differences from that of DMS variability (**Figure 3.2a**). Therefore, the similarity in DMS and DMS_{VC} trends suggests that oceanic factors drove the variability features, particularly the DMS enhancements. For instance, on the afternoon of 11 November, highly elevated levels of DMS_{VC} (300-800 ppt) were associated with a local upwelling event and a strong salinity gradient despite the high MBLH and photochemical loss. In region R3, the differences ($\sim$100–200 ppt) between DMS and DMS_{VC} during the morning of 19 and 21 November were associated with significant changes in oceanic parameters and VC (**Figure 3.2**), respectively. Except during 10-12 November, all the enhancements in DMS_{VC} were slightly higher than those observed in the DMS mixing ratio. In summary, the analysis clearly shows that the dilution of DMS in the MBL does not alter the variability, particularly the features attributed to the changes in oceanic biogeochemical conditions.

The analysis of 5-day backward trajectories revealed that air masses advected over R1 originated over the highly productive western Arabian Sea, off the Somalia coast. The bloom of phytoplankton off the coast of Somalia starts in mid-November and peaks during January–February

(Liao et al., 2017). Whereas, local air masses that originated from the shelf regions of the eastern Arabian Sea (EAS) prevailed over R3. It is important to note that the northern part of the EAS is influenced by the convective mixing leading to phytoplankton blooms in winter (Madhupratap et al., 1996). In particular, widespread blooms of dinoflagellate, green *Noctiluca*, have been reported in the north-EAS regions during the winter season. In contrast to the R1 and R3 regions, the back trajectories over R2 were influenced by the long-range transport of continental air masses, which resulted in a drastic decline of DMS in the MBL. DMS levels are clearly enhanced for air masses that travelled over the oceanic regions and dropped considerably in samples of air masses that stayed predominantly in the continental and free tropospheric regions (see **Figure 3.1c-e**).

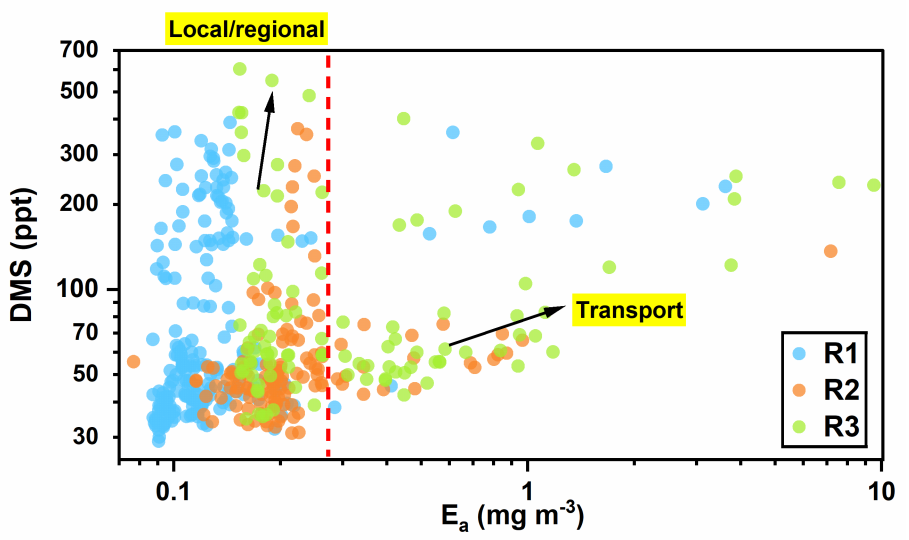

Figure 3.4: *Log-log scatter plot of DMS mixing ratio versus chlorophyll exposure of air masses (E_a) along 48-hour back-trajectories. A red vertical dashed line broadly distinguishes the measurements affected by predominant contributions from local sources (left) and transport from distant sources (right).*

To quantify the contributions from long-range transport of biogenic DMS in the measured air mass, we calculated the chlorophyll exposure of air masses (E_a) along 2-day back-trajectory (**Eq. 2.5**). E_a could be a useful parameter for quantitative understanding of the variations in atmospheric concentration of DMS with the exposure of the air masses to the phyto-

plankton at the ocean surface before reaching the measurement location, while accounting for the loss and free tropospheric intrusions. The scatter plot between DMS and E_a (**Figure 3.4**) shows an overall increase in DMS with E_a. The DMS values diverge at different slope rates for E_a <0.18 and >0.18 mg m^{-3}, suggesting that the enhancements in DMS from local or regional sources are more prominent than from transported air masses. About 12% of the measurements with enhancements (>100 ppt) in DMS levels correspond to the measurements of air masses with high E_a (>0.18 mg m^{-3}). Greater transport-based DMS enhancements are observed in R1 and R3, than in the R2 region. About 60% and 70% of air masses with higher E_a (>0.18 mg m^{-3}) were measured in the regions R1 and R3, respectively. E_a values were lowest for the air masses measured along R2, mainly due to continental transport on most days of measurements in the central Arabian Sea (**Figure 3.1d**).

The DMS mixing ratios measured in the MBL of the southeast and coastal Arabian Sea (22.5–709 ppt) are higher than those reported over other tropical oceanic regions. The DMS mixing ratios of up to 300 ppt were reported in the western tropical Indian Ocean during the Asian summer monsoon (Zavarsky et al., 2018b). Andreae et al. (1993) reported DMS mixing ratios between 20–100 ppt during July-September, and Williams et al. (2004) reported a mean value of 50 ppt during October-November over the tropical Atlantic Ocean. The DMS mixing ratio reported over the tropical Pacific Ocean ranged between 2–220 ppt in October (Marandino et al., 2013) and 22–157 ppt in August-September (Simpson et al., 2014). However, the mixing ratios over the central Arabian Sea (62$\pm$53 ppt) are close to the values reported over other oligotrophic open ocean regions (Marandino et al., 2013 and references therein).

3.3.3 Diurnal variation of atmospheric DMS concentration

We investigated the periodicity observed on shorter time scales in the time series of DMS mixing ratio to characterize its local time dependence in the MBL. The spatial variability in seawater DMS is considered to be largely

dependent on the overall Chl-a concentration and typical biological characteristics, such as phytoplankton productivity and community composition, within the three oceanic regions of R1, R2 and R3. In the region R1, the DMS mixing ratio shows a clear diurnal cycle with two broad peaks during the morning and evening, with hourly median values in the range of 41-140 ppt. The diurnal cycle in region R2 shows lesser variability (38-56 ppt) compared to those in R1 and R3 (Figure 3.5), which is consistent with a study by Royer et al. (2015) reporting lesser DMS variability in oligotrophic waters than in the productive regions.

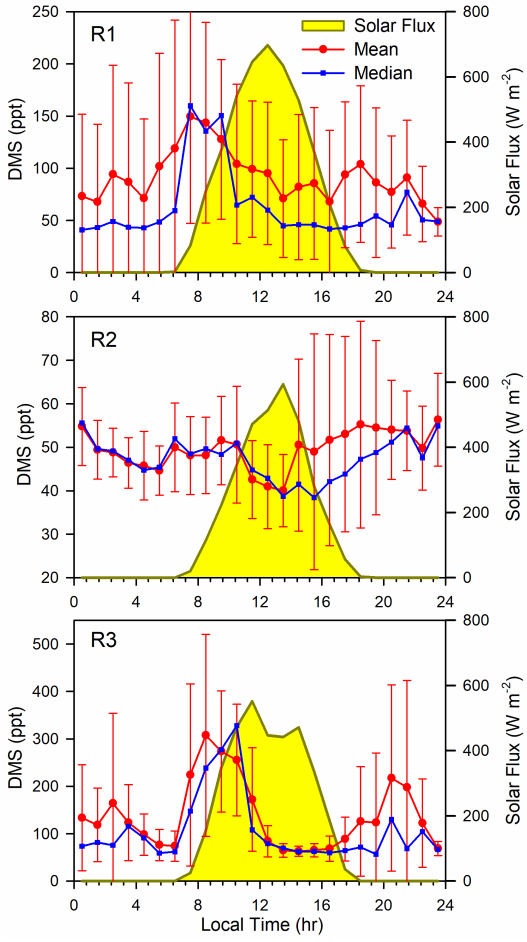

Figure 3.5: *Average (±1σ) and median diurnal variations of the DMS mixing ratio and mean solar flux measured over the three different regions of the Arabian Sea during 3-23 November 2021.*

The distinct diurnal variation of DMS in region R2 characterizes the measurements under lesser anthropogenic influences and lower oceanic productivity. Several studies have reported similar diurnal cycles of DMS, with

late afternoon minimum and early morning maximum, in cleaner marine air (e.g., de Bruyn et al., 2002; Lawson et al., 2020; Marandino et al., 2007). The daytime decrease is consistent with those observed in other regions, explained by the DMS+OH oxidation reaction. The increase in median DMS concentrations after sunset and higher levels during nighttime is attributed to lower air-sea exchange due to weaker source, and reduced NO_3 oxidation compared to R1 and R3. The higher mean mixing ratios in the evening hours and deviation from the median pattern in the diurnal pattern over R2 (**Figure 3.5b**) could be due to occurrences of anomalous DMS spikes induced by local meteorological disturbances during 17–18 November. The diurnal amplitude of DMS (maximum/minimum ratio of $\sim$1.5) in the central Arabian Sea was within the range (1.2–1.7) reported for the remote marine atmosphere (de Bruyn et al., 2002; Lawson et al., 2020a; Sciare et al., 2000). For example, the diurnal measurements at Cape Grim baseline (40–70 ppt) (Ayers and Gillett, 2000), over the tropical Indian Ocean (25–60 ppt) (Warneke and de Gouw, 2001), and at Kiritimati in the tropical Pacific (120-–200 ppt) (Bandy et al., 1996) show similar patterns to that over the central Arabian Sea.

In addition to atmospheric processes, the DMS concentrations in seawater could be a more important factor in controlling its diurnal variability over R2 than in R1 and R3. The central Arabian Sea is known to be oligotrophic during fall-intermonsoon (October–November) due to strong surface stratification (Kumar et al., 2000). The nutrient limitation facilitates the growth of marine cyanobacteria such as *Trichodesmium*, *Synechococcus*, and *Prochlorococcus* in surface waters of the central Arabian Sea. However, cyanobacteria are low DMSP-producing phytoplankton (McParland & Levine, 2019), resulting in low sea surface DMS concentrations (Stefels et al., 2007) and reduced air-sea exchanges, particularly under low wind conditions. However, previous studies have shown that, depending on solar radiation, the DMS diurnal cycle in nutrient-limited water is controlled by microbial production and consumption (Royer et al., 2016; Toole & Siegel, 2004). Royer et al. (2016) reported that the production of DMS in surface

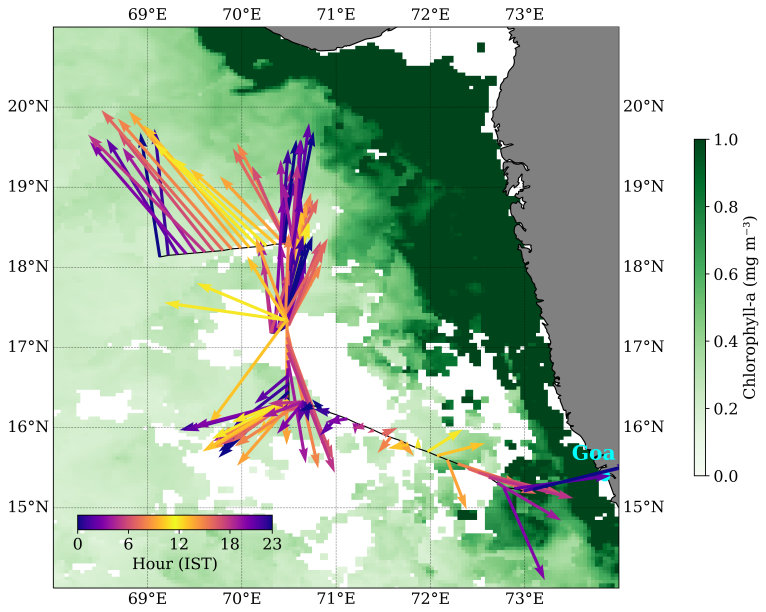

Figure 3.6: *Wind direction along the cruise track in the coastal region of the northeast Arabian Sea (19–23 November; R3) overlaid on the campaign composite MODIS-A Chl-a map. The color of the arrow indicates the time (hr) of the day, respectively.*

waters increases with solar radiation at dawn and reaches its maximum value at dusk. The DMS diurnal variations over the productive regions of R1 and R3 show nearly similar features. In polluted marine air of R3, the DMS mixing ratio shows stronger variability (hourly median: 57–328 ppt) with two sharp peaks, the first after sunrise and the second at sunset. However, compared to region R1, the levels of DMS during the early morning hours were much lower than the diurnal maximum value, resulting in a more pronounced diurnal variation in region R3. In the near-coastal region, the nighttime DMS minimum can be attributed to dilution due to the land breeze circulation (**Figure 3.6**) and $DMS + NO_3$ reaction (Bardouki et al., 2003; Osthoff et al., 2009). The NO_3 levels are typically high in coastal MBL due to proximity to the land/anthropogenic activities (Stark et al., 2005). Higher levels of NO_3 precursors (NO_X and O_3) have been reported in the coastal MBL (e.g., Debaje & Johnson Jeyakumar, 2011; Jia et al., 2017; Lal et al., 2006; Tadic et al., 2020) due to the ship exhausts, outflow of continental pollutants, secondary chemical production, etc. The higher NO_3 concentrations can result in an increased nighttime DMS loss in the coastal

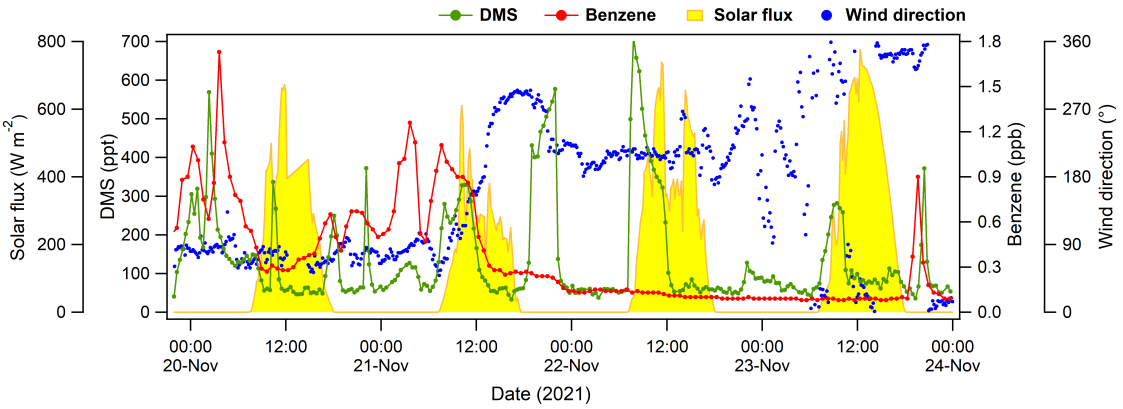

Figure 3.7: *Time series of DMS and benzene mixing ratios elucidating the effect of polluted continental and cleaner marine air masses in the northeast coastal region of the Arabian Sea during 20-23 November 2021.*

MBL than over the open ocean. Marandino et al. (2007) have reported similar diurnal variation of atmospheric DMS in the equatorial upwelling region of the tropical Pacific Ocean, with an increase in the evening and a sharp decrease just before midnight, suggesting oxidation loss by NO_3 radicals.

However, in this study, the nighttime DMS mixing ratio over R3 exhibited higher fluctuations when winds were from the land, compared to the maritime winds (**Figure 3.7**). To investigate this short-term variability in nighttime DMS measurements, we have used the benzene mixing ratio data measured during the present campaign. Benzene is a relatively long-lived VOC (lifetime ~2 weeks) emitted mainly from traffic and industrial sources, and has been used as a tracer to identify the air masses influenced by anthropogenic sources in the coastal marine atmosphere (Bourtsoukidis et al., 2019; de Gouw et al., 2005). The OH reaction rates of DMS (6.5×10^{-12} $\mathrm{cm^3\,molecule^{-1}\,s^{-1}}$) and benzene ($1.2 \times 10^{-12}$ $\mathrm{cm^3\,molecule^{-1}\,s^{-1}}$) are of a similar order. But the NO_3 rate constant (k_{NO_3}) of benzene ($\sim 10^{-17}$ $\mathrm{cm^3\,molecule^{-1}\,s^{-1}}$) is several orders of magnitude lower than that of DMS ($\sim 9.8 \times 10^{-13}$ $\mathrm{cm^3\,molecule^{-1}\,s^{-1}}$) (Atkinson et al., 1988; Atkinson & Arey, 2003). Therefore, the levels of benzene are expected to show a lesser response to NO_3 chemistry than DMS, and its nighttime variability indicates the extent of the continental influence. The multiple sharp peaks of

DMS observed during the nights of 20-21 November were observed during highly elevated benzene mixing ratios and continental winds. Interestingly, during these nights, the increasing (decreased) DMS mixing ratios coincide with the decreasing (increasing) benzene mixing ratios. These sharp DMS enhancements could be due to the rapid consumption of NO_3 by more reactive VOCs, such as alkenes and terpenoids (with higher $k_{NO_3} \sim 10^{-11}$–10^{-13} cm^3 $molecule^{-1}$ s^{-1}) present at larger concentrations in continental outflow. In contrast, during 22-23 November, when the winds were predominantly from the oceanic regions and benzene concentrations were much lower (0.1-0.3 ppb), a clear diurnal pattern was observed with a smoother nighttime decline in DMS associated with DMS-NO_3 chemistry. However, irrespective of the nighttime variability pattern, the higher magnitudes of the DMS peaks measured in maritime air masses over R3 than those in polluted air masses establish the role of increased NO_3 chemistry under the influence of continental air masses.

The nighttime DMS chemistry could significantly affect the SOA formation, particularly over the coastal regions influenced by terrestrial/anthropogenic outflow. The interference of continental air masses in the NO_3 oxidation pathway of DMS can also alter the expected secondary sulfate yield as well as aerosol composition (Chen & Jang, 2012). The changes in aerosol composition can influence CCN efficiency at a given supersaturation by modifying the particle hygroscopicity and size distribution (Sun & Ariya, 2006), thereby modulating cloud droplet concentrations (Xu et al., 2023). Subsequently, changes in aerosol composition from the modulation of DMS-NO_3 chemistry in MBL can affect the cloud radiative properties and regional climate dynamics (Manavi et al., 2025) and add to the uncertainties in predictions of DMS-derived aerosols over the Arabian Sea. Thus, it is essential to incorporate the airmass interactions in the secondary aerosol formation over the coastal waters of the Arabian Sea, particularly to account for the interference of highly reactive species, present in continental outflow, in the nighttime DMS oxidation pathways.

3.3.4 Effect of salinity changes on DMS

Among the factors, salinity is known to be extensively regulated by the DMS/DMSP production and its accumulation in seawater (Stefels et al., 2007). Several studies have reported a multi-fold increase in seawater DMS concentrations with the increase of salinity, especially in subpolar and polar waters (Herr et al., 2019; Park et al., 2019). To assess the effect of salinity on DMS production influencing its variability in marine atmosphere, we have calculated temporal change in salinity and examined its relation with the atmospheric DMS variability. The temporal change in salinity was calculated as a time derivative over a 2-hour interval using salinity data measured at adjacent points (index ± 1) at each hour.

$$\dot{S} = \frac{\partial S}{\partial t} = \frac{\Delta S}{\Delta t} = \frac{S_{i+1} - S_{i-1}}{2} \tag{3.1}$$

Where $\dot{S}$ is the rate of change in salinity (hr^{-1}) and i is the index number of hour under consideration. The hourly diurnal matrices of the DMS mixing ratio and salinity gradient are shown in **Figure 3.8**. The values of $\dot{S}$ were between -0.3 to 0.2 hr^{-1}, showing higher salinity gradient in the R1 and R3 regions. In most cases, the enhancements in the DMS mixing ratio coincided or followed the sharp changes in salinity. For instance, on 9 November, a rise in DMS can be observed with onset of a dip in salinity at a gradient of -0.1 hr^{-1} at 05 hr and intensified to 360 ppt coinciding with peak gradient of -0.15 hr^{-1} at 06 hr. Other prominent DMS features on 6, 20 and 21 November were associated with the salinity gradients in the range of +0.05 to +0.17 hr^{-1}. Although the enhancements in DMS do not show a clear dependence on the magnitude or direction (increase or decrease) of the salinity gradient, the DMS peaks tend to coincide with positive salinity gradients more often than negative gradients. Salinity and DMS levels do not show a direct relation (as discussed in **section 3.3.2**), however, the present analysis indicates a possible link between short-term salinity fluctuations and variability of DMS flux into the MBL. Shenoy et al. (2002) have reported high seawater DMS concentrations associated with

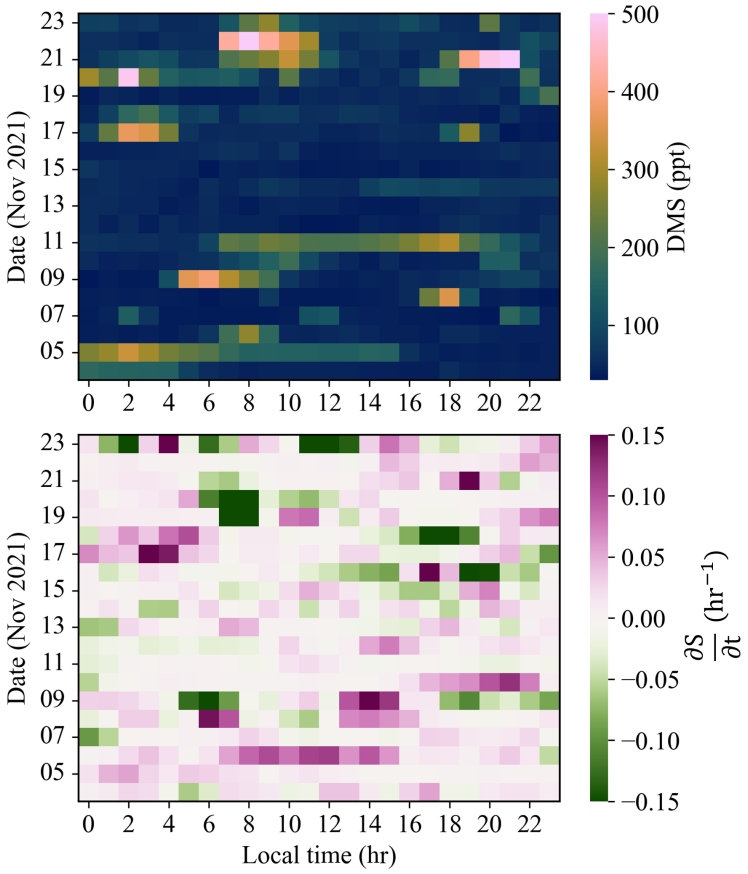

Figure 3.8: *Diurnal matrices of hourly DMS mixing ratio (top) and sea surface salinity (S) gradient (bottom) of the measurements over the Arabian Sea during 4–23 November 2021.*

the salinity front in the tropical Indian Ocean. Niki et al. (2007) reported rapid release of DMSP by a dinoflagellate species on salinity down-shock, and subsequent conversion of DMSP to DMS by the same species.

Salinity shocks can lead to stress-induced enhancements in the biological production of DMSP in seawater. DMSP, the precursor of DMS in seawater, is classified as a compatible solute as it serves physiological functions without disrupting cellular processes in phytoplankton (Keller & Korjeff-Bellows, 1996; Stefels, 2000). Salinity fluctuations can cause physiological stress in marine phytoplankton, triggering increased intracellular production and higher rates of DMSP release in phytoplankton during osmotic adjustments (Krist, 1996). Though salinity shocks can induce osmotic stress, the change in intracellular DMSP and its release also depend on phytoplankton species, nutrient availability, and microbial interactions (Burdett

et al., 2015; Gwinn et al., 2019; Kettles et al., 2014; Liang et al., 2023). In addition to the oxidative trigger, the salinity changes associated with nutrient-rich upwelling events can also enhance DMS flux by increasing surface biomass production through upwelled nutrients and/or facilitating the transport of DMS from subsurface/deeper surface to the interfacial surface waters. Deeper surface waters can have accumulated DMS from biological activity due to its slower loss to the atmosphere via air-sea exchange (Liang et al., 2023; Zindler et al., 2012). Upwelling events are triggered by strong winds and characterized by cooler SST and T_a (Aguirre et al., 2021).

In (**Figure 3.9**), the drastic changes in salinity and SST were seen to occur around several DMS peaks. The increased levels of DMS on 11 and 17-18 November in the central Arabian Sea associated with salinity fluctuations induced by the upwelling episodes are shown in **Figure 3.9** and discussed in Section 3.2. The incidences of increased SST and decreased salinity were most evidently observed on 7 November (**Figure 3.9c**) and 21 November (**Figure 3.9c**), which could be due to small-scale overturning of surface waters and leading to upwelling of nutrient-rich subsurface waters. These overturning processes could be driven by the rapid fluctuations in meteorological parameters or an increase in the density of surface water from a steady rise and fall in salinity and SST, respectively, preceding the DMS events. Asher et al. (2017) have reported that the recently upwelled, saline waters and phytoplankton productivity provide favorable conditions for DMS accumulation.

As shown in **Figure 3.9b** and **c**, the sharp DMS peaks observed at midnight and afternoon hours are inconsistent with the typical diurnal feature of DMS in MBL and coincide with strong salinity gradients. Typically, the afternoon and nighttime DMS variability is dominated by loss via OH chemistry in the afternoon hours, and lack of photosynthetic activity of phytoplankton and NO_3 loss during the nighttime. However, the anomalous rise of DMS levels from low baseline values, prompting an increase of 330 ppt at midnight (0300 hr; **Figure 3.9b**) and 160 ppt in afternoon (1200 hr; **Figure 3.9c**) could be triggered by a rise in DMS exchange in response

to a localized salinity gradient. The measurements of anomalously broad morning peaks of DMS coincided with or immediately followed a steep gradient in salinity (**Figure 3.9d-f**). These features indicate large DMS fluxes caused by salinity stress, which decelerated its OH removal, leading to broad morning peaks.

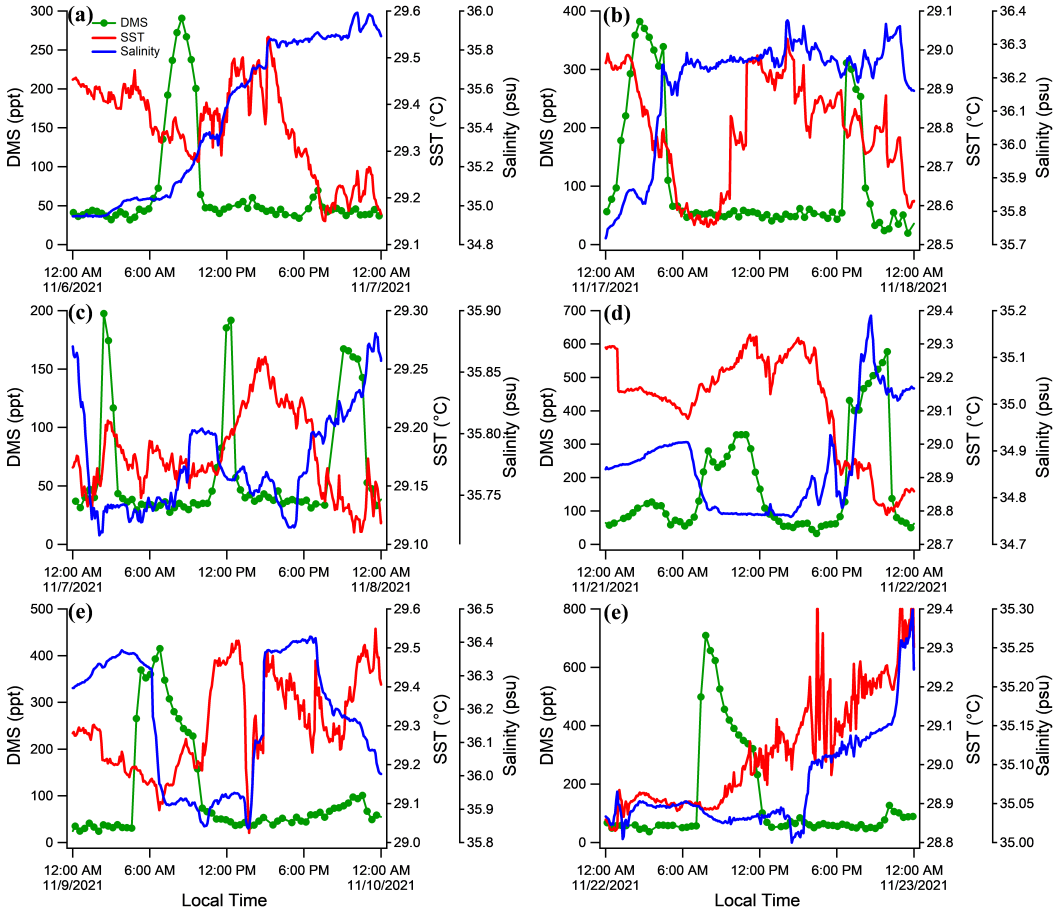

Figure 3.9: *Variation of DMS (green), salinity (blue), and SST (red) during the most noticeable salinity gradient events over the Arabian Sea, including the dates. (a) 6 November 2021, (b) 17 November 2021, (c) 7 November 2021, (d) 21 November 2021, (e) 9 November 2021, and (f) 22 November 2021*

The investigation of DMS mixing ratio and salinity gradient data signifies the impact of direct transport (upwelling) of DMS-rich subsurface waters and indirectly through biogeochemical production. Nevertheless, the salinity up- and down-shocks (>1) are reported to increase DMS production (Asher et al., 2017; Magalhães et al., 2012), while in our study, it ranged between -0.3 to 0.2 hr^{-1} of observation in spatiotemporal domain (**Figure**

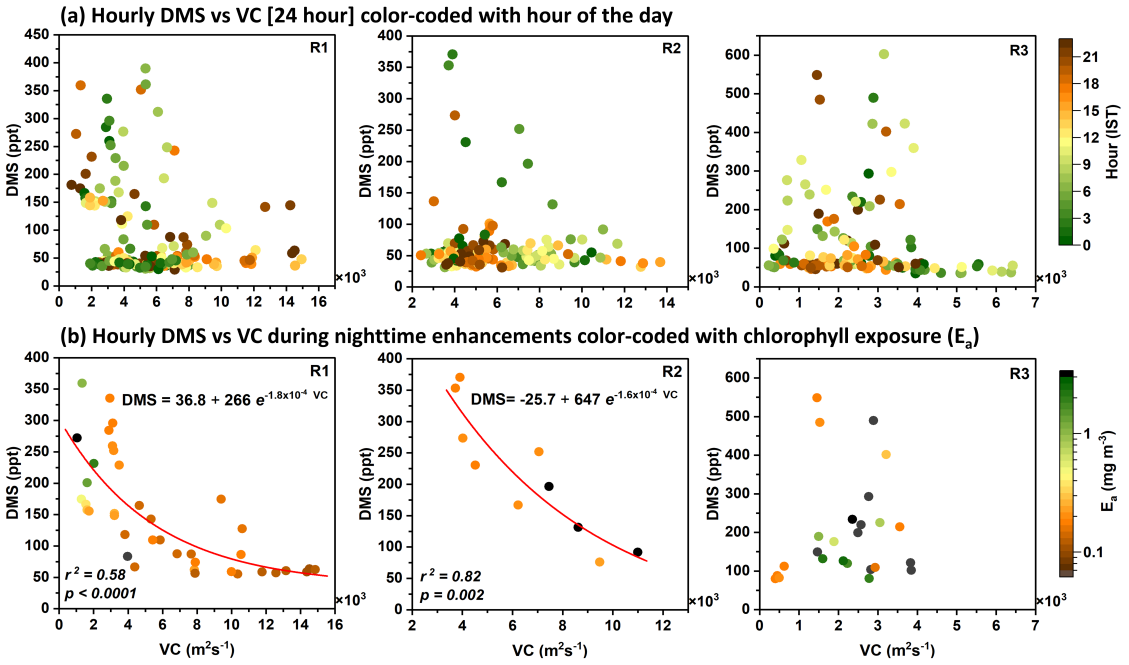

Figure 3.10: *Scatterplots between (a) DMS mixing ratio (all day and night data, color-coded with local time of the day) and (b) nighttime DMS enhancements (color-coded with Ea) and VC over R1, R2, and R3 transects. The red curve represents exponential decay fits.*

3.8). This emphasizes that a detailed investigation of the phytoplankton community structure is essential to understand the sensitive responses of DMS variability to small salinity variations in the Arabian Sea.

3.3.5 Impact of meteorological and oceanic parameters on nighttime DMS enhancements

3.3.5.1 Dilution of DMS in the MBL

The relationships between the DMS mixing ratio and VC in the three transects of R1, R2, and R3 are shown in **Figure 3.10a**. The DMS data measured during a localized upwelling event on 11 November were excluded from the analysis. DMS levels during this event, despite high VC values, were predominantly driven by oceanic conditions and were thus considered outliers. Mostly, the data points with the elevated DMS levels (100-602 ppt) were associated with relatively lower VC values (< 8 × 103 m^2 s^{-1}) throughout the campaign. Most enhancements in the DMS mixing

ratio were measured during early morning and nighttime hours, which coincide with relatively lower VC values. The photochemistry and boundary layer dynamics act simultaneously during the afternoon (12-16 hr), but separating the effects of ventilation and photochemical loss during this period is difficult. Therefore, except for some data points, the combined photo-oxidation and dilution-driven loss could have resulted in the lower DMS mixing ratios ($<$ 70 ppt) during the afternoon. Overall, but particularly during nighttime, the DMS mixing ratios show a decreasing trend with the increasing VC, highlighting the important role of atmospheric dilution in controlling DMS variability over the Arabian Sea. We segregated the nighttime DMS spikes ($DMS_{nighttime} >$ 55 ppt in R1 & R2; $>$80 ppt in R3) to parameterize its dependence on VC (**Figure 3.10b**).

The enhanced nighttime DMS concentrations in regions R1 and R2 declined as VC increased, but no clear relationship was observed in region R3. The DMS-VC relations during nighttime enhancements in R1 and R2 regions can be described by the following exponential decay functions. In region R1,

$$[DMS]_i = 36.8 + 266\ e^{-1.8 \times 10^{-4}\ \mathrm{VC}_i} \tag{3.2}$$

In region R2,

$$[DMS]_i = -25.7 + 647\ e^{-1.6 \times 10^{-4}\ \mathrm{VC}_i} \tag{3.3}$$

In region R3, the lack of any clear relationships could be due to the increased significance of nighttime radical chemistry attributed to the influence of continental outflow. The nighttime data points with a significant Chl-a exposure (Ea: 1-4 mg m-3) of air masses measured in R3 were relatively higher than those in other regions. Moreover, the lower VC values ($<$ 7×103 $m^2\ s^{-1}$) suggest less efficient ventilation in this region. The simultaneous interactions of various oceanic-atmospheric processes, including higher biomass abundance and increased DMS-NO_3 chemistry, contribute to the complexities in quantifying the direct dependence of DMS on VC in coastal environments.

3.3.5.2 Impact of sea surface parameters

We further investigated the correlations of DMS mixing ratios with sea surface temperature (SST) and salinity separately, using data from the three transects (**Figure 3.11**). Over regions R1 and R2, DMS mixing ratios exhibited a positive correlation with SST and a negative correlation with salinity.

In region R1, the DMS–SST correlation was weak ($r^2 = 0.29$), while the correlation with salinity was strong ($r^2 = 0.68$). Conversely, in region R2, the DMS mixing ratio was particularly sensitive to SST changes, showing an excellent positive correlation ($r^2 = 0.88$), but a weaker negative correlation with salinity ($r^2 = 0.37$). Although with smaller magnitudes than those observed in regions R1 and R3, the nighttime spikes in the R2 region were associated with an overall slight variation in SST by $\sim$ 0.4 $^{\circ}$C. The DMS mixing ratio in R3 shows poor correlations with SST and salinity; however, enhancements were measured at relatively lower SST values. As influenced significantly by local/regional transport (**Figure 3.4**), the low (high) DMS levels in region R1 were associated with high (low) wind speed (**Figure 3.11a**) and low (high) E_a (**Figure 3.11**b). The DMS spikes observed at night occurred during low winds in R1 ($<$ 7 m s^{-1}) and R3 (1–10 m s^{-1}), while those in region R2 were associated with stronger winds ($>$ 10 m s^{-1}). However, the DMS mixing ratio in R3 does not show any clear trends with either wind speed or E_a.

In summary, the results in region R2 suggest that wind-driven exchange and SST can be significant factors in DMS enhancements in the MBL over oligotrophic open oceans. The nutrient-poor open-ocean waters, shallow stratified mixed layer, and lower winds allow the DMS to accumulate under synergetic microbial activity, leading to nighttime DMS enhancements and spikes in the MBL when wind speed briefly increases (Royer et al., 2015). In the open ocean and offshore waters of R1, local biogeochemistry and oceanic conditions play a more crucial role in DMS enhancements, given the negligible influence of continental/anthropogenic air masses as observed in R1. On the contrary, in coastal waters, complex wind flow, heterogeneous

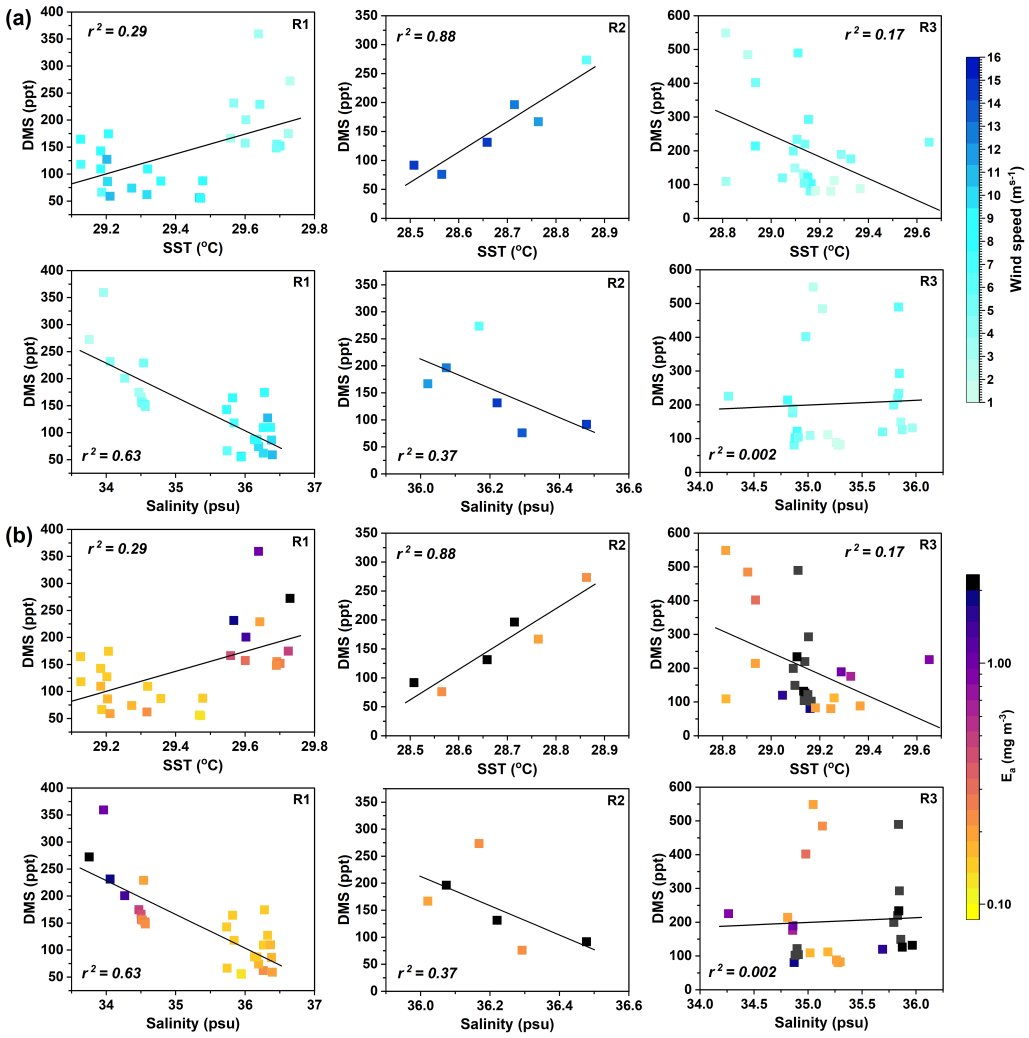

Figure 3.11: *Correlations of DMS mixing ratio (nighttime enhancements) with SST and salinity over the R1, R2, and R3 transects. The data points are color-coded with (a) wind speed and (b) air mass chlorophyll exposure (E_a). The black line in each panel represents a linear regression fit.*

air masses, and simultaneous interactions of various oceanic and atmospheric processes contribute to the difficulty in studying the dependence of DMS variability on different parameters.

3.3.6 Influence of seawater nitrate availability on DMS exchange

Besides salinity change, limiting nutrients in seawater is another physiochemical parameter that can impact the release of DMSP from phytoplankton cells (Andreae et al., 1999; Sunda et al., 2002; 2007) and, thus,

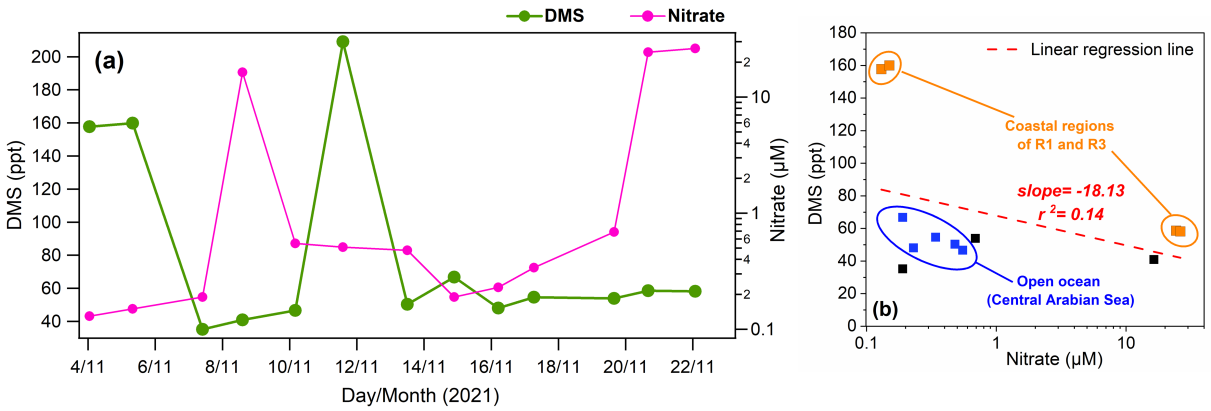

Figure 3.12: *(a) Variation of DMS mixing ratio with the surface seawater nitrate concentration sampled at different oceanographic sampling stations, (b) DMS vs nitrate scatterplot (excluding station L6) with linear regression fit for all data points. Data points from the coastal (orange) and oligotrophic open ocean (blue) regions are highlighted.*

the amount of DMS emission into the atmosphere. To assess the role of nitrogen (N)-limitation on the DMS levels, we examined the relations between the DMS mixing ratio and seawater nitrate concentration measured at different stations during the campaign (**Figure 3.12**), considering that the atmospheric DMS mixing ratio is strongly driven by its concentration in seawater. Overall, the time series of DMS mixing ratio and nitrate concentration tend to show anti-correlated variation as shown in **Figure 3.12a**. However, the relationship is highly inconsistent due to drastic changes in the biogeochemical regime and other atmospheric processes between all 13 stations.

The DMS and nitrate concentrations show a weak negative correlation ($r^2 = 0.14$; slope $= -18.13$ ppt μM^{-1}) over the Arabian Sea (**Figure 3.12b**). The anomalously high DMS (209 ppt) values at L6 station (**Figure 3.1a**), associated with the changes in salinity and biomass abundances, caused by an upwelling event, are excluded from this analysis. As shown in **Figure 3.12b**, the measurements over distinct biogeochemical regimes of coastal regions dominated by diatoms and dinoflagellate species (Hardikar et al., 2017; Krishnankutty et al., 2019) and the stratified oligotrophic (nitrate < 1 μM, phosphate < 0.4 μM) open ocean (dominated by *Prochlorococcus*

and *Synechococcus*) reveal an increase in the DMS mixing ratios with the decrease in nitrate in the surface seawater with r^2 values of 0.42 and 0.99, respectively. The N-limited conditions have been known to enhance the cellular DMSP concentrations in individual species of diatoms, dinoflagellates, and coccolithophores in culture experiments (Bucciarelli & Sunda, 2003; Litchman et al., 2002; Spielmeyer & Pohnert, 2012; Sunda et al., 2007). Previous studies have reported substantially higher seawater DMS concentrations associated with the lower nitrogen levels in coastal upwelling (Zindler et al., 2012) and subarctic Pacific (Herr et al., 2019) regions. The N-limitation can exert oxidative stress on phytoplankton cells by inhibiting photosynthetic activity and restricting antioxidant enzyme synthesis. This leads to increased production of intracellular DMSP or DMSP lyase products (i.e., DMS and acrylate), which are highly effective antioxidants to prevent oxidative damage (Litchman et al., 2002; Sunda et al., 2007). Sunda et al. (2007) reported a 20-fold increase in DMS from DMSP lyases by coccolithophore species in response to N-limited conditions, as DMS is ∼60 times more effective antioxidant than DMSP. Moreover, combined oxidative stress from N-limitation and UV radiation has been reported to result in a significant increase in seawater DMS (Litchman et al., 2002). Thus, N-limitation could be an important factor controlling the DMS levels in the stratified surface waters of the tropical oceans.

3.3.7 DMS flux and comparison with previous studies

DMS fluxes, estimated using **Eq. 2.11** (**F1** hereafter), are in the range of 20–141 μmol m^{-2} d^{-1} with a mean of $\sim$ 62$\pm$47 μmol m^{-2} d^{-1}. The higher fluxes (127–141 μmol m^{-2} d^{-1}) over the southern Arabian Sea were associated with patches of high Chl-a concentrations. On the other hand, lower fluxes (20–40 μmol m^{-2} d^{-1}) were calculated over the central Arabian Sea. However, in contrast to the findings of Shenoy and Kumar (2007), our flux estimates revealed lower DMS fluxes in the coastal regions ($\sim$ 22 μmol m^{-2} d^{-1}) than in the open ocean ($\sim$ 80 μmol m^{-2} d^{-1}).

Table 3.2: *The estimated bottom-up DMS air-sea fluxes (μmol m^{-2} d^{-1}), using satellite PAR data in F1 method, at different CTD stations along the cruise track. Concentration of DMS in surface seawater estimated using G18.*

Station	**Date & time**	**Lat (°N)**	**Lon (°E)**	**C_w** (nM)	**F_{DMS}**
1	04-11-2021 01:00	9.58	75.53	14.04	21.76
3	07-11-2021 09:45	6.8	71.89	11.66	40.85
4	08-11-2021 14:15	5.5	70.04	16.47	127.30
5	10-11-2021 04:00	4	68.02	22.79	141.54
6	11-11-2021 14:00	6.01	68.05	18.53	137.68
7	13-11-2021 12:00	9.33	68.07	12.86	82.66
8	14-11-2021 21:30	11.95	68.05	14.40	39.92
9	16-11-2021 05:00	14	68	11.00	28.14
10	17-11-2021 06:30	16	67.99	10.53	37.55
11	19-11-2021 15:40	18.3	70.5	11.89	31.51
12	20-11-2021 16:00	17.29	70.5	12.97	19.59
13	22-11-2021 01:35	16.3	70.5	12.26	31.85

We speculate two major factors that could account for this discrepancy: first, the anomalously high DMS flux in the southern Arabian Sea due to high biomass abundance and local oceanic processes, as discussed in Section 3.3.2. Secondly, the fluxes reported by Shenoy and Kumar (2007) are based solely on the seawater DMS concentration and wind speed data, while we observed no apparent direct relationship between atmospheric DMS and wind speed.

The fluxes estimated using the F1 method are significantly higher than the previously reported inter-monsoon values of 0.1–13 (mean∼3.13) μmol m^{-2} d^{-1} over the Arabian Sea. It is important to highlight that the estimates of C_w using the G18 parameterizations are found to be highly sensitive to photosynthetically active radiation (PAR) values (Galí et al., 2018), and thus, the F1 flux estimation carries a large uncertainty due to the poor temporal resolution of PAR satellite data.

The values of C_w, calculated using satellite PAR data (**Table 3.2**), are overestimated compared to previously reported concentrations of ~ 1.4 nM

Table 3.3: *The estimated bottom-up DMS air-sea fluxes (μmol m^{-2} d^{-1}), using in situ PAR in surface waters (3–5 m) in F1 method, at different CTD stations along the track. Concentration of DMS in surface seawater estimated using* ***G18****.*

Station	Date & time	Lat (°N)	Lon (°E)	C_w (nM)	F_{DMS}
1	04-11-21 13:05	9.54	75.55	3.24	9.66
1	04-11-21 15:15	9.59	75.53	3.25	8.57
5	10-11-21 11:19	4.01	68.01	3.18	20.06
5	10-11-21 14:56	4.00	68.01	3.20	23.82
7	13-11-21 12:06	9.33	68.04	2.45	13.93
7	13-11-21 15:44	9.33	68.07	2.45	8.84
10	17-11-21 11:22	15.98	67.97	2.48	0.36
11	19-11-21 15:41	18.30	70.50	2.72	8.24
11	19-11-21 17:26	18.30	70.46	2.72	4.94
				Mean	**10.94±7.29**

in coastal and 5.8 nM in open ocean regions of the Arabian Sea. However, the estimates of C_w values ($\sim$ 10.4 nM) using *in situ* PAR data show better agreement. Consequently, the fluxes estimated using satellite-derived products were $\sim$ 6 times higher than the mean flux of $\sim$ 11 μmol m^{-2} d^{-1} calculated using *in situ* PAR (**Table 3.3**). To address the large differences among the estimates, there is a need for regional parameterization schemes to improve the DMS flux climatology over the northern Indian Ocean.

The nighttime build-up rates of DMS_{VC} estimated for three different instances (**Figure 3.13**) over the central Arabian Sea have been used for the top-down flux (**F2** hereafter) estimation. On most other days, the sharp fluctuations in nighttime DMS_{VC} show a complex response of DMS to atmospheric chemistry and changes in oceanic conditions, opposing the assumptions in F2. Moreover, the reduced influences of continental and anthropogenic pollutants in the open ocean minimize the nighttime DMS loss from NO_3 oxidation compared to coastal or polluted regions (Stark et al., 2007), favouring its accumulation under a stable MBL. The nutrient-depleted open ocean waters support a coherent diel cycle due to tightly coupled DMS-

DMSP conversion from light-synchronized microbial interactions (Royer et al., 2016). Thus, oligotrophic open ocean waters are more suitable for top-down flux analysis based on nighttime atmospheric build-up than coastal or high-productivity waters.

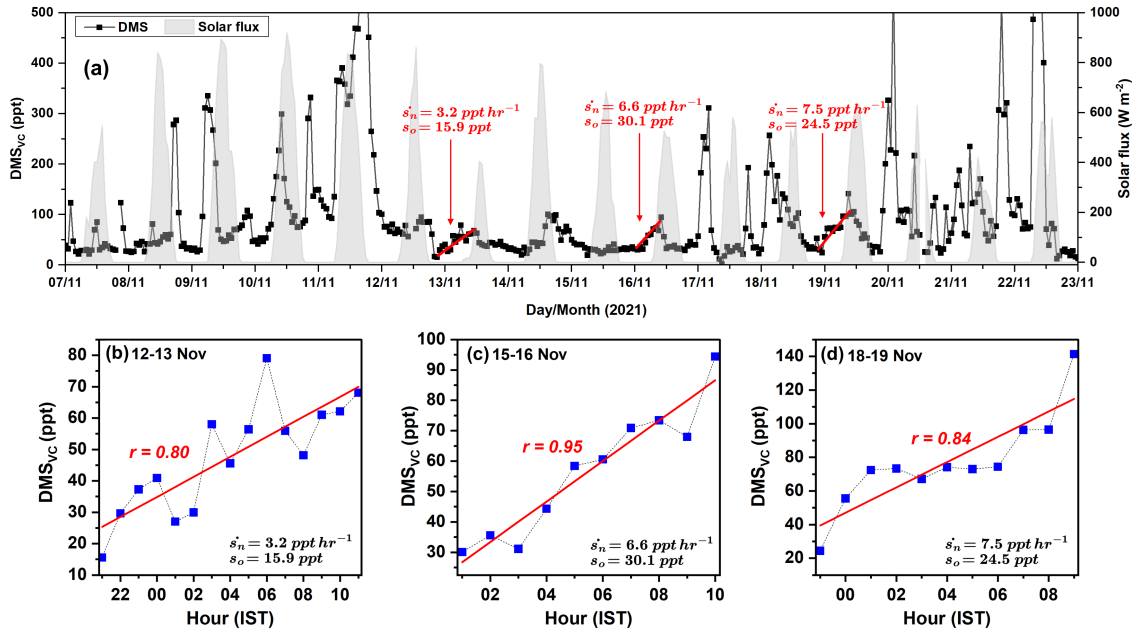

Figure 3.13: *(a) Time series of atmospheric DMS mixing ratio and solar radiation flux during 7-22 November 2021. The nighttime build-up of DMS_{VC} during (b) 12-13 November, (c) 15-16 November, and (d) 18-19 November 2021 over the R2 region in the Arabian Sea. The red line represents the linear regression fit, and so and $\dot{s}_n$ represent the initial mixing ratio and build-up rate in the MBL, respectively.*

F2 was calculated using **Eq. 2.21** and n, and thus, for the three periods, is derived from **Figure 3.13**. The parameter w_e is taken as 5 mm s^{-1} following the study by Warneke and de Gouw (2001) over the western tropical Indian Ocean, and h is taken as the mean MBLH (ERA-5 reanalysis data) during the build-up period. The mean F2 flux of 4.2±2.07 μmol m^{-2} d^{-1} is comparable to the top-down flux of ~2.15 μmol m^{-2} d^{-1} reported over the western tropical Indian Ocean (Warneke and de Gouw, 2001). Despite the conceptual differences, the F2 fluxes (2.46–6.59 μmol m^{-2} d^{-1}; **Table 3.4**) are comparable to the F1 fluxes near most of the stations (**Table 3.3**), except station 5 with intense Chl-a patches (**Figure 3.1**). Although

F2 flux estimates lie toward the lower end of the F1 fluxes, the mean of F2 estimates is approximately half of the mean F1 flux (10.94±7.29 μmol m^{-2} d^{-1}). However, the F1 method could provide higher fluxes using afternoon data points when the photochemical loss of DMS by OH radicals is considered.

Table 3.4: *The DMS air-sea fluxes estimated using the top-down approach over the central Arabian Sea during the post-monsoon season 2021.*

Period	**Flux (μmol m^{-2} d^{-1})**
12–13 November	2.46
15–16 November	6.59
18–19 November	4.81
Mean	**4.62±2.07**

The DMS fluxes estimated using the F1 method with *in situ* PAR data in the present study are compared with previously reported values over the Arabian Sea and also over other oceanic regions of the world (**Figure 3.14**). Despite lower primary production during the post-monsoon, the Arabian Sea DMS flux estimates are higher compared to most other ocean basins. However, the uncertainty in indirect, parameterization-based flux calculations (present study; Shenoy et al., 2007; Bell et al., 2021) is higher than direct flux measurements (Garbe et al., 2014; Marandino et al., 2007, 2009; Yang et al., 2011).

The high 1σ variability shown in **Figure 3.14**, particularly in the Arabian Sea (present study), Bay of Bengal (Shenoy & Kumar, 2007), and South Pacific (Marandino et al., 2009) was associated with diverse spatial (e.g., oligotrophic and upwelling/coastal) or seasonal coverage in the oceanic basins. The parametrized C_w in our study, 2.9±0.4 nM, are well within the range of mean C_w in other basins (1.6–3.8 nM; **Table 3.3**). The studies cited in **Figure 3.14** have reported elevated DMS fluxes for biologically productive regions (upwelling zones, frontal zones) relative to low productivity regimes (like gyres and equatorial warm pools), which is consistent

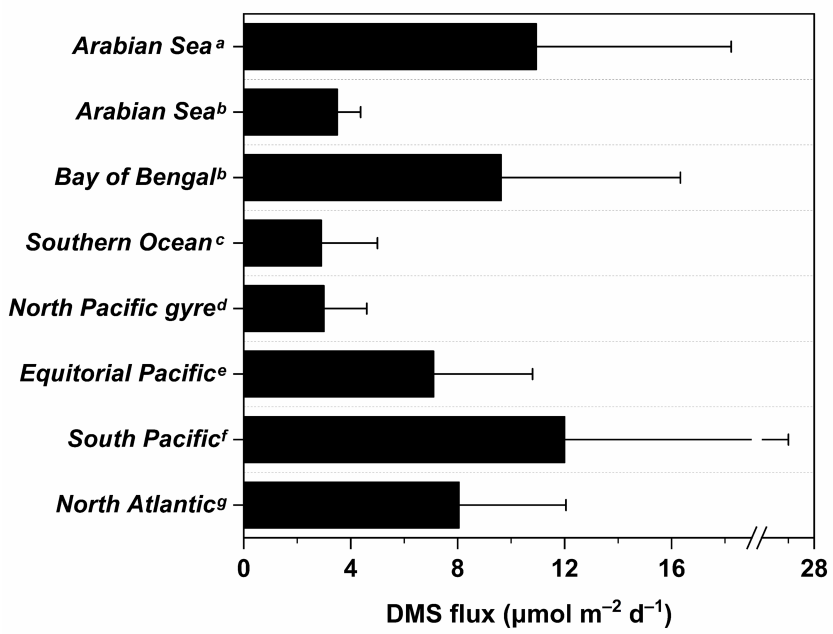

Figure 3.14: *Comparison of DMS fluxes reported for different oceanic regions of the world. Present study[a], Shenoy & Kumar, 2007[b], Yang et al., 2011[c], Marandino et al., 2007[d], Yang et al., 2011[e], Marandino et al., 2009[f], Bell et al., 2021[g].*

with our findings.

However, despite the chlorophyll dependence on seawater DMS, parameters like windspeed thresholds, SST and mixed layer dynamics were found to play a pivotal role in air-sea exchange in these studies. The mean flux ($\sim$ 11 μmol m^{-2} d^{-1}; **Table 3.3**) is $\sim$ 3 times higher than reported in a previous study conducted during 1998–99 over the Arabian Sea in the fall inter-monsoon, suggesting a substantial increase in the DMS flux from the Arabian Sea over the last two decades. Based on extrapolation of the estimated flux to the entire basin, the emissions from the Arabian Sea account for $\sim$ 10% of the average global annual DMS emissions (28.1 Tg S yr^{-1}; L11).

3.4 Conclusion

For the first time, the high time-resolution measurements of the DMS mixing ratio were conducted in the marine air of the Arabian Sea dur-

ing the post-monsoon season of 2021. The effects of physicochemical and meteorological parameters were analyzed to investigate the spatiotemporal distributions of DMS over both coastal and open oceanic regions. The DMS mixing ratios were highest over the coastal Arabian Sea (116$\pm$120 ppt), followed by the southeast Arabian Sea (98$\pm$87 ppt), and lowest over the central Arabian Sea (62$\pm$53 ppt). The large diurnal and day-to-day variations of the DMS mixing ratio, associated with the changes in physicochemical and meteorological conditions, reveal the complex interplay of oceanic emissions, photochemistry, and transport of distinct air masses. The mean DMS mixing ratios over the three regions vary significantly with Chl-a concentration and air trajectory. The analysis of chlorophyll exposure to back trajectories suggests greater enhancements in DMS from local or regional sources than from transported air masses. However, the short-term, small-scale variability seems to be largely controlled by the local hydrography, such as changes in salinity associated with physical forcings at the surface.

The diurnal patterns showed distinct characteristics over the oligotrophic open ocean and productive coastal regions. However, the daytime OH oxidation loss strongly influenced the diurnal dependence of DMS throughout the study period. The transport of polluted continental air, with lower DMS concentrations but presumably higher NO_3 concentrations, influenced the DMS measurements in the northeast coastal regions. The episodes of sharp increase in DMS mixing ratios were mostly associated with the strong salinity gradients (-0.3 to +0.2 hr^{-1}) caused by the local upwelling and surface overturning processes. Atmospheric DMS showed a distinct regional response to seawater nitrate concentration and increased under nitrogen-limited conditions. The nighttime enhancements of the DMS mixing ratio revealed a decline with increasing dilution level. However, the effectiveness of VC in DMS variability in MBL can be influenced by factors such as coastal proximity, ocean productivity, and the transport of air masses. The significance of SST, salinity, and wind speeds in driving the nighttime DMS enhancements was found to be dependent on local biogeochemistry.

The estimated DMS air-sea fluxes of $\sim$11 μmol m^{-2} d^{-1} in this study

are almost three times greater than those reported over the tropical Indian Ocean. The bottom-up DMS flux estimated using the global parameterization schemes tends to overestimate the estimations from *in situ* data, highlighting the need for regional parameterization schemes addressing the complex biogeochemistry in this productive basin of the northern Indian Ocean.

These results highlight the complexity and heterogeneous nature of DMS flux dynamics in the Arabian Sea and could be pivotal in understanding the primary factors driving the DMS emissions under varied oceanic and atmospheric conditions. The DMS measurements and the relationships with several variables could be a valuable regional representation of DMS emissions from the Arabian Sea for the global biogeochemical and chemistry-climate simulations. Regional variations in pollution and background oxidant concentrations can substantially affect sulfate aerosol formation rates, as demonstrated by the simultaneous nighttime variability of DMS and benzene emissions. Understanding these pathways is essential for modelling marine sulfur emissions' impacts on atmospheric chemistry and climate dynamics. In addition, detailed studies are required to investigate the diverse phytoplankton community structure to assess the roles of different physicochemical factors controlling seawater DMS production.

Chapter 4

Impact of oceanic emission and atmospheric transport on DMS distribution over the Bay of Bengal

Key takeaways

- Continental and oceanic air masses led to distinct west-east and east-west longitudinal distributions of DMS over the central Bay of Bengal
- Relationship with nutrient and picophytoplankton data emphasizes the role of complex biogeochemical processes in the spatial variation of DMS
- Based on campaign mean DMS flux of 4.9 ± 3.2 μmol m^{-2} d^{-1}, the annual sulfur emissions from the Bay of Bengal are estimated to be $\sim$0.14 Tg S yr^{-1}, with large uncertainties due to limited seasonal coverage.

4.1 Introduction

The Bay of Bengal basin (5–22°N; 80–100°E, area $\sim 2.6 \times 10^6$ km^2) in the northeast Indian Ocean is bounded by India and Sri Lanka on the west, Bangladesh and the Ganges-Brahmaputra-Meghna delta on the north, and Myanmar on the east. The Andaman Sea is a marginal sea separated from the Bay of Bengal by the Andaman and Nicobar Islands and connected to it

via multiple channels through the Andaman and Nicobar archipelago. The Andaman Sea lies between 90–100°E of longitude and 2–16°N of latitude, covering $\sim 32\%$ of the northeast Indian Ocean. It is bounded by Myanmar in the north and east and Thailand, Malaysia, and Indonesia to the south. The Andaman Sea is relatively shallow ($<$ 100 m) in the coastal regions of Myanmar, Thailand, and the Andaman Islands but deep ($>$ 4000 m) in the central region.

The river influx also plays a critical role in shaping the biogeochemistry of the Bay of Bengal and the northern Andaman Sea, especially near the Andaman Islands (Gauns et al., 2005; Groß et al., 2022). The Bay of Bengal receives the highest amount of rainfall in the Indian Ocean (Qi & Wang, 2015) and large riverine influxes ($\sim 2.95 \times 10^{12}$ m^3 yr^{-1}; Sengupta et al., 2006) from a few of the world's major river systems, namely the *Brahmaputra*, *Ganga*, *Godavari*, and *Mahanadi* (Varkey et al., 1996). The freshwater input from the river discharge into the Bay of Bengal is highest during the post-monsoon season (Sarma et al., 2009), which leads to strong surface stratification (Mahadevan et al., 2016). The stratification inhibits the vertical supply of nutrients, causing reduced surface productivity and oligotrophic conditions in the open ocean (Gauns et al., 2005; Kumar et al., 2002). However, the river runoff supplies large amounts of nutrients and organic matter, enhancing the primary production in coastal regions (Rao et al., 2015). The stratified shallow mixed layer also sustains the occurrence of a strong oxygen minimum zone (OMZ) in subsurface waters throughout the year (Bristow et al., 2017; Rixen et al., 2020). Atmospheric depressions and cyclones drive turbulent vertical mixing, particularly in the southern Bay of Bengal, upwelling nutrient-rich subsurface waters, and triggering isolated Chl-a blooms (Latha et al., 2015). 3–5 times of increase in primary productivity associated with cyclonic eddies have been reported in the Bay of Bengal (Kumar et al., 2005; Sarma et al., 2019).

The Andaman Sea receives freshwater from the *Irrawaddy*, *Sittang*, *Salween*, and other smaller rivers (Pargaonkar & Vinayachandran, 2022), significantly influencing salinity, nutrient levels, and vertical circulation.

The SMC during May–September pushes the major riverine influx from the north of Andaman into the Andaman Sea. In early post-monsoon (October), the weakening of the SW monsoon can transport nutrient-rich waters from the *Irrawaddy* River system into the Andaman Sea (Pargaonkar & Vinayachandran, 2022). This surface current turns completely south-westward by the end of October/early November (Chatterjee et al., 2017). The transport of nutrient-rich riverine waters mixed with coastal and offshore waters leads to a rise in Chl-a after a period of lower concentrations during the SW monsoon.

Significant spatial and seasonal variability in DMS concentration and fluxes in the Bay of Bengal has been reported in previous literature. Shenoy et al. (2000; 2007) reported high seawater DMS concentrations (1–8 nM) and fluxes in the range of 2–10 μmol m^{-2} d^{-1} over the Bay of Bengal, associated with upwelling of nutrient-rich waters and stronger southwest (SW) winds. Compared to the southwest monsoon, lower DMS fluxes (1–5 μmol m^{-2} d^{-1}) were reported during the post-monsoon season, attributed to weaker winds and reduced vertical mixing (Shenoy et al., 2007). The cyclonic activities, which occur mostly in the post-monsoon season over the Bay of Bengal, can temporarily enhance DMS flux by enhancing vertical mixing and nutrient supply to the surface waters. For example, Kumari et al. (2019) have reported changes in seawater DMS concentration and flux during the passage of cyclone Hudhud during 7–14 October 2014 in the coastal waters of the Bay of Bengal. The DMS concentrations of 8.8–33.5 and 0.4–3.9 nM and fluxes of 5.8 ± 3 and 2.8 ± 2 μmol m^{-2} d^{-1} were reported for the pre-cyclone and post-cyclone periods, respectively. About 30% higher DMS concentration during the pre-cyclone period was due to intensified upwelling and increased nutrient availability. Elevated levels of DMS fluxes (up to 8 μmol m^{-2} d^{-1}) have also been reported in coastal regions of the Bay of Bengal, due to enhanced nutrient input from river discharge in the post-monsoon season (Rao et al., 2015). Recently, Peng et al. (2024) reported the seawater DMS concentration and estimated flux over the eastern Indian Ocean (EIO) covering the central Bay of Bengal

during October–November 2020. In this study over the EIO, variations in seawater DMS concentrations of 2–10 nM and fluxes of 2–12 μmol m^{-2} d^{-1} were attributed to biogeochemical processes influenced by the Wyrtki jets, Bay of Bengal runoff (BBR), and South Equatorial Current (SEC).

Previous studies indicate that the dynamical forcings and atmospheric processes become increasingly important in determining the DMS concentrations in the Bay of Bengal. Sarin et al. (2010) reported that the nss-SO_4^{2-} contributes significantly to sulfate aerosol in the Bay of Bengal, especially in the polluted MBL. However, the understanding of processes driving the exchange and regulating the levels of DMS in the MBL of the Bay of Bengal and its implications on the atmospheric processes is still lacking.

This study was conducted using the first high time-resolution, continuous shipborne measurements of atmospheric DMS concentration over the northeast Indian Ocean during the post-monsoon season of 2021, covering the Bay of Bengal and Andaman Sea basins. The main objective of this study is to investigate the complex interplay of air-sea exchange, microbial community, coral reef emissions, atmospheric photochemistry, and continental outflow influencing the diurnal and day-to-day variations of atmospheric DMS. We have also further estimated the air-sea fluxes of DMS over the study area through different approaches using measured atmospheric DMS and parameterized seawater concentrations.

4.2 Ship Campaign

A shipborne experimental campaign onboard ORV *Sagar Kanya* (SK#373) was conducted over the northeast Indian Ocean in the post-monsoon season, from 25 September to 14 October 2021. The cruise started from Chennai port (13.08°N, 80.29°E) on the eastern coast of India, sailed eastward longitudinally over the Bay of Bengal, entered the Andaman Sea at the northern tip of the Andaman Islands, and sailed westward from south of Little Andaman to Chennai port. The cruise track covered during the campaign has been divided into three transects (Figure 4.1): T1 (west-east,

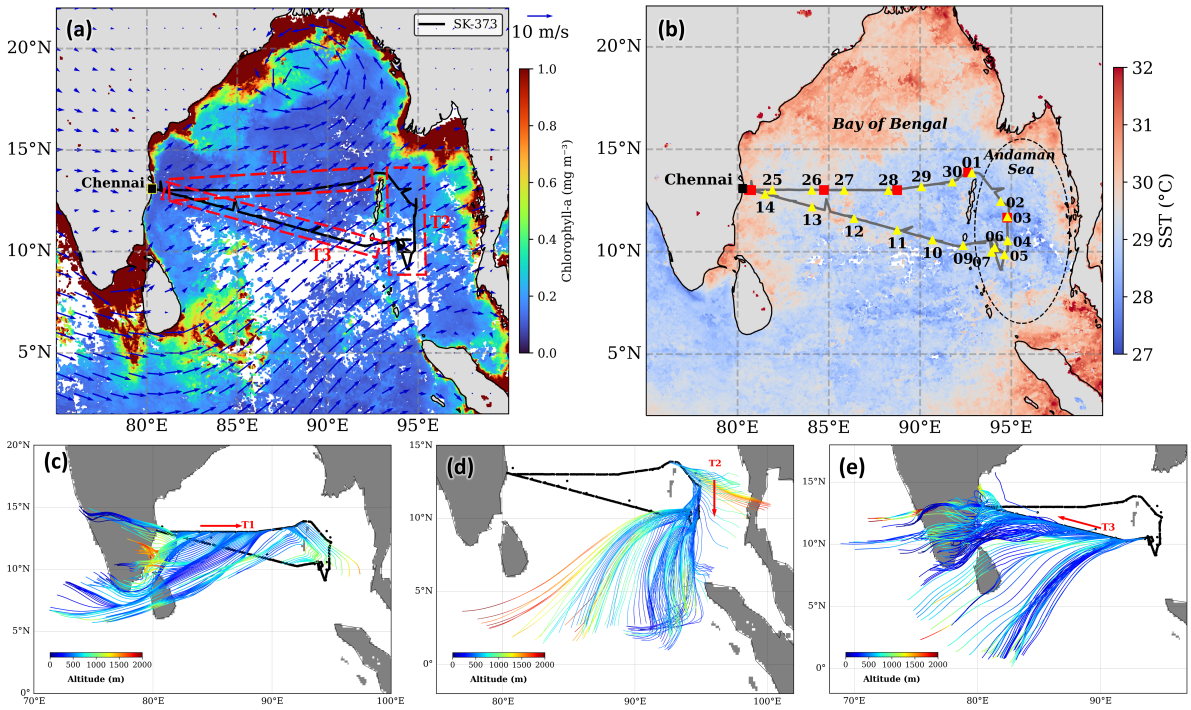

Figure 4.1: *Composite maps of (a) Chl-a (mg m^{-3}) and (b) SST (°C), retrieved from the MODIS-Aqua for the cruise period (25 September–14 October 2021). The numbers (yellow triangles) along the cruise track in (b) represent the reference date (days in September (25–30) and October (1–14) 2021 at 00 hr LT). Red squares and labels represent the water sampling station.*

13–14°N; 80–93°E, 25–30 September 2021), T2 (Andaman Sea, 9–14°N; 93–95°E, 1–8 October 2021), and T3 (east-west, 10–13°N; 80–93°E, 9–14 October 2021). T1 (onward; Chennai port to Andaman Sea) and T3 (return; Andaman Sea to Chennai port) are the longitudinal transects over the Bay of Bengal, while T2 is a latitudinal transect over the Andaman Sea. The SST and surface Chl-a concentration in the study region (9–15°N; 80–96°E) varied between 28–29.5°C and 0.1–0.3 mg m^{-3}, respectively (**Figure 4.1**). Typically, the SST over the Bay of Bengal exhibits a bimodal annual pattern with a primary peak in the pre-monsoon (April–May) and a secondary peak in the post-monsoon season (October). The distribution of SST showed a north-to-south decreasing pattern in the study region during the campaign (**Figure 4.1b**).

In the post-monsoon season, the wind pattern over the northern Indian

Ocean represents a transition from the strong southwest (SW) to northeast (NE), driven by the seasonal progression of the Intertropical Convergence Zone (ITCZ) (Gupta et al., 2024). The wind field map from the European Centre for Medium-Range Weather Forecasts Reanalysis 5 (ERA-5 reanalysis) shows the prevalence of SW winds over the Bay of Bengal (**Figure 4.1a**). The monsoonal winds drive the Southwest Monsoon Current (SMC; June–October), which is an eastward current that advects high salinity waters from the Arabian Sea to the southwest Bay of Bengal and parts of the Andaman Sea (Vinayachandran et al., 2013).

The patches of high Chl-a concentrations observed in the southwest Bay of Bengal (**Figure 4.1a**) are associated with the SMC hydrodynamics around Sri Lanka and the remnants of the Sri Lanka Dome (de Vos et al., 2014; Gomes et al., 2016). The equatorial westerlies during the inter-monsoon season (October–November) drive the strong eastward surface currents in the equatorial Indian Ocean (EIO; 2°N–2°S), also known as Wyrtki jet (Prerna et al., 2019; Wyrtki, 1973). The warm equatorial surface waters are advected eastward, deepening the thermocline in the eastern EIO and shallowing in the western EIO, which triggers phytoplankton blooms in the western EIO.

4.3 Results and Discussion

4.3.1 Time series variations of atmospheric DMS concentration

The DMS mixing ratio varied in the range of 44–426 ppt during the campaign, with lower mixing ratios (77 ± 23 ppt) along the T1 transect than along the T3 transect (103 ± 37 ppt) over the Bay of Bengal (**Figure 4.2a**). The difference in mean DMS observed over T1, T2, and T3 were statistically significant (χ^2=120.41, K-W p$<$0.0001 [α=0.05]). The background atmospheric DMS concentrations, calculated as the 5th percentile (Apte et al., 2017), along T2 and T3 (50–55 ppt) were higher than that of 47 ppt along the T1 transect. The differences in the background DMS concentrations are consistent with the MODIS-derived Chl-a data, which shows lower

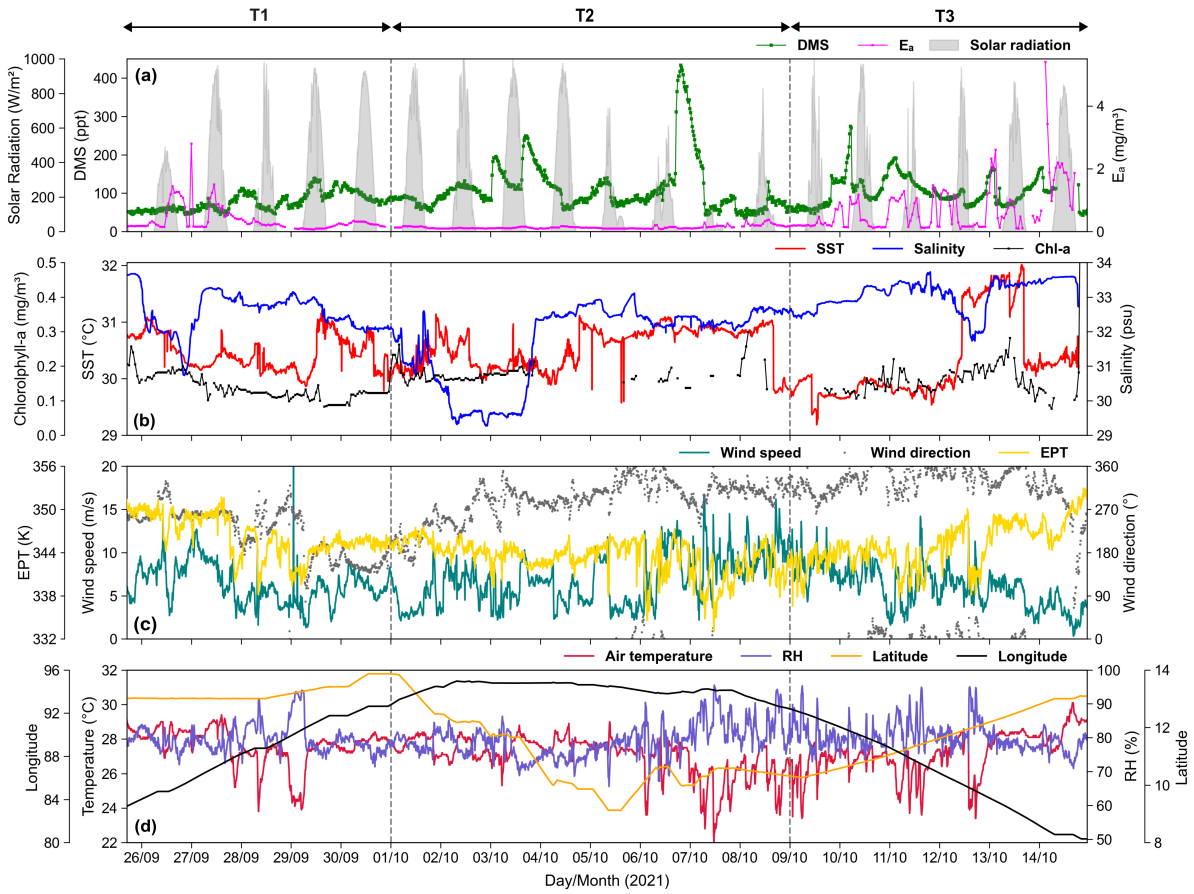

Figure 4.2: *Time series variations of (a) DMS mixing ratio, chlorophyll-exposure of air masses (E_a), and solar flux, (b) SST, salinity and Chl-a, (c) equivalent potential temperature (EPT), wind speed and wind direction, (d) Temperature, relative humidity (RH), latitude, and longitude over the Bay of Bengal during 25 September–14 October 2021.*

concentrations of 0.08–0.25 mg m^{-3} along T1 than 0.08–0.79 mg m^{-3} along T3. However, contrary to the observations over the Bay of Bengal, the higher DMS concentrations (112 ± 68 ppt) over the Andaman Sea were associated with the lower Chl-a concentrations (0.13–0.29 mg m^{-3}). Despite substantial day-to-day variability of the DMS, several enhancement events led to an overall higher average value in the MBL of the Andaman Sea (T2) than those measured in the Bay of Bengal along T1 and T3. Prominent peaks of DMS between 5–8 October suggest the influence of intense local sources, including the emissions from corals around the Andaman Islands (Jackson, Gabric, Woodhouse, et al., 2020).

The DMS enhancements exceeding 200 ppt on 3 October and 150 ppt on

Table 4.1: *The mean (± standard deviation) of the DMS mixing ratio, and meteorological and hydrographic parameters along the three different transects over the Bay of Bengal during 25 September–14 October 2021.*

Parameters	**Onward-BOB (T1)**	**Andaman Sea (T2)**	**Return-BOB (T3)**	**All data**
DMS (ppt)†	77±23 [1]	112±68 [3]	103±37 [2]	99±52 [1.5]
Wind speed (m s^{-1})	6.31±2.15	6.78±2.74	6.06±2.28	6.43±2.46
SST (°C)	30.45±0.3	30.54±0.35	30.29±0.72	30.44±0.5
Salinity	32.57±0.56	31.67±1.17	33.07±0.44	32.35±1.04
Solar flux (W/m^2)	191±284	163±267	159±250	169±266
Pressure (mb)	1005±2	1008±1	1005±1	1006±2
Temperature (°C)	27.6±1.1	27.0±1.1	27.2±1.2	27.2±1.2
Relative humidity (%)	79.7±3.9	79±4.6	80.2±3.6	79.6±4.2
Chl-a (mg m^{-3})	0.14±0.03	0.18±0.03	0.18±0.13	0.16±0.08

†Standard error [SE]

12 October coincided with strong salinity gradients of 2–4 (**Figure 4.2b**), suggesting increased DMSP production by phytoplankton in response to osmotic stress (Kettles et al., 2014; Speeckaert et al., 2019). Royer et al. (2015) have reported sharp changes in seawater DMS concentrations associated with local salinity and SST gradients in the equatorial Pacific, indicating a direct or indirect influence of hydrographic parameters. Shenoy et al.(2000) have also reported the impact of salinity change on the seawater DMSP concentrations in the Bay of Bengal. However, in our study, no clear correlation was found between salinity and DMS levels, as DMS peaks were observed at both low and high salinity values. Therefore, in addition to salinity, several other factors, such as heterogeneity in biogeochemical properties like phytoplankton abundance and taxonomy, localized emissions from coral reefs, and meteorological conditions, could influence the oceanic emissions of DMS over the Bay of Bengal.

The wind speed varied in the range of 2–15 m s^{-1} during the campaign, with rapid fluctuations under unstable atmospheric conditions between 6–8

October (**Figure 4.2c**). The lower DMS mixing ratios ($\sim 55 \pm 6$ ppt) measured at the beginning of the T1 transect during 25–26 September were associated with the prevalence of strong westerly winds (5–10 m s^{-1}). This indicates the dilution of atmospheric DMS by the rapid continental winds from peninsular India, leading to lower DMS levels. On the contrary, the higher mixing ratios (90.3 ± 22.5 ppt) during 28–30 September were associated with the weaker SW winds, transporting oceanic air masses. The 5-day backward trajectories reveal that the periods of low and high DMS levels observed along T1 and T3 were associated with air masses transported from continental and biologically productive oceanic regions, respectively (**Figure 4.1c**).

The DMS mixing ratio over the Andaman Sea (T2) shows much larger variations (44–426 ppt) than those measured along the T1 and T3 longitudinal transects over the Bay of Bengal. A prominent DMS peak (> 400 ppt) centred between 19–20 hr on 06 October in the Andaman Sea was associated with rapid changes in wind direction and transport from the coral shelf regions in eastern Andaman (discussed in detail in Chapter 5). However, the reduced DMS levels (∼44–80 ppt) observed during 07–08 October coincided with significant meteorological disturbances marked by large fluctuations in wind speed (5–15 m s^{-1}), a drop in air temperature by ∼5°C, higher relative humidity of 85–90%, and events of precipitation or dense cloud cover. The unstable atmospheric conditions and intense convective activities marked by the sharp variations in equivalent potential temperature (EPT; θ_E) (**Figure 4.2c**) could have modulated the DMS levels in this episode.

Except for enhancement events along T2, the nighttime DMS mixing ratio in the MBL tends to decrease with increasing wind speed (**Figure 4.3**). Stronger dilution by the DMS-deficit continental air masses over T1 than the marine air masses over T3 could be one of the factors leading to distinct longitudinal variations of DMS both along the transects. The impact of vertical mixing and air mass intrusion on DMS concentration is discussed in Section 4.3.4. Further, the DMS enhancement associated with

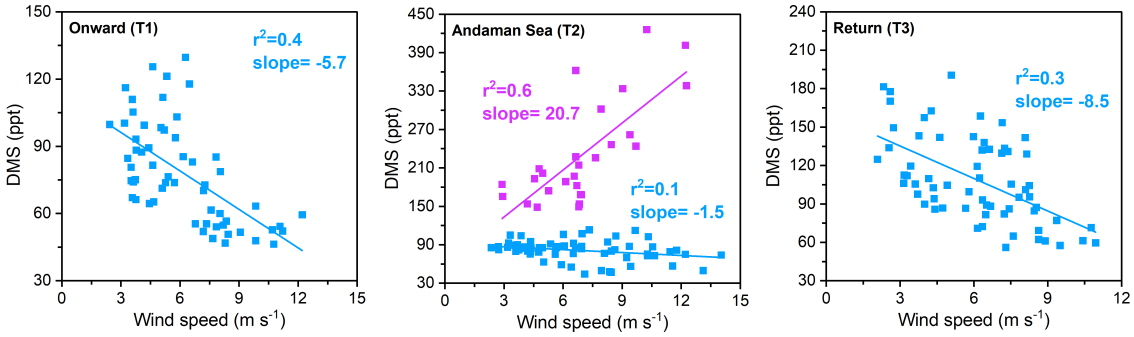

Figure 4.3: *Scatterplot of the nighttime DMS mixing ratios vs wind speed over the T1, T2, and T3 transects over the Bay of Bengal during 27 September-14 October 2021. Coral influences DMS concentrations over the Andaman Sea are marked in purple.*

coral reef emissions over the Andaman Sea increased with wind speed, revealing increased air-sea exchange of DMS under high wind conditions. The backward trajectories along T3 reveal the transport of marine air masses from the productive coastal and EIO regions (see **Figure 4.1e**), which could have led to enhanced DMS mixing ratios. The analysis of back trajectories and wind parameters over T1 suggests the impact of continental outflow and a possible chemical loss of DMS due to its reaction with the NO_3 radical. To qualify the contributions of biogenic DMS from long-range transport, we have calculated the chlorophyll exposure of air masses (E_a) along the 48-hour back trajectories (Eq. 2.5). E_a is a useful diagnostic parameter linking the atmospheric DMS levels with the air mass exposure to oceanic phytoplankton prior to arrival at the measurement site, while also accounting for DMS loss processes and intrusions from the free troposphere. **Figure 4.2a** shows an overall increase in E_a during the east-west (T3) transect, attributed to the southwest (SW) transport of air masses from the productive waters of the Palk Strait, coastal region of Sri Lanka, and EIO with high phytoplankton biomass as indicated in the Chl-a map (**Figure 4.1a**). Yan et al.(2024) have established a strong correlation between the atmospheric DMS mixing ratio and E_a in the western Pacific Continental Sea. However, despite elevated E_a near the coast, the lower DMS concentrations during 26–27 October along T1 indicate the dominant influence of dilution in the continental outflow regime. E_a and DMS mixing

ratio do not show any relations over the Andaman Sea, supporting our discussion on the effect of localized sources in the region. The DMS mixing ratios measured along T3 (45–225 ppt; 103 ± 37 ppt) are slightly higher than the values reported over several other open ocean regions, such as the equatorial Pacific warm pool (59 ± 17 ppt; Marandino et al., 2007), North Pacific gyre (44 ± 28 ppt; Marandino et al., 2007), western equatorial Pacific (76 ± 52 ppt; Marandino et al., 2013), North Atlantic Gulf Stream waters (21 ± 9 ppt; Matrai et al., 1996), and tropical Pacific (42 ± 27 ppt; Kato et al., 2007). However, the DMS mixing ratios measured during the T1 transect are comparable to those over the central Arabian Sea (62 ± 53 ppt; Gupta et al., 2025). The background levels of DMS obtained during the present campaign are higher than those over the Arabian Sea in November 2021 (Gupta et al., 2025).

4.3.2 Longitudinal variation of DMS along east-west and west-east transects

The DMS levels in the Bay of Bengal increased west to east along both T1 and T3 longitudinal transects (**Figure 4.4**). Higher afternoon background DMS ($\sim$ 70–90 ppt) were measured along T3, compared to 45–60 ppt over the T1 transect. The instances of anomalously low DMS mixing ratios of $\sim$ 40–50 ppt in the coastal ($\sim 80^{\circ}$E) and open ocean ($\sim 92^{\circ}$E) were due to influences of continental transport and episodes of heavy rain, respectively. Interestingly, all broad peaks of DMS along T3 occurred around midnight hours (**Figure 4.4a**), which could be due to the entrainment of subsurface DMS into the oceanic mixed layer leading to enhanced oceanic emissions (Simó & Dachs, 2002) and reduced photo-oxidative loss in the atmosphere.

Decreased radical chemistry due to dominance of cleaner marine air mass and consequently lower NO_3 concentration could be a crucial factor in elevated nighttime levels particularly in offshore and open ocean regions of T3. In contrast, several major DMS enhancements along T1 were observed during daytime, and were associated with anomalously high-wind episodes

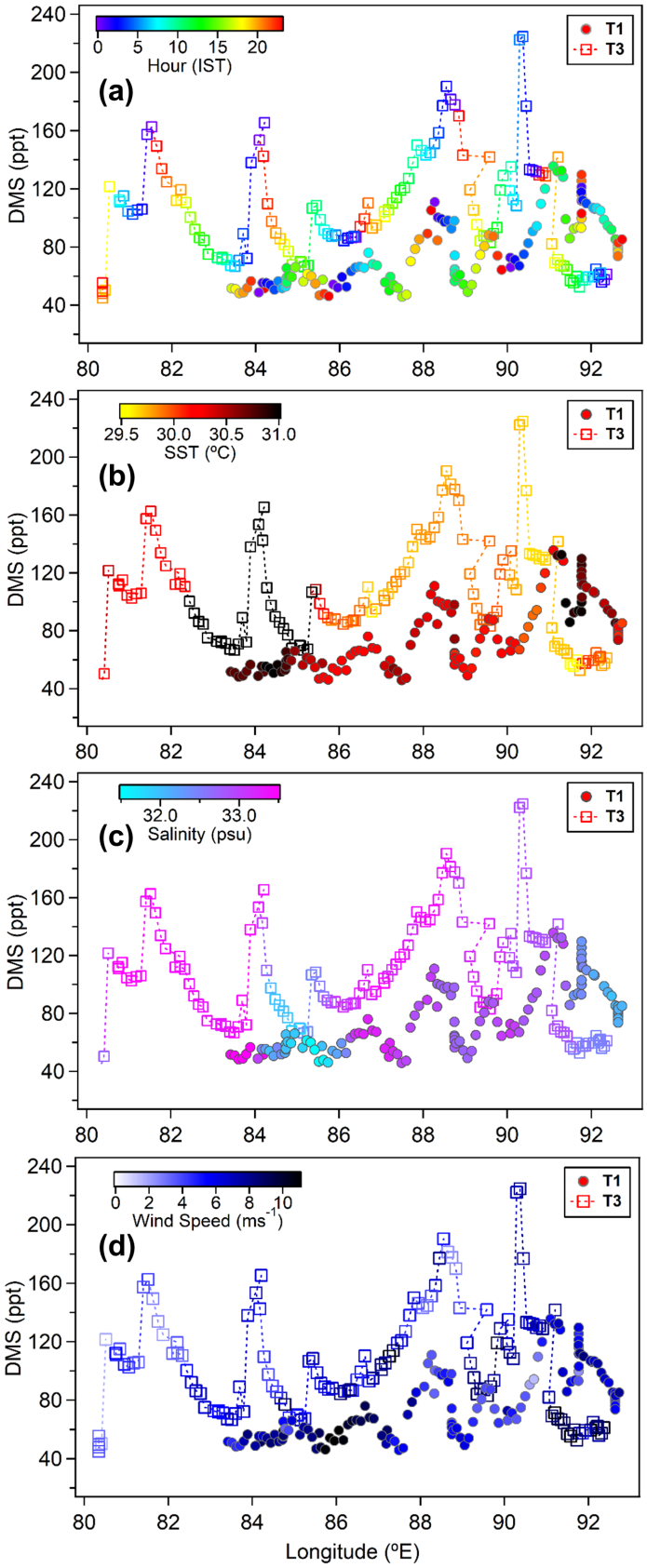

Figure 4.4: *Longitudinal variations of the DMS mixing over the Bay of Bengal during the T1 (triangles) and T3 (open square) transects, color-coded with (a) hour of the day in IST, (b) SST, (c) salinity, and (d) wind speed.*

(**Figure 4.4d**) and transport from the coral-rich Andaman shelf region (**Figure 4.5**). In the open ocean regions (> 82°E), except around 92°E, the higher DMS levels were typically associated with lower SST and higher salinity values (**Figure 4.4b**, **c**).

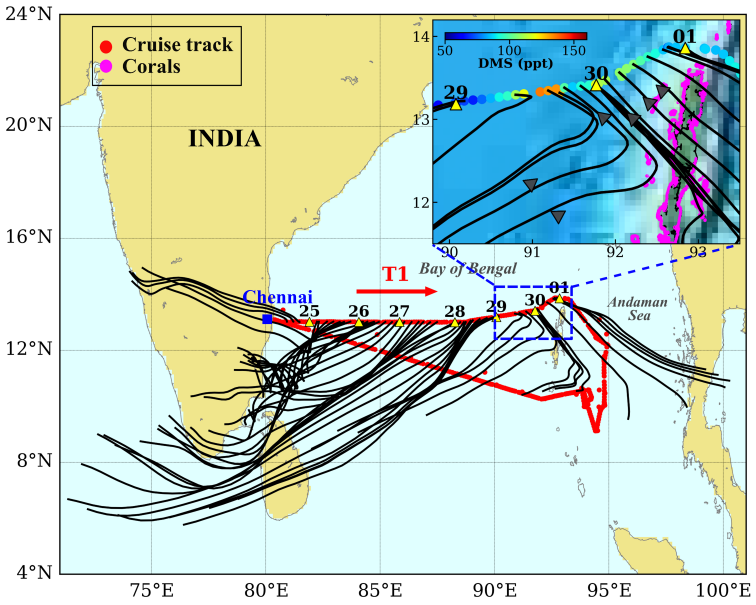

Figure 4.5: *Air mass back-trajectories over the Bay of Bengal during the T1 transect (25-30 September 2021). The inset plot shows the observed DMS mixing along the track during 29–30 September 2021.*

4.3.3 Diurnal variation of DMS

The mean and median diurnal patterns of the DMS mixing ratio have been investigated to understand the causes of short-scale variations along the three transects covered during the campaign (**Figure 4.6**). The hourly mean diurnal DMS varied in the ranges of 65–85 ppt and 80–110 ppt along T1 and T3, respectively, over the Bay of Bengal, and 90–150 ppt along T2 over the Andaman Sea. The diurnal patterns show enhancements in the morning (06–08 hr), followed by a gradual decline to the lowest concentrations in the afternoon. The median DMS patterns show a significant build-up from evening to midnight over T1 and T3. The $\mathrm{DMS} + \mathrm{OH}$ oxidation reaction can be a major factor leading to the daytime decrease of the DMS mixing ratio in the tropical MBL (Chen et al., 2018). The effect of $\mathrm{DMS} + \mathrm{OH}$ oxidation on diurnal variability is particularly noticeable during the DMS

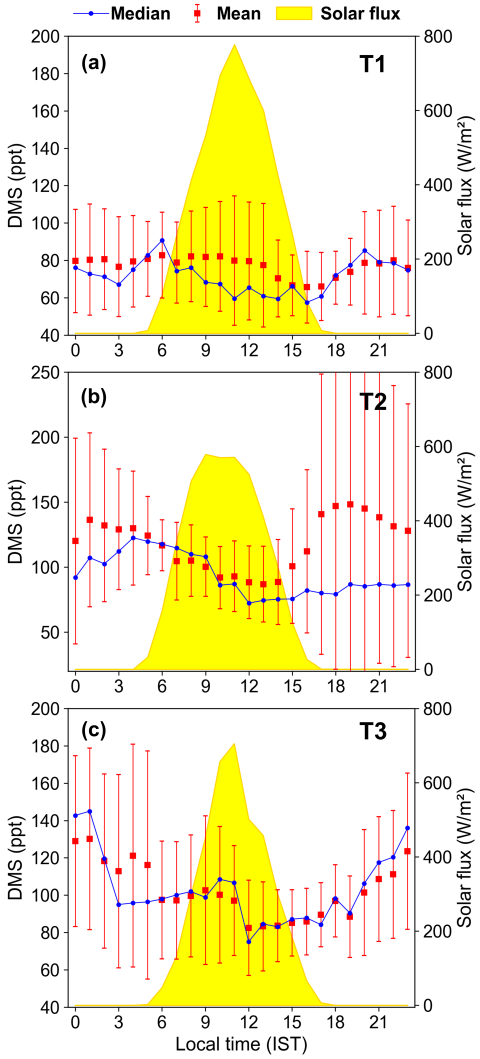

Figure 4.6: *The average ($\pm 1\sigma$) and median diurnal patterns of the DMS mixing ratio and mean solar radiation flux measured in the MBL along (a) T1 and (c) T3 transects in the Bay of Bengal, and (b) T2 transect in the Andaman Sea, during 25 September–14 October 2021.*

enhancement events on 3 and 12 October (**Figure 4.6a,c**). Despite elevated DMS levels triggered by salinity and SST change on 3 and 12 October (**Figure 4.7a,c**), a significant decline in the daytime DMS mixing ratios indicates loss from OH-oxidation under clear or partly cloudy conditions. However, measurements on cloudy days show a daytime (06–17 hrs) build-up of DMS in the MBL (e.g., **Figure 4.7b**), indicating reduced photo-oxidation of DMS. The nighttime measurements near the polluted eastern coastal regions of India along T1 and T3 could have been strongly influenced by the $\mathrm{DMS} + \mathrm{NO_3}$ reaction, contributing to the observed gradual decline of the

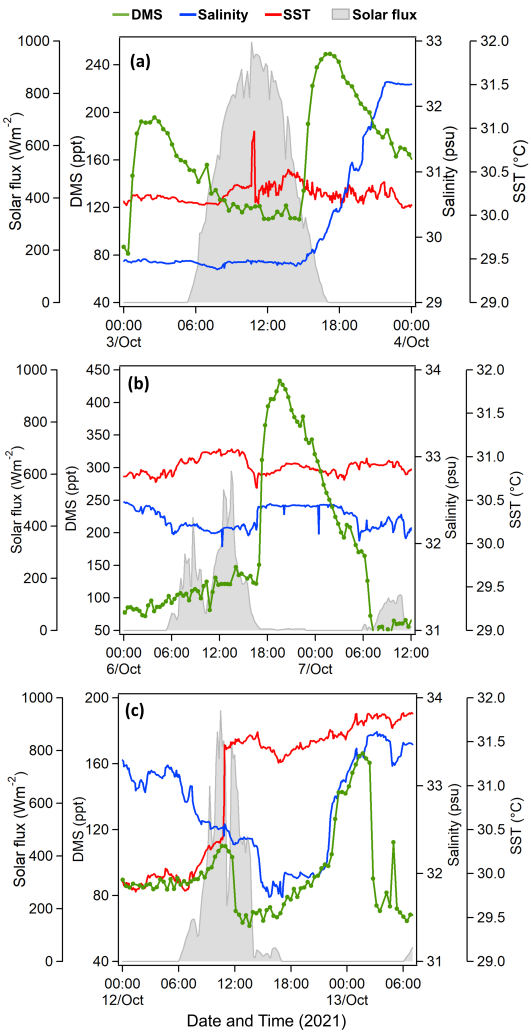

Figure 4.7: *The diurnal features of salinity, SST, and DMS mixing ratio for selected days over the Bay of Bengal.*

DMS mixing ratio from midnight to early morning (Stark et al., 2007).

Except in the early morning (03–06 hr), the DMS mean and median diurnal patterns over T3 exhibit similar levels and variability (**Figure 4.6c**). However, there are significant differences between mean and median patterns in the daytime (07–15 hr) over T1 (**Figure 4.6a**) and in the night-early morning over T2 (**Figure 4.6b**). The differences between the mean and median DMS patterns, with large standard deviations, suggest the impact of varied sources in response to changes in meteorological and sea surface parameters. In particular, the significant differences over T2 in the Andaman Sea can be attributed to anomalous DMS enhancements near the localized sources, as discussed in Section 3.3.1. Similarly, on 29 September

over T1 in the Bay of Bengal, despite the loss of DMS by OH-oxidation, the higher daytime mixing ratios were associated with the change in wind direction and back trajectory, indicating transport from the coral shelf of Andaman Islands (**Figure 4.5**).

To a large extent, the diurnal cycles of DMS in the MBL of the Bay of Bengal (**Figure 4.6a, c**) are similar to those observed over oligotrophic open ocean regions (Royer et al., 2015 and references therein). We have reported similar diurnal variability of the DMS mixing ratio in the oligotrophic central Arabian Sea in November 2021 (Gupta et al., 2025). The diurnal cycles of DMS, with a late afternoon minimum and an early morning maximum, have been reported at Cape Grim (40–70 ppt) (Ayers & Gillett, 2000), over the western Arabian Sea (25–60 ppt) (Warneke & de Gouw, 2001), at Kiritimati in the tropical Pacific (120–200 ppt) (Bandy et al., 1996), and in the Gulf of Maine in the North Atlantic (50–150 ppt) (Stark et al., 2007). The average diurnal amplitude of DMS (maximum/minimum ratio) of ∼1.42 in the Bay of Bengal is comparable to that of ∼1.5 over the central Arabian Sea (Gupta et al., 2025) and is within the range (1.2–1.7) reported in the remote marine atmosphere with moderate to low ocean productivity (de Bruyn et al., 2002; Lawson et al., 2020a; Sciare et al., 2000).

4.3.4 Impact of atmospheric instability and convective downdrafts on DMS variability

A rapid change in θ_E and other meteorological variables in the MBL indicates the presence of convective activities, particularly the downdraft events in the post-monsoon season over the Bay of Bengal (Sahu & Lal, 2006). Typically, θ_E of an air parcel in the lower troposphere declines sharply during the downdrafts and quickly recovers via near-surface fluxes (Alland et al., 2021). The instantaneous and large fluctuations in wind parameters characterize the effects of localized convective downdrafts, also called microbursts (La & Messager, 2021; Windmiller et al., 2023). Therefore, in addition to the advection of air masses (transport) from different regions, vertical mixing associated with convective downdrafts and atmospheric in-

stability can cause short-term variations of the DMS mixing ratio in the tropical MBL.

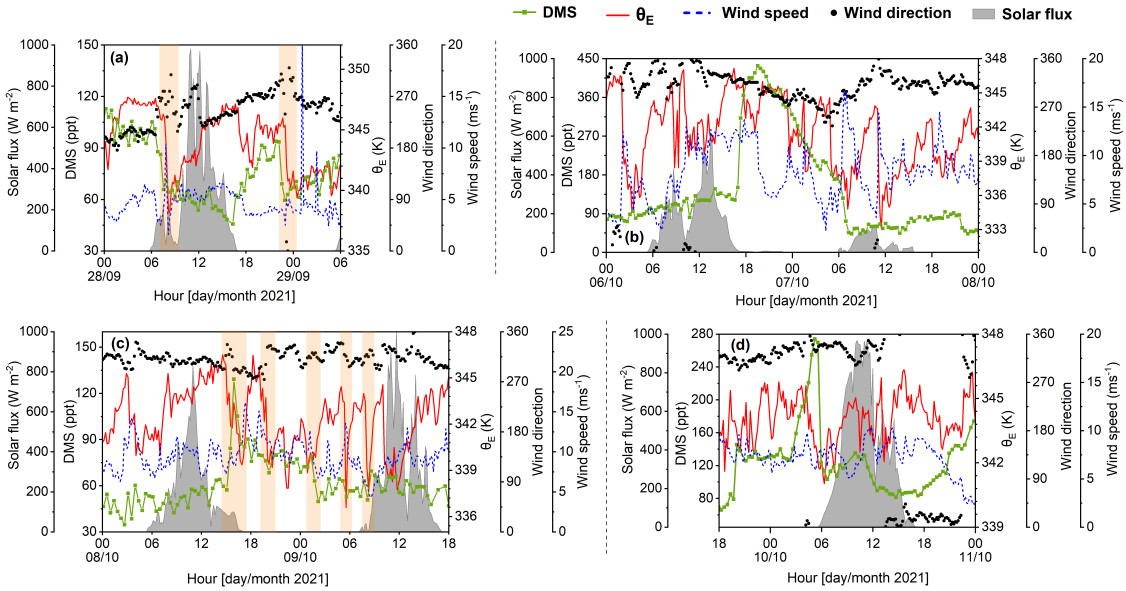

Figure 4.8: *The variations in DMS mixing ratios, equivalent potential temperature (θ_E), solar flux, wind speed, and wind direction during (a) 28–29 September, (b) 6–7 October, (c) 8–9 October, and (d) 9–10 October 2021 over the Bay of Bengal.*

The variations in θ_E during 6–9 October indicate the occurrence of multiple convective downdraft events (**Figure 4.8b,c**). The drops in the DMS mixing ratio, coinciding with a sharp decline in θ_E and abrupt changes in wind parameters were observed during 28–29 September and 6–10 October. For example, sudden drops (~ 250 ppt) in the DMS mixing ratio were associated with a sharp decrease in θ_E (~ 8–10 K) in the early morning (06–07 hr) and midnight (23–00 hr) of 28–29 September (**Figure 4.8a**). The measurements of consistently low DMS concentrations in the Andaman Sea (**Figure 4.8b**) were associated with recurring high amplitude fluctuations in θ_E during rain and thunderstorm events and indicate presence of intense convective downdrafts. However, despite the vigorous mixing in the MBL, a DMS peak (~ 450 ppt) on 6 October at ~ 17 hr suggests measurements near an intense and localized DMS source. During 8–9 October, very low DMS concentrations of ~ 60 ppt in nighttime were observed with a drop in θ_E (~ 5 K) and remained low due to the recurring downdrafts (**Figure 4.8c**).

Although the amplitudes of θ_E fluctuations during 9–10 October (**Figure 4.8d**) were smaller than in other instances, similar reductions in the DMS mixing ratios were observed in the daytime.

In addition to intrusion of DMS-deficient free tropospheric air, reduced air-sea exchange of DMS due to the stratification of the ocean surface during rainfall events could contribute to the decreased DMS mixing ratio. During the post-monsoon season, meteorological disturbances like tropical cyclones and convective activity play a growing role in the Bay of Bengal as the warmer SST increases moisture content, boosts heat fluxes, reduces vertical wind shear, and enhances atmospheric instability, making the Bay of Bengal conducive for the development of convective systems (Balaguru et al., 2014). These convective clouds can also bring substantial rainfall without intensifying cyclonic disturbances in October (Zuidema, 2003).

4.3.5 Role of picophytoplankton in DMS emissions

The small-scale variability of atmospheric DMS in marine air can also be controlled by the biomass abundance and bacterial metabolic activities (Bullock et al., 2017). In the inter-monsoon periods, the phytoplankton composition in the open Bay of Bengal and Andaman Sea is dominated by cyanobacteria, including picophytoplankton (*Prochlorococcus* and *Synechococcus*) and *Trichodesmium* (Hegde et al., 2008; Jyothibabu et al., 2014, 2017; Mitbavkar et al., 2020; Wei et al., 2020), followed by lower abundances of diatoms in the central Bay of Bengal (Löscher, 2021; Paul et al., 2007). However, in coastal waters of the Bay of Bengal, large abundances of diatoms and Dinophyceae have been reported (Baliarsingh et al., 2015; Manigandan et al., 2024; Vajravelu et al., 2018).

Although cyanobacteria and diatoms are low DMSP-producing phytoplankton species (McParland & Levine, 2019), the spatial differences in nutrient availability and population density in surface waters can modulate the seawater concentrations and, subsequently, the air-sea fluxes of DMS. Nonetheless, previous studies have shown that picophytoplankton can also

be an important source of DMSP in warm oligotrophic surface seawaters (Corn et al., 1996).

We have used picophytoplankton (*Synechococcus* and *Prochlorococcus*) cell abundance and nutrient concentrations measured in the surface seawaters at five stations to investigate their impact on regional variability of observed DMS. Sampling stations S1 and S2 were located in the open central Bay of Bengal, S3 in the north of Andaman Islands, S4 in the central Andaman Sea, and S5 in the coastal Bay of Bengal. Although DMS concentrations showed an overall increase with the *Synechococcus* cell abundance, its relation with *Prochlorococcus* was not consistent. Peng et al. (2024) have also reported a boosting impact of *Synechococcus* and *Prochlorococcus* abundances on the seawater DMS(P) concentrations in the Bay of Bengal during the post-monsoon season of 2020. However, discrepancies in DMS-picophytoplankton variability over stations S1 and S2 in our data suggest influence of additional processes.

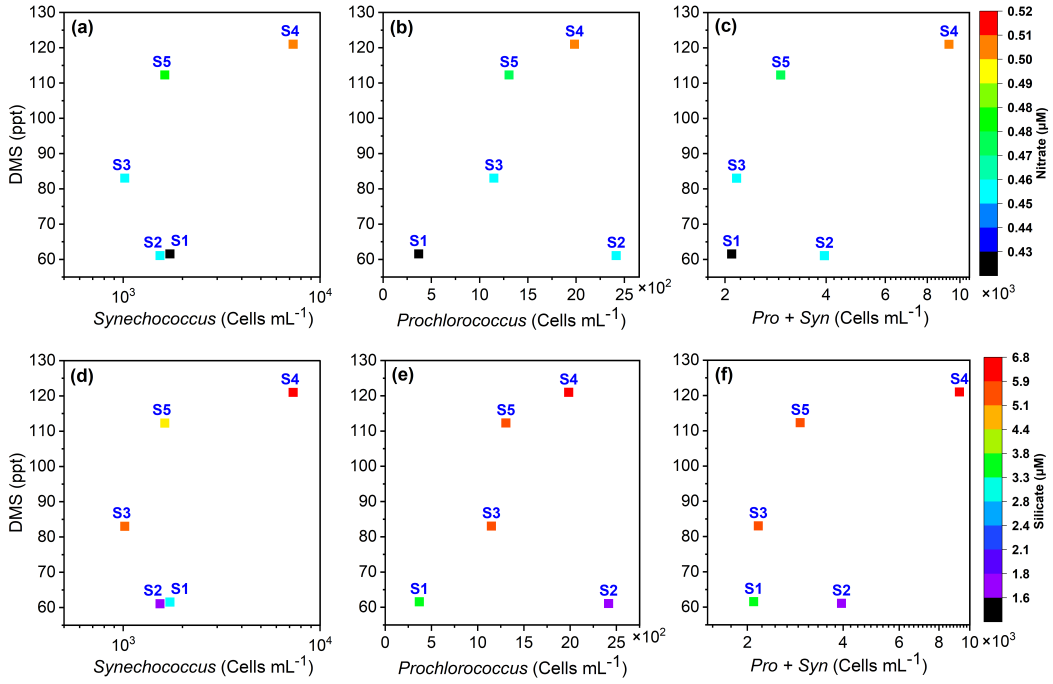

Figure 4.9: *Scatterplots of the DMS mixing ratio with Synechococcus, Prochlorococcus, and combined cell abundance color-coded with (a-c) silicate and (d-f) nitrate concentrations in the surface seawater at different stations (S1-S5) in the Bay of Bengal during post-monsoon 2021.*

Further analysis of silicate (SiO_4^{3-}) and nitrate (NO_3^-) nutrient concentrations at each station reveal an increase of DMS mixing ratio with increasing nitrate concentrations at all stations except for station S2 (**Figure 4.9**). Despite similar nitrate levels and higher abundances of *Synechococcus* and *Prochlorococcus* cells, the DMS levels at S2 were lower than those at S3. However, silicate concentration at station S2 was also lower (< 1.8 μM) than at other stations (**Figure 4.9d-f**). Silicate-rich waters favour diatom growth (Kristiansen & Hoell, 2002) with silicate > 2 μM, and high silicate to nitrate ratios provide optimal conditions for the development of diatoms (EGGE & Aksnes, 1992; Sommer, 1994).

Even though the abundance and diversity of diatoms are typically low in oligotrophic open ocean waters as their growth is limited by nitrate or phosphate availability, they can still thrive in nitrate-depleted waters (Bender et al., 2014). Despite the nitrate-limited conditions (< 1 μM) in our observations (**Figure 4.9a-c**), DMS levels are higher for relatively higher nitrate and silicate concentrations. Thus, the abundance of diatoms could be a critical modulator of DMS concentration in the Bay of Bengal. The diatoms have also been reported to be major contributors to the DMS concentration in the upper 40 m water column of the Bay of Bengal (6–20°N) (Shenoy et al., 2006). Moreover, the intercellular DMSP in diatoms can increase up to 16-fold under stress induced by nitrate-limitation (Bucciarelli & Sunda, 2003; Sunda et al., 2007).

Paul et al. (2007) have reported a strong relationship between diatoms (accounting for 97.5% of the phytoplankton species) and seawater DMS in the Bay of Bengal during the summer monsoon of 2001. Manigandan et al. (2024) have also reported the dominance of diatoms in southwest coastal waters of the Bay of Bengal in the post-monsoon season, supporting the enhancement of diatom populations with silicate availability. Moreover, instances of co-occurrence of cyanobacteria and diatoms and their symbiotic relationships have been highlighted in different parts of the northern Indian Ocean (Kulkarni et al., 2010; Manjumol et al., 2018; Pujari et al., 2019).

4.3.6 Estimation of DMS flux over the Bay of Bengal

Though the measurements are limited, the available literature data show significant spatial and seasonal variations of the seawater DMS concentration in the Bay of Bengal. Higher seawater DMS concentrations (1–8 nM) and fluxes (2–10 μmol m^{-2} d^{-1}) had been observed over the Bay of Bengal in the summer monsoon, attributed to the upwelling of nutrient-rich waters and stronger southwest (SW) winds (Shenoy et al., 2000; 2007). While relatively lower DMS fluxes (1–5 μmol m^{-2} d^{-1}) were reported in the post-monsoon season, attributed to weaker transition winds and reduced vertical mixing (Shenoy et al., 2007).

Kumari et al. (2019) have reported changes in seawater DMS concentration and flux in the coastal waters of the Bay of Bengal during the passage of cyclone Hudhud during 7–14 October 2014. This reduction was attributed to strong salinity stratification from heavy rainfall and runoff, which limited nutrient upwelling and phytoplankton growth. The seawater DMS concentrations of 8.8–33.5 and 0.4–3.9 nM and fluxes of 5.8 ± 3 and 2.8 ± 2 μmol m^{-2} d^{-1} were reported for the pre- and post-cyclone periods, respectively. Rao et al. (2015) have reported elevated DMS fluxes (up to 8 μmol m^{-2} d^{-1}) in the coastal Bay of Bengal due to the nutrient supply from riverine discharge during the post-monsoon season. In a recent study by Peng et al. (2024), the variations in the seawater DMS concentration (2–10 nM) and flux (2–12 μmol m^{-2} d^{-1}) over the eastern Indian Ocean (EIO) covering the central Bay of Bengal during October–November 2020 were attributed to biogeochemical processes influenced by the Wyrtki jets, Bay of Bengal runoff (BBR), and South Equatorial Current (SEC). In this study, C_w (2.35–2.70 nM) estimated using G18 with satellite Chl-a, were nearly the same at all the stations (**Table 4.2**). The parametrized C_w values (mean: 2.5 ± 0.2 nM) in the present study are well within the range of mean C_w values reported for other basins (1.6–3.8 nM). Our estimates of C_w are comparable to the measurements by Peng et al. (2024) between 0–15°N in the open Bay of Bengal (~3–7 nM) during the post-monsoon season of 2020.

Table 4.2: *The estimated surface water (depth 2 m) concentrations and air-sea fluxes of DMS at different CTD stations along the cruise track.*

St.	Date and time (IST)	Lat (°N)	Lon (°E)	C_w[a] (nM)	u (m s^{-1})	C_a (ppt)	F_{DMS}[b]
S1	26/09/2021 10:30	13.01	84.74	2.70	12.5	62	29.38
S2	28/09/2021 10:30	13.00	88.74	2.35	5.8	61	5.73
S3	30/09/2021 14:30	13.87	92.64	2.40	6	83	6.26
S4	03/10/2021 11:00	11.66	94.78	2.70	5.5	119	5.94
S5	14/10/2021 10:30	13.00	80.75	2.42	4	112	2.89

[a] Concentration of DMS in surface seawater estimated using **G18**.
[b] Air-sea flux of DMS (μmol m^{-2} d^{-1}) estimated using the bottom-up ($F_{b\text{-}u}$) parameterization.

Flux estimates using the bottom-up approach (F_{b-u} hereafter) range between 2.9–6.7 μmol m^{-2} d^{-1} over most stations (**Figure 4.2**). However, the F_{b-u} value corresponding to wind speed $u > 10$ m s^{-1}, at station S1, increased by an order of magnitude (29.4 μmol m^{-2} d^{-1}), despite the low atmospheric DMS concentrations over S1. In contrast, the lowest F_{b-u} values at the coastal station (S5) were noted during calm winds, despite the high atmospheric DMS concentrations. This indicates that the parameterizations in the F_{b-u} approach could overestimate the flux when wind speed is greater than 10 m s^{-1} over the low Chl-a regions and underestimate it in low wind speed regions. The tendency of gas-transfer-velocity parameterization to overestimate the DMS flux has been highlighted in other studies (Yang et al., 2011), but could also arise from the coarse temporal resolution of the Chl-a data and the dilution effect caused by stronger winds.

Further, the nighttime build-up rates of DMS at five different locations (**Figure 4.10**) in the open ocean were used to calculate the DMS flux using the top-down approach (Eq. 2.11; F_{t-d} hereafter). The highest flux of ~ 10.22 μmol m^{-2} d^{-1} was estimated over N5 (**Table 4.3**) during 9–10 October in the open Bay of Bengal, where the DMS measurements experienced minimal atmospheric loss, as discussed in Section 3.3.1. The fluxes (~ 2.5 μmol m^{-2} d^{-1}) over N1 and N2 along the T1 transect are lower than the fluxes of ~ 4.7 μmol m^{-2} d^{-1} over N3 and N4 along the T2 transect.

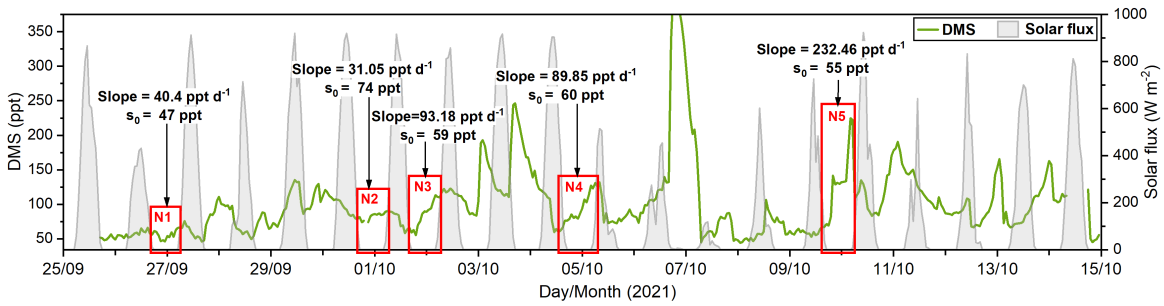

Figure 4.10: *Time series variations of the DMS mixing ratio and solar flux over the Bay of Bengal during 25 September–14 October 2021. Red boxes highlight the nighttime DMS used to calculate the build-up rate (slope) and mixing ratio (so) at the beginning of build-up for top-down estimations of DMS flux.*

Nonetheless, the F_{t-d} values (mean $\sim 4.9 \pm 3.2$ μmol m^{-2} d^{-1}) are comparable to F_{b-u} (mean $\sim 5.2 \pm 1.6$ μmol m^{-2} d^{-1} [for $u < 10$ m s^{-1}]). The DMS fluxes estimated over the open Bay of Bengal ($F_{t-d} \sim 3.5 \pm 1.2$ μmol m^{-2} d^{-1}) in this study are $\sim$2 times higher than that of ~ 1.6 μmol m^{-2} d^{-1} estimated during the Bay of Bengal Monsoon Experiment (BOBMEX) campaign in the post-monsoon season of 1998 (Shenoy & Kumar, 2007). However, our estimates for the post-monsoon season are still lower than the summer monsoon flux (~ 11.5 μmol m^{-2} d^{-1}) over the Bay of Bengal reported by Shenoy & Kumar (2007).

Table 4.3: *The top-down estimates of air-sea fluxes of DMS (F_{DMS}) using the nighttime build-up of DMS in the MBL. $\dot{S}_n$ represents the nighttime build-up rate, while S_0 refers to the DMS mixing ratio measured at the beginning of the build-up period.*

S. No.	**Dates (2021)**	**$\dot{S}_n$(ppt d^{-1})**	**S_0 (ppt)**	**F_{DMS}(μmol m^{-2}d^{-1})**
N1	26-27 Sep	40.4	47	2.42
N2	30 Sep-01 Oct	31.05	74	2.51
N3	01-02 Oct	93.18	59	4.73
N4	04-05 Oct	89.85	60	4.61
N5	09-10 Oct	232.46	55	10.22
			Mean	**4.9 $\pm$ 3.2**

The DMS fluxes over the Bay of Bengal were on the higher end of the range reported for other oligotrophic regions, such as the western Pacific Ocean (~ 3.68 μmol m^{-2} d^{-1}; Xu et al., 2021), Mediterranean Sea (~ 2.5 μmol m^{-2} d^{-1}; Simó & Grimalt, 1998), south Pacific gyre (~ 3.8 μmol m^{-2} d^{-1}; Marandino et al., 2009), north Pacific gyre (3.0 ± 1.6 μmol m^{-2} d^{-1}), etc. The studies cited in **Figure 4.11** have reported elevated DMS fluxes in the biologically productive regions (upwelling or frontal zones) compared to low productivity regimes (like gyres and equatorial warm pools), which is consistent with our findings. Interestingly, the monthly mean DMS fluxes of 2–10 μmol m^{-2} d^{-1} retrieved from the climatological datasets over the Bay of Bengal in October (Hulswar et al., 2022; Lana et al., 2011) are comparable to the present estimates. Based on the DMS fluxes estimated in the present study, the annual sulfur emission is ~ 0.14 Tg S yr^{-1} over the Bay of Bengal. However, this value could be underestimated as it does not account for the DMS fluxes during the monsoon season, which can be significantly larger than the post-monsoon season, as reported in previous studies (Shenoy & Kumar, 2007).

4.3.7 DMS variability across the northern Indian Ocean

The unprecedented high-resolution atmospheric DMS measurements over the Arabian Sea (Gupta et al., 2025) and Bay of Bengal [provide an excellent opportunity to highlight the key variability features attributed to the distinct oceanic and atmospheric conditions in these two basins of the northern Indian Ocean in the post-monsoon season](). The regional variability of DMS over the Arabian Sea was driven primarily by local biogeochemistry and biomass abundance, while the Bay of Bengal, air mass source, and transport played a significant role. Most DMS enhancements over the Arabian Sea were associated with local biomass abundance, and only 12% of enhancements correspond to airmass transport with high E_a (> 0.18). On the other hand, the elevated (lower) DMS levels in the Bay of Bengal were primarily measured in high (low) E_a regimes, indicating lesser impact of local sources and significant contributions from DMS-rich

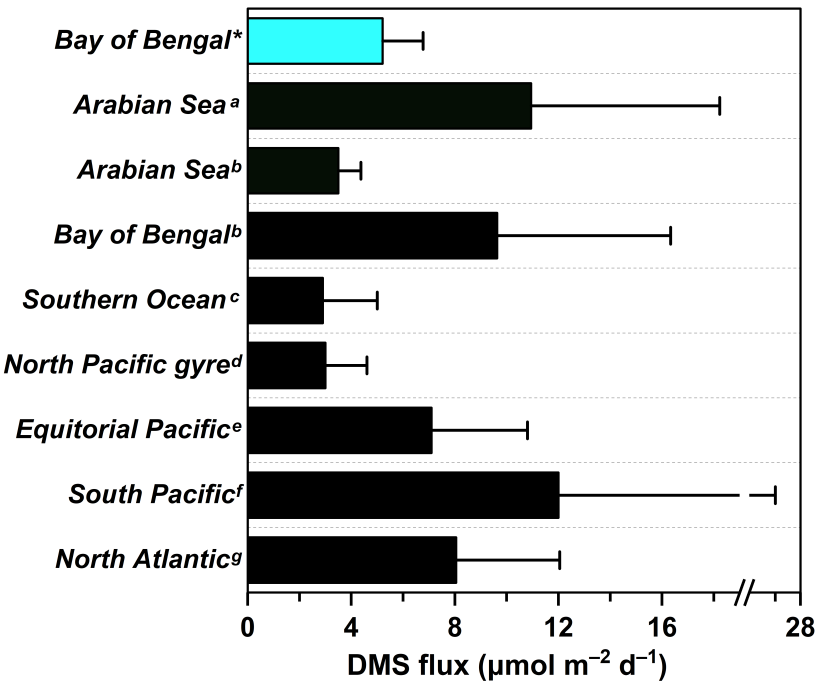

Figure 4.11: *Comparison of DMS fluxes reported for the different oceanic regions of the world. [*present study, [a–g] Gupta et al., 2025 and references therein]*

air masses from productive southwest regions, including coastal Sri Lanka. Influences of coral emissions were most prominent in the eastern Bay of Bengal, then the rest of the northern Indian Ocean, where transport from the coral-rich Andaman Shelf was a major contributor to the DMS enhancements. Furthermore, the short-term DMS variability in the Arabian Sea was influenced primarily by surface ocean processes, particularly salinity fluctuations. However, over the Bay of Bengal, atmospheric instabilities, including convective downdraft events, contributed strongly to the short-term changes in DMS. Our studies over both basins establish the effect of atmospheric ventilation on the DMS levels in the MBL of the open and offshore waters of the northern Indian Ocean, except for regions with strong local DMS emission sources such as the coastal Arabian Sea and Andaman Sea.

The DMS mixing ratios in the Bay of Bengal and central Arabian Sea showed lower spatial-temporal variability than the high Chl-a waters of the Arabian Sea. This could be associated with the oligotrophic biogeochemical

conditions in both the open ocean regions of the northern Indian Ocean during the post-monsoon season. Royer et al. (2015) have reported larger DMS variability scales of up to 200 km in oligotrophic open ocean waters than in tropical coastal waters (< 15 km). The studies over the Arabian Sea (Gupta et al., 2025) and southern coastal regions of the Indian subcontinent show that the interactions of continental and marine air masses can modulate the DMS oxidation chemistry and variability in the MBL of the northern Indian Ocean.

The DMS flux from the Arabian Sea (~ 11 μmol m^{-2} d^{-1}; Gupta et al., 2025) during the post-monsoon season is twice the flux from the Bay of Bengal during the same season (~ 4.9 μmol m^{-2} d^{-1}; this study). Based on these flux data, we estimate an annual DMS emission of 1.21 Tg yr^{-1} from the northern Indian Ocean. However, this estimate could be subject to uncertainties due to limited availability of seasonally resolved measurements as discussed in Section 4.3.6. In summary, consideration of atmospheric processes, including enrichment/dilution from air mass transport and convective instabilities under varying biogeochemical regimes, is crucial for reducing the uncertainties in model studies investigating the roles of atmospheric DMS on secondary aerosol production and cloud formation over the northern Indian Ocean.

4.4 Conclusion

This study presents the first shipborne *in situ* measurements of the DMS mixing ratio in the MBL of the Bay of Bengal and Andaman Sea during the post-monsoon season of the year 2021. Analysis of high time-resolution DMS data reveals large variations with distinct longitudinal dependencies in the central Bay of Bengal caused by the interplay of oceanic and atmospheric parameters. The episodes of convective downdrafts and mesoscale instabilities over the central Bay of Bengal caused short-term fluctuations in the DMS mixing ratio. The intermittent measurements of relatively lower and higher DMS mixing ratios were due to the transport of air masses from

peninsular India and high Chl-a coastal regions of Sri Lanka, respectively. The continental outflow and transport of air masses with higher E_a were predominant factors in lower and higher DMS levels measured during the west-east and east-west longitudinal transects, respectively. Though the DMS diurnal features varied depending on the measurements in coastal and open oceanic regions, the impact of daytime photo-oxidation loss by OH radical was evident throughout the campaign. The diurnal variability of DMS in the coastal regions reflected the combined effects of oceanic emissions, transport of continental air, and nighttime radical chemistry. The transport of air masses from the Andaman shelf region caused significant enhancements in the DMS mixing ratio around the Andaman Islands.

The DMS level increased with the increasing silicate concentrations over the picophytoplankton abundance, indicating significant DMS emissions from diatoms. The mean DMS flux of $\sim 4.9 \pm 3.2$ μmol m^{-2} d^{-1}, calculated based on nighttime build-up at different locations, is comparable to the climatological fluxes over the study region. An average open-ocean flux of DMS (3.5 ± 1.2 μmol m^{-2} d^{-1}) was almost twice the values reported during the BOBMEX-1998 post-monsoon expedition. Though atmospheric processes were able to explain many of the DMS variability features, further studies are required to investigate the role of phytoplankton community structure in DMS production and emissions to assess the roles of different physico-chemical factors controlling seawater DMS production. The contribution of significant DMS emissions from the coral reefs to the non-sea-salt sulfate (nss-SO_4^{2-}) aerosol formation over the Bay of Bengal and Andaman Sea can be an important aspect for future investigations.

Chapter 5

Effect of DMS emissions from coral reefs around the Andaman Islands

Key takeaways

- Tidal stress-induced emissions from corals in the Invisible Bank and Andaman shelf region significantly enhanced DMS levels over the Andaman Sea
- Corals are an important source of DMS to the MBL over the Andaman Sea, with an estimated flux of ~ 0.5 μmol m^{-2} hr^{-1} under tidal stress and an annual sulfur emission of ~ 1.43 Gg S yr^{-1} from the Andaman and Nicobar coral reef area

5.1 Introduction

In addition to marine phytoplankton, emissions from coral reefs are a significant source of atmospheric DMS at regional scale (Jackson et al., 2020a; Jones et al., 2018). High concentrations of DMSP (up to ~ 54 μM) and DMS (up to ~ 19 μM) have been measured in coral reef-dense areas of the Great Barrier Reef (GBR) region (Broadbent & Jones, 2004; Swan, 2022). The DMS emissions from coral reefs are associated with the metabolic activities of coral polyps and their endosymbiont zooxanthellae (algae) in coral tissues, and the coral bacterial community (Broadbent & Jones, 2004; Deschaseaux et al., 2019; Guibert et al., 2020; Raina et al., 2013). Although

not well quantified, the production and emission of DMS and DMSP from coral reefs are recognized to be highly sensitive to oxidative stresses caused by air exposure, alleviated UV-irradiance, warmer SST, desiccation, and hypoxia (Deschaseaux et al., 2014; Fiddes et al., 2021). The DMS(P) synthesis by coral polyps in the absence of algal endosymbionts highlights crucial climatic implications of coral bleaching under thermal stress (Raina et al., 2013). DMS from coral reefs can be emitted into the atmosphere via sea-to-air exchange processes or directly during aerial exposure of corals (Jackson et al., 2022). Thus, shallow depths and warm SST of the tropical coral reef shelf waters can facilitate high production and exchange of DMS. The annual flux of DMS from the global coral reef regions, based on emissions from the extensively studied GBR, is estimated to be ~ 0.3 Tg S yr^{-1}, which is $\sim 1.7\%$ of global DMS flux data. These DMS flux estimates are significant considering its release only from $\sim 0.2\%$ of the surface ocean (Fiddes et al., 2021; Jackson et al., 2020b).

The Andaman Sea is surrounded by extensive coral reefs in the Andaman and Nicobar Islands, along the coastline of Myanmar and Thailand, and the northwest tip of Sumatra. The Andaman and Nicobar Islands are one of the major coral reef regions of India, surrounded by narrow, linear, and well-developed fringing reefs in almost all the islands (Saroj et al., 2016). The total area occupied by coral reefs around the Andaman and Nicobar Islands is $\sim$ 1021 km^2 (SAC, 2010). Lakshmi et al. (2021) reported a large diversity of reef-building corals in 5 locations between 12–13°N.

As discussed in the previous chapter (Chapter 4), despite the stratified surface waters and a similar surface biogeochemistry as the Bay of Bengal, large DMS enhancements were observed in our measurements over the Andaman Sea compared to the Bay of Bengal. This highlighted influence of strong DMS source. In this chapter, we have investigated the role of coral reefs in the DMS enhancements over the Andaman Sea during SK#373 campaign in the eastern part of the northern Indian Ocean. Continuous measurements of DMS were conducted over the Andaman Sea [9–14°N; 93–95°E] during 1–8 October 2021.

5.2 Results and Discussion

5.2.1 Impact of coral reef emissions and environmental factors on DMS variability over the Andaman Sea

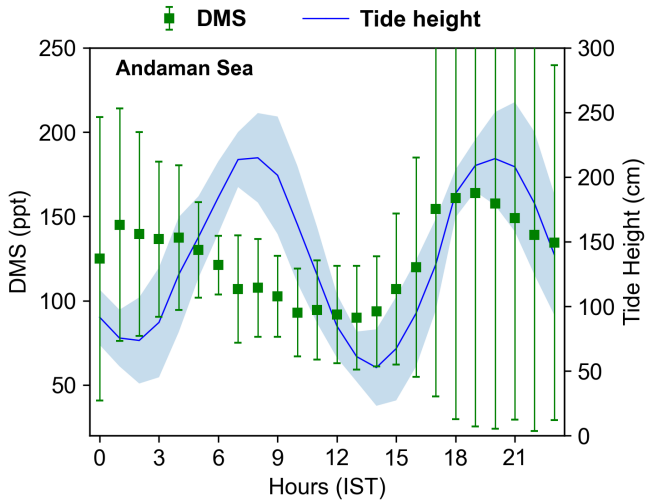

Figure 5.1: *Diurnal variation of the DMS mixing ratio over the Andaman Sea (green) and tidal height at the Aerial Bay coast (blue), Andaman Islands.*

Diurnal analysis of DMS mixing ratios and tide data suggests that the high DMS variability in our measurements over the Andaman Sea is largely affected by the coral reefs surrounding the Andaman Islands (**Figure 5.1**). The tide height data measured at Port Blair and Aerial Bay stations situated in the Andaman Islands revealed that the coast regions experience a semi-diurnal tide cycle. As shown in **Figure 5.1**, the DMS peak in the evening ($\sim$ 17 hr) coincides with the up-slope in the tide height between 14–18 hr, while another DMS peak at $\sim$ 01 hr LT occurs during the tidal low between 0–3 hr. A similar diurnal pattern of DMS mixing ratio has been reported by Jackson et al. (2020b) from long-term measurements at Heron Island in the GBR. Coral reefs have been recognized to release substantial amounts of DMSP, DMSO, and DMS in the seawater, and directly to the atmosphere due to aerial exposure during the low tides (Hopkins et al., 2016). Although corals could certainly make significant emissions of DMS over the Andaman Sea, the events of DMS mixing ratio seem to also be

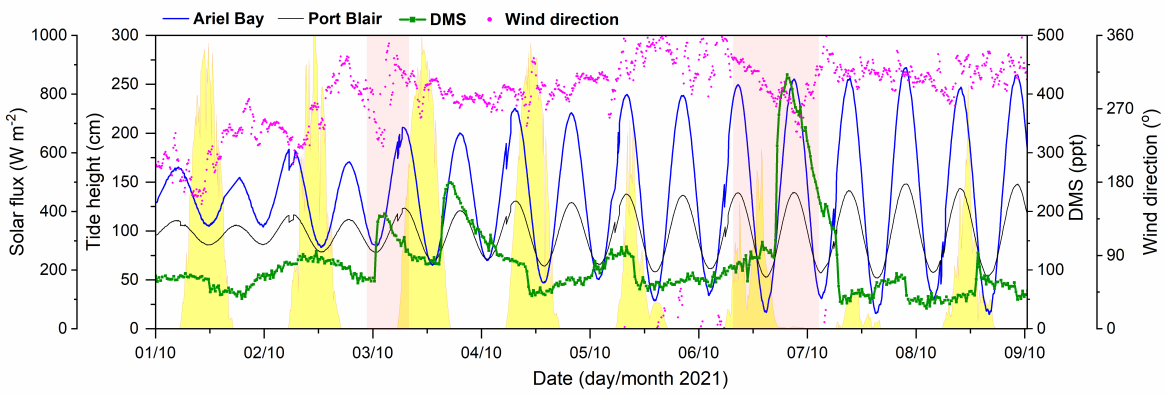

Figure 5.2: *Time series variations of the DMS mixing ratio and wind direction over the Andaman Sea and tidal heights recorded at Aerial Bay and Port Blair stations during 1-8 October 2021.*

regulated by meteorological factors and atmospheric processes controlling both the exchange and build-up in the MBL.

Further, tidal height and wind direction data were used to investigate the influences of coral emissions in the time series variation of the DMS mixing ratio over the Andaman Sea during 1–8 October 2021 (**Figure 5.2**). The highest DMS enhancement ($\Delta\mathrm{DMS} \sim 300$ ppt) above the background concentration (~ 110 ppt) over the Andaman Sea were observed during 6–7 October. This pronounced increase in the DMS mixing ratio was associated with the rapid change in wind direction from the north to northwest, leading to transport of air masses from the Andaman shelf region. In addition, the time series of the tide height data recorded at Port Blair and Aerial Bay stations reveal low tides, with large tidal amplitude, on the evening of 6 October, just prior to the DMS event. The transport of air masses from the exposed coral reefs in the upwind of the measurement locations could have led to the enhanced DMS levels. During 6–7 October, the rainfall events in the island region, around Port Blair (**Table 5.1**), and along the ship track in the Andaman Sea were recorded.

Other considerable peaks of DMS in this region were observed following the low tides at midnight (~ 200 ppt) and afternoon (~ 270 ppt) on 3 October. The DMS afternoon background levels (afternoon low due to photochemical loss) on 3 October were also elevated compared to other days

in the Andaman Sea. The spikes ($\Delta \sim 120$ ppt & 170 ppt at 00 and 14 hr, respectively) in DMS in these events are occurring at the tidal low, forming a peak at the upslope of tidal height (**Figure 5.2**).

Table 5.1: *Meteorological conditions at Port Blair, Andaman Islands, during 6–7 October 2021.*

Date	Time	Weather	Temperature (°C)	RH (%)
06-10-2021	02:30	Light rain. Overcast.	26	95
	05:30	Drizzle. Overcast.	25	95
	08:30	Light rain. Overcast.	24	96
	11:30	Light rain. Overcast.	25	98
	14:30	Rain. Overcast.	24	95
	17:30	Light rain. Overcast.	24	96
	20:30	Overcast.	25	97
	23:30	Overcast.	25	98
07-10-2021	02:30	Light rain. Overcast.	26	95
	05:30	Drizzle. Overcast.	25	95
	08:30	Light rain. Overcast.	24	96
	11:30	Light rain. Overcast.	25	98
	14:30	Rain. Overcast.	24	95
	17:30	Light rain. Overcast.	24	96
	20:30	Overcast.	25	97
	23:30	Overcast.	25	98

The measurement points of elevated DMS on 3 October are located parallel to the invisible bank (IB), which is a shallow submerged plateau to the east of the Andaman Islands (**Figure 5.3a**). The NOAA-coral data revealed presence of benthic corals in the central Andaman Sea and IB

(**Figure 5.3c**). The depth of IB can range from 2–100 m. The DMS enhancements on 3 October match strikingly well with IB depth variations, with high concentrations beside the shallow centre of IB and decreasing DMS levels as the ship moves away from the centre. The afternoon spikes in atmospheric DMS observed on 6 October are 2-3 times higher than on 3 October, which could be primarily due to higher tidal amplitude and lower solar flux on 6 October. Common wind conditions as of 6 October were observed, such as sudden changes in wind direction and relatively higher winds. The tidal lows render the coral reefs in shallow shelf

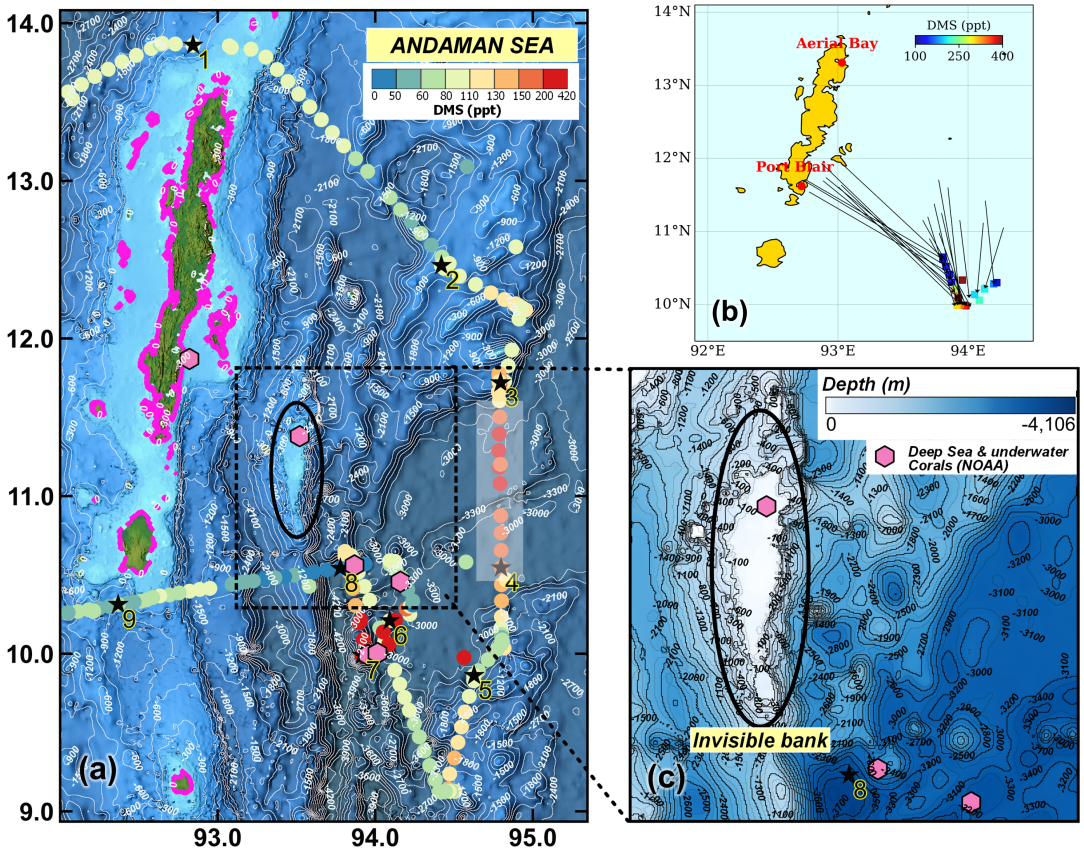

Figure 5.3: *(a) Bathymetric map of the Andaman Sea with DMS mixing ratio along the cruise track, (b) in situ wind vector over measurement location for the highlighted DMS episode during 6-7 October 2021, and (c) Invisible Bank and underwater coral data from NOAA. The contours represent the ocean depth in meters (m).*

waters exposed to the atmosphere, which releases a burst of DMS into the atmosphere. A consequent release of DMSP in the seawater after

resubmersion enhances the DMS concentrations in seawater (Hopkins et al., 2016). The oxidative stress, and hence the release of DMS from corals, is proportional to the extent of exposure. The presence of corals also suggests high DMS concentration from production by zooxanthellae in the coastal waters surrounding the Andaman Nicobar Islands. Swan et al. (2017) have reported the intense spikes of the atmospheric DMS concentration at low tides when convective precipitation fell onto the aerially exposed platform reef at Heron Island, southern GBR, Australia. This study established that the occurrence of rain events can intensify the low-tide emission of DMS from coral reefs. The rainfall events and the NW winds could have provided a favourable condition for the release of DMS from the coral reefs surrounding the Andaman Islands, followed by the dispersion of DMS-rich air masses over the central Andaman Sea. It is recognised that extensive fringing reefs are present throughout the Andaman Sea and they are particularly well developed in the Andaman and Nicobar Islands, along the coastline of Myanmar and Thailand, and the northern tip of Sumatra (Brown, 2007). The fringing reefs (dominated by *Alcyonarians* and *Acropora* species) are found to be well developed on the eastern sides of the islands, with the only 'barrier' reef on the west coast of the Andaman Islands. The experiments have shown that hard corals such as *Acropora spp.*, which is a dominant coral in the Indo-Pacific, can produce substantial amounts of seawater and atmospheric DMS (E. Deschaseaux et al., 2018; G. Jones et al., 2018). The reef-building corals in the Andaman region (12-13°N) are dominated by *Acropora* genus, recorded in 28 species of hard corals among a total of 124 species (Laxmilatha et al., 2021). Furthermore, the background DMS levels on 3 October were higher than on other days of measurements in the Andaman Sea (**Figure 5.2**). Two crucial factors could be supplementing the enhancements and the excessive background concentrations on 3 October: Transport of DMS through air mass travelling from DMS-rich warm tropical coral reef regions along the coast of Sumatra (**Figure 5.4**) as seen in air mass back-trajectory over the Anadama Sea transect (see Figure 4.1b); And increased

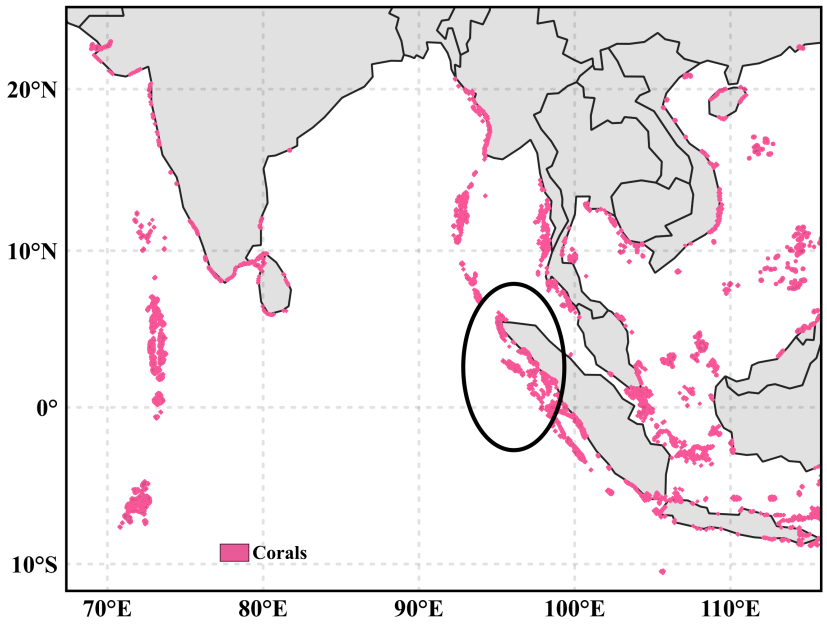

Figure 5.4: *Coral distribution map of the tropical Indian Ocean, the black circle represents the air mass back trajectory passage for the observations during 3-4 October 2021.*

DMSP production by local phytoplankton biomass in response to salinity fluctuations. Additionally, the coastal regions of Sumatra are marked with a bleaching alert around the sampling period (**Figure 5.4**), which could lead to higher DMSP production in the coral reef waters due to thermal stress.

Coral polyps and their endosymbiotic organisms upregulate the biosynthesis of DMSP and DMS under oxidative stresses caused by elevated SST and solar irradiance, salinity down shock from riverine discharge, and aerial exposure at low tide (Hopkins et al., 2016; Jackson et al., 2020b; Swan et al., 2017). DMS can be released directly into the atmosphere on exposure of corals to air during low tide, or via SST and wind-dependent air-sea exchange processes, particularly in shallow warm shelf waters harbouring corals (Hopkins et al., 2016; Jackson et al., 2022; Swan et al., 2017). The enhancement of DMS is not limited only to aerial exposure of corals; they also release a burst of DMS in the water after resubmersion, which typically declines in an hour via oxidation to DMSO (Hopkins et al., 2016). The amount of DMS ($\sim$18.7 μM) reported in coral mucus ropes, released as

a stress response, has been found to be the highest among natural marine substances (Swan, 2022).

5.2.2 DMS flux from coral reefs of the Andaman Islands

DMS flux from the coral reef region can be estimated using the photochemical mass-balance equation (**Eq. 5.1**) for DMS, under the assumption of a well-mixed atmospheric boundary layer (Ayers et al., 1995; Chen et al., 1999; Swan et al., 2017):

$$\frac{d[\mathrm{DMS}]}{dt} = F_{\mathrm{DMSH}} - k[\mathrm{OH}][\mathrm{DMS}] + w_e\left([\mathrm{DMSt}] - [\mathrm{DMS}]\right)H \tag{5.1}$$

where $\frac{d[\mathrm{DMS}]}{dt}$ is the change in DMS per unit time, F_{DMSH} is the air-sea flux of DMS, $[\mathrm{OH}]$ and $[\mathrm{DMS}]$ are the mean concentrations of OH radical and DMS in MBL, $[\mathrm{DMSt}]$ and w_e are the DMS concentration and entrainment velocity in the transition layer between MBL and free troposphere or the entrainment zone, H is the mean height of the MBL during 11–15 hr, and k is the overall rate constant for first-order reactions of OH with DMS.

It is based on the top-down approach, similar to the gas flux estimation method discussed in **Section 2.7**, with an additional term accounting for the photochemical loss during daytime. [DMS$_t$] is considered to be zero as the concentration of DMS transferred to the free troposphere is negligible due to rapid oxidation by radical species in the tropical MBL. DMS flux from coral reefs is determined using the following equation:

$$F_{\mathrm{DMS}} = H \times \left(\frac{d[\mathrm{DMS}]}{dt} + k[\mathrm{OH}][\mathrm{DMS}]\right) + w_e[\mathrm{DMS}] \tag{5.2}$$

We used the two low-tide associated afternoon peaks of DMS mixing ratios, observed on 3 and 6 October, for the calculation of coral reef DMS emissions from the northern Indian Ocean. The MBL height is taken from ERA5 reanalysis data product (Hersbach et al., 2018), and mean values of 792 m and 595 m are used for measurement locations covered during 3 and 6 October peaks, respectively. k is taken as the integrated reaction rate

constant value of 6.5×10^{-12} cm^3 molecules^{-1} s^{-1} at 25°C and 1 atm pressure, incorporating the OH abstraction and addition reactions (Atkinson et al., 1988). The OH concentrations were taken to be 1.8×10^5 molecules cm^{-3} for the eastern Bay of Bengal around the Andaman and Nicobar Islands during September–November (Kuttippurath et al., 2023). The OH concentration around this region is considerably lower than the rest of the basin due to loss of OH associated with volcanic SO_2. w_e is taken as 5 mm s^{-1} following the study by Warneke and de Gouw (2001) conducted over the western tropical Indian Ocean. The coral reef emission fluxes calculated for 3 and 6 October are 0.4 and 0.6 μmol m^{-2} hr^{-1}, respectively. Since the OH radical concentration is a function of solar flux, OH concentration could be a critical factor, adding to the uncertainty in our flux estimates as the solar flux was substantially higher on 3 October than on 6 October with mostly cloudy weather.

The emission estimates from low-tide exposure of corals in the Andaman Sea are almost three times less than the estimates received from the low-tide DMS release GBR region ($\sim$1.5 μmol m^{-2} d^{-1}; Swan et al., 2022). The estimates of global coral-reef-derived DMS emissions are essentially based on the extrapolation of flux from the GBR, which can overestimate the DMS emissions from global coral reef regions. Our estimates can provide important insights into the contribution of coral-reef-DMS emissions from the northern tropical Indian Ocean. The annual sulfur emissions from the total Andaman coral reef area can be estimated to be $\sim$1.43 Gg S yr^{-1}. Our estimates would be beneficial in investigating the contributions of coral reef-derived DMS to aerosol formation over the Andaman Sea.

5.3 Conclusion

This study highlights the significance of coral reef emissions in the elevated DMS mixing ratios (112$\pm$69 ppt) observed over the Andaman Sea. These elevated levels are primarily influenced by emissions from coral reefs along the Andaman Islands, the Invisible Bank, and the warm equatorial reef waters

near the Sumatra coast. The DMS flux resulting from the aerial exposure of coral reefs during low tides was estimated to be $\sim$0.5 μmol m^{-2} hr^{-1}. Through spatial extrapolation, we estimate an annual DMS sulfur emission of about 1.43 Gg S yr^{-1} from coral reef regions surrounding the Andaman Islands. This highlights the potential influence of coral reefs on nss-SO_4^{2-} aerosol formation over the Andaman Sea. Furthermore, the strong DMS emissions from the coral reefs of the Andaman Sea highlight their potential in influencing regional aerosol and climate dynamics in the coral reef regions of the northern Indian Ocean. Our findings emphasize the need to constrain the coral reef emissions from the northern Indian Ocean for improved modeled estimates of regional DMS emissions.

Chapter 6

Variability of atmospheric DMS along the southern coastal region of the Indian subcontinent

Key takeaways

- Strong dilution of atmospheric DMS during continental outflow along the coastal waters of the Indian subcontinent
- Higher isoprene abundances in continental outflow modulate the DMS chemistry and its diurnal cycle in coastal marine air
- Emissions from coral reefs are an important source of DMS enhancements in the coastal MBL of the northern Indian Ocean

6.1 Introduction

The DMS climatologies have shown that ~11% of the global DMS flux comes from coastal regions despite covering only 9.7% of the ocean surface area (Lana et al., 2011; Zhou et al., 2024). Notable coastal DMS hotspots include the Chile coast, southern Alaskan coast, southwest coast of Africa, polar shelf, and the coastal provinces of the Arabian Sea and Bay of Bengal (Hulswar et al., 2022). Coastal waters are usually characterized by elevated DMS concentrations (2–50 nM) associated with nutrient-rich riverine input and wind-driven upwelling (Asher et al., 2017; Zhao et al., 2022; Zindler et al., 2012), greater Chl-a concentrations and microbial activity (O'Brien

et al., 2022), and DMSP-enhancing phytoplankton assemblages (Bepari et al., 2020; Borker et al., 2022; Gao et al., 2025; Zhang et al., 2017).

Royer et al. (2015) have found that the spatial variability scales of DMS are smallest with variability length scales (VLS) < 15 km in tropical/subtropical coastal regions and highest in the oligotrophic open ocean with VLS up to ~ 200 km. The rapid variability (VLS ~ 7 km) in coastal areas is primarily related to high productivity and bloom patchiness, predominantly driven by biogeochemical rather than physical parameters.

In addition, emissions from dense coral reefs in tropical coastal shelves (Hoegh-Guldberg et al., 2017) can also contribute to substantial DMS variability. Laboratory experiments have reported that aerial exposure of coral reefs during low tides can directly release DMS into the tropical atmosphere (approximately 23°N to 23°S). However, DMS emissions from coral reefs are not presently accounted for in existing climatologies and Earth System models (Hopkin et al., 2016 and references therein).

Previous studies have reported high DMS concentrations and fluxes in estuaries and coastal ocean waters surrounding peninsular India (Bepari et al., 2020; Borker et al., 2022; Shenoy & Kumar, 2007; Shenoy & Patil, 2003; Viswanadham et al., 2016). Shenoy and Kumar (2007) documented significant seasonal variability in DMS seawater concentration (1.2–525.6 nM) in coastal waters of the Arabian Sea and Bay of Bengal. The highest values were reported in the southwest (SW) monsoon, with DMS concentrations as high as 526 nM in the western coastal waters of India (Shenoy & Kumar, 2007), significantly exceeding the concentration reported along the eastern coast (up to 16 nM; Rao et al., 2015). The DMS enhancements in the coastal Arabian Sea are driven primarily by upwelling and phytoplankton composition (Dias et al., 2023). While in the Bay of Bengal, riverine nutrient influx, variable nutrient stress, and seasonal salinity fronts are the major factors, with impacts varying latitudinally (Rao et al., 2015). Surface stratification and tropical cyclone (TC) events (Kumari et al., 2019) can also lead to reduced DMS levels in surface waters of the coastal Bay of Bengal. The DMS concentrations (3.6 ± 5.7 nM) in estuaries on the east coast of

India have been reported to be higher than most estuaries globally, with a large seasonal variability driven primarily by phytoplankton biomass and species composition (Viswanadham et al., 2016). An annual DMS flux of ~ 20 μmol m^{-2} d^{-1} has been estimated from the coastal waters of India (Bepari et al., 2020; Shenoy & Kumar, 2007).

Gupta et al. (2025) conducted the first measurements of atmospheric DMS in the Arabian Sea and reported elevated DMS mixing ratios of $\sim 116 \pm 120$ ppt (30–709 ppt) over the eastern coastal waters of India. Transport of continental pollutants, with higher nighttime NO_3 concentrations in coastal regions (Stark et al., 2007), can alter the DMS chemistry in otherwise cleaner marine air (Gupta et al., 2025).

The present study is based on the first shipborne *in situ* measurements of atmospheric DMS concentration over the tropical coastal waters surrounding the southern Indian subcontinent. We analyzed high time-resolution DMS data to investigate the key processes controlling the regional and short-term variability over the coastal waters of Sri Lanka, India, and the Laccadive Sea. We also used simultaneously measured isoprene mixing ratio data to assess the impact of the outflow of terrestrial air masses on DMS levels in the coastal MBL.

6.2 Cruise Campaign

The shipborne campaign was conducted over the southern coastal regions of India and Sri Lanka, and the Laccadive Sea, onboard ORV *Sagar Kanya*, during 27–31 October 2021. The cruise started from Chennai port, sailed along the eastern and southern coast of Sri Lanka, and across the Laccadive Sea, and reached Kochi port on 31 October 2021. The ship was anchored near the Kochi port during 1–2 November 2021. The surface waters of the coastal Bay of Bengal and the Laccadive Sea show contrasting hydrographic and biogeochemical properties, with a transition near the southern tip of Sri Lanka. The Chl-a concentrations were high in the Laccadive Sea (**Figure 6.1a**), while the SST was warmer along the eastern coast of Sri Lanka than in the Laccadive Sea during the campaign (**Figure 6.1b**).

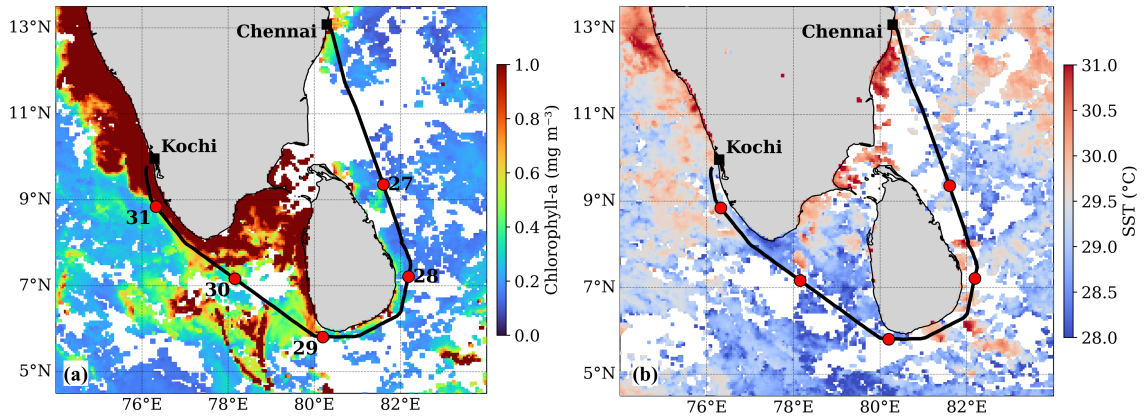

Figure 6.1: *Ship track (black line) over the southern coastal waters of India and Sri Lanka, and the Laccadive Sea on the MODIS (a) Chl-a and (b) SST composite maps during 24-31 October 2021. The red circles along the track represent the measurement date (day of October at 00 hr LT).*

The distributions of SST and Chl-a in this region are primarily controlled by the change in surface current dynamics associated with the transition in wind flow from southwest (SW) to northeast (NE) winds. During this period, the centre of flow convergence of the monsoonal currents and the upwelling shifts towards the west of Sri Lanka (de Vos et al., 2014). In October, the East India Coastal Current starts flowing southward along the east coast of the Indian subcontinent, transporting warmer, low-salinity surface waters to the east coast of Sri Lanka (Vinayachandran et al., 2005). This pattern subsequently leads to higher sea levels and high SSTs in the southeast Arabian Sea, called the Lakshadweep high (LH) or 'Arabian Sea mini warm pool' (Shankar and Shetye, 1997). The LH is an anticyclonic eddy formed off the southwest coast of India and east of the Lakshadweep islands (Ernst et al., 2022 and references therein). The Laccadive Sea and the west coast of Sri Lanka also experience higher rainfall and cloud cover than the east coast in October (Marambe et al., 2015).

6.3 Results and Discussion

6.3.1 Spatio-temporal distribution of DMS over the study region

The observed DMS mixing ratio, SST, SSS, and meteorological parameters show contrasting features along the tracks over the Sri Lanka coast and

the Laccadive Sea (**Figure 6.2**). DMS levels were substantially higher over the east coast of Sri Lanka (34–228 ppt) than over the southern coast of Sri Lanka and offshore Laccadive Sea (**Figure 6.2a**). The measurements along the east coast of Sri Lanka were influenced by the predominant E–SE winds transporting marine air from the southern Bay of Bengal (**Figure 6.2f**). Contrastingly, terrestrial outflow, driven by stronger NE winds from the continental regions of Sri Lanka and peninsular India, prevailed over the Laccadive Sea (**Figure 6.2f**).

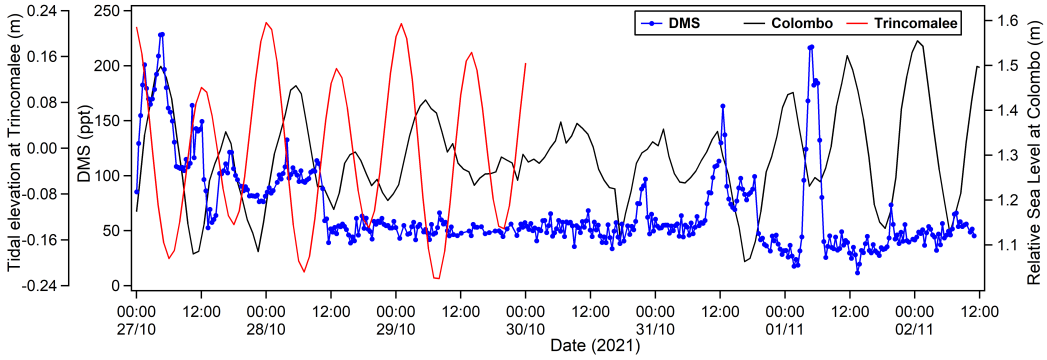

Figure 6.3: *Time series of tide height data at Trincomalee and Colombo stations in Sri Lanka during different periods of the campaign.*

The elevated DMS levels (150–230 ppt) and higher background (~ 100 ppt) concentrations over the northeast coastal waters of Sri Lanka were associated with relatively low wind speeds and higher air temperatures (27–32 °C) (**Figure 6.2b, e**). As inferred from the VC data (discussed in **Section 6.3.3**) and tide height at Trincomalee station (**Figure 6.3**), the accumulation of DMS and emissions from coral reefs during low tides could have led to the elevated DMS mixing ratios in this region.

Coral reefs can be a significant local source of atmospheric DMS (Jackson et al., 2020a; Jones et al., 2018). The coastal regions of Sri Lanka harbour several coral reef habitats, mostly fringing reefs, along ~2% of its coastline (Ellepola et al., 2021; Rajasuriya & White, 1995). Extensive fringing reefs are found along the east coast and are better developed than the reefs along the southwestern coast (Perera, 2011). The development of coral reefs along the southern coast is inhibited primarily due to increased sedimentation by intense rainfall during the southwest (SW) monsoon (Ellepola et al., 2021).

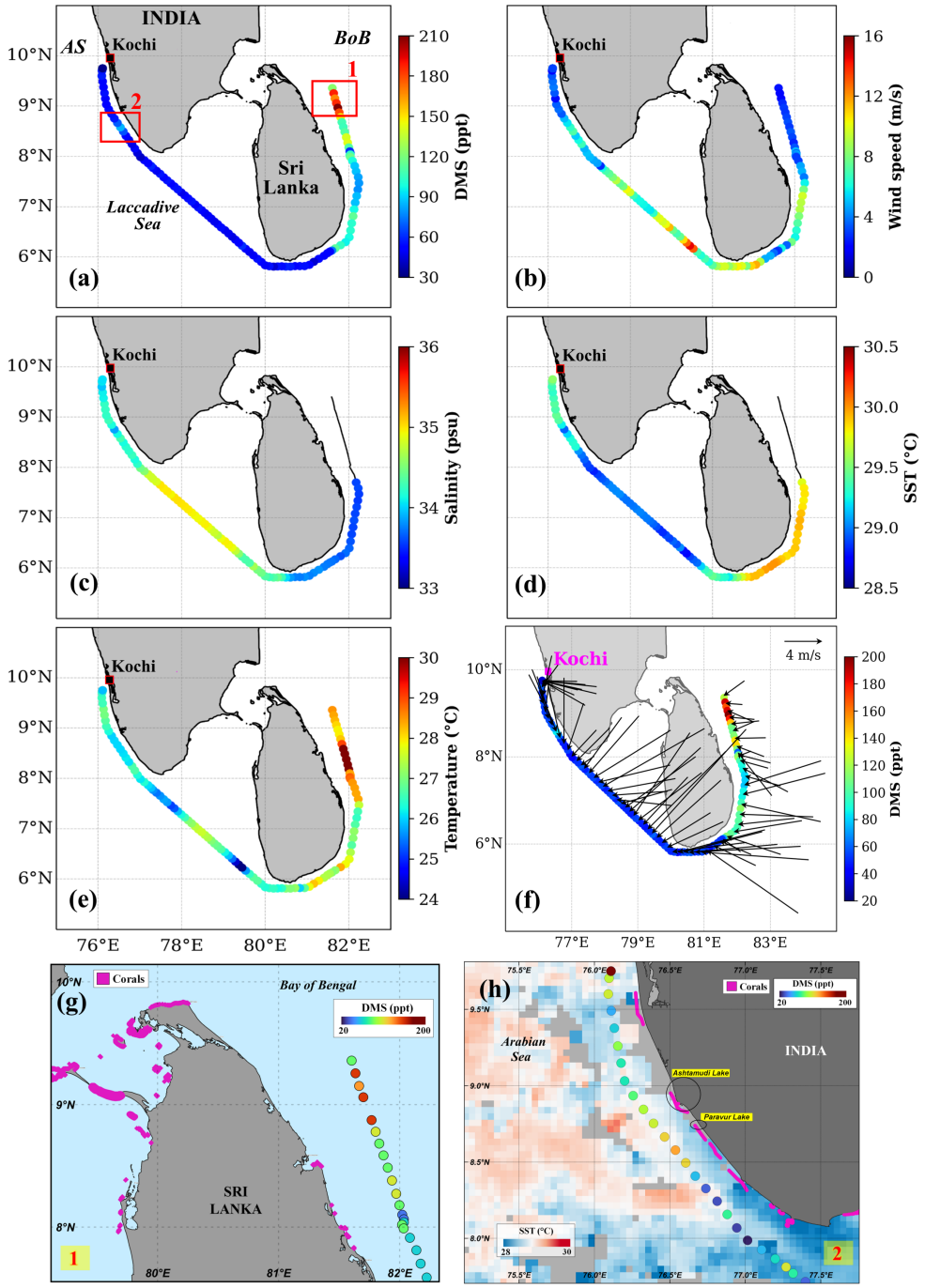

Figure 6.2: *Variability of (a) DMS mixing ratio, (c) salinity, (d) SST, (e) temperature, and (b, f) wind parameters along the cruise track during the campaign (27-31 October 2021). AS and BOB in panel (a) represents Arabian Sea and Bay of Bengal, respectively; (g) coral distribution around southern parts of the Indian subcontinent, and (h) SSTs, corals and Estuarine systems near the cruise track (colored with DMS mixing ratio) in southwest coast of India, highlighted by red rectangle 2 in (a).*

Despite the presence of corals, the decrease in DMS mixing ratio along the east coast can be attributed to dilution from stronger winds, photochemical degradation, and ocean tidal phase. The analysis of tide height data at Trincomalee station on the east coast shows that the occurrences of DMS peaks (> 100 ppt) coincide with the low tide periods (**Figure 6.3**). Aerial exposure of coral reefs during the low tides results in large emissions (3–11 mmol m^{-2} d^{-1}) of gas-phase DMS directly into the atmosphere (Hopkins et al., 2016). Additionally, thermal- and UV-stress from warmer SSTs and higher solar flux in the northeast coastal waters of Sri Lanka could have facilitated an increase in DMS emissions from coral reefs in this region (Deschaseaux et al., 2014; Fiddes et al., 2021). Jackson et al. (2020b) have also reported negative and positive correlations of atmospheric DMS with tide height and SST, respectively, over the Southern GBR.

Another anomalous DMS enhancement of ~ 100 ppt was observed over the Laccadive Sea along the southwest coast of India (**Figure 6.2h**). The southwest coast of India, particularly along south Kerala, harbours patchy growth of hard coral reefs in the intertidal regions (Baiju et al., 2019; Jasmine et al., 2009). This enhancement in DMS also coincides with the negative anomalies in SST ($\sim 0.7^{\circ}$C) and salinity (~ 0.7) (**Figure 6.2d, c**), suggesting the influence of estuaries and riverine waters (**Figure 6.2h**). Except for some localized DMS enhancements, the differences in prevailing meteorological and sea surface conditions could have played a major role in DMS variations along the track.

6.3.2 Time series of DMS mixing ratio with oceanic and meteorological parameters

The time series variations showed large spatio-temporal variations of DMS mixing ratios (34–228 ppt) over the eastern coastal waters of Sri Lanka and the southwest coast of India, while levels were consistently low (40–68 ppt) over the Laccadive Sea with no substantial variability (**Figure 6.4**). The average DMS mixing ratio of 111 ± 38 ppt over the east coast of Sri Lanka was about 2 times higher than the southern coast of Sri Lanka (52 ± 5 ppt)

and the Laccadive Sea (53 ± 7 ppt). The background DMS mixing ratio, calculated as the 5th percentile (Apte et al., 2017) of hourly data, over the Sri Lankan coastal waters (~ 67 ppt) was also higher than over the Laccadive Sea (~ 41 ppt).

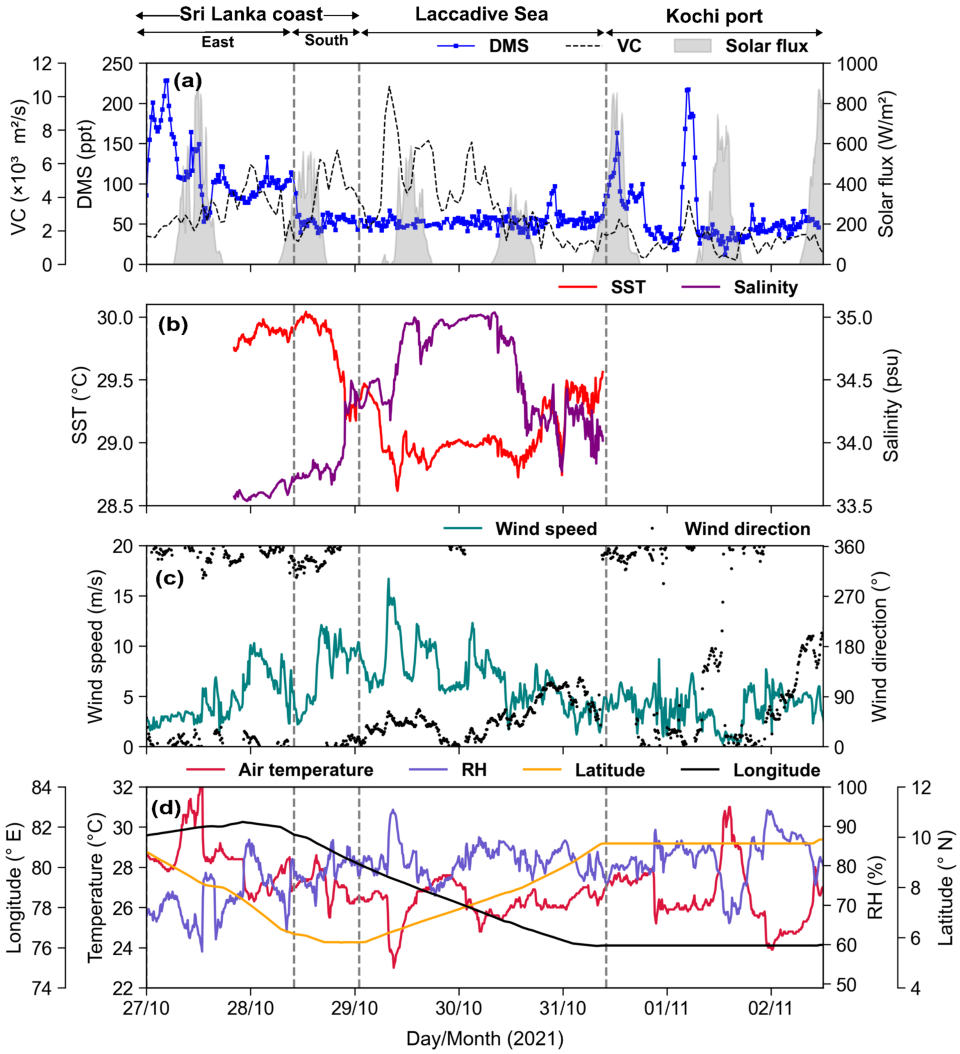

Figure 6.4: *Time series variations of (a) DMS mixing ratio and ventilation coefficient (VC), (b) SST and Salinity, (c) wind speed and direction, (d) temperature and relative humidity along with latitude and longitude along the track over southern coastal regions of the Indian subcontinent during 27 October–2 November 2021.*

The analysis of solar flux data indicates that cloudy conditions prevailed during the measurements over the Laccadive Sea. This may have inhibited the metabolic production of DMS by phytoplankton (Toole et al., 2006), leading to a decrease in air-sea flux in this region. However, the Chl-a con-

centrations in the Laccadive Sea were higher and could have resulted from shifting the upwelling center towards the west of Sri Lanka, highlighting the dynamic oceanic properties observed along the cruise track (as discussed in Section 6.2). The sharp decline in DMS mixing ratio over the southern coast of Sri Lanka with drastic changes in SST ($\Delta \sim -2.5^{\circ}$C) and salinity ($\Delta \sim 2.5$) indicates the transition in biogeochemical and hydrographic properties between the Bay of Bengal and Arabian Sea (**Figure 6.4b**).

Overall, higher (lower) DMS mixing ratios were observed to be associated with higher (lower) SSTs and lower (higher) salinity during the campaign (**Figure 6.4b**). In comparison to the Laccadive Sea, higher SST (29.9 ± 0.1 $^{\circ}$C) and lower salinity (33.6 ± 0.1) values were measured along the eastern coast of Sri Lanka (**Table 6.1**). The elevated DMS levels on 27 October (02–05 hr, IST) can be attributed mainly to emissions from exposed corals along the eastern coast during the low tide period (**Figure 6.3**). In addition, the lack of DMS+OH loss reaction and calm winds could have contributed to the build-up of DMS at night, and led to the highly elevated levels. The DMS peak on the night of 30 October along the southwest coast of India in the Laccadive Sea coincided with a simultaneous decrease in SST and salinity, indicating the influence of estuarine waters.

Repeated occurrences of dinoflagellate blooms of *Karenia mikimotoi* have been reported along the southwest coast of India, particularly the Kerala coast, during the post-monsoon season (Li et al., 2019 and references therein). *K. mikimotoi* blooms prefer warm SSTs, high nutrient levels and stratified waters, and therefore, are mostly found in estuaries and coastal waters (Robin et al., 2013). Culture experiments have demonstrated a higher release of DMSP ($\sim$195 fmol cell^{-1}) and DMS ($\sim$86 fmol cell^{-1}) from *K. mikimotoi* compared to other marine microalgae (Yang et al., 2022). The transport of DMS from the estuarine and productive coastal waters along the southwest coast of India could contribute to the elevated DMS along the Kerala coast and near Kochi port regions. However, despite the high Chl-a concentrations, the DMS levels in the MBL of the Laccadive Sea were lower than those along the coastal waters of Sri Lanka and India. It

Table 6.1: *Mean (± standard deviation) of DMS mixing ratio, meteorological and hydrographic parameters over eastern and southern coastal waters of Sri Lanka (SL), Laccadive Sea, Kochi port, and during the entire campaign (27 October–2 November 2021).*

Parameters	SL–east coast	SL–south coast	Laccadive sea	Kochi port	All data
DMS (ppt)†	113±37 [6]	52±5 [1]	53±7 [1]	59±39 [6]	74±36 [1.5]
Wind speed (m s^{-1})	4.7±2.2	8.1±2.9	6.8±2.8	3.9±1.4	6.2±2.8
SST (°C)	29.87±0.06	29.72±0.3	29.06±0.2	–	29.32±0.4
Salinity	33.61±0.05	33.91±0.25	34.57±0.36	–	34.29±0.5
Solar flux (W/m^2)	131±212	157±200	84±131	158±240	125±191
Pressure (mb)	1008±1	1008±1	1010±1	1009±1	1009±2
Temperature (°C)	28.33±1.28	27.08±0.65	26.24±0.81	26.54±1.48	27.06±1.33
RH (%)	72±6	79±3	81±4	82±6	78±6
Chl-a (mg m^{-3})	0.55±0.15	1.18±1.52	2.23±4.58	0.84±0.02	1.5±3.41
MBLH (m)	707±150	533±54	518±148	388±131	577±165
VC (m^2s^{-1})	3106±1159	4345±1708	3793±2359	1439±703	3571±1986

†Standard error [SE]

also suggests the crucial influence of atmospheric processes in controlling the DMS levels over coastal regions of the Indian subcontinent.

6.3.3 Impact of atmospheric ventilation and terrestrial outflow on DMS variability

The time series of the DMS mixing ratio tends to show anti-correlated variations with wind speed and ventilation coefficient (VC), highlighting the impact of atmospheric ventilation on DMS variability along the cruise track. The lower and higher DMS mixing ratios over the Laccadive Sea and east coast of Sri Lanka were associated with stronger (6.8 ± 2.8 m s^{-1}) and moderate (4.7 ± 2.2 m s^{-1}) winds, respectively (**Figure 6.4c**; **Table 6.1**). The lower DMS mixing ratios over the Laccadive Sea were associated with

consistently higher VC values, implying a stronger ventilation effect. In contrast, the DMS enhancement episodes observed along the east coast of Sri Lanka coincide with the lower VC values ($< 4 \times 10^4$ m^2 s^{-1}) (**Figure 6.4a**). However, this inverse relationship between DMS and VC is not consistent in the measurements near Kochi port. The effect of atmospheric ventilation was particularly stronger over regions with continentally-influenced winds, as observed over the southern coast of Sri Lanka, the Laccadive Sea, and near Kochi port (**Figure 6.4c**). The contributions of continental (anthropogenic + terrestrial biogenic) sources to atmospheric DMS are much lower compared to the oceanic sources (Andreae & Crutzen, 1997; Lana et al., 2011). As a result, the lower DMS levels in the MBL of the Laccadive Sea can primarily be attributed to the outflow of DMS-depleted air masses from continental regions.

Isoprene mixing ratio, measured along segments of the cruise track, is analyzed to support the impact of continental outflow on DMS variability. Contrary to DMS, the isoprene mixing ratio increased during the transition from marine to continental air masses (**Figure 6.5a**). On 28 October, a significant decrease in the DMS mixing ratio over the southern coastal waters of Sri Lanka coincides with a gradual increase in isoprene from ~ 0.2 ppb to > 0.4 ppb. Although oceanic emissions are one of the sources of isoprene that contribute ~0.1–11.6 Tg C yr^{-1} to the global isoprene budget (Exton et al., 2015; Shaw et al., 2010), the contribution from terrestrial vegetation is significantly higher than oceanic emissions (440–660 Tg C yr^{-1}; Guenther et al., 2006). Therefore, the terrestrial outflow could significantly enhance the isoprene levels in coastal MBL. Several studies have reported high isoprene mixing ratios in the tropical MBL due to contributions from terrestrial sources (e.g., Yokouchi et al., 1999). Tripathi et al. (2020a) reported that transport from terrestrial sources resulted in elevated isoprene concentrations (0.60 ± 0.21 ppb) over the northeast coastal waters of the Arabian Sea during the pre-monsoon season.

An anti-correlation ($r^2 = 0.59$) between the isoprene and DMS mixing ratios suggests their distinct source characteristics in the coastal marine

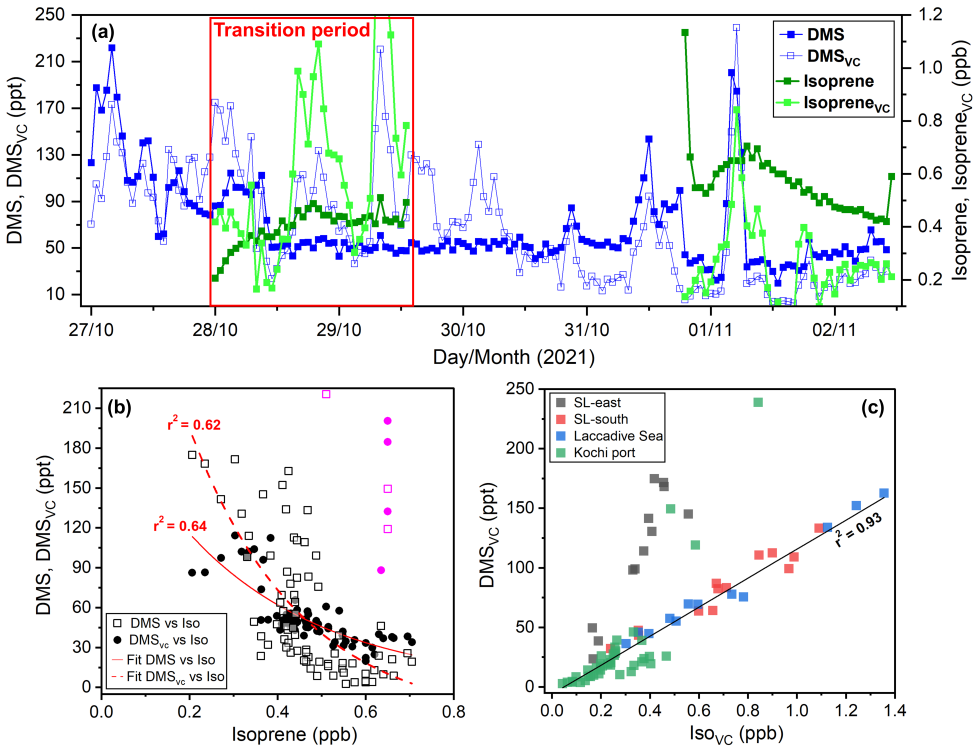

Figure 6.5: *(a) Variations of measured and VC-normalized DMS and isoprene mixing ratios. The red rectangle highlights the changes in DMS and isoprene during the transition from marine to terrestrial winds (28–29 October 2021) over the southern coastal waters of Sri Lanka. (b) Scatterplot of DMS and* DMS_{VC} *with isoprene mixing ratios during the campaign. Exponential fits* ($p < 0.0001$) *are given in red solid and dashed lines for DMS vs. isoprene and* DMS_{VC} *vs. isoprene, respectively. (c) Scatterplot between* DMS_{VC} *and* Iso_{VC} *color-coded for the measurements along the different segments of the cruise track.*

atmosphere (**Figure 6.5b**). The measurements of lower DMS levels in continentally-influenced air masses are also consistent with our studies over the Arabian Sea (Gupta et al., 2025) and Bay of Bengal (Gupta and Sahu, 2025) during the post-monsoon season. However, VC-normalized DMS (DMS_{VC}) and isoprene (Iso_{VC}) mixing ratios showed a strong positive correlation ($r^2 = 0.94$), particularly over the Laccadive Sea and southern coastal waters of Sri Lanka (**Figure 6.5c**) with land-influenced air masses. This could be due to the significant impact of oceanic emissions of isoprene over high Chl-a waters of the Laccadive Sea and DMS emissions from the productive southern coastal waters of Sri Lanka (**Figure 6.1**). Marine

phytoplankton can also be an important source of isoprene in the MBL, particularly in high Chl-a regions (Shaw et al., 2010). It also emphasizes the crucial role of ventilation in the low DMS levels in continentally influenced air masses. Additionally, the highly elevated DMS_{VC} (> 100 ppt) during moderate levels of Iso_{VC} (0.1–0.6 ppb) over the eastern coastal waters of Sri Lanka and Kochi port (**Figure 6.5c**) shows a significant contribution of oceanic sources of DMS over the region.

Alternatively, depending on the species composition, marine phytoplankton can also be an important source of isoprene to the marine atmosphere over the high Chl-a regions (Shaw et al., 2010). The major production mechanisms of marine isoprene are photochemical degradation of dissolved organic matter in the sea surface microlayer (SML) (Ciuraru et al., 2015), and metabolic production by certain phytoplankton species (Meskhidze et al., 2015). Therefore, the higher Chl-a concentrations in the surface waters of the Laccadive Sea (**Figure 6.1a**) can be an important source of marine isoprene to the MBL. Dani and Loreto (2017) proposed a source trade-off arising from the natural selection of the metabolic pathway responsible for isoprene or DMS production by different phytoplankton groups. Thus, the dominance of phytoplankton functional groups favouring isoprene emissions could also lead to decreased DMS levels. However, due to the unavailability of phytoplankton composition data during the campaign, a conclusive role of the biogeochemical source trade-off between isoprene and DMS could not be established in this study. The emission of marine isoprene also depends on light intensity and temperature (Booge et al., 2018), making it complex to separate the oceanic background and terrestrial contribution.

The change in air mass source over the tropical coastal regions could have significant implications for the secondary aerosol composition in the coastal MBL. Influx of terrestrial volatile organic compounds (VOCs) can modify the DMS radical chemistry, consequently influencing the distribution of DMS oxidation products responsible for secondary sulfate aerosol formation in the marine atmosphere. Although the emission factor of isoprene is much higher than that of monoterpenes (MTs), the secondary organic aerosol

(SOA) yield from MTs is ~ 16 times higher than from isoprene. Hu et al. (2013) found significant levels of isoprene- and MT-derived SOA tracers (36 and 20 ng m^{-3}, respectively) in marine air samples across a large latitudinal range, and the highest concentrations of isoprene SOA tracer (2-methyltetrols) were reported in coastal MBL with land-origin air masses. Yang et al. (2020) have reported the impact of vegetation emissions and fossil fuel combustion controlling the organic aerosols over the western coast of Sri Lanka.

Further investigations are required to elucidate the relative contributions of marine isoprene emissions in the productive coastal waters of the northern Indian Ocean. Our study also underscores a critical gap in understanding the impact of marine and terrestrial biogenic volatile organic compounds (BVOCs), particularly isoprene and terpenoids, on the aerosol chemistry and composition in the coastal MBL around the Indian subcontinent.

6.3.4 Diurnal characteristics of DMS mixing ratio

The investigation of air-sea exchange and oxidation processes is complex due to the significant influences of meteorology-driven dilution on DMS variability. However, to a certain extent, DMS_{VC} accounts for the relative dilution effects driven by varying boundary layer dynamics and wind speed along the cruise track (Gupta et al., 2025). We have used DMS_{VC} mixing ratio to investigate the impact of local emissions and atmospheric oxidation processes controlling the short-term variability in different air masses.

The time series of DMS_{VC} over the coastal waters of Sri Lanka and offshore Laccadive Sea during 27–30 October exhibits a clear diurnal periodicity, characterized by a daytime (10–16 hr IST) decline and an increase in the evening/nighttime. During this period, the daytime max/min ratio of DMS_{VC} was highest on 28 October along the southern coast of Sri Lanka (~ 6.2 ppt ppt^{-1}), and lowest along the east coast of Sri Lanka (~ 2.4 ppt ppt^{-1}). Additionally, despite substantial OH loss (daytime max/min ~ 4 ppt ppt^{-1}) on 29 October in the Laccadive Sea region, the

elevated daytime DMS_{VC} (minima $\sim$ 72 ppt) and the highest nighttime build-up (up to $\sim$ 225 ppt) suggest strong emissions from marine biological activities. Satellite data also revealed higher Chl-a concentrations over the Laccadive Sea than the east coast of Sri Lanka during the campaign period (**Figure 6.1**).

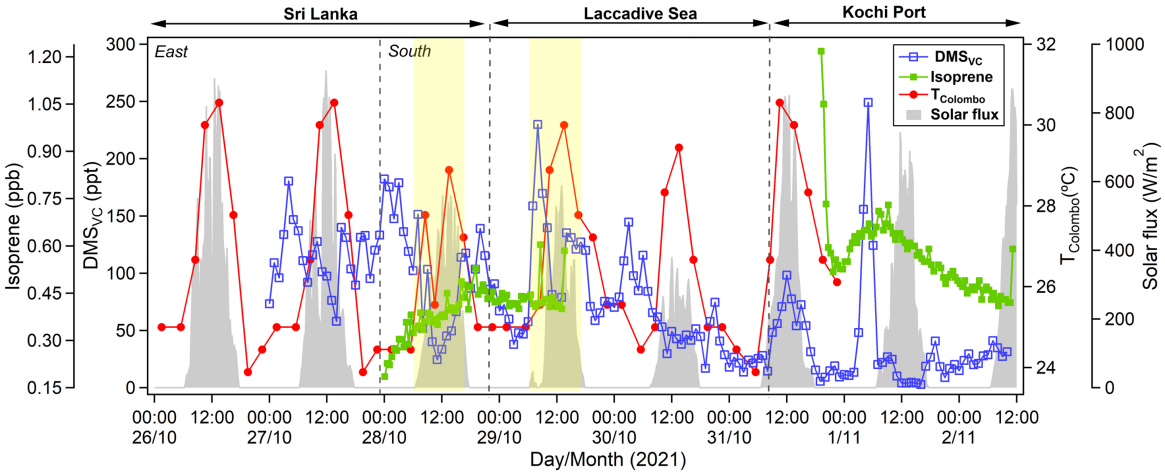

Figure 6.6: *VC-normalized DMS (DMS_{VC}), isoprene, and solar flux along the cruise track over the southern coastal waters of the Indian subcontinent during 27 October November 2021, and air temperature in Colombo, Sri Lanka ($T_{colombo}$) during 27-31 October 2021.*

The lowest DMS concentration in the late afternoon (14–16 hr LT) along the east coast of Sri Lanka is consistent with the diurnal feature measured in the open ocean and coastal regions of the Arabian Sea (Gupta et al., 2025). The pattern is also consistent with typical diurnal cycles of DMS reported over other ocean regions, characterized by a build-up in the early morning and lower values during the late afternoon (Lawson et al., 2020; Marandino et al., 2007; Yvon and Saltzman, 1996). Unlike the variability along the east coast, DMS_{VC} levels over the southern coastal waters of Sri Lanka and Laccadive Sea tend to increase after a dip at $\sim$ 12 hr LT during 28–29 October. This change could be driven by higher abundances of isoprene and other reactive biogenic volatile organic compounds (BVOCs) in the continental outflow (Figure 6.5).

Sri Lanka has a total forested area of $\sim$ 29.6%, with dense tropical

evergreen forests in the southwest region of the island (Volk et al., 2012). Tripathi et al. (2021) have reported very high isoprene concentrations (1.05 ± 0.43 ppb) at a tropical evergreen forest site in the Western Ghats of India. Therefore, the continental outflow from the forested regions of the southern Indian subcontinent can efficiently transport isoprene and other BVOCs to the surrounding coastal marine atmospheres. However, the effect of terrestrial outflow may not essentially be limited to the coastal MBL, as we have measured high isoprene (1.02 ± 0.07 ppb) and low DMS (55 ± 5 ppt) mixing ratios over the offshore waters of the western Bay of Bengal (13°E; 83.5–86°E) during September–October 2021 (Gupta and Sahu, 2025).

The nighttime DMS_{VC} mixing ratios along the east coast were higher than those over the southern coast and the Laccadive Sea (**Figure 6.6**). The nighttime DMS_{VC} peaks (~ 180–250 ppt) along the east coast (02–05 hr IST; 27 October) and at Kochi port (02–05 hr IST; 1 November) coincided with the low tide periods (Figure 6.3). These peaks could be attributed to the emissions from coral reefs, as discussed in **Section 6.3.1**. However, unlike the measurements over the Laccadive Sea and southern coast of Sri Lanka, a clear nighttime build-up of DMS_{VC} was observed along the east coast of Sri Lanka on 27–28 October and at Kochi port on 2 November.

This discrepancy appears to be driven by the transport of anthropogenic plumes with elevated NO_x, resulting in increased NO_3 concentrations (Stark et al., 2007). This could lead to rapid nighttime DMS loss, inhibiting the accumulation of DMS in the MBL of the Laccadive Sea. The nighttime DMS build-up near Kochi port on 2 November may also have been influenced by cleaner air due to rainfall events, but requires further investigation. The high nighttime DMS_{VC} variability in the land–influenced air masses during the campaign could be due to the varying abundance of reactive hydrocarbons (rate constant $k_{NO_3} \sim 10^{-11}$–10^{-13} cm^3 $molecule^{-1}$ s^{-1}). Therefore, along with the dilution due to transport of DMS-depleted air masses, more reactive species can modulate DMS–NO_3 chemistry in the coastal MBL (Gupta et al., 2025).

6.3.5 Impact of continental outflow on the oxidation capacity of coastal MBL

The OH-reaction rate constant of isoprene ($k_{\mathrm{OH+isoprene}} = 100 \times 10^{-12}$ cm^3 molecule^{-1} s^{-1}) is an order of magnitude higher than that of DMS ($k_{\mathrm{OH+DMS}} = 7.6 \times 10^{-12}$ cm^3 molecule^{-1} s^{-1}) (Atkinson & Arey, 2003; Burkholder et al., 2020). Thus, the outflow of isoprene-rich terrestrial air masses can significantly influence the oxidation capacity of the coastal MBL (Yáñez-Serrano et al., 2015). The increased isoprene concentrations in the afternoon can lead to faster consumption of OH radicals, reducing OH availability for DMS oxidation. The isoprene mixing ratio increased by up to 0.5 ppb during the transition from oceanic to continental air masses between 28–29 October (**Figure 6.4a**). This could be one of the factors leading to the early occurrence (11–12 hr) of DMS daytime minima on 28 and 29 October, characterized by transport of isoprene-rich air masses over the southern coastal waters of Sri Lanka.

We calculated the OH-reactivity (R_{OH}) of isoprene and DMS to quantify their relative significance in influencing the oxidation capacity using the following formula (Nölscher et al., 2014; Sahu et al., 2025b):

$$\mathrm{R_{OH}} = k_{\mathrm{OH}_i} \times [\mathrm{VOC}_i] \tag{6.1}$$

where k_{OH_i} is the OH-reaction rate constant of VOC$_i$ and $[\mathrm{VOC}_i]$ is the measured concentration.

Table 6.2: *The OH-reaction rate constants and mean (± standard deviation) of mixing ratios and OH-reactivity of DMS and isoprene during the daytime of 28 October 2021.*

Compound	**Mixing ratio (ppt)**	**k_{OH} (cm^{3}molecules^{-1} s^{-1}) at 298K**	**OH-Reactivity (s^{-1})**
DMS	407±40	7.6×10^{-12}[a]	0.009±0.002
Isoprene	53±11	100×10^{-12}[b]	1.001±0.097

[a]Burkholder et al., 2020; [b]Atkinson & Arey, 2003

During 28–29 October, the R_{OH} of isoprene was approximately two orders of magnitude higher than that of DMS (**Table 6.2**), indicating that the high concentrations of isoprene impeded the daytime oxidation of DMS by faster consumption of OH radicals. Further, the competitive scavenging of OH radicals is not limited to isoprene, as the rapid outflow of other reactive biogenic terrestrial (e.g., $\alpha-, \beta-$pinenes, limonene, etc.) and anthropogenic (e.g., aromatics, NO_x, etc.) species to the coastal MBL can result in reduced OH availability for DMS (Pfannerstill et al., 2019; Zannoni et al., 2017).

6.4 Conclusion

The first high time-resolution shipborne *in situ* measurements of atmospheric DMS mixing ratio were conducted over the southern coastal regions of the Indian subcontinent in the post-monsoon season. Higher DMS mixing ratios (113 ± 37 ppt) observed along the east coast of Sri Lanka were influenced by marine air masses from the Bay of Bengal. Despite higher Chl-a concentrations, the lower DMS mixing ratios (53 ± 7 ppt) over the Laccadive Sea were attributed to dilution caused by the rapid outflow of DMS-depleted terrestrial air masses, as confirmed by elevated isoprene levels. The DMS levels were more sensitive to transport patterns and wind conditions than the oceanic productivity, and showed elevated values at lower winds.

The analysis of tide data indicates substantial DMS enhancements over coastal waters along northeast Sri Lanka and southwest India due to emissions from coral reefs at higher sea surface temperatures. The diurnal pattern of the ventilation coefficient-normalized DMS (DMS_{VC}) mixing ratio reveals reduced photochemical loss of DMS in the afternoon hours under the continental outflow. The concurrent decrease in DMS and increase in isoprene were associated with the transition from marine to terrestrial air masses. In the continental outflow regime, the OH-reactivity of isoprene (1 ± 0.1 s^{-1}) was about two orders of magnitude higher than that of DMS (0.01 ± 0.002 s^{-1}). These results suggest that continental outflow with higher concentrations of isoprene and other reactive species from the forested

regions of Sri Lanka can modulate the DMS oxidation rate in the MBL.

The outflow of BVOCs in the MBL can have important implications for secondary aerosol formation, as the yield of isoprene-derived SOA has been reported to increase significantly (~51–146%) in the presence of DMS (Chen & Jang, 2012). Further, the compositional changes due to the addition of organics to marine sulfate aerosol can lead to a decrease in the hygroscopicity of the marine aerosols (Meskhidze et al., 2011) and eventually change the CCN activity and cloud properties (Gantt et al., 2012). This complex interplay of oceanic and terrestrial air masses controlling the atmospheric chemistry can have significant implications for aerosol chemical composition in the surrounding coastal regions of the southern Indian subcontinent. Therefore, simultaneous and time-resolved measurements of aerosol composition along with precursor gases are required to understand their formation processes in different air masses.

Chapter 7

Sources and processes controlling isoprene distribution over the northern Indian Ocean

Key takeaways

- Terrestrial outflow from vegetation sources in peninsular India significantly contributed to isoprene in the marine air of the Bay of Bengal
- The photochemical production of isoprene at the SML is a prominent source in the open ocean of the Arabian Sea
- Reduced isoprene levels associated with increasing Chl-a suggest chemical and biological consumption of isoprene in high productive coastal waters of the Bay of Bengal

7.1 Introduction

In the global marine atmosphere, most of the measurement-based studies of isoprene have been reported over the different regions of the Pacific and Atlantic Oceans (Arnold et al., 2009; Baker et al., 2000; Lewis et al., 1999; Liakakou et al., 2007; Mungall et al., 2017; Saito et al., 2000). In particular, measurements of isoprene in marine air and seawater of the tropical Indian Ocean remain scarce (Table 1.1). Nonetheless, the average surface isoprene concentration in the eutrophic tropical Indian

Ocean has been reported to be ~50 pmol L^{-1} at higher SST (>28°C), which is significantly higher than those measured in subtropical, sub-polar, and polar waters (Ooki et al., 2015; Zavarksky et al., 2018a). Thus far, Tripathi et al. (2020a) is the only study providing atmospheric isoprene measurements over the open ocean regions of the Arabian Sea. The study reported elevated isoprene concentrations (0.16–1.12 ppb) in marine air of the oligotrophic Arabian Sea during the spring inter-monsoon season, mainly associated with the *Trichodesmium* (cyanobacteria) and *Thalassiosira* (diatoms) blooms at high SST. Modelling studies have further suggested that marine isoprene-derived secondary organic aerosol (SOA) can constitute over 30% of the monthly-averaged sub-micron organic carbon fraction of marine aerosols across tropical oceanic regions (30°S – 30°N) (Gantt et al., 2009). However, to accurately quantify the role of isoprene in marine organic aerosol formation, climate models require extensive *in situ* observations, particularly in understudied areas of the tropical Indian Ocean (Arnold et al., 2009; Gantt et al., 2010; Shaw et al., 2010).

This chapter is based on the first high time-resolved shipborne *in situ* measurements of isoprene mixing ratio over the Bay of Bengal and Arabian Sea in the post-monsoon. The main aim of this study is to investigate the roles of terrestrial outflow and oceanic processes in controlling the distributions of isoprene in the MBL. We also investigated the short-term and diurnal variations associated with changes in surface hydrographic and meteorological parameters, and the role of photochemistry.

7.2 Ship Campaign

The high-resolution atmospheric isoprene concentrations were measured onboard ORV *Sagar Kanya* over the Bay of Bengal (SK#373) and Arabian Sea (SK#374) during the post-monsoon season 2021. The details of these campaigns and cruise tracks are provided in Chapters 3 and 4. The

statistics of SST, salinity, Chl-a, wind speed, air temperature, relative humidity, and surface pressure do not show significant differences between the measurements during the onward (T1, west-east) and return (T2, east-west) longitudinal transects over the Bay of Bengal (Table 4.1). However, analysis of wind data measured during this campaign (SK#373) reveals the predominance of SW-W and NW-NE winds during T1 and T2 transects, respectively (**Figure 7.1**).

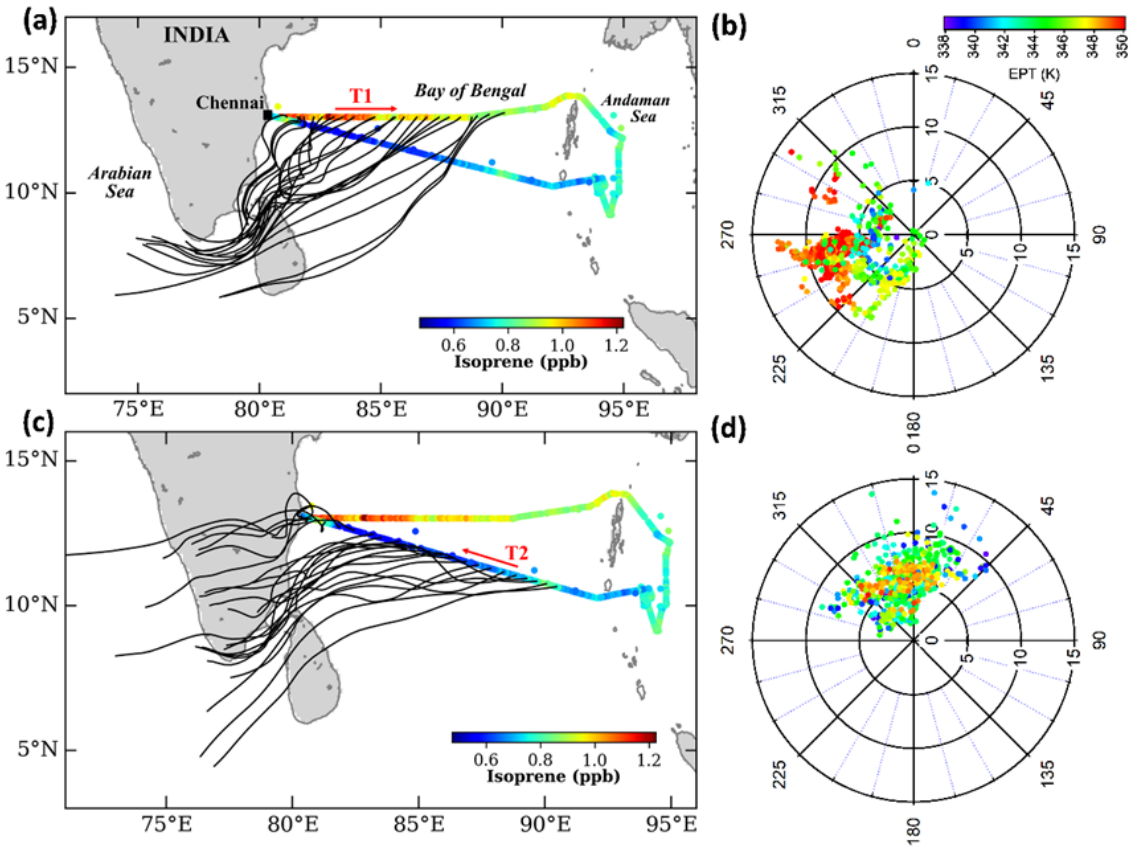

Figure 7.1: *The ship track, covering two longitudinal transects of (a) T1 (onward, west to east) and (c) T2 (return, east to west), is color-coded with the isoprene mixing ratio over the Bay of Bengal measured during 25 September-14 October 2021. The black curves show 48-hour HYSPLIT back-trajectories (Draxler & Hess, 1998) at 100 m altitude (AMSL) along both transects. The polar plots of wind parameters (wind speed, m s_{-1}) and wind direction color-coded with the EPT (K) during the (b) T1 and (d) T2 transects, respectively.*

7.3 Results and Discussion

7.3.1 Time series of isoprene mixing ratio over the Bay of Bengal

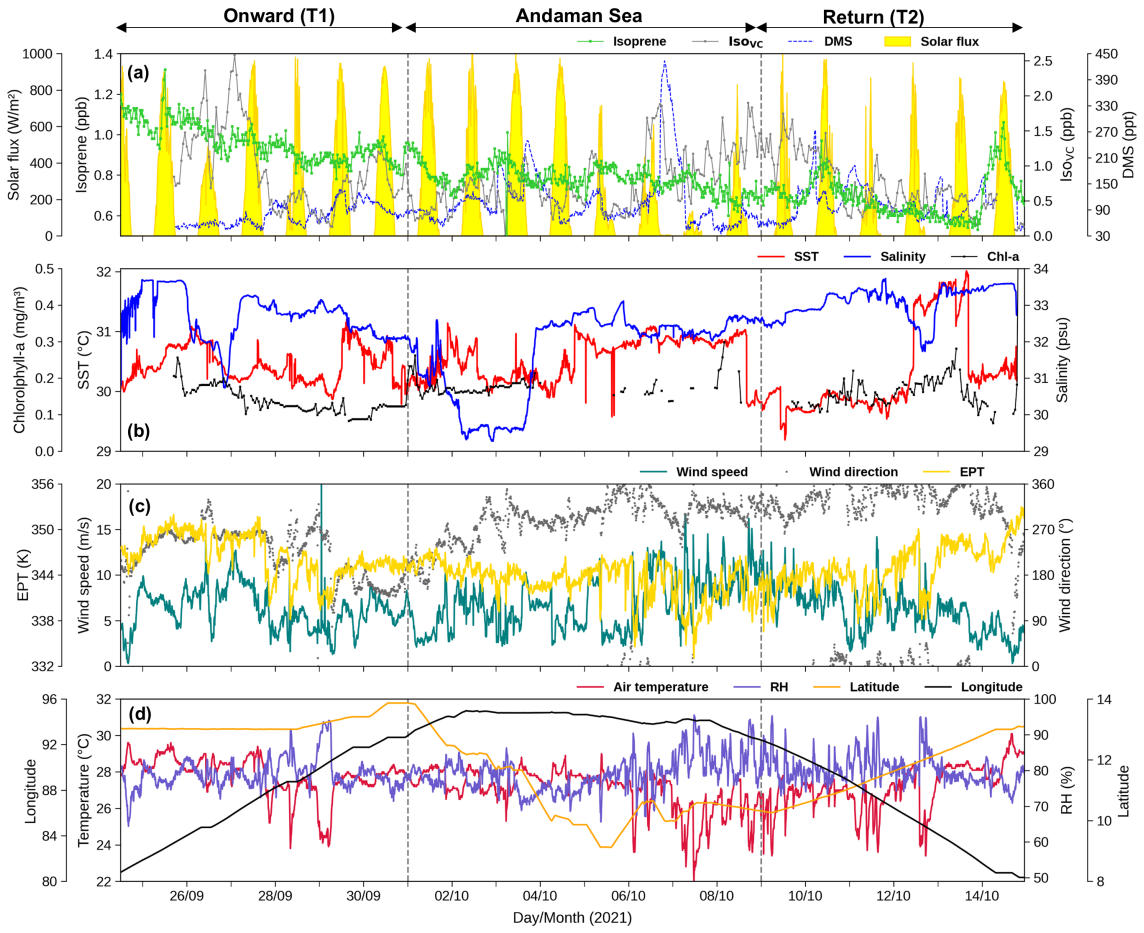

Figure 7.2: *Time series variations of the (a) isoprene mixing ratio, Iso_{VC}, DMS, (b) SST, salinity, and (c-d) meteorological parameters during onward (T1, west-east) and return (T2, east-west) transects in the Bay of Bengal, and the Andaman Sea transect.*

The time series variations of isoprene mixing ratio, Iso_{VC}, SST, salinity, and meteorological parameters along the onward (T1) and the return (T2) transects are shown in **Figure 7.2**. At the beginning of T1, during 25–27 September, the higher isoprene levels of 0.88–1.15 ppb were associated with stronger westerly winds, higher ambient air temperatures (27–29 °C), and lower surface pressures (1000–1005 mb). The back trajectories during periods of elevated isoprene levels reveal the transport of continentally-

influenced air masses from peninsular India and Sri Lanka (**Figure 7.1**). Lower isoprene levels of 0.82–0.97 ppb observed during the latter phase of T1, particularly on 28 September, were associated with the lighter SW winds, higher pressures (1004–1008 mb), and lower air temperatures (24–27.5 °C). Back trajectory analysis during this period shows air mass transport within the MBL of the Bay of Bengal, contributing to the lower isoprene concentrations. The time series of Iso_{VC} along T1 shows a clear contrast with a significantly higher mean value of 1.45 ± 0.5 ppb during W winds compared to that of 0.44 ± 0.14 ppb during the SW winds.

Along the return transect (T2) between 10 and 12 October, the isoprene mixing ratio declined rapidly as the ship moved westward from the open ocean towards the east coast of India. The higher mixing ratios of 0.80 ± 0.06 ppb on 10 October over the open ocean and lower mixings of 0.64 ± 0.04 ppb during 11–12 October near the coast were associated with predominant NW and NE winds, respectively. The NW and NE winds suggest the transport of continental and oceanic air masses with relatively higher and lower isoprene levels, respectively. In addition to the role of distinct air masses, the lower isoprene concentrations along this transect were mostly associated with the rapid changes in meteorological parameters with higher RH (75–94%), lower air temperatures (23.3–28.5 °C), and cloudy conditions. The analysis of back trajectories along T2 suggests lesser influences of continental air masses than T1. Unlike the measurements along T1, the time series of isoprene and Iso_{VC} show similar variations along T2 with some exceptions. Overall, the trends of isoprene and Iso_{VC} show an anti-correlated variation with salinity along both T1 and T2 transects. However, events of sharp reductions in isoprene and Iso_{VC} levels were associated with sudden drops in air temperature and SST (discussed in **Section 7.3.2**).

In a few cases, such as during the afternoon of 27 September and 12 October, the drops in isoprene concentrations were marked by simultaneous

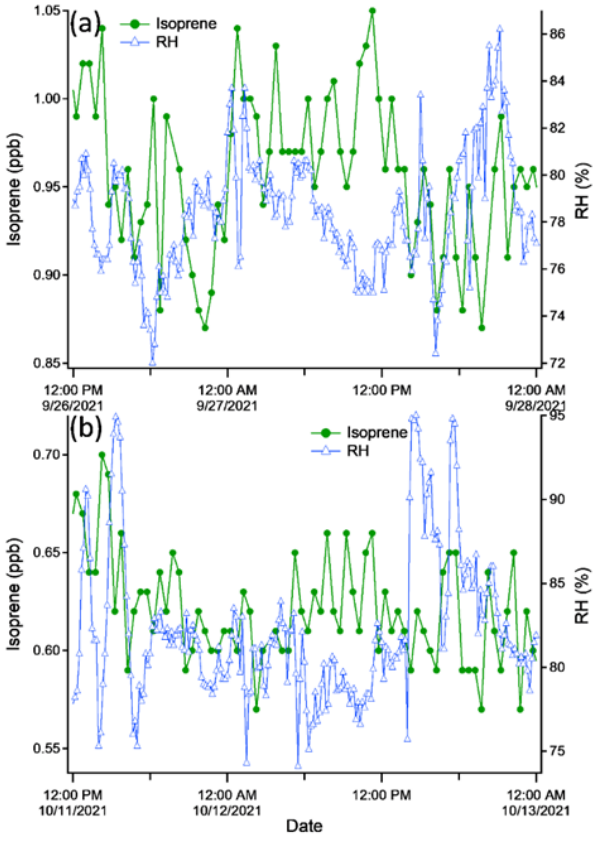

Figure 7.3: *The time series variations of isoprene mixing ratio and relative humidity (RH) during the segments of (a) onward (T1, west-east) and (b) return (T2, east-west) transects over the Bay of Bengal.*

changes in meteorological parameters, particularly by the decrease of RH and wind speed. As shown in **Figure 7.2c**, the simultaneous declines of equivalent potential temperature (EPT, θ_e) indicate the intrusions of higher altitude air masses during these low isoprene events. Sahu and Lal (2006) have reported observations of sudden downdrafts of ozone-rich free tropospheric air masses in the central Bay of Bengal during the fall inter-monsoon period. Additionally, the anomalies in meteorological parameters, e.g., wind speed, wind direction, RH, etc., characterize the effect of downdrafts in the tropical MBL (Folkins et al., 1999; Folkins & Martin, 2005).

Further, the time series variations of isoprene and relative humidity (RH) show an anti-correlated tendency during the segments of T1 and T2 transects (**Figure 7.3**). Along both transects, measurements of short-term

increase and decrease in mixing ratios were associated with the decrease and increase in RH, respectively. For instance, the events of elevated isoprene concentrations (> 1 ppb) along T1 are marked by a sharp decline in RH ($< 76\%$). The relations of atmospheric isoprene with RH support the intermittent impact of isoprene-rich terrestrial air masses in the MBL.

Overall, the variability of isoprene and DMS showed an inverse relationship along both longitudinal transects over the Bay of Bengal, likely driven by the influence of terrestrial air masses. However, the variability patterns of isoprene and DMS mixing ratios over the Andaman Sea displayed a mixed trend. The mean isoprene mixing ratio (0.80$\pm$0.06 ppb) over the Andaman Sea were lower than the Bay of Bengal (0.85 $\pm$0.19 ppb) as demonstrated by Welch's t-test ($p<0.0001$). Although the fluctuations in isoprene concentrations were less prominent than those of DMS, the isoprene levels followed the DMS variability trend during 2–7 October, except for coral-related enhancements observed in the evenings of 3 and 6 October. However, the assessment of $\mathrm{Iso_{VC}}$ revealed a variability pattern similar to that of DMS throughout measurements in the Andaman Sea. This could be attributed to two factors: the transport of terrestrial isoprene in the air mass from the Andaman shelf region, and stress-induced emissions of isoprene from coral reefs and marine ecosystem.

Along with DMS, Swan et al. (2016) have reported isoprene production by *Acropora aspera* coral from the GBR. Peak isoprene emissions occurred when corals were physically stressed by agitation, accompanied by mucus release. Conversely, no substantial isoprene or mucus release was detected in undisturbed *A. aspera* fragments (Dawson et al., 2021). The daytime decline of isoprene due to photochemistry is evident on all days over the Andaman Sea, except 2 October. The increase in isoprene on 2 October was associated with transition to southwest (SW; 180–270°) winds and significant changes in salinity ($\Delta \sim 3$) and SST ($\Delta \sim \pm 1^{\circ}$C), which is also consistent with corresponding DMS variability.

7.3.2 Diurnal and short-term variations of isoprene over the northern Indian Ocean

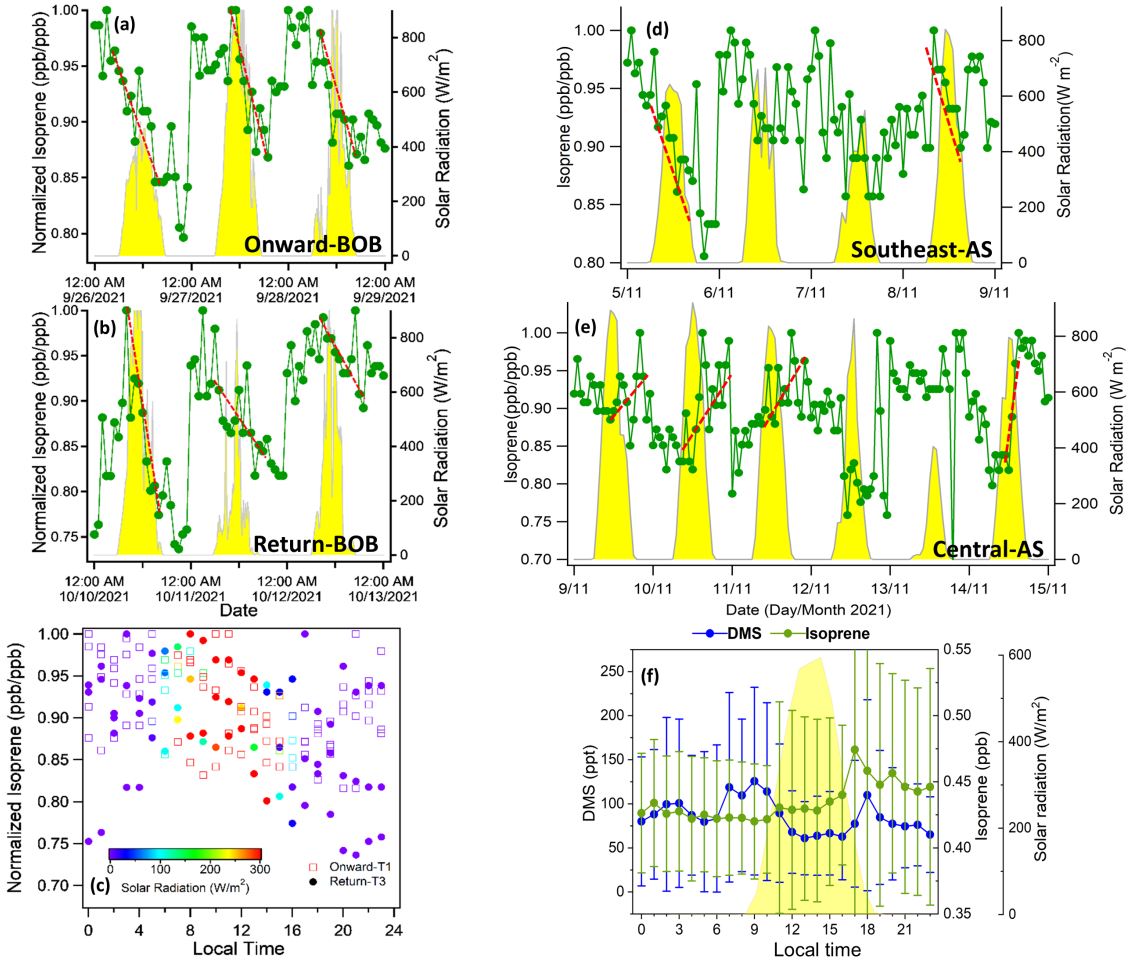

Figure 7.4: *The time series variations of the normalized isoprene mixing ratio to the daily maximum, and solar radiation flux along (a) onward (T1, west-east) and (b) return (T2, east-west) transects in the Bay of Bengal, and (d) southeast, and (e) central Arabian Sea. The red dashed lines indicate daytime decline. Diurnal variation of (c) normalized isoprene mixing ratios over the Bay of Bengal, and (f) observed isoprene and DMS mixing ratios over the Arabian Sea.*

The time series of isoprene mixing ratio data exhibited significant day-to-day variations, making it difficult to infer an overall diurnal dependence. Therefore, to scale the impact of transient spikes and day-to-day variability, the hourly isoprene mixing ratio data have been normalized to the corresponding daily maximum value (e.g., Ferracci et al., 2024; Wohl et

al., 2020). The normalized isoprene data during both longitudinal transects in the Bay of Bengal show higher values (mostly >0.95 ppb ppb^{-1}) in the early morning hours, which declined below 0.85 ppb ppb^{-1} by late afternoon hours. The isoprene levels and rate of decline for the clear-sky days were significantly higher than those for the cloudy days. For example, the normalized isoprene concentrations declined from ∼1.0 ppb ppb^{-1} at sunrise to ∼0.86 and 0.74 ppb ppb^{-1} in the evenings of the clear-sky days on 27 September and 10 October, respectively. Some hour-to-hour fluctuations, deviating from the decreasing trend lines, were associated with the changes in solar flux and meteorological and sea surface parameters, as noticed during the cloudy days of 11-12 October. On the afternoon of 12 October, the normalized concentration showed a lesser decline than that seen on other days. This could be due to a sudden increase in SST from 30.4-31.5 °C between 10:30–11:00 IST, enhancing the air-sea exchange of isoprene and counterbalancing the loss due to OH oxidation (**Figure 7.4b**). The composite diurnal patterns of the normalized-isoprene (**Figure 7.4c**) demonstrate a decline of 15-20% in the afternoon compared to early morning during both transects. This establishes the effect of photo-oxidation loss by reaction with OH radical, leading to lower daytime isoprene concentrations.

However, despite the high solar flux, the normalized isoprene data in the Arabian Sea show an increase from 0.75–0.85 ppb ppb^{-1} in early morning to 0.95–1.0 ppb ppb^{-1} in late afternoon hours (**Figure 7.4e**). This pattern is more consistent in the central Arabian Sea than in the southeast Arabian Sea, similar to those observed over the Bay of Bengal (**Figure 7.4d**). The rate of decline of normalized isoprene in the southeast Arabian Sea is more prominent near the coast (1.0 to 0.8 ppb ppb^{-1}) than over the offshore open ocean waters of the Arabian Sea. We further examined the campaign mean diurnal variations of the isoprene and DMS mixing ratios over the Arabian Sea (**Figure 7.4f**). Isoprene exhibited an apparent increase during 12–17 hr LT with maximum diurnal concentrations ∼17 hr LT, while DMS

continued to decrease till ~17 hr LT due to its photochemical loss. These results suggest that the photochemical production of isoprene at the SML could be a prominent source in the open ocean of the Arabian Sea. The SML is an organic-rich layer at the air-sea interface, where photosensitized reactions involving dissolved organic matter and UV exposure lead to abiotic production and direct emission of isoprene from the sea surface (Ciuraru et al., 2015). Based on the global modelling study, Conte et al. (2020) have reported significant contributions (0.39 Tg C yr^{-1}; 0.29–0.49 Tg C yr^{-1}) directly from the SML to the total global marine isoprene emissions into the atmosphere. On the other hand, the contributions from the terrestrial sources over the Bay of Bengal and the southeast Arabian Sea were higher than those from oceanic sources. Relationships between daily mean DMS and isoprene mixing ratios also support the contribution of terrestrial and marine isoprene over both the basins (**Figure 7.5**). The daily mean mixing ratios of DMS and isoprene show an inverse relation in the Bay of Bengal, indicating the predominant terrestrial and oceanic sources of isoprene and DMS, respectively. Over the Arabian Sea, except near the Kochi port, isoprene mixing ratios show lesser variability (0.35–0.5 ppb), while DMS showed relatively large variability (40–200 ppt).

Several studies have reported the diurnal dependence of isoprene in the MBL of different oceanic regions. However, unlike the present study, the isoprene measurements in the MBL of most other oceanic regions have shown relatively higher daytime concentrations due to increased marine emissions from the metabolic activity of phytoplankton (Shaw et al., 2010). Tripathi et al. (2020a) reported higher daytime concentrations (0.69 ± 0.06 ppb) than nighttime (0.44 ± 0.08 ppb) in the MBL of the Arabian Sea in the spring inter-monsoon season. The higher daytime isoprene mixing ratios measured at coastal stations of Cape Grim (Tasmania) and Mace Head (Ireland) were attributed to terrestrial influences (Lewis et al., 1999; 2001). Colomb et al. (2009) reported higher isoprene mixing ratios in the

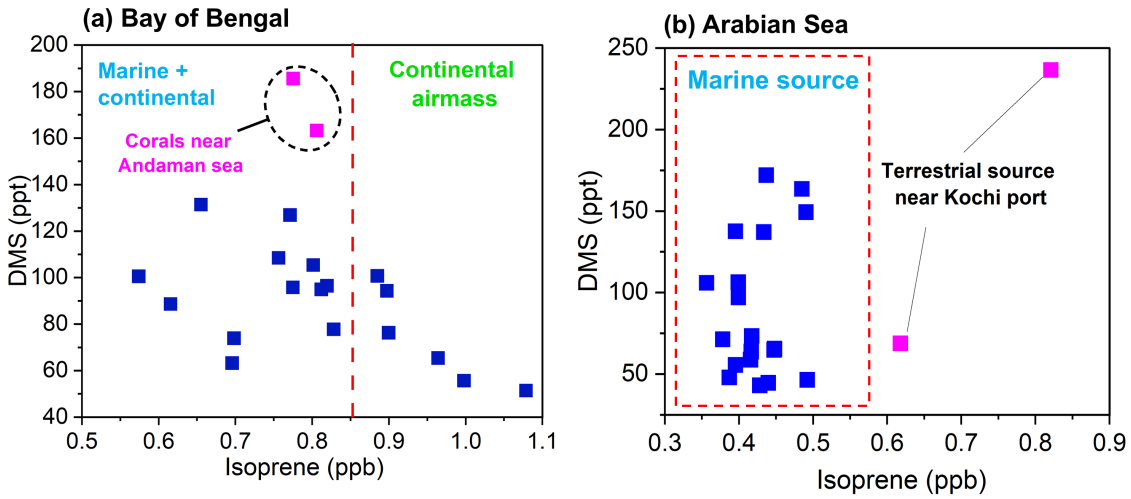

Figure 7.5: *Scatter plot between the daily mean DMS and isoprene mixing ratios over the (a) Bay of Bengal during 27 September-14 October 2021 and (b) Arabian Sea during 3-24 November 2021.*

forenoon hours (10:00–12:00 LT) in the MBL of the southern Indian Ocean during December 2004. The observations in the MBL of the Southern Ocean show higher mixing ratios during the daytime with a peak in the morning hours and lower values at night (Ferracci et al., 2024). Wohl et al. (2020) have reported $\sim 12\%$ higher daytime isoprene mixing ratios than the nighttime values in the Atlantic sector of the Southern Ocean during February–April 2019.

7.3.3 Longitudinal dependence of isoprene mixing ratio in the Bay of Bengal

The dependencies of isoprene on atmospheric pressure were investigated as functions of longitude, wind speed, and air temperature (**Figure 7.6**). The occurrences of relatively lower (< 1006 mb) and higher (> 1006 mb) atmospheric pressures at different locations along the ship track indicate the dominance of land-influenced and marine air masses, respectively. The variability in isoprene measurements was significantly higher in land-influenced air masses (0.83$\pm$0.22; range 0.55–1.15 ppb) than in the oceanic air masses (0.81$\pm$0.14; 0.58–1.0 ppb), based on F-test (F=2.5, p$<$0.0001). This was also associated with relatively stable and fluctuating meteorological conditions

in continental and marine air masses, respectively.

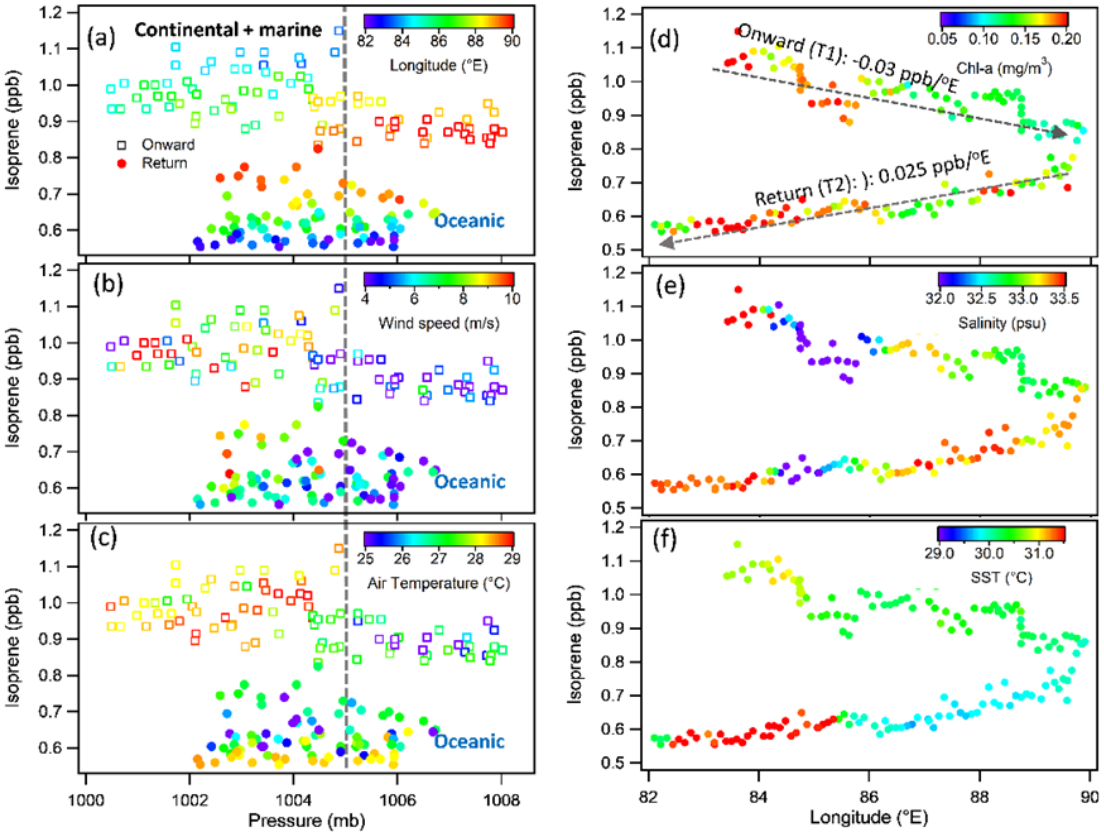

Figure 7.6: *The left panels (a-c) show the relationships between the isoprene mixing ratio and ambient air pressure in two distinct regimes, representing predominant influences of continental air (low pressures) and oceanic air (higher pressures). The right panels (d-f) show the longitudinal dependence of the isoprene as a function of the Chl-a concentration, salinity, and SST during the onward (T1, west-east) and return (T2, east-west) transects over the Bay of Bengal.*

In **Figure 7.6d-f**, we have further investigated the longitudinal dependence of isoprene as a function of Chl-a, salinity, and SST along the two transects between 82–90°E. Along T1, the isoprene mixing ratio varied in the range of 0.88–1.15 ppb and gradually decreased west-to-east (-0.03 ppb $^{\circ}E^{-1}$). In contrast, it varied between 0.55–0.86 ppb and gradually increased west-to-east (0.025 ppb $^{\circ}E^{-1}$) along T2. The isoprene mixing ratios were higher throughout the T1 longitudinal transect than T2, with average values of 0.96 ± 0.07 and 0.62 ± 0.06 ppb, respectively. A decreasing tendency in isoprene levels from the coast to the open ocean along T1 can be

attributed mainly to increased loss and dilution in the land-influenced air masses transporting terrestrial isoprene into the MBL. As shown in **7.1b**, the measurements of isoprene along the T1 transect were mostly influenced by the SW/W winds. The measurements with stronger winds (> 5 m s^{-1}) and higher θ_e (> 348 K) indicate the transport of continental-influenced air masses. The biogenic emission from dense vegetation in peninsular India is known to be an important source of isoprene and other BVOCs (Tripathi et al., 2021). Therefore, rapid transport of air masses from this region led to elevated isoprene levels over the coastal Bay of Bengal.

Despite relatively elevated Chl-a concentrations, lower isoprene mixing ratios (< 0.6 ppb) over the coastal waters (82–84°E) along T2 coincided with the higher SST (> 31°C) and salinity (> 33.5). Ooki et al. (2015) have reported elevated seawater isoprene concentrations (29–75 pmol/L) in the eutrophic tropical Indian Ocean (10°N–12°S), including the southern Bay of Bengal, in the KH-09-5 campaign during November 2009 to January 2010. A satellite-based study by Zhang and Gu (2022) has reported a negative correlation between marine isoprene emission flux and SST in tropical oceans. Simó et al. (2022) have reported an exponential increase in isoprene production between -0.8 °C and 23 °C, but a drastic drop at higher SST. Further, the decrease in marine isoprene emission from the productive and warm coastal waters could be explained by a substantial chemical and biological consumption of isoprene in seawater (Simó et al., 2022). In fact, the isoprene consumption rates in Chl-a rich surface waters have been similar to or greater than ventilation rates to the atmosphere. Thus, the lower isoprene mixing ratios in the coastal Bay of Bengal during the T2 transect could be due to the lower terrestrial inputs and lesser marine fluxes. Moreover, the measurements of isoprene along T2 were influenced mainly by the NW–NE winds (**7.1d**), influenced by the air masses with lower θ_e and long-range transport from the less productive open ocean regions of the Indian Ocean.

7.3.4 Contributions of surface oceanic processes and terrestrial outflow

In addition to meteorological and photochemical processes, the temporal and spatial variations of biological and physical parameters in the sea surface drive the air-sea exchange of isoprene in the MBL (Zhang and Gu, 2022). As shown in **Figure 7.7**, the isoprene mixing ratio along T1 exhibits an increasing trend with SST, with significant enhancements with just $\sim 1^{\circ}$C (30 to 31°C) rise in SST. The sharp increases in isoprene mixing ratio (0.88 to 1.0 ppb) and $\mathrm{Iso_{VC}}$ on the evening of 26 September were associated with a sudden increase in salinity from 30.2 to 32.3 (**7.2a**). However, the isoprene mixing ratio does not show a clear relation with a significant change in salinity from 30.7 to 33.7.

Although noticed clearly along T1, the isoprene mixing ratio shows increasing trends with the air temperature (26–29°C) associated with decreasing RH levels throughout the campaign (**Figure 7.7c**). The $\mathrm{Iso_{VC}}$ levels also increased rapidly with the increasing ambient air temperature, particularly along T1 (**Figure 7.8a**). The exponential response of $\mathrm{Iso_{VC}}$ to increasing air temperature in the present study resembles the temperature-dependent emission of isoprene from terrestrial vegetation in the tropics (e.g., Kalogridis et al., 2014; Sahu et al., 2017), providing evidence of the transport from terrestrial biogenic sources. Except for a few points, the relations of the isoprene mixing ratio with SST, Chl-a, and salinity appear coincidental, as the terrestrial outflow influenced the measurements over the coastal productive water during this transect (T1). Therefore, instead of marine emissions, the dominance of terrestrial outflow controls the longitudinal variations of isoprene along T1. A recent study by Wang et al. (2024) has reported the contributions of oceanic emissions and terrestrial outflows to the atmospheric concentrations of various NMHCs, including isoprene, in the marginal seas of China. The findings indicate that terrestrial outflows

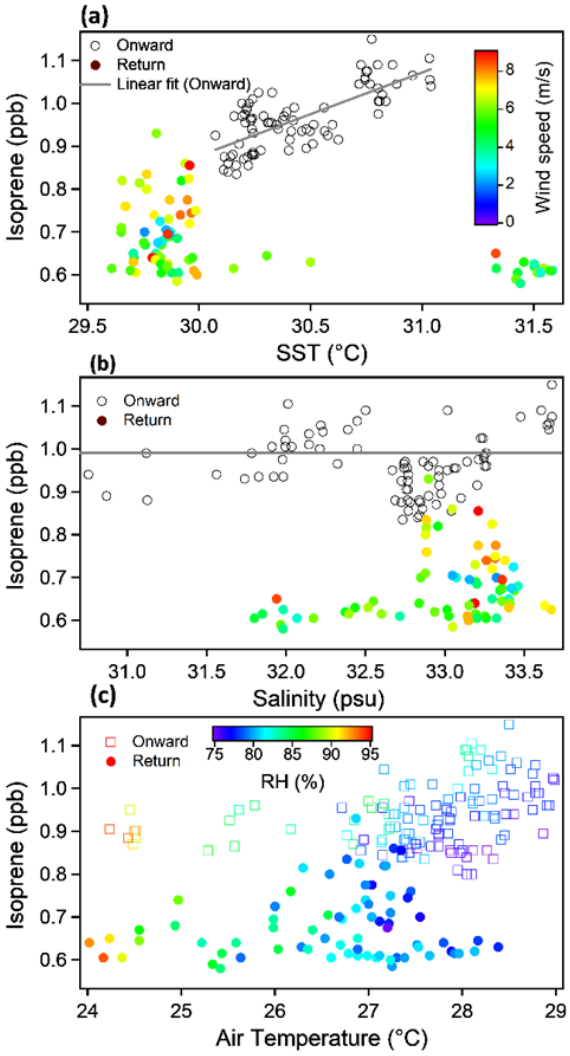

Figure 7.7: *The dependencies of the isoprene mixing ratio with (a) SST, (b) salinity, and (c) air temperature along the onward (T1) and return (T2) longitudinal transects over the Bay of Bengal during September-October 2021.*

significantly influence the variability of atmospheric NMHCs, responsible for 69.6% of the alkenes and isoprene observed in this region.

The enhanced isoprene concentrations along T2 over the open ocean were associated with the lower Chl-a (< 0.1 mg m^{-3}) and higher salinity (> 32.7) values. In contrast, relatively lower isoprene mixing ratios were associated with higher SST ($>$ 30°C) and lower salinity (< 32.6) values. However, the data points with lower isoprene concentrations were measured in biologically productive (Chl-a: 0.15–0.22 mg m^{-3}) near the coastal regions (82–84°E). The isoprene mixing ratio along T2 decreased exponentially

with the increasing Chl-a concentration (**Figure 7.8b**). This relationship with Chl-a further validates the substantial role of chemical and biological consumption of isoprene in seawater (Acuña Alvarez et al., 2009; Simó et al., 2022), confirming the lower marine isoprene emission over productive surface coastal waters along T2.

Overall, the contrasting relations of the isoprene mixing ratios with oceanic parameters along T1 and T2 highlight the complex interplay of air-sea exchange processes and terrestrial outflow.

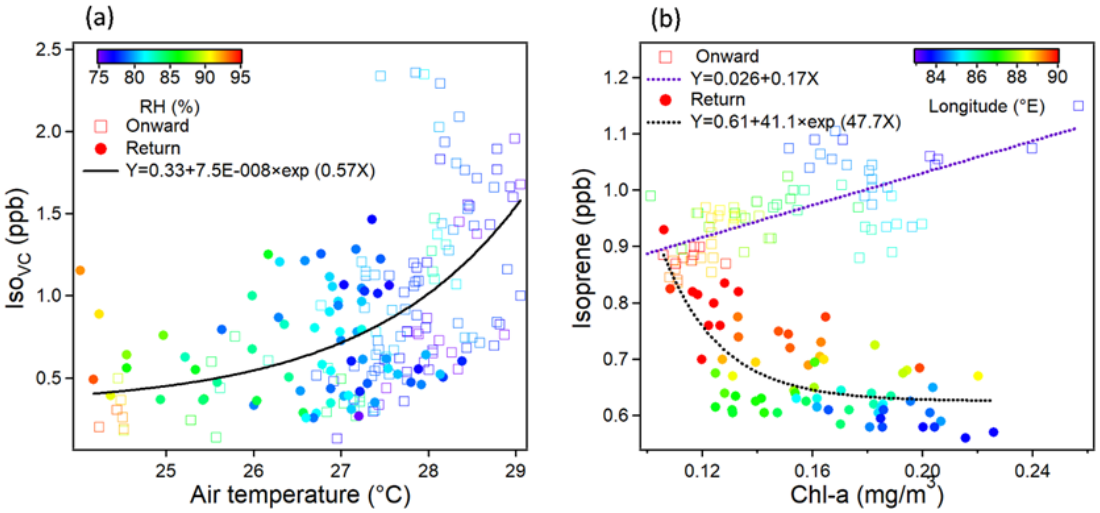

Figure 7.8: *The relations of (a) VC-normalized isoprene (Iso_{VC}) mixing ratio with air temperature and (b) isoprene mixing ratio with Chl-a concentration along the onward and return longitudinal transects over the Bay of Bengal during September-October 2021. The black curve in panel (a) shows an exponential fit of all data points. The dotted curves in panel (b) show linear and exponential fits along the onward and return longitudinal transects, respectively.*

7.4 Conclusion

The longitudinal dependence of atmospheric isoprene over the central Bay of Bengal can be described by a decrease from coastal India to open ocean during the west-east (1.15–0.88 ppb) transect, but a decrease from open ocean towards the coast during the east-west (0.86–0.55 ppb) transect. The higher and lower isoprene mixing ratios in the MBL of the Bay of

Bengal in the post-monsoon season were associated with the measurements of terrestrial outflow and marine air masses, respectively. In addition to the transport of distinct air masses from peninsular India and cleaner marine regions, the complex interplay of air-sea exchange and fluctuations in sea surface physical and meteorological factors controlled the short-term variations of isoprene in the MBL. The composite diurnal pattern of isoprene mixing ratio in the Bay of Bengal shows higher values in the early morning hours and declines during the daytime, with the lowest in the afternoon, indicating the significance of OH oxidation loss. However, the photo-production of isoprene at the SML is a prominent source in the open ocean Arabian Sea.

Except for certain locations, the impact of air-sea exchange on isoprene variability linked to biogeochemical processes appears to be a minor factor due to the high background concentrations caused by the dominance of terrestrial outflow. VC-normalized isoprene mixing ratios tend to show an exponential increase with increasing air temperature in the MBL, resembling the temperature-dependent emission from terrestrial vegetation in the tropics. Along with the relation between $\mathrm{Iso_{VC}}$ and air temperature, the back trajectory analysis also supports significant contributions of isoprene from terrestrial sources. However, the decrease in isoprene concentrations with Chl-a during the transport of oceanic air over the productive (Chl-a $>$0.20 mg $\mathrm{m^{-3}}$) and warmer (SST $>$ 31°C) surface coastal waters indicates a substantial chemical and biological consumption of isoprene in seawater.

The contributions of terrestrial outflow can vary significantly as the regions of the northern Indian Ocean experience strong seasonal changes in wind circulation. Further, seasonal variations in SST, salinity, and Chl-a can have a substantial impact on the air-sea exchange of isoprene and other oceanic trace gases. Therefore, the key factors governing the level and variability of reactive trace gases in the MBL of the northern Indian Ocean need a detailed evaluation based on comprehensive measurements in different seasons.

Chapter 8

Summary and Scope of Future Research

8.1 Summary

This thesis presents a comprehensive analysis of the first high time-resolution *in situ* shipborne measurements of atmospheric DMS and isoprene mixing ratios over different basins of the northern Indian Ocean, including the Arabian Sea, the Bay of Bengal, the Andaman Sea, the Laccadive Sea, and the coastal waters of Sri Lanka, during the post-monsoon season. The measurements were conducted during two ship campaigns onboard ORV *Sagar Kanya*, SK#373 and SK#374, in the eastern and western basins of the northern Indian Ocean, respectively. Using state-of-the-art TD-GC-FPD/FID-based analyzers, continuous measurements of DMS, C_2–C_6 NMHCs, and C_6–C_{12} NMHCs were performed at a resolution of 24, 30, and 40 min, respectively. The data were analysed to investigate the spatiotemporal distributions of DMS and isoprene in the MBL of the northern Indian Ocean, and the role of oceanic and meteorological variables in their variability.

DMS mixing ratios exhibited large spatial and temporal variability across the different oceanic regions, which were more pronounced over coastal waters compared to the open ocean. The highest DMS concen-

trations were observed over the highly productive waters of the Arabian Sea, with a regional mean of 116±120 ppt. The DMS flux of 10.9±7.3 μmol m^{-2} d^{-1} estimated over the Arabian Sea was also substantially higher than 4.9±3.2 μmol m^{-2} d^{-1} over the Bay of Bengal. In contrast, isoprene mixing ratios in the MBL of the Bay of Bengal (0.82±0.15 ppb) were nearly twice as high as those measured over the Arabian Sea (0.44±0.08 ppb). Notably, the factors and processes controlling the day-to-day and diurnal variability of atmospheric DMS (**Table 8.1**) and isoprene show distinct regional differences.

In the Arabian Sea, the DMS mixing ratios in the southeast (98±87 ppt) and northeast (116±120 ppt) coastal regions were higher than in the oligotrophic central Arabian Sea (62±53 ppt). Regions with higher Chl-a concentration typically showed enhanced DMS mixing ratios attributed to high biomass abundance and phytoplankton metabolic activity. Episodes of sudden increases in DMS were often associated with salinity gradients of -0.3 to +0.2 hr^{-1} and SST fluctuations, indicating that salinity fronts, localized upwelling, and surface-overturing processes played crucial roles in modulating DMS levels.

DMS mixing ratios were higher along the east-west (103±37 ppt) longitudinal transect than the west-east (77±24 ppt) longitudinal transect over the Bay of Bengal. This distinct longitudinal variability was driven by the predominance of air masses from continental and productive oceanic regions, respectively, supported by chlorophyll exposure (E_a) values. Atmospheric instabilities such as downdraft events played a significant role in the short-term variability of DMS over the region. Despite a relatively lower DMS background (~47 ppt) and E_a (<0.5 mg m^{-3}), higher mean DMS over the Andaman Sea suggests significant influence of strong localized sources. In the Andaman Sea, the higher mean DMS mixing ratios of ~112±68 ppt were found to be significantly influenced by emissions from coral reefs of the Andaman Islands and benthic corals of the Invisible Bank, particularly

during low tide. DMS enhancements from coral reefs increased with wind speed and under higher SST conditions. A flux of ~0.5 μmol m^{-2} hr^{-1} was estimated for coral reef emissions, extrapolated into an annual regional sulfur emission of ~1.43 Gg S yr^{-1}. However, underrepresented in global models, the findings of our study highlight that the coral reef emissions can potentially be an important source of sulfur in the tropical Indian Ocean. The estimated DMS air-sea fluxes over the Arabian Sea and Bay of Bengal were considerably higher than the last reported fluxes over the region, about two decades ago.

The diurnal patterns of DMS showed distinct regional characteristics over the oligotrophic open ocean waters of the central Arabian Sea and Bay of Bengal, and productive coastal and offshore waters. Despite distinct regional features, the impact of OH-driven daytime oxidation on DMS variability was consistent over all the study regions covered during the campaigns. However, the nighttime chemistry varied significantly based on the continental influence. Transport of polluted continental air introduced high NO_x environments that enhanced DMS-NO_3 chemistry at night in coastal regions. In addition, the transport of more reactive terrestrial VOCs in continental outflow impacted the DMS oxidation rates, especially in the northeast Arabian Sea and the Laccadive Sea. Nighttime DMS enhancements in open ocean and offshore waters of the Arabian Sea and Laccadive Sea were also associated with accumulation under low ventilation conditions.

In addition to that, nutrients and flow cytometry data indicated that the variability in DMS was also linked to nutrient dynamics. In the Arabian Sea, higher DMS levels were measured in the nitrate-limited environments. In the Bay of Bengal, a positive relationship between DMS levels and *Synechococcus*, observed essentially under high silicate conditions in the Bay of Bengal, indicates the complex impact of picophytoplankton and diatom abundances on DMS fluxes and atmospheric levels.

The DMS levels and variability patterns over the coastal waters of the Indian subcontinent exhibit higher dependence on dilution and wind conditions than on biomass abundance. The higher (113±37 ppt) and lower (53±7 ppt) DMS levels measured over the east coast of Sri Lanka and Laccadive Sea were due to the dominance of marine and continentally-influenced air masses, respectively. Analysis of tide height data shows substantial DMS enhancements (>200 ppt) due to stress-induced coral reef emissions at higher SST over northeast Sri Lanka and southwest India. Analysis of simultaneously measured DMS and isoprene mixing ratios reveals complex chemical interactions over the coastal region of the Indian subcontinent. Under the influence of continental outflow, isoprene reactivity (1±0.1 s^{-1}) far exceeded that of DMS (0.01±0.002 s^{-1}), potentially modulating the oxidation capacity of the coastal marine atmosphere. The interaction between terrestrial BVOCs and DMS could alter the aerosol chemical composition and CCN properties in the MBL. Previous studies have shown that the presence of DMS can enhance secondary organic aerosol (SOA) yields from isoprene.

The investigations of the first high-time-resolution measurements of isoprene mixing ratios over the Bay of Bengal and Arabian Sea suggest a strong interplay of terrestrial outflow and oceanic emissions in driving the atmospheric isoprene variability over the northern Indian Ocean. Over the Bay of Bengal, the decreasing west-east (1.15-0.88 ppb) and east-west (0.86-0.55 ppb) longitudinal trends were associated with the dominance of land-influenced and oceanic air masses, respectively. The ventilation-normalized isoprene data during the west-east longitudinal transect increased exponentially with the increasing air temperature, resembling terrestrial vegetation emission patterns. This highlights that while marine sources of isoprene exist, terrestrial outflow from the Indian subcontinent was the major contributor of isoprene in the MBL of the Bay of Bengal. A decrease in isoprene levels with increasing Chl-a during the east-west longitudinal

transect suggested microbial or photochemical consumption of isoprene in seawater.

Table 8.1: *The key parameters controlling the variability of the atmospheric DMS over different basins of the northern Indian Ocean.*

Arabian Sea	**Bay of Bengal**	**Andaman Sea**	**Southern coastal waters of the Indian sub-continent**
Processes controlling regional (synoptic)-scale variability			
• Local biogeochemistry, particularly Chl-a, was a prominent factor, with a regional impact of air mass transport. • Dilution in open and offshore waters	• Air mass transport (E_a) was the major factor • Dilution in coastal waters	• Influence of emissions from coral reefs around the Andaman Islands	• Atmospheric dilution by terrestrial outflow • Influence of emissions from coral reefs under thermal stress
Processes controlling mesoscale and short-term variability			
• Salinity gradients	• Atmospheric instabilities such as convective downdraft events	• Atmospheric instabilities such as downdraft events	• Atmospheric chemistry modulated by terrestrial outflow
Biogeochemical factors			
• Nutrient stress: Nitrate limitation	• DMS levels increased with diatoms & pico-phytoplankton abundance	• DMS levels increased with diatoms & pico-phytoplankton abundance	• Dinoflagellate *K. mikimotoi* in estuarine and coastal waters off the Kerala coast could have led to DMS enhancement
Air Sea flux ($\mu mol\ m^{-2}\ d^{-1}$)			
~10.9±7.3	~4.9±3.2	Coral reef emissions ~ 0.5	

8.2 Scope of Future Research

The findings of this thesis provide important advances in our understanding of sources and atmospheric processes controlling the levels and variability of DMS and isoprene in the marine air of the northern Indian Ocean. However, they also open up multiple critical avenues for future research:

1. **Role of atmospheric DMS in CCN formation and regional chemistry-climate interactions over the northern Indian Ocean**

   Our findings present the imperative for future research investigating the impact of the elevated atmospheric DMS concentrations over the northern Indian Ocean on the formation of secondary aerosols and CCN activity. As oxidation of DMS is a major natural source of sulfate aerosols, it can substantially modulate cloud microphysical properties and alter the regional radiative balance and climate of the region. These first *in situ* measurements provide a unique opportunity to investigate how regional DMS variability translates into CCN production and cloud characteristics, an area still under-sampled and largely unexplored in the Indian Ocean. Comprehensive future work integrating experimental campaigns and modelling is essential for quantifying these effects and enhancing our understanding of chemistry-climate feedbacks over the northern Indian Ocean and surrounding regions, particularly concerning the regional climate response and monsoon behaviour.

2. **Marine isoprene flux and implications for atmospheric chemistry**

   The observed elevated isoprene levels over the northern Indian Ocean raise important questions about their sources and impact. Future studies should prioritize quantifying the contributions of air-sea fluxes of isoprene, which would require measurement of its concentration in

seawater combined with other flux estimation techniques. Additionally, given its high reaction rates with major atmospheric oxidants (OH and NO_3) and its potential to drive secondary aerosol formation, investigating the influence of elevated isoprene levels on the marine atmospheric oxidation capacity is crucial to determine their influence on the aerosol budget.

Moreover, the transport of terrestrial air masses, particularly from the Indian subcontinent, may profoundly impact the composition and chemical processes of reactive trace gases in the MBL. The measurements and detailed modelling studies characterizing these interactions will advance our understanding of the complex couplings between continental outflow and marine atmospheric chemistry in the land-locked basins of the northern Indian Ocean.

3. **Seasonal and interannual variability**

   This study has focused on investigating the sources and atmospheric processes controlling the variability features of DMS and isoprene in the post-monsoon season of 2021. However, studies conducted during BOBMEX-1998 and INDOEX-1999 experiments showed large seasonal variability in DMS seawater concentrations. Therefore, seasonal observations of these important trace gases are essential to estimate their annual emissions. Additionally, the higher DMS flux estimated in the present study compared to the observations during previous campaigns highlights the need for long-term measurements of DMS and other BVOCs to assess the potential changes in response to climate change.

4. **Augmentation with satellite data and improved regional parameterizations**

   The overestimation of oceanic DMS in the Indian Ocean region through global parameterization schemes observed in our study suggests the requirement of region-specific parameterizations accounting for local

wind regimes, sea state, SST, and biological activity, and other important factors. This requires integration of high-resolution *in situ* data and satellite-derived parameters (e.g., SST, Chl-a, aerosol optical depth) in regional chemistry-climate models to improve simulations of DMS and isoprene emissions and their climate feedbacks.

5. **Seawater measurements and the role of Phytoplankton Community composition in BVOC emissions in the northern Indian Ocean**

   Although DMS and isoprene emissions are linked to phytoplankton productivity, the lack of concurrent seawater measurements limits our ability to determine the specific contributions of different phytoplankton groups, such as diatoms, dinoflagellates, and coccolithophores, in the northern Indian Ocean. Future research integrating seawater measurements of DMS with pigment analysis and flow cytometry can help examine the DMS emission potentials from different phytoplankton functional groups under varying nutrient regimes.

6. **Coral reef DMS emissions under a changing climate**

   The substantial DMS emissions from coral reefs highlight the need for focused studies to examine the impact of bleaching events and ocean warming on DMS emissions from reef ecosystems. This is particularly crucial to assess their contribution to non-sea-salt sulfate aerosol (nss-SO_4^{2-}) formation under climate change scenarios.

Thus, this research highlights important knowledge gaps and suggests several directions for future research to advance our understanding of the effect of marine DMS and BVOCs on the atmospheric processes and regional climate over the northern Indian Ocean.

BIBLIOGRAPHY

Acuña Alvarez, L., Exton, D. A., Timmis, K. N., Suggett, D. J., and McGenity, T. J. (2009). Characterization of marine isoprene-degrading communities. Environmental Microbiology, 11(12), 3280–3291.https://doi.org/10.1111/j.1462-2920.2009.02069.x

Aguirre, C., Garreaud, R., Belmar, L., Farías, L., Ramajo, L., and Barrera, F. (2021). High-Frequency Variability of the Surface Ocean Properties Off Central Chile During the Upwelling Season. Frontiers in Marine Science, 8. https://www.frontiersin.org/journals/marine-science/articles/10.3389/fmars.2021.702051

Ahmed, A., Kurian, S., Gauns, M., Chndrasekhararao, A. V., Mulla, A., Naik, B., Naik, H., and Naqvi, S. W. A. (2016). Spatial variability in phytoplankton community structure along the eastern Arabian Sea during the onset of south-west monsoon. Continental Shelf Research, 119, 30–39. https://doi.org/10.1016/j.csr.2016.03.005

Alland, J. J., Tang, B. H., Corbosiero, K. L., and Bryan, G. H. (2021). Combined Effects of Midlevel Dry Air and Vertical Wind Shear on Tropical Cyclone Development. Part I: Downdraft Ventilation. Journal of the Atmospheric Sciences, 78(3), 763–782. https://doi.org/10.1175/JAS-D-20-0054.1

Andreae, M. O., and Crutzen, P. J. (1997). Atmospheric Aerosols: Biogeochemical Sources and Role in Atmospheric Chemistry. Science, 276(5315), 1052–1058. https://doi.org/10.1126/science.276.5315.1052

Andreae, T. W., Andreae, M. O., Bingemer, H. G., and Leck, C. (1993). Measurements of dimethyl sulfide and H2S over the western North Atlantic and the tropical Atlantic. Journal of Geophysical Research: Atmospheres, 98(D12), 23389–23396. https://doi.org/10.1029/91JD03016

Apte, J. S., Messier, K. P., Gani, S., Brauer, M., Kirchstetter, T. W., Lunden, M. M., Marshall, J. D., Portier, C. J., Vermeulen, R. C. H., and Hamburg, S. P. (2017). High-Resolution Air Pollution Mapping with Google Street View Cars: Exploiting Big Data. Environmental Science and Technology, 51(12), 6999–7008. https://doi.org/10.1021/acs.est.7b00891

Arnold, S. R., Spracklen, D. V., Williams, J., Yassaa, N., Sciare, J., Bonsang, B., Gros, V., Peeken, I., Lewis, A. C., Alvain, S., and Moulin, C. (2009). Evaluation of the global oceanic isoprene source and its impacts on marine organic carbon aerosol. Atmos. Chem. Phys., 10.

Asher, E. C., Dacey, J. W. H., Stukel, M., Long, M. C., and Tortell, P. D. (2017). Processes driving seasonal variability in DMS, DMSP, and DMSO concentrations and turnover in coastal Antarctic waters. Limnology and Oceanography, 62(1), 104–124. https://doi.org/10.1002/lno.10379

Atkinson, R., and Arey, J. (2003). Atmospheric Degradation of Volatile Organic Compounds. Chemical Reviews, 103(12), 4605–4638.https://doi.org/10.1021/cr0206420

Atkinson, R., Aschmann, S. M., and Pitts, J. N. Jr. (1988). Rate constants for the gas-phase reactions of the nitrate radical with a series of organic compounds at 296 .+-. 2 K. The Journal of Physical Chemistry, 92(12), 3454–3457. https://doi.org/10.1021/j100323a028

Ayers, G. P., and Cainey, J. M. (2007). The CLAW hypothesis: A review of the major developments. Environmental Chemistry, 4(6), 366–374.

Ayers, G. P., and Gillett, R. W. (2000). DMS and its oxidation products in the remote marine atmosphere: Implications for climate and atmospheric chemistry. Journal of Sea Research, 43(3), 275–286. https://doi.org/10.1016/S1385-1101(00)00022-8

Baiju, P. T., Prabhakaran, M. P., Pereira, F. G. B., and Jayaprakas, V. (2019). Rocky reef associated macro invertebrates and urochordates of South Kerala Coast, India. Research Journal of Marine Sciences, 7(2), 1–19.

Baker, A. R., Turner, S. M., Broadgate, W. J., Thompson, A., McFiggans, G. B., Vesperini, O., Nightingal, P. D., Liss, P. S., and Jickells, T. D. (2000). Distribution and sea-air fluxes of biogenic trace gases in the eastern Atlantic Ocean. Global Biogeochemical Cycles, 14(3). https://doi.org/10.1029/1999GB001219

Balaguru, K., Taraphdar, S., Leung, L. R., and Foltz, G. R. (2014). Increase in the intensity of postmonsoon Bay of Bengal tropical cyclones. Geophysical Research Letters, 41(10), 3594–3601.https://doi.org/10.1002/2014GL060197

Baliarsingh, S. K., Srichandan, S., Naik, S., Sahu, K., Lotliker, A., and Kumar, T. (2015). Seasonal variation of phytoplankton community composition in coastal waters off Rushikulya Estuary, East Coast of India. Indian Journal of Geo-Marine Sciences, 44, 1–19.

Bandy, A. R., Thornton, D. C., Blomquist, B. W., Chen, S., Wade, T. P., Ianni, J. C., Mitchell, G. M., and Nadler, W. (1996). Chemistry of dimethyl sulfide in the equatorial Pacific atmosphere. Geophysical Research Letters, 23(7), 741–744. https://doi.org/10.1029/96GL00779

Banerjee, P., and Prasanna Kumar, S. (2014). Dust-induced episodic phytoplankton blooms in the Arabian Sea during winter monsoon. Journal of Geophysical Research: Oceans, 119(10), 7123–7138.https://doi.org/10.1002/2014JC010304

Bardouki, H., Berresheim, H., Vrekoussis, M., Sciare, J., Kouvarakis, G., Oikonomou, K., Schneider, J., and Mihalopoulos, N. (2003). Gaseous (DMS, MSA, SO_2,

H_2SO_4 and DMSO) and particulate (sulfate and methanesulfonate) sulfur species over the northeastern coast of Crete. Atmospheric Chemistry and Physics, 3(5), 1871–1886.https://doi.org/10.5194/acp-3-1871-2003

Barlow, R. G., Mantoura, R. F. C., and Cummings, D. G. (1999). Monsoonal influence on the distribution of phytoplankton pigments in the Arabian Sea. Deep Sea Research Part II: Topical Studies in Oceanography, 46(3), 677–699. https://doi.org/10.1016/S0967-0645(98)00123-4

Barnes, I., Hjorth, J., and Mihalopoulos, N. (2006). Dimethyl Sulfide and Dimethyl Sulfoxide and Their Oxidation in the Atmosphere. Chemical Reviews, 106(3), 940–975. https://doi.org/10.1021/cr020529+

Beale, R., Dixon, J. L., Arnold, S. R., Liss, P. S., and Nightingale, P. D. (2013). Methanol, acetaldehyde, and acetone in the surface waters of the Atlantic Ocean. Journal of Geophysical Research: Oceans, 118(10). https://doi.org/10.1002/jgrc.20322

Beale, R., Liss, P. S., and Nightingale, P. D. (2010). First oceanic measurements of ethanol and propanol. Geophysical Research Letters, 37(24).https://doi.org/10.1029/2010GL045534

Bell, T. G., Landwehr, S., Miller, S. D., de Bruyn, W. J., Callaghan, A. H., Scanlon, B., Ward, B., Yang, M., and Saltzman, E. S. (2017). Estimation of bubble-mediated air–sea gas exchange from concurrent DMS and CO2 transfer velocities at intermediate–high wind speeds. Atmospheric Chemistry and Physics, 17(14), 9019–9033.https://doi.org/10.5194/acp-17-9019-2017

Bell, T. G., Porter, J. G., Wang, W.-L., Lawler, M. J., Boss, E., Behrenfeld, M. J., and Saltzman, E. S. (2021). Predictability of Seawater DMS During the North Atlantic Aerosol and Marine Ecosystem Study (NAAMES). Frontiers in Marine Science, 7. https://www.frontiersin.org/articles/10.3389/fmars.2020.596763

Bemal, S., and Anil, A. C. (2016). Genetic and ecophysiological traits of Synechococcus strains isolated from coastal and open ocean waters of the Arabian Sea. FEMS Microbiology Ecology, 92(11), fiw162. https://doi.org/10.1093/femsec/fiw162

Bender, S. J., Durkin, C. A., Berthiaume, C. T., Morales, R. L., and Armbrust, E. V. (2014). Transcriptional responses of three model diatoms to nitrate limitation of growth. Frontiers in Marine Science. https://www.frontiersin.org/journals/marine-science/articles/10.3389/fmars.2014.00003

Bepari, K. F., Shenoy, D. M., Chndrasekhara Rao, A. V., Kurian, S., Gauns, M. U., Naik, B. R., and Naqvi, S. W. A. (2020). Dynamics of dimethylsulphide and associated compounds in the coastal waters of Goa, west coast of India. Journal of Marine Systems, 207, 103228. https://doi.org/10.1016/j.jmarsys.2019.103228

Bhatti, Y. A., Revell, L. E., Schuddeboom, A. J., McDonald, A. J., Archibald, A. T., Williams, J., Venugopal, A. U., Hardacre, C., and Behrens, E. (2023). The sensitivity of Southern Ocean atmospheric dimethylsulfide (DMS) to modeled oceanic

DMS concentrations and emissions. Atmospheric Chemistry and Physics, 23(24), 15181–15196. https://doi.org/10.5194/acp-23-15181-2023

Blake, N. J., Blake, D. R., Chen, T.-Y., Collins Jr., J. E., Sachse, G. W., Anderson, B. E., and Rowland, F. S. (1997). Distribution and seasonality of selected hydrocarbons and halocarbons over the western Pacific basin during PEM-West A and PEM-West B. Journal of Geophysical Research: Atmospheres, 102(D23), 28315–28331. https://doi.org/10.1029/97JD02538

Blake, N. J., Blake, D. R., Simpson, I. J., Meinardi, S., Swanson, A. L., Lopez, J. P., Katzenstein, A. S., Barletta, B., Shirai, T., Atlas, E., Sachse, G., Avery, M., Vay, S., Fuelberg, H. E., Kiley, C. M., Kita, K., and Rowland, F. S. (2003). NMHCs and halocarbons in Asian continental outflow during the Transport and Chemical Evolution over the Pacific (TRACE-P) Field Campaign: Comparison With PEM-West B. Journal of Geophysical Research: Atmospheres, 108(D20). https://doi.org/10.1029/2002JD003367

Booge, D., Marandino, C. A., Schlundt, C., Palmer, P. I., Schlundt, M., Atlas, E. L., Bracher, A., Saltzman, E. S., and Wallace, D. W. R. (2016). Can simple models predict large-scale surface ocean isoprene concentrations? Atmospheric Chemistry and Physics, 16(18), 11807–11821. https://doi.org/10.5194/acp-16-11807-2016

Booge, D., Schlundt, C., Bracher, A., Endres, S., Zäncker, B., and Marandino, C. A. (2018). Marine isoprene production and consumption in the mixed layer of the surface ocean – a field study over two oceanic regions. Biogeosciences, 15(2), 649–667. https://doi.org/10.5194/bg-15-649-2018

Borker, S. G., Shenoy, D. M., Bepari, K. F., Kurian, S., and Uskaikar, H. (2022). Variation of biogenic sulphur compounds in the estuarine and coastal waters of Goa, West coast of India. Indian Journal of Geo-Marine Sciences, 51(06), 517–528.https://doi.org/10.56042/ijms.v51i06.56976

Boucher, O., Moulin, C., Belviso, S., Aumont, O., Bopp, L., Cosme, E., von Kuhlmann, R., Lawrence, M. G., Pham, M., Reddy, M. S., Sciare, J., and Venkataraman, C. (2003). DMS atmospheric concentrations and sulphate aerosol indirect radiative forcing: A sensitivity study to the DMS source representation and oxidation. Atmospheric Chemistry and Physics, 3(1), 49–65. https://doi.org/10.5194/acp-3-49-2003

Bourtsoukidis, E., Ernle, L., Crowley, J. N., Lelieveld, J., Paris, J.-D., Pozzer, A., Walter, D., and Williams, J. (2019). Non Methane Hydrocarbon (C2–C8) sources and sinks around theArabian Peninsula [Preprint]. Gases/Field Measurements/Troposphere/Chemistry (chemical composition and reactions).https://doi.org/10.5194/acp-2019-92

Bristow, L. A., Callbeck, C. M., Larsen, M., Altabet, M. A., Dekaezemacker, J., Forth, M., Gauns, M., Glud, R. N., Kuypers, M. M. M., Lavik, G., Milucka, J., Naqvi, S. W. A., Pratihary, A., Revsbech, N. P., Thamdrup, B., Treusch, A. H., and Canfield, D. E. (2017). N2 production rates limited by nitrite availability

in the Bay of Bengal oxygen minimum zone. Nature Geoscience, 10(1), Article 1.https://doi.org/10.1038/ngeo2847

Broadbent, A. D., and Jones, G. B. (2004). DMS and DMSP in mucus ropes, coral mucus, surface films and sediment pore waters from coral reefs in the Great Barrier Reef. Marine and Freshwater Research, 55(8), 849–855.

Brown, B. (2007). Coral reefs of the Andaman Sea—An integrated perspective. In Oceanography and Marine Biology (Vol. 45, pp. 173–194).https://doi.org/10.1201/9781420050943.ch5

Brüggemann, M., Hayeck, N., and George, C. (2018). Interfacial photochemistry at the ocean surface is a global source of organic vapors and aerosols. Nature Communications, 9(1). https://doi.org/10.1038/s41467-018-04528-7

Bucciarelli, E., and Sunda, W. G. (2003). Influence of CO2, nitrate, phosphate, and silicate limitation on intracellular dimethylsulfoniopropionate in batch cultures of the coastal diatom Thalassiosira pseudonana. Limnology and Oceanography, 48(6), 2256–2265. https://doi.org/10.4319/lo.2003.48.6.2256

Bullock, H. A., Luo, H., and Whitman, W. B. (2017). Evolution of Dimethylsulfoniopropionate Metabolism in Marine Phytoplankton and Bacteria. Frontiers in Microbiology, 8, 637.https://doi.org/10.3389/fmicb.2017.00637

Burdett, H. L., Hatton, A. D., and Kamenos, N. A. (2015). Effects of reduced salinity on the photosynthetic characteristics and intracellular DMSP concentrations of the red coralline alga, Lithothamnion glaciale. Marine Biology, 162(5), 1077–1085. https://doi.org/10.1007/s00227-015-2650-8

Burkholder, J. B., Sander, S. P., Abbatt, J. P. D., Barker, J. R., Cappa, C. D., Crounse, J. D., Dibble, T. S., Huie, R. E., Kolb, C. E., Kurylo, M. J., Orkin, V. L., Percival, C. J., Seinfeld, J. H., Talukdar, R. K., Tyndall, G. S., Wallington, T. J., and Wine, P. H. (2020). Chemical Kinetics and Photochemical Data for Use in Atmospheric Studies, Evaluation No. 19 (No. JPL Publication 19-5). Jet Propulsion Laboratory, California Institute of Technology. https://jpldataeval.jpl.nasa.gov/

Caldwell, P. C., M. A. Merrifield, P. R. Thompson (2015), Sea level measured by tide gauges from global oceans — the Joint Archive for Sea Level holdings (NCEI Accession 0019568), Version 5.5, NOAA National Centers for Environmental Information, Dataset, doi:10.7289/V5V40S7W.

Carpenter, L. J., Archer, S. D., and Beale, R. (2012). Ocean-atmosphere trace gas exchange. Chemical Society Reviews, 41(19).https://doi.org/10.1039/c2cs35121h

Carpenter, L. J., MacDonald, S. M., Shaw, M. D., Kumar, R., Saunders, R. W., Parthipan, R., Wilson, J., and Plane, J. M. C. (2013). Atmospheric iodine levels influenced by sea surface emissions of inorganic iodine. Nature Geoscience, 6(2). https://doi.org/10.1038/ngeo1687

Chance, R., Baker, A. R., Carpenter, L., and Jickells, T. D. (2014). The distribution of iodide at the sea surface. Environmental Science: Processes and Impacts, 16(8), 1841–1859. https://doi.org/10.1039/C4EM00139G

Charlson, R. J., Lovelock, J. E., Andreae, M. O., and Warren, S. G. (1987). Oceanic phytoplankton, atmospheric sulphur, cloud albedo and climate. Nature, 326(6114), Article 6114. https://doi.org/10.1038/326655a0

Chatterjee, A., Shankar, D., McCreary, J. P., Vinayachandran, P. N., and Mukherjee, A. (2017). Dynamics of Andaman Sea circulation and its role in connecting the equatorial Indian Ocean to the Bay of Bengal. Journal of Geophysical Research: Oceans, 122(4), 3200–3218. https://doi.org/10.1002/2016JC012300

Chen, Q., Sherwen, T., Evans, M., and Alexander, B. (2018). DMS oxidation and sulfur aerosol formation in the marine troposphere: A focus on reactive halogen and multiphase chemistry. Atmospheric Chemistry and Physics, 18(18), 13617–13637. https://doi.org/10.5194/acp-18-13617-2018

Chen, T., and Jang, M. (2012). Secondary organic aerosol formation from photooxidation of a mixture of dimethyl sulfide and isoprene. Atmospheric Environment, 46, 271–278. https://doi.org/10.1016/j.atmosenv.2011.09.082

Chen, Y., and Schäfer, H. (2019). Towards a systematic understanding of structure–function relationship of dimethylsulfoniopropionate-catabolizing enzymes. Molecular Microbiology, 111(6), 1399–1403. https://doi.org/10.1111/mmi.14230

Chowdhury, M., and Biswas, H. (2023). A coherent status of summer monsoon phytoplankton communities (2017–2018) along the Western Indian continental shelf: Implications for fisheries. Science of The Total Environment, 878, 162963. https://doi.org/10.1016/j.scitotenv.2023.162963

Ciuraru, R., Fine, L., Pinxteren, M. V., D'Anna, B., Herrmann, H., and George, C. (2015). Unravelling New Processes at Interfaces: Photochemical Isoprene Production at the Sea Surface. Environmental Science and Technology, 49(22), 13199–13205.https://doi.org/10.1021/acs.est.5b02388

Colomb, A., Gros, V., Alvain, S., Sarda-Esteve, R., Bonsang, B., Moulin, C., Klüpfel, T., and Williams, J. (2009). Variation of atmospheric volatile organic compounds over the Southern Indian Ocean (3049S). Environmental Chemistry, 6(1), 70–82.

Conte, L., Szopa, S., Aumont, O., Gros, V., and Bopp, L. (2020). Sources and Sinks of Isoprene in the Global Open Ocean: Simulated Patterns and Emissions to the Atmosphere. Journal of Geophysical Research: Oceans, 125(9), e2019JC015946. https://doi.org/10.1029/2019JC015946

Cooper, D. J., and Saltzman, E. S. (1993). Measurements of atmospheric dimethylsulfide, hydrogen sulfide,and carbon disulfide during GTE/CITE 3. Journal of Geophysical Research: Atmospheres, 98(D12), 23397–23409. https://doi.org/10.1029/92JD00218

Corn, M., Belviso, S., Partensky, F., Simon, N., and Christaki, U. (1996). Origin and Importance of Picoplanktonic DMSP. In R. P. Kiene, P. T. Visscher, M. D. Keller, and G. O. Kirst (Eds.), Biological and Environmental Chemistry of DMSP and Related Sulfonium Compounds (pp. 191–201). Springer US. https://doi.org/10.1007/978-1-4613-0377-0_17

Crawford, A. M., Stunder, B. J. B., Ngan, F., and Pavolonis, M. J. (2016). Initializing HYSPLIT with satellite observations of volcanic ash: A case study of the 2008 Kasatochi eruption. Journal of Geophysical Research: Atmospheres, 121(18), 10,786-10,803. https://doi.org/10.1002/2016JD024779

Cui, L., Xiao, Y., Hu, W., Song, L., Wang, Y., Zhang, C., Fu, P., and Zhu, J. (2023). Enhanced dataset of global marine isoprene emissions from biogenic and photochemical processes for the period 2001–2020. Earth System Science Data, 15(12), 5403–5425. https://doi.org/10.5194/essd-15-5403-2023

Cui, T., Green, H. S., Selleck, P. W., Zhang, Z., O'Brien, R. E., Gold, A., Keywood, M., Kroll, J. H., and Surratt, J. D. (2019). Chemical Characterization of Isoprene- and Monoterpene-Derived Secondary Organic Aerosol Tracers in Remote Marine Aerosols over a Quarter Century. ACS Earth and Space Chemistry, 3(6), 935–946. https://doi.org/10.1021/acsearthspacechem.9b00061

Dacey, J. W. H., Wakeham, S. G., and Howes, B. L. (1984). Henry's law constants for dimethylsulfide in freshwater and seawater. Geophysical Research Letters, 11(10), 991–994.https://doi.org/10.1029/GL011i010p00991

Dacey, J. W., and Zemmelink, H. J. (2001). Air–Sea Transfer: Dimethyl Sulfide, COS, CS2, NH4, Non-Methane Hydrocarbons, Organo-Halogens*. In J. H. Steele (Ed.), Encyclopedia of Ocean Sciences (Second Edition) (pp. 157–162). Academic Press. https://doi.org/10.1016/B978-012374473-9.00063-1

Dani, K. G. S., and Loreto, F. (2017). Trade-Off Between Dimethyl Sulfide and Isoprene Emissions from Marine Phytoplankton. Trends in Plant Science, 22(5), 361–372. https://doi.org/10.1016/j.tplants.2017.01.006

Davie-Martin, C. L., Giovannoni, S. J., Behrenfeld, M. J., Penta, W. B., and Halsey, K. H. (2020). Seasonal and Spatial Variability in the Biogenic Production and Consumption of Volatile Organic Compounds (VOCs) by Marine Plankton in the North Atlantic Ocean. Frontiers in Marine Science, Volume 7-2020. https://doi.org/10.3389/fmars.2020.611870

Davison, B. M., and Allen, A. G. (1994). A method for sampling dimethylsulfide in polluted and remote marine atmospheres. Atmospheric Environment, 28(10), 1721–1729. https://doi.org/10.1016/1352-2310(94)90182-1

Dawson, R. A., Crombie, A. T., Pichon, P., Steinke, M., McGenity, T. J., and Murrell, J. C. (2021). The microbiology of isoprene cycling in aquatic ecosystems. Aquatic Microbial Ecology, 87, 79–98.

de Boyer Montégut, C., Madec, G., Fischer, A. S., Lazar, A., and Iudicone, D. (2004). Mixed layer depth over the global ocean: An examination of profile data and a profile-based climatology. Journal of Geophysical Research: Oceans, 109(C12). https://doi.org/10.1029/2004JC002378

de Bruyn, W. J., Harvey, M., Cainey, J. M., and Saltzman, E. S. (2002). DMS and SO2 at Baring Head, New Zealand: Implications for the Yield of SO2 from DMS. Journal of Atmospheric Chemistry, 41(2), 189–209.https://doi.org/10.1023/A:1014252106572

de Gouw, J. A., Goldan, P. D., Warneke, C., Kuster, W. C., Roberts, J. M., Marchewka, M., Bertman, S. B., Pszenny, A. A. P., and Keene, W. C. (2003). Validation of proton transfer reaction-mass spectrometry (PTR-MS) measurements of gas-phase organic compounds in the atmosphere during the New England Air Quality Study (NEAQS) in 2002. Journal of Geophysical Research: Atmospheres, 108(D21). https://doi.org/10.1029/2003JD003863

de Gouw, J. A., Middlebrook, A. M., Warneke, C., Goldan, P. D., Kuster, W. C., Roberts, J. M., Fehsenfeld, F. C., Worsnop, D. R., Canagaratna, M. R., Pszenny, A. A. P., Keene, W. C., Marchewka, M., Bertman, S. B., and Bates, T. S. (2005). Budget of organic carbon in a polluted atmosphere: Results from the New England Air Quality Study in 2002. Journal of Geophysical Research: Atmospheres, 110(D16). https://doi.org/10.1029/2004JD005623

de Jonge, R. W., Xavier, C., Olenius, T., Elm, J., Svenhag, C., Hyttinen, N., Nieradzik, L., Sarnela, N., Kristensson, A., Petäjä, T., Ehn, M., and Roldin, P. (2024). Natural Marine Precursors Boost Continental New Particle Formation and Production of Cloud Condensation Nuclei. Environmental Science & Technology, 58(25), 10956–10968. https://doi.org/10.1021/acs.est.4c01891

de Vos, A., Pattiaratchi, C. B., and Wijeratne, E. M. S. (2014). Surface circulation and upwelling patterns around Sri Lanka. Biogeosciences, 11(20), 5909–5930. https://doi.org/10.5194/bg-11-5909-2014

Debaje, S., and Johnson Jeyakumar, S. (2011). High ozone at coastal sites in India. International Journal of Remote Sensing, 32(4), 993–1015. https://doi.org/10.1080/01431160903505294

Deschaseaux, E., Hardefeldt, J., Jones, G., and Reichelt-Brushett, A. (2018). High zinc exposure leads to reduced dimethylsulfoniopropionate (DMSP) levels in both the host and endosymbionts of the reef-building coral Acropora aspera. Marine Pollution Bulletin, 126, 93–100.https://doi.org/10.1016/j.marpolbul.2017.10.070

Deschaseaux, E. S. M., Jones, G. B., Deseo, M. A., Shepherd, K. M., Kiene, R. P., Swan, H. B., Harrison, P. L., and Eyre, B. D. (2014). Effects of environmental factors on dimethylated sulfur compounds and their potential role in the antioxidant system of the coral holobiont. Limnology and Oceanography, 59(3), 758–768.https://doi.org/10.4319/lo.2014.59.3.0758

Deschaseaux, E., Stoltenberg, L., Hrebien, V., Koveke, E. P., Toda, K., and Eyre, B. D. (2019). Dimethylsulfide (DMS) fluxes from permeable coral reef carbonate sediments. Marine Chemistry, 208, 1–10. https://doi.org/10.1016/j.marchem.2018.11.008

Dias, A. B., Kurian, S., Vijayan, N. T., Gauns, M., Khichi, R., Pratihary, A. K., Borker, S. G., and Shenoy, D. M. (2023). Recurrence of Gonyaulax polygramma bloom in the southeastern Arabian Sea. Environmental Monitoring and Assessment, 195(6), 635. https://doi.org/10.1007/s10661-023-11278-7

Draxler, R. NOAA - Air Resources Laboratory - FAQ - How Do I Estimate the Absolute (in Km) and Relative (%) Errors When Using the HYSPLIT Trajectory Model, September 23, 2008. http://www.arl.noaa.gov/faq hg11.php.

Draxler, R., and Hess, G. (1998). An overview of the HYSPLIT_4 modeling system for trajectories, dispersion, and deposition. Australian Meteorological Magazine, 47, 295–308.

Edtbauer, A., Stönner, C., Pfannerstill, E. Y., Berasategui, M., Walter, D., Crowley, J. N., Lelieveld, J., and Williams, J. (2020). A new marine biogenic emission: Methane sulfonamide (MSAM), dimethyl sulfide (DMS), and dimethyl sulfone (chem$DMSO_2$) measured in air over the Arabian Sea. Atmospheric Chemistry and Physics, 20(10), 6081–6094. https://doi.org/10.5194/acp-20-6081-2020

EGGE, J., and Aksnes, D. (1992). Silicate as Regulating Nutrient in Phytoplankton Competition. Marine Ecology-Progress Series, 83, 281–289.https://doi.org/10.3354/meps083281

Ellepola, G., Harischandra, S., and Ranawana, K. B. (2021). Spatial analysis of geophysical and environmental factors characterize distinct coral reef habitats around Sri Lanka; implications for management. Ocean and Coastal Management, 210, 105667.https://doi.org/10.1016/j.ocecoaman.2021.105667

Ernst, P. A., Subrahmanyam, B., and Trott, C. B. (2022). Lakshadweep High Propagation and Impacts on the Somali Current and Eddies During the Southwest Monsoon. Journal of Geophysical Research: Oceans, 127(3), e2021JC018089. https://doi.org/10.1029/2021JC018089

Exton, D. A., Mcgenity, T. J., Steinke, M., Smith, D. J., and Suggett, D. J. (2015). Uncovering the volatile nature of tropical coastal marine ecosystems in a changing world. Global Change Biology, 21(4). https://doi.org/10.1111/gcb.12764

Exton, D. A., Suggett, D. J., McGenity, T. J., and Steinke, M. (2013). Chlorophyll-normalized isoprene production in laboratory cultures of marine microalgae and implications for global models. Limnology and Oceanography, 58(4), 1301–1311.https://doi.org/10.4319/lo.2013.58.4.1301

Ferracci, V., Weber, J., Bolas, C. G., Robinson, A. D., Tummon, F., Rodríguez-Ros, P., Cortés-Greus, P., Baccarini, A., Jones, R. L., Galí, M., Simó, R., Schmale, J., and Harris, Neil. R. P. (2024). Atmospheric isoprene measurements reveal

larger-than-expected Southern Ocean emissions. Nature Communications, 15(1), 2571.https://doi.org/10.1038/s41467-024-46744-4

Fiddes, S. L., Woodhouse, M. T., Lane, T. P., and Schofield, R. (2021). Coral-reef-derived dimethyl sulfide and the climatic impact of the loss of coral reefs. Atmos. Chem. Phys., 21(8), 5883–5903. https://doi.org/10.5194/acp-21-5883-2021

Fischer, E., and Jones, G. (2012). Atmospheric dimethysulphide production from corals in the Great Barrier Reef and links to solar radiation, climate and coral bleaching. Biogeochemistry, 110(1), 31–46. https://doi.org/10.1007/s10533-012-9719-y

Flood, V. A., Strong, K., Whaley, C. H., Chen, J., Wunch, D., Drummond, J. R., Colebatch, O., Gillespie, L., and Mostafavi Pak, N. (2025). The Impact of the 2023 Canadian Forest Fires on Air Quality in Southern Ontario. Journal of Geophysical Research: Atmospheres, 130(5), e2024JD042254. https://doi.org/10.1029/2024JD042254

Folkins, I., Loewenstein, M., Podolske, J., Oltmans, S. J., and Proffitt, M. (1999). A barrier to vertical mixing at 14 km in the tropics: Evidence from ozonesondes and aircraft measurements. Journal of Geophysical Research, 104(D18), 22095–22102.https://doi.org/10.1029/1999JD900404

Folkins, I., and Martin, R. V. (2005). The Vertical Structure of Tropical Convection and Its Impact on the Budgets of Water Vapor and Ozone. Journal of the Atmospheric Sciences, 62(5), 1560–1573. https://doi.org/10.1175/JAS3407.1

Franchini, F., and Steinke, M. (2017). Protocols for the Quantification of Dimethyl Sulfide (DMS) and Other Volatile Organic Compounds in Aquatic Environments. In T. J. McGenity, K. N. Timmis, and B. Nogales (Eds.), Hydrocarbon and Lipid Microbiology Protocols: Petroleum, Hydrocarbon and Lipid Analysis (pp. 161–177). Springer Berlin Heidelberg. https://doi.org/10.1007/8623_2016_206

Fuller, N. J., Tarran, G. A., Cummings, D. G., Woodward, E. M. S., Orcutt, K. M., Yallop, M., Le Gall, F., and Scanlan, D. J. (2006). Molecular analysis of photosynthetic picoeukaryote community structure along an Arabian Sea transect. Limnology and Oceanography, 51(6), 2502–2514. https://doi.org/10.4319/lo.2006.51.6.2502

Galí, M., Devred, E., Levasseur, M., Royer, S.-J., and Babin, M. (2015). A remote sensing algorithm for planktonic dimethylsulfoniopropionate (DMSP) and an analysis of global patterns. Remote Sensing of Environment, 171, 171–184. https://doi.org/10.1016/j.rse.2015.10.012

Galí, M., Levasseur, M., Devred, E., Simó, R., and Babin, M. (2018). Sea-surface dimethylsulfide (DMS) concentration from satellite data at global and regional scales. Biogeosciences, 15(11), 3497–3519. https://doi.org/10.5194/bg-15-3497-2018

Galí, M., and Simó, R. (2015). A meta-analysis of oceanic DMS and DMSP cycling processes: Disentangling the summer paradox. Global Biogeochemical Cycles, 29(4), 496–515.https://doi.org/10.1002/2014GB004940

Gandhi, N., Singh, A., Prakash, S., Ramesh, R., Raman, M., Sheshshayee, M. S., and Shetye, S. (2011). First direct measurements of N2 fixation during a Trichodesmium bloom in the eastern Arabian Sea. Global Biogeochemical Cycles, 25(4). https://doi.org/10.1029/2010GB003970

Gantt, B., Meskhidze, N., and Kamykowski, D. (2009). A new physically-based quantification of marine isoprene and primary organic aerosol emissions. Atmospheric Chemistry and Physics, 9(14), 4915–4927. https://doi.org/10.5194/acp-9-4915-2009

Gantt, B., Meskhidze, N., Zhang, Y., and Xu, J. (2010). The effect of marine isoprene emissions on secondary organic aerosol and ozone formation in the coastal United States. Atmospheric Environment, 44(1), 115–121.https://doi.org/10.1016/j.atmosenv.2009.08.027

Gantt, B., Xu, J., Meskhidze, N., Zhang, Y., Nenes, A., Ghan, S. J., Liu, X., Easter, R., and Zaveri, R. (2012). Global distribution and climate forcing of marine organic aerosol – Part 2: Effects on cloud properties and radiative forcing. Atmospheric Chemistry and Physics, 12(14), 6555–6563. https://doi.org/10.5194/acp-12-6555-2012

Gao, X., Chen, J., Zhai, X., Liu, Q., Zhang, L., Hu, Y., Zhu, M., Liu, Y., Zhao, X., Zhu, X., Yang, G., and Liu, J.-H. (2025). Driving Factors of Dimethylated Sulfur Compounds in the Pearl River Estuary and Its Adjacent Coastal Waters: The Nonnegligible Role of Synechococcus. Journal of Geophysical Research: Oceans, 130(3), e2024JC021764. https://doi.org/10.1029/2024JC021764

Garbe, C. S., Rutgersson, A., Boutin, J., de Leeuw, G., Delille, B., Fairall, C. W., Gruber, N., Hare, J., Ho, D. T., Johnson, M. T., Nightingale, P. D., Pettersson, H., Piskozub, J., Sahlée, E., Tsai, W., Ward, B., Woolf, D. K., and Zappa, C. J. (2014). Transfer Across the Air-Sea Interface. In P. S. Liss and M. T. Johnson (Eds.), Ocean-Atmosphere Interactions of Gases and Particles (pp. 55–112). Springer Berlin Heidelberg. https://doi.org/10.1007/978-3-642-25643-1_2

Garrison, D. L., Gowing, M. M., Hughes, M. P., Campbell, L., Caron, D. A., Dennett, M. R., Shalapyonok, A., Olson, R. J., Landry, M. R., Brown, S. L., Liu, H.-B., Azam, F., Steward, G. F., Ducklow, H. W., and Smith, D. C. (2000). Microbial food web structure in the Arabian Sea: A US JGOFS study. Deep Sea Research Part II: Topical Studies in Oceanography, 47(7), 1387–1422. https://doi.org/10.1016/S0967-0645(99)00148-4

Gauns, M., Madhupratap, M., Ramaiah, N., Jyothibabu, R., Fernandes, V., Paul, J. T., and Prasanna Kumar, S. (2005). Comparative accounts of biological productivity characteristics and estimates of carbon fluxes in the Arabian Sea and the Bay of Bengal. Biogeochemical Processes in the Northern Indian Ocean, 52(14), 2003–2017.

Ghahreman, R., Gong, W., Galí, M., Norman, A.-L., Beagley, S. R., Akingunola, A., Zheng, Q., Lupu, A., Lizotte, M., Levasseur, M., and Leaitch, W. R. (2019). Dimethyl sulfide and its role in aerosol formation and growth in the Arctic summer

– a modelling study. Atmospheric Chemistry and Physics, 19(23), 14455–14476. https://doi.org/10.5194/acp-19-14455-2019

Giorio, C., Doussin, J.-F., D'Anna, B., Mas, S., Filippi, D., Denjean, C., Mallet, M. D., Bourrianne, T., Burnet, F., Cazaunau, M., Chikwililwa, C., Desboeufs, K., Feron, A., Michoud, V., Namwoonde, A., Andreae, M. O., Piketh, S. J., and Formenti, P. (2022). Butene Emissions From Coastal Ecosystems May Contribute to New Particle Formation. Geophysical Research Letters, 49(10), e2022GL098770. https://doi.org/10.1029/2022GL098770

Goes, J. I., and Gomes, H. do R. (2016). An Ecosystem in Transition: The Emergence of Mixotrophy in the Arabian Sea. In P. M. Glibert and T. M. Kana (Eds.), Aquatic Microbial Ecology and Biogeochemistry: A Dual Perspective (pp. 155–170). Springer International Publishing. https://doi.org/10.1007/978-3-319-30259-1_13

Goldan, P. D., Kuster, W. C., Williams, E., Murphy, P. C., Fehsenfeld, F. C., and Meagher, J. (2004). Nonmethane hydrocarbon and oxy hydrocarbon measurements during the 2002 New England Air Quality Study. Journal of Geophysical Research: Atmospheres, 109(D21). https://doi.org/10.1029/2003JD004455

Gomes, H. do R., deRada, S., Goes, J. I., and Chai, F. (2016). Examining features of enhanced phytoplankton biomass in the Bay of Bengal using a coupled physical-biological model. Journal of Geophysical Research: Oceans, 121(7), 5112–5133. https://doi.org/10.1002/2015JC011508

Gómez-Consarnau, L., Klein, N. J., Cutter, L. S., and Sañudo-Wilhelmy, S. A. (2021). Growth rate-dependent synthesis of halomethanes in marine heterotrophic bacteria and its implications for the ozone layer recovery. Environmental Microbiology Reports, 13(2).https://doi.org/10.1111/1758-2229.12905

Gondwe, M., Krol, M., Gieskes, W., Klaassen, W., and de Baar, H. (2003). The contribution of ocean-leaving DMS to the global atmospheric burdens of DMS, MSA, SO2, and NSS SO4=. Global Biogeochemical Cycles, 17(2).https://doi.org/10.1029/2002GB001937

Groß, E., Di Pane, J., Boersma, M., and Meunier, C. L. (2022). River discharge-related nutrient effects on North Sea coastal and offshore phytoplankton communities. Journal of Plankton Research, 44(6), 947–960.https://doi.org/10.1093/plankt/fbac049

Guenther, A., Hewitt, C. N., Erickson, D., Fall, R., Geron, C., Graedel, T., Harley, P., Klinger, L., Lerdau, M., Mckay, W. A., Pierce, T., Scholes, B., Steinbrecher, R., Tallamraju, R., Taylor, J., and Zimmerman, P. (1995). A global model of natural volatile organic compound emissions. Journal of Geophysical Research: Atmospheres, 100(D5), 8873–8892. https://doi.org/10.1029/94JD02950

Guenther, A., Jiang, X., Heald, C. L., Sakulyanontvittaya, T., Duhl, T., Emmons, L. K., and Wang, X. (2012). The Model of Emissions of Gases and Aerosols from Nature version 2.1 (MEGAN2.1): An extended and updated framework for

modeling biogenic emissions. Geoscientific Model Development, 5(6), 1471–1492. https://doi.org/10.5194/gmd-5-1471-2012

Guenther, A., Karl, T., Harley, P., Wiedinmyer, C., Palmer, P. I., and Geron, C. (2006). Estimates of global terrestrial isoprene emissions using MEGAN (Model of Emissions of Gases and Aerosols from Nature). Atmospheric Chemistry and Physics, 6(11), 3181–3210. https://doi.org/10.5194/acp-6-3181-2006

Guibert, I., Bourdreux, F., Bonnard, I., Pochon, X., Dubousquet, V., Raharivelomanana, P., Berteaux-Lecellier, V., and Lecellier, G. (2020). Dimethylsulfoniopropionate concentration in coral reef invertebrates varies according to species assemblages. Scientific Reports, 10(1), 9922. https://doi.org/10.1038/s41598-020-66290-5

Gupta, M., Sahu, L. K., Tripathi, N., Sudheer, A. K., and Singh, A. (2025). Processes Controlling DMS Variability in Marine Boundary Layer of the Arabian Sea During Post-Monsoon Season of 2021. Journal of Geophysical Research: Atmospheres, 130(9), e2024JD042547. https://doi.org/10.1029/2024JD042547

Gupta, M., Tripathi, N., Malik, T. G., and Sahu, L. K. (2024). A review on air–sea exchange of reactive trace gases over the northern Indian Ocean. Journal of Earth System Science, 133(2), 77. https://doi.org/10.1007/s12040-024-02268-5

Gwinn, J. K., Robertson, A., and Kiene, R. P. (2019). Effect of Salinity on DMSP Production in Gambierdiscus belizeanus (Dinophyceae). Journal of Phycology, 55(6), 1401–1411. https://doi.org/10.1111/jpy.12923

Hackenberg, S., Andrews, S. J., Airs, R., Arnold, S., Bouman, H., Brewin, R., Chance, R. J., Cummings, D., Dall'Olmo, G., and Lewis, A. (2017). Potential controls of isoprene in the surface ocean. Global Biogeochemical Cycles, 31(4), 644–662.

Hackenberg, S. C., Andrews, S. J., Airs, R., Arnold, S. R., Bouman, H. A., Brewin, R. J. W., Chance, R. J., Cummings, D., Dall'Olmo, G., Lewis, A. C., Minaeian, J. K., Reifel, K. M., Small, A., Tarran, G. A., Tilstone, G. H., and Carpenter, L. J. (2017). Potential controls of isoprene in the surface ocean. Global Biogeochemical Cycles, 31(4), 644–662. https://doi.org/10.1002/2016GB005531

Hallquist, M., Wenger, J. C., Baltensperger, U., Rudich, Y., Simpson, D., Claeys, M., Dommen, J., Donahue, N. M., George, C., Goldstein, A. H., Hamilton, J. F., Herrmann, H., Hoffmann, T., Iinuma, Y., Jang, M., Jenkin, M. E., Jimenez, J. L., Kiendler-Scharr, A., Maenhaut, W., … Wildt, J. (2009). The formation, properties and impact of secondary organic aerosol: Current and emerging issues. Atmospheric Chemistry and Physics, 9(14), 5155–5236. https://doi.org/10.5194/acp-9-5155-2009

Hardikar, R., Haridevi, C. K., Chowdhury, M., Shinde, N., Ram, A., Rokade, M. A., and Rakesh, P. S. (2017). Seasonal distribution of phytoplankton and its association with physico-chemical parameters in coastal waters of Malvan, west coast of India. Environmental Monitoring and Assessment, 189(4), 151. https://doi.org/10.1007/s10661-017-5835-4

Hareesh Kumar, P. V., and Mathew, B. (1997). Salinity distribution in the Arabian Sea. Indian Journal of Marine Sciences, 26(3), 271–277.

Harris, J. M., Draxler, R. R., and Oltmans, S. J. (2005). Trajectory model sensitivity to differences in input data and vertical transport method. Journal of Geophysical Research: Atmospheres, 110(D14). https://doi.org/10.1029/2004JD005750

Hastenrath, S., Nicklis, A., and Greischar, L. (1993). Atmospheric-hydrospheric mechanisms of climate anomalies in the western equatorial Indian Ocean. Journal of Geophysical Research: Oceans, 98(C11), 20219–20235. https://doi.org/10.1029/93JC02330

Hatton, A. D., Malin, G., and Liss, P. S. (1999). Distribution of biogenic sulphur compounds during and just after the southwest monsoon in the Arabian Sea. Deep Sea Research Part II: Topical Studies in Oceanography, 46(3), 617–632. https://doi.org/10.1016/S0967-0645(98)00120-9

Hegde, S., Anil AC, Patil JS, Mitbavkar S, Krishnamurthy V, and Gopalakrishna VV. (2008). Influence of environmental settings on the prevalence of Trichodesmium spp. In the Bay of Bengal. Marine Ecology Progress Series, 356, 93–101.

Herr, A. E., Kiene, R. P., Dacey, J. W. H., and Tortell, P. D. (2019). Patterns and drivers of dimethylsulfide concentration in the northeast subarctic Pacific across multiple spatial and temporal scales. Biogeosciences, 16(8), 1729–1754. https://doi.org/10.5194/bg-16-1729-2019

Hersbach, H., Bell, B., Berrisford, P., Biavati, G., Horanyi, A., Munoz Sabater, J., et al. (2018). ERA5 hourly data on single levels from 1959 to present. Copernicus Climate Change Service (C3S) Climate Data Store (CDS). doi:10.24381/cds.adbb2d47

Hoegh-Guldberg, O., Poloczanska, E. S., Skirving, W., and Dove, S. (2017). Coral Reef Ecosystems under Climate Change and Ocean Acidification. Frontiers in Marine Science, Volume 4-2017. https://www.frontiersin.org/journals/marine-science/articles/10.3389/fmars.2017.00158

Hoffmann, E. H., Tilgner, A., Schrödner, R., Bräuer, P., Wolke, R., and Herrmann, H. (2016). An advanced modeling study on the impacts and atmospheric implications of multiphase dimethyl sulfide chemistry. Proceedings of the National Academy of Sciences of the United States of America, 113(42), 11776–11781. https://doi.org/10.1073/pnas.1606320113

Hopkins, F. E., Bell, T. G., Yang, M., Suggett, D. J., and Steinke, M. (2016). Air exposure of coral is a significant source of dimethylsulfide (DMS) to the atmosphere. Scientific Reports, 6(1), Article 1. https://doi.org/10.1038/srep36031

Hu, Q.-H., Xie, Z.-Q., Wang, X.-M., Kang, H., He, Q.-F., and Zhang, P. (2013). Secondary organic aerosols over oceans via oxidation of isoprene and monoterpenes from Arctic to Antarctic. Scientific Reports, 3(1), 2280. https://doi.org/10.1038/srep02280

Hulswar, S., Simó, R., Galí, M., Bell, T. G., Lana, A., Inamdar, S., Halloran, P. R., Manville, G., and Mahajan, A. S. (2022). Third revision of the global surface seawater dimethyl sulfide climatology (DMS-Rev3). Earth System Science Data, 14(7), 2963–2987. https://doi.org/10.5194/essd-14-2963-2022

Iannone, R. (2024). splitr: Use the HYSPLIT model from inside R (Version 0.4.0.9000) [Computer software]. https://github.com/rich-iannone/splitr

Jackson, R. L., Gabric, A. J., Cropp, R., and Woodhouse, M. T. (2020a). Dimethylsulfide (DMS), marine biogenic aerosols and the ecophysiology of coral reefs. Biogeosciences, 17(8), 2181–2204. https://doi.org/10.5194/bg-17-2181-2020

Jackson, R. L., Gabric, A. J., Woodhouse, M. T., Swan, H. B., Jones, G. B., Cropp, R., and Deschaseaux, E. S. M. (2020b). Coral Reef Emissions of Atmospheric Dimethylsulfide and the Influence on Marine Aerosols in the Southern Great Barrier Reef, Australia. Journal of Geophysical Research: Atmospheres, 125(7), e2019JD031837. https://doi.org/10.1029/2019JD031837

Jackson, R. L., Woodhouse, M. T., Gabric, A. J., and Cropp, R. A. (2022). CMIP6 projections of ocean warming and the impact on dimethylsulfide emissions from the Great Barrier Reef, Australia. Frontiers in Marine Science, 9. https://www.frontiersin.org/journals/ marine-science/articles/10.3389/fmars.2022.910420

Jasmine, S., George, R. M., Manisseri, M. K., and Kingsly, J. (2009). Hard coral diversity along southwest coast of India. Journal of the Marine Biological Association of India, 51(2), 189–193.

Jia, J., Ladstätter-Weißenmayer, A., Hou, X., Rozanov, A., and Burrows, J. P. (2017). Tropospheric ozone maxima observed over the Arabian Sea during the pre-monsoon. Atmospheric Chemistry and Physics, 17(8), 4915–4930. https://doi.org/10.5194/acp-17-4915-2017

Jones, C. E., Hornsby, K. E., Sommariva, R., Dunk, R. M., Glasow, R. V., McFiggans, G., and Carpenter, L. J. (2010). Quantifying the contribution of marine organic gases to atmospheric iodine. Geophysical Research Letters, 37(18). https://doi.org/10.1029/2010GL043990

Jones, G. B., Fischer, E., Deschaseaux, E. S. M., and Harrison, P. L. (2014). The effect of coral bleaching on the cellular concentration of dimethylsulphoniopropionate in reef corals. Journal of Experimental Marine Biology and Ecology, 460, 19–31. https://doi.org/10.1016/j.jembe.2014.06.003

Jones, G., Curran, M., Deschaseaux, E., Omori, Y., Tanimoto, H., Swan, H., Eyre, B., Ivey, J., McParland, E., Gabric, A., and Cropp, R. (2018). The Flux and Emission of Dimethylsulfide From the Great Barrier Reef Region and Potential Influence on the Climate of NE Australia. Journal of Geophysical Research: Atmospheres, 123(24), 13,835-13,856.https://doi.org/10.1029/2018JD029210

Jyothibabu, R., Karnan, C., Jagadeesan, L., Arunpandi, N., Pandiarajan, R. S., Muraleedharan, K. R., and Balachandran, K. K. (2017). Trichodesmium blooms and warm-core ocean surface features in the Arabian Sea and the Bay of Bengal. Marine Pollution Bulletin, 121(1), 201–215. https://doi.org/10.1016/j.marpolbul.2017.06.002

Jyothibabu, R., Win, N. N., Shenoy, D. M., Swe, U. T., Pratik, M., Thwin, S., and Jagadeesan, L. (2014). Interplay of diverse environmental settings and their influence on the plankton community off Myanmar during the Spring Intermonsoon. Journal of Marine Systems, 139, 446–459..https://doi.org/10.1016/j.jmarsys.2014.08.003

Kalogridis, C., Gros, V., Sarda-Esteve, R., Langford, B., Loubet, B., Bonsang, B., Bonnaire, N., Nemitz, E., Genard, A.-C., Boissard, C., Fernandez, C., Ormeño, E., Baisnée, D., Reiter, I., and Lathière, J. (2014). Concentrations and fluxes of isoprene and oxygenated VOCs at a French Mediterranean oak forest. Atmospheric Chemistry and Physics, 14(18), 10085–10102. https://doi.org/10.5194/acp-14-10085-2014

Kato, S., Ui, T., Uematsu, M., and Kajii, Y. (2007). Trace gas measurements over the northwest Pacific during the 2002 IOC cruise. Geochemistry, Geophysics, Geosystems, 8(6). https://doi.org/10.1029/2006GC001241

Kato, S., Watari, M., Nagao, I., Uematsu, M., and Kajii, Y. (2009). Atmospheric trace gas measurements during SEEDS-II over the northwestern pacific. SEEDS II: The Second Subarctic Pacific Iron Experiment for Ecosystem Dynamics Study, 56(26), 2918–2927. https://doi.org/10.1016/j.dsr2.2009.07.002

Keerthi, M. G., Lengaigne, M., Levy, M., Vialard, J., Parvathi, V., de Boyer Montégut, C., Ethé, C., Aumont, O., Suresh, I., Akhil, V. P., and Muraleedharan, P. M. (2017). Physical control of interannual variations of the winter chlorophyll bloom in the northern Arabian Sea. Biogeosciences, 14(15), 3615–3632. https://doi.org/10.5194/bg-14-3615-2017

Keller, M. D., Bellows, W. K., and Guillard, R. R. L. (1989). Dimethyl Sulfide Production in Marine Phytoplankton. In Biogenic Sulfur in the Environment (Vol. 393, pp. 167–182). American Chemical Society. https://doi.org/10.1021/bk-1989-0393.ch011

Keller, M. D., and Korjeff-Bellows, W. (1996). Physiological Aspects of the Production of Dimeyhtlsulfoniopropionate (DMSP) by Marine Phytoplankton. In R. P. Kiene, P. T. Visscher, M. D. Keller, and G. O. Kirst (Eds.), Biological and Environmental Chemistry of DMSP and Related Sulfonium Compounds (pp. 131–142). Springer US. https://doi.org/10.1007/978-1-4613-0377-0_12

Kerrison, P., Suggett, D. J., Hepburn, L. J., and Steinke, M. (2012). Effect of elevated pCO2 on the production of dimethylsulphoniopropionate (DMSP) and dimethylsulphide (DMS) in two species of Ulva (Chlorophyceae). Biogeochemistry, 110(1), 5–16. https://doi.org/10.1007/s10533-012-9707-2

Kettles, N. L., Kopriva, S., and Malin, G. (2014). Insights into the Regulation of DMSP Synthesis in the Diatom Thalassiosira pseudonana through APR Activity, Proteomics

and Gene Expression Analyses on Cells Acclimating to Changes in Salinity, Light and Nitrogen. PLOS ONE, 9(4), e94795. https://doi.org/10.1371/journal.pone.0094795

Kilgour, D. B., Jernigan, C. M., Zhou, S., Brito de Azevedo, E., Wang, J., Zawadowicz, M. A., and Bertram, T. H. (2024). Contribution of Speciated Monoterpenes to Secondary Aerosol in the Eastern North Atlantic. ACS ESandT Air, 1(8), 789–800.https://doi.org/10.1021/acsestair.3c00112

Kondo, J. (1975). Air-sea bulk transfer coefficients in diabatic conditions. Boundary-Layer Meteorology, 9(1), 91–112https://doi.org/10.1007/BF00232256

Krishnankutty, S., Joseph C, A., P D, V., Thajudeen, J., P S, V., A.V., S., and Abdulla, M. H. (2019). Hydrographic, seasonal diversity, distribution and abundance of phytoplankton in coastal waters off Cochin—South-eastern Arabian Sea. Indian Journal of Geo-Marine Sciences, 48, 319–326.

Kristiansen, S., and Hoell, E. E. (2002). The importance of silicon for marine production. In O. Vadstein and Y. Olsen (Eds.), Sustainable Increase of Marine Harvesting: Fundamental Mechanisms and New Concepts: Proceedings of the 1st Maricult Conference held in Trondheim, Norway, 25–28 June 2000 (pp. 21–31). Springer Netherlands. https://doi.org/10.1007/978-94-017-3190-4_3

Krüger, K., and Quack, B. (2013). Introduction to special issue: The TransBrom Sonne expedition in the tropical West Pacific. Atmospheric Chemistry and Physics, 13(18), 9439–9446. https://doi.org/10.5194/acp-13-9439-2013

Krüger, O., and Graßl, H. (2011). Southern Ocean phytoplankton increases cloud albedo and reduces precipitation. Geophysical Research Letters, 38(8). https://doi.org/10.1029/2011GL047116

Kulkarni, V., Chitari, R., Narale, D., Patil, J., and Anil, A. (2010). Occurrence of cyanobacteria—Diatom symbiosis in the Bay of Bengal: Implications in biogeochemistry. Current Science, 99:736.

Kumar, S. P., Ishida, A., Yoneyama, K., Ramesh Kumar, M. R., Kashino, Y., and Mitsudera, H. (2005). Dynamics and thermodynamics of the Indian Ocean warm pool in a high-resolution global general circulation model. Biogeochemical Processes in the Northern Indian Ocean, 52(14), 2031–2047. https://doi.org/10.1016/j.dsr2.2005.05.008

Kumar, S. P., Madhupratap, M., Kumar, M. D., Gauns, M., Muraleedharan, P. M., Sarma, V. V. S. S., and De Souza, S. N. (2000). Physical control of primary productivity on a seasonal scale in central and eastern Arabian Sea. Journal of Earth System Science, 109(4), 433–441. https://doi.org/10.1007/BF02708331

Kumar, S. P., Muraleedharan, P. M., Prasad, T. G., Gauns, M., Ramaiah, N., Souza, S. N. D., Sardesai, S., and Madhupratap, M. (2002). Why is the Bay of Bengal less productive during summer monsoon compared to the Arabian Sea? Geophysical Research Letters, 29(24). https://doi.org/10.1029/2002GL016013

Kumari, V. R., Sarma, V. V. S. S., Rao, G. D., Viswanadham, R., Navita, B., Srinivas, T. N. R., Krishna, M. S., and Reddy, N. P. C. (2019). Modifications in the trace gases flux by a very severe cyclonic storm, Hudhud, in the coastal Bay of Bengal. Journal of Earth System Science, 128(5), 121. https://doi.org/10.1007/s12040-019-1157-y

Kuttippurath, J., Ardra, D., Raj, S., and Feng, W. (2023). A seasonal OH minimum region over the Indian Ocean? Atmospheric Environment, 295, 119536.https://doi.org/10.1016/j.atmosenv.2022.119536

La, T. V., and Messager, C. (2021). Convective System Dynamics Viewed in 3D Over the Oceans. Geophysical Research Letters, 48(5), e2021GL092397. https://doi.org/10.1029/2021GL092397

Lakshmi, R. S., Prakash, S., Lotliker, A. A., Baliarsingh, S. K., Samanta, A., Mathew, T., Chatterjee, A., Sahu, B. K., and Nair, T. M. B. (2021). Physicochemical controls on the initiation of phytoplankton bloom during the winter monsoon in the Arabian Sea. Scientific Reports, 11(1), 13448. https://doi.org/10.1038/s41598-021-92897-3

Lal, S., Chand, D., Sahu, L. K., Venkataramani, S., Brasseur, G., and Schultz, M. G. (2006). High levels of ozone and related gases over the Bay of Bengal during winter and early spring of 2001. Atmospheric Environment, 40(9).https://doi.org/10.1016/j.atmosenv.2005.10.060

Lana, A., Bell, T. G., Simó, R., Vallina, S. M., Ballabrera-Poy, J., Kettle, A. J., Dachs, J., Bopp, L., Saltzman, E. S., Stefels, J., Johnson, J. E., and Liss, P. S. (2011). An updated climatology of surface dimethlysulfide concentrations and emission fluxes in the global ocean: UPDATED DMS CLIMATOLOGY. Global Biogeochemical Cycles, 25(1), n/a-n/a. https://doi.org/10.1029/2010GB003850

Lapere, R., Haddon, A., Price, R., Marelle, L., Monahan, A. H., Steiner, N., Raut, J.-C., Bastien, L., and Thomas, J. (2025). Oceanic DMS strongly affects aerosols and clouds in the Arctic. Preprint. https://hal.science/hal-05374106v1

Latha, T., Rao, K., Nagamani, P., Amminedu, E., Choudhury, S., Dutt, C., and Dadhwal, V. (2015). Impact of Cyclone PHAILIN on Chlorophyll-a Concentration and Productivity in the Bay of Bengal. International Journal of Geosciences, 6, 473–480.https://doi.org/10.4236/ijg.2015.65037

Lawson, S. J., Law, C. S., Harvey, M. J., Bell, T. G., Walker, C. F., de Bruyn, W. J., and Saltzman, E. S. (2020a). Methanethiol, dimethyl sulfide and acetone over biologically productive waters in the southwest Pacific Ocean. Atmos. Chem. Phys., 20(5), 3061–3078. https://doi.org/10.5194/acp-20-3061-2020

Lawson, S. J., Law, C. S., Harvey, M. J., Bell, T. G., Walker, C. F., de Bruyn, W. J., and Saltzman, E. S. (2020b). Methanethiol, dimethyl sulfide and acetone over biologically productive waters in the southwest Pacific Ocean. Atmospheric Chemistry and Physics, 20(5), 3061–3078. https://doi.org/10.5194/acp-20-3061-2020

Laxmilatha, P., Jasmine, S., Kingsly, H. J., Ameri, S., and Labeeb, K. A. (2021). Coral reef biodiversity of selected sites in Andaman and Nicobar Islands. Marine Fisheries Information Service, Technical and Extension Series, 248, 24–29.

Levasseur, M. (2013). Impact of Arctic meltdown on the microbial cycling of sulphur. Nature Geoscience, 6(9), 691–700.https://doi.org/10.1038/ngeo1910

Lévy, M., Lengaigne, M., Bopp, L., Vincent, E. M., Madec, G., Ethé, C., Kumar, D., and Sarma, V. V. S. S. (2012). Contribution of tropical cyclones to the air-sea CO2 flux: A global view. Global Biogeochemical Cycles, 26(2).https://doi.org/10.1029/2011GB004145

Lewis, A. C., Carpenter, L. J., and Pilling, M. J. (2001). Nonmethane hydrocarbons in Southern Ocean boundary layer air. Journal of Geophysical Research: Atmospheres, 106(D5), 4987–4994.

Lewis, A. C., McQuaid, J. B., Carslaw, N., and Pilling, M. J. (1999). Diurnal cycles of short-lived tropospheric alkenes at a north Atlantic coastal site. Atmospheric Environment, 33(15). https://doi.org/10.1016/S1352-2310(98)00429-4

Li, M., Zhang, Q., Streets, D. G., He, K. B., Cheng, Y. F., Emmons, L. K., Huo, H., Kang, S. C., Lu, Z., Shao, M., Su, H., Yu, X., and Zhang, Y. (2014). Mapping Asian anthropogenic emissions of non-methane volatile organic compounds to multiple chemical mechanisms. Atmospheric Chemistry and Physics, 14(11), 5617–5638.https://doi.org/10.5194/acp-14-5617-2014

Li, X., Dong, Y., Zhang, Y., Shi, Z., and Yao, J. (2023). Climatology of Planetary Boundary Layer Height over Jiangsu, China, Based on ERA5 Reanalysis Data. Atmosphere, 14(9). https://doi.org/10.3390/atmos14091330

Li, X., Yan, T., Yu, R., and Zhou, M. (2019). A review of karenia mikimotoi: Bloom events, physiology, toxicity and toxic mechanism. Harmful Algae, 90, 101702. https://doi.org/10.1016/j.hal.2019.101702

Li, X.-J., Liang, H.-R., Zhuang, G.-C., Wu, Y.-C., Li, S.-T., Zhang, H.-H., Montgomery, A., and Yang, G.-P. (2022). Annual Variations of Isoprene and Other Non-Methane Hydrocarbons in the Jiaozhou Bay on the East Coast of North China. Journal of Geophysical Research: Biogeosciences, 127(3), e2021JG006531. https://doi.org/10.1029/2021JG006531

Liakakou, E., Vrekoussis, M., Bonsang, B., Donousis, C., Kanakidou, M., and Mihalopoulos, N. (2007). Isoprene above the Eastern Mediterranean: Seasonal variation and contribution to the oxidation capacity of the atmosphere. Atmospheric Environment, 41(5). https://doi.org/10.1016/j.atmosenv.2006.09.034

Liang, S.-M., Zhai, X., Li, C.-X., Xin, M., Sun, P., Liu, X.-L., Liu, L., and Wang, B.-D. (2023). Distribution and physical–biological controls of dimethylsulfide in the western tropical Indian Ocean during winter monsoon. Frontiers in Marine Science, 10.

Liao, X., Du, Y., Zhan, H., Wang, T., and Feng, M. (2017). Wintertime Phytoplankton Blooms in the Western Equatorial Indian Ocean Associated With the Madden-Julian Oscillation. Journal of Geophysical Research: Oceans, 122(12), 9855–9869. https://doi.org/10.1002/2017JC013203

Liss, P. S., Marandino, C. A., Dahl, E. E., Helmig, D., Hintsa, E. J., Hughes, C., Johnson, M. T., Moore, R. M., Plane, J. M. C., Quack, B., Singh, H. B., Stefels, J., von Glasow, R., and Williams, J. (2014). Short-Lived Trace Gases in the Surface Ocean and the Atmosphere. In P. S. Liss and M. T. Johnson (Eds.), Ocean-Atmosphere Interactions of Gases and Particles (pp. 1–54). Springer Berlin Heidelberg. https://doi.org/10.1007/978-3-642-25643-1_1

Liss, P. S., and Slater, P. G. (1974). Flux of Gases across the Air-Sea Interface. Nature, 247(5438), 181–184. https://doi.org/10.1038/247181a0

Litchman, E., Neale, P. J., and Banaszak, A. T. (2002). Increased sensitivity to ultraviolet radiation in nitrogen-limited dinoflagellates: Photoprotection and repair. Limnology and Oceanography, 47(1), 86–94. https://doi.org/10.4319/lo.2002.47.1.0086

Löscher, C. R. (2021). Reviews and syntheses: Trends in primary production in the Bay of Bengal – is it at a tipping point? Biogeosciences, 18(17), 4953–4963. https://doi.org/10.5194/bg-18-4953-2021

MacDonald, S., and Moore, R. M. (2007). Seasonal and spatial variations in methyl chloride in NW Atlantic waters. Journal of Geophysical Research: Oceans, 112(5). https://doi.org/10.1029/2006JC003812

MacKellar, M. C., McGowan, H. A., Phinn, S. R., and Soderholm, J. S. (2013). Observations of Surface Energy Fluxes and Boundary-Layer Structure Over Heron Reef, Great Barrier Reef, Australia. Boundary-Layer Meteorology, 146(2), 319–340. https://doi.org/10.1007/s10546-012-9767-9

Madhupratap, M., Kumar, S. P., Bhattathiri, P. M. A., Kumar, M. D., Raghukumar, S., Nair, K. K. C., and Ramaiah, N. (1996). Mechanism of the biological response to winter cooling in the northeastern Arabian Sea. Nature, 384(6609), 549–552. https://doi.org/10.1038/384549a0

Magalhães, C., Salgado, P., Kiene, R. P., and Bordalo, A. A. (2012). Influence of salinity on dimethyl sulfide and methanethiol formation in estuarine sediments and its side effect on nitrous oxide emissions. Biogeochemistry, 110(1), 75–86. https://doi.org/10.1007/s10533-011-9690-z

Mahadevan, A., Spiro Jaeger, G., Freilich, M., Omand, M., Shroyer, E. L., and Sengupta, D. (2016). Freshwater in the Bay of Bengal: Its fate and role in air-sea heat exchange. Oceanography, 29(2), 72–81. https://doi.org/10.5670/oceanog.2016.40

Mahajan, A. S., Fadnavis, S., Thomas, M. A., Pozzoli, L., Gupta, S., Royer, S.-J., Saiz-Lopez, A., and Simó, R. (2015). Quantifying the impacts of an updated global dimethyl sulfide climatology on cloud microphysics and aerosol radia-

tive forcing. Journal of Geophysical Research: Atmospheres, 120(6), 2524–2536. https://doi.org/10.1002/2014JD022687

Mahajan, A. S., Prados-Roman, C., Hay, T. D., Lampel, J., Pöhler, D., Groβmann, K., Tschritter, J., Frieβ, U., Platt, U., Johnston, P., Kreher, K., Wittrock, F., Burrows, J. P., Plane, J. M. C., and Saiz-Lopez, A. (2014). Glyoxal observations in the global marine boundary layer. Journal of Geophysical Research, 119(10).https://doi.org/10.1002/2013JD021388

Mahajan, A. S., Tinel, L., Sarkar, A., Chance, R., Carpenter, L. J., Hulswar, S., Mali, P., Prakash, S., and Vinayachandran, P. N. (2019). Understanding Iodine Chemistry Over the Northern and Equatorial Indian Ocean. Journal of Geophysical Research: Atmospheres, 124(14). https://doi.org/10.1029/2018JD029063

Manavi, S. E. I., Aktypis, A., Siouti, E., Skyllakou, K., Myriokefalitakis, S., Kanakidou, M., and Pandis, S. N. (2025). Atmospheric aerosol spatial variability: Impacts on air quality and climate change. One Earth, 8(3). https://doi.org/10.1016/j.oneear.2025.101237

Manigandan, V., Sarangi, R. K., Jeyapragash, D., and Ayyappan, S. (2024). Environmental-driven dynamics of phytoplankton assemblages in the Bay of Bengal, Southeast coast of India. Marine Ecology, 45(5), e12812.https://doi.org/10.1111/maec.12812

Manjumol, C. C., Linoy Libini, C., Albert Idu, K. A., Mohamed, K. S., and Kripa, V. (2018). Occurrence of Diatom – Diazotrophic association in the coastal surface waters of south Andaman, India. Symbiosis, 76(3), 293–302. https://doi.org/10.1007/s13199-018-0559-y

Marambe, B., Punyawardena, R., Silva, P., Premalal, S., Rathnabharathie, V., Kekulandala, B., Nidumolu, U., and Howden, M. (2015). Climate, Climate Risk, and Food Security in Sri Lanka: The Need for Strengthening Adaptation Strategies. In W. Leal Filho (Ed.), Handbook of Climate Change Adaptation (pp. 1759–1789). Springer Berlin Heidelberg. https://doi.org/10.1007/978-3-642-38670-1_120

Marandino, C. A., De Bruyn, W. J., Miller, S. D., and Saltzman, E. S. (2007). Eddy correlation measurements of the air/sea flux of dimethylsulfide over the North Pacific Ocean. Journal of Geophysical Research: Atmospheres, 112(D3). https://doi.org/10.1029/2006JD007293

Marandino, C. A., De Bruyn, W. J., Miller, S. D., and Saltzman, E. S. (2009). Open ocean DMS air/sea fluxes over the eastern South Pacific Ocean. Atmospheric Chemistry and Physics, 9(2), 345–356. https://doi.org/10.5194/acp-9-345-2009

Marandino, C. A., Tegtmeier, S., Krüger, K., Zindler, C., Atlas, E. L., Moore, F., and Bange, H. W. (2013). Dimethylsulphide (DMS) emissions from the western Pacific Ocean: A potential marine source for stratospheric sulphur? Atmospheric Chemistry and Physics, 13(16), 8427–8437. https://doi.org/10.5194/acp-13-8427-2013

Marie, D., Simon, N., Guillou, L., Partensky, F., and Vaulot, D. (2000). Flow Cytometry Analysis of Marine Picoplankton. In R. A. Diamond and S. Demaggio (Eds.), In Living Color: Protocols in Flow Cytometry and Cell Sorting (pp. 421–454). Springer Berlin Heidelberg. https://doi.org/10.1007/978-3-642-57049-0_34

Masdeu-Navarro, M., Mangot, J.-F., Xue, L., Cabrera-Brufau, M., Kieber, D. J., Rodríguez-Ros, P., Gardner, S. G., Bergauer, K., Herndl, G. J., Marrasé, C., and Simó, R. (2024). Diel variation of seawater volatile organic compounds, DMSP-related compounds, and microbial plankton inside and outside a tropical coral reef ecosystem. Frontiers in Marine Science, Volume 11-2024. https://www.frontiersin.org/journals/marine-science/articles/10.3389/fmars.2024.1341619

Mathew, T., Prakash, S., Shenoy, L., Chatterjee, A., Udaya Bhaskar, T. V. S., and Wojtasiewicz, B. (2021). Observed variability of monsoon blooms in the north-central Arabian Sea and its implication on oxygen concentration: A bio-argo study. Deep Sea Research Part II: Topical Studies in Oceanography, 184–185, 104935.https://doi.org/10.1016/j.dsr2.2021.104935

Matrai, P. A., Cooper, D. J., and Saltzman, E. S. (1996). Frontal enhancement of dimethylsulfide concentrations across a Gulf Stream meander. Journal of Marine Systems, 7(1), 1–8.https://doi.org/10.1016/0924-7963(95)00013-5

Mayer, K. J., Sauer, J. S., Dinasquet, J., and Prather, K. A. (2020). CAICE Studies: Insights from a Decade of Ocean-Atmosphere Experiments in the Laboratory. Accounts of Chemical Research, 53(11).https://doi.org/10.1021/acs.accounts.0c00504

McGillis, W. R., Dacey, J. W. H., Frew, N. M., Bock, E. J., and Nelson, R. K. (2000). Water-air flux of dimethylsulfide. Journal of Geophysical Research: Oceans, 105(C1), 1187–1193.https://doi.org/10.1029/1999JC900243

McGowan, H., Lensky, N. G., Abir, S., and Saunders, M. (2022). Coral Reef Coupling to the Atmospheric Boundary Layer Through Exchanges of Heat, Moisture, and Momentum: Case Studies From Tropical and Desert Fringing Coral Reefs. Frontiers in Marine Science, Volume 9-2022. https://www.frontiersin.org/journals/marine-science/articles/10.3389/fmars.2022.900679

McParland, E. L., and Levine, N. M. (2019). The role of differential DMSP production and community composition in predicting variability of global surface DMSP concentrations. Limnology and Oceanography, 64(2), 757–773.https://doi.org/10.1002/lno.11076

Mesarchaki, E., Yassaa, N., Hein, D., Lutterbeck, H. E., Zindler, C., and Williams, J. (2014). A novel method for the measurement of VOCs in seawater using needle trap devices and GC–MS. Marine Chemistry, 159, 1–8. https://doi.org/10.1016/j.marchem.2013.12.001

Meskhidze, N., and Nenes, A. (2006). Phytoplankton and Cloudiness in the Southern Ocean. Science, 314(5804), 1419–1423.https://doi.org/10.1126/science.1131779

Meskhidze, N., Sabolis, A., Reed, R., and Kamykowski, D. (2015). Quantifying environmental stress-induced emissions of algal isoprene and monoterpenes using laboratory measurements. Biogeosciences, 12(3), 637–651.https://doi.org/10.5194/bg-12-637-2015

Meskhidze, N., Xu, J., Gantt, B., Zhang, Y., Nenes, A., Ghan, S. J., Liu, X., Easter, R., and Zaveri, R. (2011). Global distribution and climate forcing of marine organic aerosol: 1. Model improvements and evaluation. Atmospheric Chemistry and Physics, 11(22), 11689–11705. https://doi.org/10.5194/acp-11-11689-2011

Minu, P., Shaju, S. S., Muhamed Ashraf, P., and Meenakumari, B. (2014). Phytoplankton community characteristics in the coastal waters of the southeastern Arabian Sea. Acta Oceanologica Sinica, 33(12), 170–179. https://doi.org/10.1007/s13131-014-0571-x

Mitbavkar, S., Anil, A. C., Narale, D. D., Chitari, R., Rao, V. T., and Gopalakrishna, V. V. (2020). Environmental influence on the picophytoplankton community structure in the central and northern Bay of Bengal. Regional Studies in Marine Science, 40, 101528. https://doi.org/10.1016/j.rsma.2020.101528

Moore, R. M. (2008). A photochemical source of methyl chloride in saline waters. Environmental Science and Technology, 42(6).https://doi.org/10.1021/es0719201

Mueller, J. L., and Lange, R. E. (1989). Bio-optical provinces of the Northeast Pacific Ocean: A provisional analysis. Limnology and Oceanography, 34(8), 1572–1586.https://doi.org/10.4319/lo.1989.34.8.1572

Müller, J.-F., Stavrakou, T., Wallens, S., De Smedt, I., Van Roozendael, M., Potosnak, M. J., Rinne, J., Munger, B., Goldstein, A., and Guenther, A. B. (2008). Global isoprene emissions estimated using MEGAN, ECMWF analyses and a detailed canopy environment model. Atmospheric Chemistry and Physics, 8(5), 1329–1341. https://doi.org/10.5194/acp-8-1329-2008

Mungall, E. L., Abbatt, J. P. D., Wentzell, J. J. B., Lee, A. K. Y., Thomas, J. L., Blais, M., Gosselin, M., Miller, L. A., Papakyriakou, T., Willis, M. D., and Liggio, J. (2017). Microlayer source of oxygenated volatile organic compounds in the summertime marine Arctic boundary layer. Proceedings of the National Academy of Sciences of the United States of America, 114(24). https://doi.org/10.1073/pnas.1620571114

Murtugudde, R. G., Signorini, S. R., Christian, J. R., Busalacchi, A. J., McClain, C. R., and Picaut, J. (1999). Ocean color variability of the tropical Indo-Pacific basin observed by SeaWiFS during 1997-1998. Journal of Geophysical Research: Oceans, 104(C8). https://doi.org/10.1029/1999jc900135

Naqvi, W. (1991). Geographical extent of denitrification in the arabian sea in relation to some physical processes. Oceanologica Acta, 14(3).

Niki, T., Shimizu, M., Fujishiro, A., and Kinoshita, J. (2007). Effects of salinity downshock on dimethylsulfide production. Journal of Oceanography, 63(5), 873–877. https://doi.org/10.1007/s10872-007-0074-x

Nölscher, A. C., Butler, T., Auld, J., Veres, P., Muñoz, A., Taraborrelli, D., Vereecken, L., Lelieveld, J., and Williams, J. (2014). Using total OH reactivity to assess isoprene photooxidation via measurement and model. Atmospheric Environment, 89, 453–463.https://doi.org/10.1016/j.atmosenv.2014.02.024

Novak, G. A., Kilgour, D. B., Jernigan, C. M., Vermeuel, M. P., and Bertram, T. H. (2022a). Oceanic emissions of dimethyl sulfide and methanethiol and their contribution to sulfur dioxide production in the marine atmosphere. Atmos. Chem. Phys., 22(9), 6309–6325. https://doi.org/10.5194/acp-22-6309-2022

Novak, G. A., Kilgour, D. B., Jernigan, C. M., Vermeuel, M. P., and Bertram, T. H. (2022b). Oceanic emissions of dimethyl sulfide and methanethiol and their contribution to sulfur dioxide production in the marine atmosphere. Atmospheric Chemistry and Physics, 22(9), 6309–6325. https://doi.org/10.5194/acp-22-6309-2022

O'Brien, J., McParland, E. L., Bramucci, A. R., Ostrowski, M., Siboni, N., Ingleton, T., Brown, M. V., Levine, N. M., Laverock, B., Petrou, K., and Seymour, J. (2022). The Microbiological Drivers of Temporally Dynamic Dimethylsulfoniopropionate Cycling Processes in Australian Coastal Shelf Waters. Frontiers in Microbiology, Volume 13-2022. https://doi.org/10.3389/fmicb.2022.894026

Okuda, Y., Hiraiwa, M., Shimizu, N., and Hashimoto, S. (2023). Production of volatile organic iodine compounds by the marine cyanobacterium Calothrix parasitica under different light intensities. Marine Chemistry, 248.https://doi.org/10.1016/j.marchem.2023.104211

Ooki, A., Nomura, D., Nishino, S., Kikuchi, T., and Yokouchi, Y. (2015). A global-scale map of isoprene and volatile organic iodine in surface seawater of the Arctic, Northwest Pacific, Indian, and Southern Oceans. Journal of Geophysical Research: Oceans, 120(6), 4108–4128. https://doi.org/10.1002/2014JC010519

Osthoff, H. D., Bates, T. S., Johnson, J. E., Kuster, W. C., Goldan, P., Sommariva, R., Williams, E. J., Lerner, B. M., Warneke, C., de Gouw, J. A., Pettersson, A., Baynard, T., Meagher, J. F., Fehsenfeld, F. C., Ravishankara, A. R., and Brown, S. S. (2009). Regional variation of the dimethyl sulfide oxidation mechanism in the summertime marine boundary layer in the Gulf of Maine. Journal of Geophysical Research: Atmospheres, 114(D7). https://doi.org/10.1029/2008JD010990

Padmakumar, K. B., Smitha, B. R., Thomas, L. C., Fanimol, C. L., SreeRenjima, G., Menon, N. R., and Sanjeevan, V. N. (2010). Blooms of Trichodesmium erythraeum in the South Eastern Arabian Sea during the onset of 2009 summer monsoon. Ocean Science Journal, 45(3), 151–157. https://doi.org/10.1007/s12601-010-0013-4

Parab, S. G., Prabhu Matondkar, S. G., Gomes, H. do R., and Goes, J. I. (2006). Monsoon driven changes in phytoplankton populations in the eastern Arabian Sea as revealed by microscopy and HPLC pigment analysis. Continental Shelf Research, 26(20), 2538–2558. https://doi.org/10.1016/j.csr.2006.08.004

Pargaonkar, S. M., and Vinayachandran, P. N. (2022). The Irrawaddy River Jet in the Andaman Sea During the Summer Monsoon. Frontiers in Marine Science, 9. https://www.frontiersin.org/journals/marine-science/articles/10.3389/fmars.2022.849179

Park, K., Kim, I., Choi, J.-O., Lee, Y., Jung, J., Ha, S.-Y., Kim, J.-H., and Zhang, M. (2019). Unexpectedly high dimethyl sulfide concentration in high-latitude Arctic sea ice melt ponds. Environmental Science: Processes and Impacts, 21(10), 1642–1649.https://doi.org/10.1039/C9EM00195F

Park, K.-T., and Lee, K. (2008). High-frequency, accurate measurement of dimethylsulfide in surface marine environments using a microporous membrane contactor. Limnology and Oceanography: Methods, 6(11), 548–557. https://doi.org/10.4319/lom.2008.6.548

Paul, J. T., Ramaiah, N., Gauns, M., and Fernandes, V. (2007). Preponderance of a few diatom species among the highly diverse microphytoplankton assemblages in the Bay of Bengal. Marine Biology, 152(1), 63–75. https://doi.org/10.1007/s00227-007-0657-5

Peng, L., Fan, C., Guo, Y., Ding, C., Wang, X., Zhang, G., and Sun, J. (2024). Spatial distribution and environmental/biological co-regulation mechanism of dimethyl sulfur compounds in the eastern Indian Ocean. Frontiers in Marine Science, 11. https://www.frontiersin.org/journals/marine-science/articles/10.3389/fmars.2024.1395292

Perera, N. (2011). Coral Reefs of Sri Lanka. The National Trust Sri Lanka.

Pfannerstill, E. Y., Wang, N., Edtbauer, A., Bourtsoukidis, E., Crowley, J. N., Dienhart, D., Eger, P. G., Ernle, L., Fischer, H., Hottmann, B., Paris, J.-D., Stönner, C., Tadic, I., Walter, D., Lelieveld, J., and Williams, J. (2019). Shipborne measurements of total OH reactivity around the Arabian Peninsula and its role in ozone chemistry. Atmospheric Chemistry and Physics, 19(17), 11501–11523.https://doi.org/10.5194/acp-19-11501-2019

Plass-Dülmer, C., Koppmann, R., Ratte, M., and Rudolph, J. (1995). Light non-methane hydrocarbons in seawater. Global Biogeochemical Cycles, 9(1), 79–100. https://doi.org/10.1029/94GB02416

Prerna, S., Chatterjee, A., Mukherjee, A., Ravichandran, M., and Shenoi, S. S. C. (2019). Wyrtki Jets: Role of intraseasonal forcing. Journal of Earth System Science, 128(1), 21.https://doi.org/10.1007/s12040-018-1042-0

Pujari, L., Wu, C., Kan, J., Li, N., Wang, X., Zhang, G., Shang, X., Wang, M., Zhou, C., and Sun, J. (2019). Diversity and Spatial Distribution of Chromophytic Phytoplankton in the Bay of Bengal Revealed by RuBisCO Genes (rbcL). Frontiers in Microbiology, 10. https://www.frontiersin.org/journals/microbiology/articles/10.3389/fmicb.2019.01501

Qi, L., and Wang, Y. (2015). Discrepancies in Different Precipitation Data Products in the Bay of Bengal during Summer Monsoon Season. Advances in Meteorology, 2015(1), 806845.https://doi.org/10.1155/2015/806845

Quinn, P. K., and Bates, T. S. (2011). The case against climate regulation via oceanic phytoplankton sulphur emissions. Nature, 480(7375), 51–56. https://doi.org/10.1038/nature10580

Raina, J.-B., Tapiolas, D. M., Forêt, S., Lutz, A., Abrego, D., Ceh, J., Seneca, F. O., Clode, P. L., Bourne, D. G., Willis, B. L., and Motti, C. A. (2013). DMSP biosynthesis by an animal and its role in coral thermal stress response. Nature, 502(7473), 677–680. https://doi.org/10.1038/nature12677

Rajasuriya, A., and White, A. (1995). Coral Reefs of Sri Lanka: Review of Their Extent, Condition, and Management Status. Coastal Management - COAST MANAGE, 23, 77–90.https://doi.org/10.1080/08920759509362257

Rao, V. D., Viswanadham, R., Bharathi, M. D., Sarma, V. V. S. S., and Kumar, M. D. (2015). Impact of river discharge on distribution of dimethyl sulfide (DMS) and its fluxes in the coastal Bay of Bengal. Journal of Sea Research, 103. https://doi.org/10.1016/j.seares.2015.05.004

Ratte, M., Plass-Dülmer, C., Koppmann, R., Rudolph, J., and Denga, J. (1993). Production mechanism of C2-C4 hydrocarbons in seawater: Field measurements and experiments. Global Biogeochemical Cycles, 7(2), 369–378.https://doi.org/10.1029/93GB00054

Rixen, T., Cowie, G., Gaye, B., Goes, J., do Rosário Gomes, H., Hood, R. R., Lachkar, Z., Schmidt, H., Segschneider, J., and Singh, A. (2020). Reviews and syntheses: Present, past, and future of the oxygen minimum zone in the northern Indian Ocean. Biogeosciences, 17(23), 6051–6080. https://doi.org/10.5194/bg-17-6051-2020

Robin, R. S., Kanuri, V. V., Muduli, P. R., Mishra, R. K., Jaikumar, M., Karthikeyan, P., Suresh Kumar, C., and Saravana Kumar, C. (2013). Dinoflagellate Bloom of Karenia mikimotoi along the Southeast Arabian Sea, Bordering Western India. Journal of Ecosystems, 2013(1), 463720. https://doi.org/10.1155/2013/463720

Rocco, M., Dunne, E., Peltola, M., Barr, N., Williams, J., Colomb, A., Safi, K., Saint-Macary, A., Marriner, A., Deppeler, S., Harnwell, J., Law, C., and Sellegri, K. (2021). Oceanic phytoplankton are a potentially important source of benzenoids to the remote marine atmosphere. Communications Earth and Environment, 2(1), 175. https://doi.org/10.1038/s43247-021-00253-0

Rosati, B., Christiansen, S., Wollesen de Jonge, R., Roldin, P., Jensen, M. M., Wang, K., Moosakutty, S. P., Thomsen, D., Salomonsen, C., Hyttinen, N., Elm, J., Feilberg, A., Glasius, M., and Bilde, M. (2021). New Particle Formation and Growth from Dimethyl Sulfide Oxidation by Hydroxyl Radicals. ACS Earth and Space Chemistry, 5(4), 801–811. https://doi.org/10.1021/acsearthspacechem.0c00333

Roxy, M. K., Ritika, K., Terray, P., Murtugudde, R., Ashok, K., and Goswami, B. N. (2015). Drying of Indian subcontinent by rapid Indian Ocean warming and a weakening land-sea thermal gradient. Nature Communications, 6(1), 7423. https://doi.org/10.1038/ncomms8423

Royer, S.-J., Galí, M., Mahajan, A. S., Ross, O. N., Pérez, G. L., Saltzman, E. S., and Simó, R. (2016). A high-resolution time-depth view of dimethylsulphide cycling in the surface sea. Scientific Reports, 6(1), Article 1. https://doi.org/10.1038/srep32325

Royer, S.-J., Galí, M., Saltzman, E. S., McCormick, C. A., Bell, T. G., and Simó, R. (2014). Development and validation of a shipboard system for measuring high-resolution vertical profiles of aqueous dimethylsulfide concentrations using chemical ionisation mass spectrometry. Environmental Chemistry, 11(3), 309–317. https://doi.org/10.1071/EN13203

Royer, S.-J., Mahajan, A. S., Galí, M., Saltzman, E., and Simó, R. (2015). Small-scale variability patterns of DMS and phytoplankton in surface waters of the tropical and subtropical Atlantic, Indian, and Pacific Oceans. Geophysical Research Letters, 42(2), 475–483. https://doi.org/10.1002/2014GL062543

SAC. (2010). Coral Reef Atlas of the World, Central Indian Ocean (p. 281). Space Application Centre, Indian Space Research Organization.

Sahu, L. K. (2012). Volatile organic compounds and their measurements in the troposphere. CURRENT SCIENCE, 102(12).

Sahu, L. K., Gupta, M., Tripathi, N., Yadav, R., Malik, T. G., and Kajino, M. (2025). Effect of Different Sources and Meteorological Processes on the Variability of VOC Composition in a Metropolitan City of Western India During Summer Season. Journal of Geophysical Research: Atmospheres, 130(9), e2024JD040867. https://doi.org/10.1029/2024JD040867

Sahu, L. K., Lal, S., and Venkataramani, S. (2006). Distributions of O3, CO and hydrocarbons over the Bay of Bengal: A study to assess the role of transport from southern India and marine regions during September–October 2002. Atmospheric Environment, 40(24), 4633–4645. https://doi.org/10.1016/j.atmosenv.2006.02.037

Sahu, L. K., and Lal, S. (2006). Changes in surface ozone levels due to convective downdrafts over the Bay of Bengal. Geophysical Research Letters, 33(10).https://doi.org/10.1029/2006GL025994

Sahu, L. K., Lal, S., and Venkataramani, S. (2010). Impact of monsoon circulations on oceanic emissions of light alkenes over Bay of Bengal. Global Biogeochemical Cycles, 24(4). https://doi.org/10.1029/2009GB003766

Sahu, L. K., Lal, S., and Venkataramani, S. (2011). Seasonality in the latitudinal distributions of NMHCs over Bay of Bengal. Atmospheric Environment, 45(14), 2356–2366.https://doi.org/10.1016/j.atmosenv.2011.02.021

Sahu, L. K., Tripathi, N., Gupta, M., Singh, V., Yadav, R., and Patel, K. (2022). Impact of COVID-19 Pandemic Lockdown in Ambient Concentrations of Aromatic Volatile Organic Compounds in a Metropolitan City of Western India. Journal of Geophysical Research: Atmospheres, 127(6), e2022JD036628. https://doi.org/10.1029/2022JD036628

Sahu, L. K., Tripathi, N., and Yadav, R. (2017). Contribution of biogenic and photochemical sources to ambient VOCs during winter to summer transition at a semi-arid urban site in India. Environmental Pollution, 229, 595–606. https://doi.org/10.1016/j.envpol.2017.06.091

Saito, T., Yokouchi, Y., and Kawamura, K. (2000). Distributions of C2-C6 hydrocarbons over the western North Pacific and eastern Indian Ocean. Atmospheric Environment, 34(25). https://doi.org/10.1016/S1352-2310(00)00249-1

Salignat, R., Rose, C., Banson, S., Berthet, S., Lupascu, A., Uitz, J., Mallet, M., Seferian, R., Rocco, M., Colomb, A., Dunne, E., Saint-Macary, A., Marriner, A., Law, C. S., and Sellegri, K. (2025). Sensitivity Study of Atmospheric DMS Simulated in WRF-Chem to Various Oceanic DMS Fields Over the South West Pacific. Journal of Geophysical Research: Atmospheres, 130(14), e2024JD042271. https://doi.org/10.1029/2024JD042271

Saltzman, E. S., King, D. B., Holmen, K., and Leck, C. (1993). Experimental determination of the diffusion coefficient of dimethylsulfide in water. Journal of Geophysical Research: Oceans, 98(C9), 16481–16486. https://doi.org/10.1029/93JC01858

hlSanchez, K. J., Roberts, G. C., Saliba, G., Russell, L. M., Twohy, C., Reeves, J. M., Humphries, R. S., Keywood, M. D., Ward, J. P., and McRobert, I. M. (2021). Measurement report: Cloud processes and the transport of biological emissions affect Southern Ocean particle and cloud condensation nuclei concentrations. Atmospheric Chemistry and Physics, 21(5), 3427–3446. https://doi.org/10.5194/acp-21-3427-2021

hlSanchez-Barrero, M. F., Goloub, P., Blarel, L., Popovici, I. E., Torres, B., Dubois, G., Podvin, T., Ducos, F., de Filippi, R., Sicard, M., Bout Roumazeilles, V., and Skonieczny, C. (2025). Aerosol variability over oceans using micro-pulse lidar and photometer: Insights from TRANSAMA ship-based campaign. EGUsphere, 2025, 1–30. https://doi.org/10.5194/egusphere-2025-3481

Sanchez, K. J., Chen, C.-L., Russell, L. M., Betha, R., Liu, J., Price, D. J., Massoli, P., Ziemba, L. D., Crosbie, E. C., Moore, R. H., Müller, M., Schiller, S. A., Wisthaler, A., Lee, A. K. Y., Quinn, P. K., Bates, T. S., Porter, J., Bell, T. G., Saltzman, E. S., … Behrenfeld, M. J. (2018). Substantial Seasonal Contribution of Observed Biogenic Sulfate Particles to Cloud Condensation Nuclei. Scientific Reports, 8(1), 3235. https://doi.org/10.1038/s41598-018-21590-9

Sarin, M., Kumar, A., Srinivas, B., Sudheer, A. K., and Rastogi, N. (2010). Anthropogenic sulphate aerosols and large Cl-deficit in marine atmospheric boundary layer of tropical Bay of Bengal. Journal of Atmospheric Chemistry, 66(1), 1–10. https://doi.org/10.1007/s10874-011-9188-z

Sarker, S., Panassa, E., Hossain, M. S., Chowdhury, S. R., Yadav, A. K., and Sharifuzzaman, S. M. (2020). A bio-physicochemical perspective of the Bay of Bengal. Journal of the Marine Biological Association of the United Kingdom, 100(4), 517–528. Cambridge Core. https://doi.org/10.1017/S0025315420000442

Sarma, V. V. S. S., Gupta, S. N. M., Babu, P. V. R., Acharya, T., Harikrishnachari, N., Vishnuvardhan, K., Rao, N. S., Reddy, N. P. C., Sarma, V. V., Sadhuram, Y., Murty, T. V. R., and Kumar, M. D. (2009). Influence of river discharge on plankton metabolic rates in the tropical monsoon driven Godavari estuary, India. Estuarine, Coastal and Shelf Science, 85(4), 515–524. https://doi.org/10.1016/j.ecss.2009.09.003

Sarma, V. V. S. S., Sampath Kumar, G., Yadav, K., Dalabehera, H. B., Rao, D. N., Behera, S., and Loganathan, J. (2019). Impact of eddies on dissolved inorganic carbon components in the Bay of Bengal. Deep Sea Research Part I: Oceanographic Research Papers, 147, 111–120. https://doi.org/10.1016/j.dsr.2019.04.005

Saroj, J., Gautam, R., Joshi, A., and Tehseen, P. (2016). REVIEW OF CORAL REEFS OF INDIA: DISTRIBUTION, STATUS, RESEARCH AND MANAGEMENT. International Journal of Science, Environment and Technology, 5, 3088–3098.

Sciare, J., Kanakidou, M., and Mihalopoulos, N. (2000). Diurnal and seasonal variation of atmospheric dimethylsulfoxide at Amsterdam Island in the southern Indian Ocean. Journal of Geophysical Research: Atmospheres, 105(D13), 17257–17265.https://doi.org/10.1029/1999JD901186

Sengupta, D., Bharath Raj, G. N., and Shenoi, S. S. C. (2006). Surface freshwater from Bay of Bengal runoff and Indonesian Throughflow in the tropical Indian Ocean. Geophysical Research Letters, 33(22). https://doi.org/10.1029/2006GL027573

Sharkey, T. D., Wiberley, A. E., and Donohue, A. R. (2008). Isoprene Emission from Plants: Why and How. Annals of Botany, 101(1), 5–18.https://doi.org/10.1093/aob/mcm240

Shaw, S. L., Gantt, B., and Meskhidze, N. (2010). Production and Emissions of Marine Isoprene and Monoterpenes: A Review. Advances in Meteorology, 2010, 408696. https://doi.org/10.1155/2010/408696

Shenoy, D. M., Joseph, S., Dileep Kumar, M., and George, M. D. (2002). Control and interannual variability of dimethyl sulfide in the Indian Ocean. Journal of Geophysical Research: Atmospheres, 107(D19), INX2 7-1.https://doi.org/10.1029/2001JD000371

Shenoy, D. M., and Kumar, M. D. (2007). Variability in abundance and fluxes of dimethyl sulphide in the Indian Ocean. Biogeochemistry, 83(1), 277–292. https://doi.org/10.1007/s10533-007-9092-4

Shenoy, D. M., Kumar, M. D., and Sarma, V. V. S. S. (2000). Controls of dimethyl sulphide in the Bay of Bengal during BOBMEX-Pilot cruise 1998. Journal of Earth System Science, 109(2), 279–283. https://doi.org/10.1007/BF02702201

Shenoy, D. M., and Patil, J. S. (2003). Temporal variations in dimethylsulphoniopropionate and dimethyl sulphide in the Zuari estuary, Goa (India). Marine Environmental Research, 56(3), 387–402. https://doi.org/10.1016/S0141-1136(02)00337-9

Shenoy, D. M., Paul, J. T., Gauns, M., Ramaiah, N., and Kumar, M. D. (2006). Spatial variations of DMS, DMSP and phytoplankton in the Bay of Bengal during the summer monsoon 2001. Marine Environmental Research, 62(2), 83–97. https://doi.org/10.1016/j.marenvres.2006.03.005

Simó, R., Cortés-Greus, P., Rodríguez-Ros, P., and Masdeu-Navarro, M. (2022). Substantial loss of isoprene in the surface ocean due to chemical and biological consumption. Communications Earth and Environment, 3(1), 20.https://doi.org/10.1038/s43247-022-00352-6

Simó, R., and Dachs, J. (2002). Global ocean emission of dimethylsulfide predicted from biogeophysical data. Global Biogeochemical Cycles, 16(4), 26-1-26–10. https://doi.org/10.1029/2001GB001829

Simó, R., and Grimalt, J. O. (1998). Spring–summer Emission of Dimethyl Sulphide from the North-western Mediterranean Sea. Estuarine, Coastal and Shelf Science, 47(5), 671–677.https://doi.org/10.1006/ecss.1998.0386

Simpson, R. M. C., Howell, S. G., Blomquist, B. W., Clarke, A. D., and Huebert, B. J. (2014). Dimethyl sulfide: Less important than long-range transport as a source of sulfate to the remote tropical Pacific marine boundary layer. Journal of Geophysical Research: Atmospheres, 119(14), 9142–9167. https://doi.org/10.1002/2014JD021643

Sindelarova, K., Granier, C., Bouarar, I., Guenther, A., Tilmes, S., Stavrakou, T., Müller, J.-F., Kuhn, U., Stefani, P., and Knorr, W. (2014). Global data set of biogenic VOC emissions calculated by the MEGAN model over the last 30 years. Atmospheric Chemistry and Physics, 14(17), 9317–9341. https://doi.org/10.5194/acp-14-9317-2014

Singh, A., and Ramesh, R. (2015). Environmental controls on new and primary production in the northern Indian Ocean. Progress in Oceanography, 131. https://doi.org/10.1016/j.pocean.2014.12.006

Sipilä, M., Berndt, T., Petäjä, T., Brus, D., Vanhanen, J., Stratmann, F., Patokoski, J., Mauldin, R. L., Hyvärinen, A.-P., Lihavainen, H., and Kulmala, M. (2010). The Role of Sulfuric Acid in Atmospheric Nucleation. Science, 327(5970), 1243–1246.https://doi.org/10.1126/science.1180315

Sommer, U. (1994). Are marine diatoms favoured by high Si:N ratios? Marine Ecology Progress Series, 115. https://doi.org/10.3354/meps115309

Speeckaert, G., Borges, A. V., and Gypens, N. (2019). Salinity and growth effects on dimethylsulfoniopropionate (DMSP) and dimethylsulfoxide (DMSO) cell quotas of Skeletonema costatum, Phaeocystis globosa and Heterocapsa triquetra. Estuarine, Coastal and Shelf Science, 226, 106275. https://doi.org/10.1016/j.ecss.2019.106275

Spielmeyer, A., and Pohnert, G. (2012). Daytime, growth phase and nitrate availability dependent variations of dimethylsulfoniopropionate in batch cultures of the diatom Skeletonema marinoi. Journal of Experimental Marine Biology and Ecology, 413, 121–130.

Sreeush, M. G., Valsala, V., Pentakota, S., Prasad, K. V. S. R., and Murtugudde, R. (2018). Biological production in the Indian Ocean upwelling zones—Part 1: Refined estimation via the use of a variable compensation depth in ocean carbon models. Biogeosciences, 15(7). https://doi.org/10.5194/bg-15-1895-2018

Stark, H., Brown, S. S., Goldan, P. D., Aldener, M., Kuster, W. C., Jakoubek, R., Fehsenfeld, F. C., Meagher, J., Bates, T. S., and Ravishankara, A. R. (2007). Influence of nitrate radical on the oxidation of dimethyl sulfide in a polluted marine environment. Journal of Geophysical Research: Atmospheres, 112(D10).https://doi.org/10.1029/2006JD007669

Stefels, J. (2000). Physiological aspects of the production and conversion of DMSP in marine algae and higher plants. Journal of Sea Research, 43(3), 183–197. https://doi.org/10.1016/S1385-1101(00)00030-7

Stefels, J., Steinke, M., Turner, S., Malin, G., and Belviso, S. (2007). Environmental constraints on the production and removal of the climatically active gas dimethylsulphide (DMS) and implications for ecosystem modelling. Biogeochemistry, 83(1), 245–275.https://doi.org/10.1007/s10533-007-9091-5

Stein, A. F., Draxler, R. R., Rolph, G. D., Stunder, B. J. B., Cohen, M. D., and Ngan, F. (2015). NOAA's HYSPLIT Atmospheric Transport and Dispersion Modeling System. Bulletin of the American Meteorological Society, 96(12), 2059–2077. https://doi.org/10.1175/BAMS-D-14-00110.1

Stohl, A. (1998). Computation, accuracy and applications of trajectories—A review and bibliography. Atmospheric Environment, 32(6), 947–966. https://doi.org/10.1016/S1352-2310(97)00457-3

Sun, J., and Ariya, P. A. (2006). Atmospheric organic and bio-aerosols as cloud condensation nuclei (CCN): A review. Atmospheric Environment, 40(5), 795–820. https://doi.org/10.1016/j.atmosenv.2005.05.052

Sunda, W., Hardison, R., Kiene, R. P., Bucciarelli, E., and Harada, H. (2007). The effect of nitrogen limitation on cellular DMSP and DMS release in marine phytoplankton: Climate feedback implications. Aquatic Sciences, 69(3), 341–351. https://doi.org/10.1007/s00027-007-0887-0

Sunda, W., Kieber, D. J., Kiene, R. P., and Huntsman, S. (2002). An antioxidant function for DMSP and DMS in marine algae. Nature, 418(6895), 317–320. https://doi.org/10.1038/nature00851

Swan, H. B. (2022). The Potential for Great Barrier Reef Regional Climate Regulation via Dimethylsulfide Atmospheric Oxidation Products. Frontiers in Marine Science, 9. https://www.frontiersin.org/journals/marine-science/articles/10.3389/fmars.2022.869166

Swan, H. B., Crough, R. W., Vaattovaara, P., Jones, G. B., Deschaseaux, E. S. M., Eyre, B. D., Miljevic, B., and Ristovski, Z. D. (2016). Dimethyl sulfide and other

biogenic volatile organic compound emissions from branching coral and reef seawater: Potential sources of secondary aerosol over the Great Barrier Reef. Journal of Atmospheric Chemistry, 73(3), 303–328. https://doi.org/10.1007/s10874-016-9327-7

Swan, H. B., Jones, G. B., Deschaseaux, E. S. M., and Eyre, B. D. (2017). Coral reef origins of atmospheric dimethylsulfide at Heron Island, southern Great Barrier Reef, Australia. Biogeosciences, 14(1), 229–239. https://doi.org/10.5194/bg-14-229-2017

Tadic, I., Crowley, J. N., Dienhart, D., Eger, P., Harder, H., Hottmann, B., Martinez, M., Parchatka, U., Paris, J.-D., Pozzer, A., Rohloff, R., Schuladen, J., Shenolikar, J., Tauer, S., Lelieveld, J., and Fischer, H. (2020). Net ozone production and its relationship to nitrogen oxides and volatile organic compounds in the marine boundary layer around the Arabian Peninsula. Atmos. Chem. Phys., 20(11), 6769–6787. https://doi.org/10.5194/acp-20-6769-2020

Tashmim, L., Porter, W. C., Chen, Q., Alexander, B., Fite, C. H., Holmes, C. D., Pierce, J., Croft, B., and Ishino, S. (2024). Contribution of expanded marine sulfur chemistry to the seasonal variability of dimethyl sulfide oxidation products and size-resolved sulfate aerosol. Atmospheric Chemistry and Physics, 24, 3379–3403. https://doi.org/10.5194/acp-24-3379-2024

Tegtmeier, S., Marandino, C., Jia, Y., Quack, B., and Mahajan, A. S. (2022). Atmospheric gas-phase composition over the Indian Ocean. Atmospheric Chemistry and Physics, 22(10), 6625–6676.https://doi.org/10.5194/acp-22-6625-2022

Tesdal, J.-E., Christian, J. R., Monahan, A. H., and von Salzen, K. (2016). Sensitivity of modelled sulfate aerosol and its radiative effect on climate to ocean DMS concentration and air–sea flux. Atmospheric Chemistry and Physics, 16(17), 10847–10864. https://doi.org/10.5194/acp-16-10847-2016

Thoppil, P. G., Wallcraft, A. J., and Jensen, T. G. (2022). Winter Convective Mixing in the Northern Arabian Sea during Contrasting Monsoons. Journal of Physical Oceanography, 52(3), 313–327. https://doi.org/10.1175/JPO-D-21-0144.1

Toole, D. A., and Siegel, D. A. (2004). Light-driven cycling of dimethylsulfide (DMS) in the Sargasso Sea: Closing the loop. Geophysical Research Letters, 31(9). https://doi.org/10.1029/2004GL019581

Tripathi, N., Girach, I. A., Kompalli, S. K., Murari, V., Nair, P. R., Babu, S. S., and Sahu, L. K. (2024). Sources and Distribution of Light NMHCs in the Marine Boundary Layer of the Northern Indian Ocean During Winter: Implications to Aerosol Formation. Journal of Geophysical Research: Atmospheres, 129(3), e2023JD039433. https://doi.org/10.1029/2023JD039433

Tripathi, N., Sahu, L. K., Patel, K., Kumar, A., and Yadav, R. (2021). Ambient air characteristics of biogenic volatile organic compounds at a tropical evergreen forest site in Central Western Ghats of India. Journal of Atmospheric Chemistry, 78(2), 139–159.https://doi.org/10.1007/s10874-021-09415-y

Tripathi, N., Sahu, L. K., Singh, A., Yadav, R., and Karati, K. K. (2020a). High Levels of Isoprene in the Marine Boundary Layer of the Arabian Sea during Spring Inter-Monsoon: Role of Phytoplankton Blooms. ACS Earth and Space Chemistry, 4(4), 583–590. https://doi.org/10.1021/acsearthspacechem.9b00325

Tripathi, N., Sahu, L. K., Singh, A., Yadav, R., Patel, A., Patel, K., and Meenu, P. (2020b). Elevated Levels of Biogenic Nonmethane Hydrocarbons in the Marine Boundary Layer of the Arabian Sea During the Intermonsoon. Journal of Geophysical Research: Atmospheres, 125(22), e2020JD032869.https://doi.org/10.1029/2020JD032869

Tyagi, G., Babu, K., and Solanki, H. A. (2020). Monitoring bio-optical response of coastal waters surrounding the Indian subcontinent to atmospheric dust deposition using satellite data. Environmental Science and Pollution Research, 27(5), 5523–5535. https://doi.org/10.1007/s11356-019-07134-2

UNEP-WCMC, WorldFish Centre, WRI, TNC, and 4.0. (2010). Global distribution of warm-water coral reefs, compiled from multiple sources including the Millennium Coral Reef Mapping Project [Dataset]. In Includes contributions from IMaRS-USF and IRD (2005), IMaRS-USF (2005), and Spalding et al. (2001). UNEP World Conservation Monitoring Centre. http://data.unep-wcmc.org/datasets/1

Vajravelu, M., Martin, Y., Ayyappan, S., and Mayakrishnan, M. (2018). Seasonal influence of physico-chemical parameters on phytoplankton diversity, community structure and abundance at Parangipettai coastal waters, Bay of Bengal, South East Coast of India. Oceanologia, 60(2), 114–127.https://doi.org/10.1016/j.oceano.2017.08.003

Varkey, M. J., Murty, V. S., and Suryanarayana, A. (1996). Physical oceanography of the Bay of Bengal and Andaman Sea. Oceanography and Marine Biology, 34, 1–70.

Vidhya, V., Jyothibabu, R., Jagadeesan, L., Rashid, C., Alok, K. T., Arunpandi, N., and Thirumurugan, R. (2022). Oxygen minimum zone copepods in the Arabian Sea and the Bay of Bengal: Their adaptations and status. Progress in Oceanography, 206, 102839. https://doi.org/10.1016/j.pocean.2022.102839

Vijayan, A. K., Reddy, B. B., Sudheesh, V., Marathe, P. H., Nampoothiri, V. N., Harikrishnachari, N. V., Kavya, P., Gupta, G. V. M., and Ramanamurthy, M. V. (2021). Phytoplankton community structure in a contrasting physico-chemical regime along the eastern Arabian Sea during the winter monsoon. Journal of Marine Systems, 215, 103501. https://doi.org/10.1016/j.jmarsys.2020.103501

Vinayachandran, P. N., Kagimoto, T., Masumoto, Y., Chauhan, P., Nayak, S. R., and Yamagata, T. (2005). Bifurcation of the East India Coastal Current east of Sri Lanka. Geophysical Research Letters, 32(15). https://doi.org/10.1029/2005GL022864

Vinayachandran, P. N., Shankar, D., Vernekar, S., Sandeep, K. K., Amol, P., Neema, C. P., and Chatterjee, A. (2013). A summer monsoon pump to keep the Bay of Bengal salty. Geophysical Research Letters, 40(9), 1777–1782. https://doi.org/10.1002/grl.50274

Viswanadham, R., Bharathi, M. D., and Sarma, V. V. S. S. (2016). Variations in Concentrations and Fluxes of Dimethylsulfide (DMS) from the Indian Estuaries. Estuaries and Coasts, 39(3), 695–706. https://doi.org/10.1007/s12237-015-0039-z

Vogt, M., Steinke, M., Turner, S., Paulino, A., Meyerhöfer, M., Riebesell, U., LeQuéré, C., and Liss, P. (2008). Dynamics of dimethylsulphoniopropionate and dimethylsulphide under different CO2 concentrations during a mesocosm experiment. Biogeosciences, 5(2), 407–419. https://doi.org/10.5194/bg-5-407-2008

Wang, J., Xue, L., Ma, Q., Xu, F., Xu, G., Yan, S., Zhang, J., Li, J., Zhang, H., Zhang, G., and Chen, Z. (2024). The role of oceanic ventilation and terrestrial outflow in atmospheric non-methane hydrocarbons over the Chinese marginal seas. Atmospheric Chemistry and Physics, 24(15), 8721–8736. https://doi.org/10.5194/acp-24-8721-2024

Wang, S., Apel, E. C., Schwantes, R. H., Bates, K. H., Jacob, D. J., Fischer, E. V., Hornbrook, R. S., Hills, A. J., Emmons, L. K., Pan, L. L., Honomichl, S., Tilmes, S., Lamarque, J. F., Yang, M., Marandino, C. A., Saltzman, E. S., Bruyn, W. de, Kameyama, S., Tanimoto, H., … Wofsy, S. C. (2020). Global Atmospheric Budget of Acetone: Air-Sea Exchange and the Contribution to Hydroxyl Radicals. Journal of Geophysical Research: Atmospheres, 125(15). https://doi.org/10.1029/2020JD032553

Wanninkhof, R. (1992). Relationship between wind speed and gas exchange over the ocean. Journal of Geophysical Research, 97(C5). https://doi.org/10.1029/92JC00188

Wanninkhof, R., Asher, W. E., Ho, D. T., Sweeney, C., and McGillis, W. R. (2009). Advances in Quantifying Air-Sea Gas Exchange and Environmental Forcing. Annual Review of Marine Science, 1(1), 213–244.https://doi.org/10.1146/annurev.marine.010908.163742

Warneke, C., and de Gouw, J. A. (2001). Organic trace gas composition of the marine boundary layer over the northwest Indian Ocean in April 2000. Atmospheric Environment, 35(34), 5923–5933. https://doi.org/10.1016/S1352-2310(01)00384-3

Warneke, C., Holzinger, R., Hansel, A., Jordan, A., Lindinger, W., Pöschl, U., Williams, J., Hoor, P., Fischer, H., Crutzen, P. J., Scheeren, H. A., and Lelieveld, J. (2001). Isoprene and Its Oxidation Products Methyl Vinyl Ketone, Methacrolein, and Isoprene Related Peroxides Measured Online over the Tropical Rain Forest of Surinam in March 1998. Journal of Atmospheric Chemistry, 38(2), 167–185. https://doi.org/10.1023/A:1006326802432

Watts, S. F. (2000). The mass budgets of carbonyl sulfide, dimethyl sulfide, carbon disulfide and hydrogen sulfide. Atmospheric Environment, 34(5). https://doi.org/10.1016/S1352-2310(99)00342-8

Webster, P. J., Moore, A. M., Loschnigg, J. P., and Leben, R. R. (1999). Coupled ocean-atmosphere dynamics in the Indian Ocean during 1997-98. Nature, 401(6751), 356–360. https://doi.org/10.1038/43848

Wei, Y., Huang D, Zhang G, Zhao Y, and Sun J. (2020). Biogeographic variations of picophytoplankton in three contrasting seas: The Bay of Bengal, South China Sea and Western Pacific Ocean. Aquatic Microbial Ecology, 84, 91–103.

Williams, J., Custer, T., Riede, H., Sander, R., Jöckel, P., Hoor, P., Pozzer, A., Wong-Zehnpfennig, S., Hosaynali Beygi, Z., Fischer, H., Gros, V., Colomb, A., Bonsang, B., Yassaa, N., Peeken, I., Atlas, E. L., Waluda, C. M., van Aardenne, J. A., and Lelieveld, J. (2010). Assessing the effect of marine isoprene and ship emissions on ozone, using modelling and measurements from the South Atlantic Ocean. Environmental Chemistry, 7(2), 171–182. https://doi.org/10.1071/EN09154

Williams, J., Holzinger, R., Gros, V., Xu, X., Atlas, E., and Wallace, D. W. R. (2004). Measurements of organic species in air and seawater from the tropical Atlantic. Geophysical Research Letters, 31(23). https://doi.org/10.1029/2004GL020012

Windmiller, J. M., Bao, J., Sherwood, S. C., Schanzer, T. D., and Fuchs, D. (2023). Predicting Convective Downdrafts From Updrafts and Environmental Conditions in a Global Storm Resolving Simulation. Journal of Advances in Modeling Earth Systems, 15(3), e2022MS003048. https://doi.org/10.1029/2022MS003048

Wohl, C., Brown, I., Kitidis, V., Jones, A. E., Sturges, W. T., Nightingale, P. D., and Yang, M. (2020). Underway seawater and atmospheric measurements of volatile organic compounds in the Southern Ocean. Biogeosciences, 17(9), 2593–2619. https://doi.org/10.5194/bg-17-2593-2020

Wohl, C., Li, Q., Cuevas, C. A., Fernandez, R. P., Yang, M., Saiz-Lopez, A., and Simó, R. (2023). Marine biogenic emissions of benzene and toluene and their contribution to secondary organic aerosols over the polar oceans. Science Advances, 9(4), eadd9031.https://doi.org/10.1126/sciadv.add9031

Wu, Y.-C., Li, J.-L., Wang, J., Zhuang, G.-C., Liu, X.-T., Zhang, H.-H., and Yang, G.-P. (2021). Occurance, emission and environmental effects of non-methane hydrocarbons in the Yellow Sea and the East China Sea. Environmental Pollution, 270, 116305.https://doi.org/10.1016/j.envpol.2020.116305

Wyrtki, K. (1973). An Equatorial Jet in the Indian Ocean. Science, 181(4096), 262–264. https://doi.org/10.1126/science.181.4096.262

Xu, F., Zhang, H.-H., Yan, S.-B., Sun, M.-X., Wu, J.-W., and Yang, G.-P. (2023). Biogeochemical controls on climatically active gases and atmospheric sulfate aerosols in the western Pacific. Environmental Research, 220, 115211. https://doi.org/10.1016/j.envres.2023.115211

Yan, S.-B., Xu, G.-B., Zhang, H.-H., Wang, J., Xu, F., Gao, X.-X., Zhang, J.-W., Wu, J.-W., and Yang, G.-P. (2024). Factors Controlling DMS Emission and Atmospheric Sulfate Aerosols in the Western Pacific Continental Sea. Journal of Geophysical Research: Oceans, 129(7), e2024JC020886. https://doi.org/10.1029/2024JC020886

Yáñez-Serrano, A. M., Nölscher, A. C., Williams, J., Wolff, S., Alves, E., Martins, G. A., Bourtsoukidis, E., Brito, J., Jardine, K., Artaxo, P., and Kesselmeier, J. (2015). Diel and seasonal changes of biogenic volatile organic compounds within and above an Amazonian rainforest. Atmospheric Chemistry and Physics, 15(6), 3359–3378. https://doi.org/10.5194/acp-15-3359-2015

Yang, M., Blomquist, B. W., Fairall, C. W., Archer, S. D., and Huebert, B. J. (2011). Air-sea exchange of dimethylsulfide in the Southern Ocean: Measurements from SO GasEx compared to temperate and tropical regions. Journal of Geophysical Research: Oceans, 116(C4). https://doi.org/10.1029/2010JC006526

Yang, Q.-Q., Li, P.-F., Duan, S.-S., Han, L., Gao, P.-P., Liu, C.-Y., and Yang, G.-P. (2022). Production of dimethylsulfoniopropionate, dimethylsulfide and acrylic acid from marine microalgae. Journal of Sea Research, 190, 102299. https://doi.org/10.1016/j.seares.2022.102299

Yassaa, N., Peeken, I., Zöllner, E., Bluhm, K., Arnold, S., Spracklen, D., Williams, J., Yassaa, N., Peeken, I., Zöllner, E., Bluhm, K., Arnold, S., Spracklen, D., and Williams, J. (2008). Evidence for marine production of monoterpenes. Environmental Chemistry, 5(6), 391–401. https://doi.org/10.1071/EN08047

Yoch, D. C. (2002). Dimethylsulfoniopropionate: Its Sources, Role in the Marine Food Web, and Biological Degradation to Dimethylsulfide. Applied and Environmental Microbiology, 68(12), 5804–5815. https://doi.org/10.1128/AEM.68.12.5804-5815.2002

Yokouchi, Y., Li, H.-J., Machida, T., Aoki, S., and Akimoto, H. (1999). Isoprene in the marine boundary layer (southeast Asian Sea, eastern Indian Ocean, and Southern Ocean): Comparison with dimethyl sulfide and bromoform. Journal of Geophysical Research: Atmospheres, 104(D7), 8067–8076. https://doi.org/10.1029/1998JD100013

Zannoni, N., Gros, V., Sarda Esteve, R., Kalogridis, C., Michoud, V., Dusanter, S., Sauvage, S., Locoge, N., Colomb, A., and Bonsang, B. (2017). Summertime OH reactivity from a receptor coastal site in the Mediterranean Basin. Atmospheric Chemistry and Physics, 17(20), 12645–12658. https://doi.org/10.5194/acp-17-12645-2017

Zavarsky, A., Booge, D., Fiehn, A., Krüger, K., Atlas, E., and Marandino, C. (2018a). The Influence of Air-Sea Fluxes on Atmospheric Aerosols During the Summer Monsoon Over the Tropical Indian Ocean: AIR-SEA FLUXES IN THE INDIAN OCEAN. Geophysical Research Letters, 45(1), 418–426. https://doi.org/10.1002/2017GL076410

Zavarsky, A., Goddijn-Murphy, L., Steinhoff, T., and Marandino, C. A. (2018b). Bubble-Mediated Gas Transfer and Gas Transfer Suppression of DMS and CO2. Journal of Geophysical Research: Atmospheres, 123(12), 6624–6647.https://doi.org/10.1029/2017JD028071

Zhang, S.-H., Sun, J., Liu, J.-L., Wang, N., Zhang, H.-H., Zhang, X.-H., and Yang, G.-P. (2017). Spatial distributions of dimethyl sulfur compounds, DMSP-lyase activity,

and phytoplankton community in the East China Sea during fall. Biogeochemistry, 133(1), 59–72. https://doi.org/10.1007/s10533-017-0308-y

Zhang, W., and Gu, D. (2022). Geostationary satellite reveals increasing marine isoprene emissions in the center of the equatorial Pacific Ocean. Npj Climate and Atmospheric Science, 5(1), Article 1. https://doi.org/10.1038/s41612-022-00311-0

Zhang, X.-H., Liu, J., Liu, J., Yang, G., Xue, C.-X., Curson, A. R. J., and Todd, J. D. (2019). Biogenic production of DMSP and its degradation to DMS—their roles in the global sulfur cycle. Science China Life Sciences, 62(10), 1296–1319. https://doi.org/10.1007/s11427-018-9524-y

Zhao, Y., Booge, D., Marandino, C. A., Schlundt, C., Bracher, A., Atlas, E. L., Williams, J., and Bange, H. W. (2022). Dimethylated sulfur compounds in the Peruvian upwelling system. Biogeosciences, 19(3), 701–714. https://doi.org/10.5194/bg-19-701-2022

Zhou, S., Chen, Y., Huang, S., Gong, X., Yang, G., Zhang, H., Herrmann, H., Wiedensohler, A., Poulain, L., Zhang, Y., Wang, F., Xu, Z., and Yan, K. (2024). A 20-year (1998–2017) global sea surface dimethyl sulfide gridded dataset with daily resolution. Earth System Science Data, 16(9), 4267–4290. https://doi.org/10.5194/essd-16-4267-2024

Zhu, J., Zhang, Y., Cheng, X., Wang, X., Sun, Q., and Du, Y. (2022). Effect of mesoscale eddies on the transport of low-salinity water from the Bay of Bengal into the Arabian Sea during winter. Geoscience Letters, 9(1), 37. https://doi.org/10.1186/s40562-022-00246-7

Zindler, C., Peeken, I., Marandino, C. A., and Bange, H. W. (2012). Environmental control on the variability of DMS and DMSP in the Mauritanian upwelling region. Biogeosciences, 9(3), 1041–1051.https://doi.org/10.5194/bg-9-1041-2012

Ziska, F., Quack, B., Abrahamsson, K., Archer, S. D., Atlas, E., Bell, T., Butler, J. H., Carpenter, L. J., Jones, C. E., Harris, N. R. P., Hepach, H., Heumann, K. G., Hughes, C., Kuss, J., Krüger, K., Liss, P., Moore, R. M., Orlikowska, A., Raimund, S., … Yokouchi, Y. (2013). Global sea-to-air flux climatology for bromoform, dibromomethane and methyl iodide. Atmospheric Chemistry and Physics, 13(17), 8915–8934. https://doi.org/10.5194/acp-13-8915-2013

Zuidema, P. (2003). Convective Clouds over the Bay of Bengal. Monthly Weather Review, 131(5), 780–798.

List of Publications

Published

1. **Gupta, M.**, Sahu, L. K., Tripathi, N., Sudheer, A. K., & Singh, A. (**2025**). Processes Controlling DMS Variability in Marine Boundary Layer of the Arabian Sea During Post-Monsoon Season of 2021. Journal of Geophysical Research: Atmospheres, 130(9), e2024JD042547. https://doi.org/10.1029/2024JD042547

2. **Gupta, M.**, Tripathi, N., Malik, T. G., & Sahu, L. K. (**2024**). A review on air–sea exchange of reactive trace gases over the northern Indian Ocean. Journal of Earth System Science, 133(2), 77. https://doi.org/10.1007/s12040-024-02268-5

3. Sahu, L. K., **Gupta, M.**, Tripathi, N., Yadav, R., & Kajino, M. (2025). Effect of different sources and meteorological processes on the variability of VOC composition in a metropolitan city of western India during summer season. Journal of Geophysical Research: Atmospheres, 130(9), e2024JD040867. https://doi.org/10.1029/2024JD040867

4. Rathore, J., Ganguly, D., Singh, V., **Gupta, M.**, Vazhathara, V. J., Biswal, A., Kunchala, R. K., Patra, P. K., Sahu, L. K., Gani, S., & Dey, S. (2025). Characteristics of Haze Pollution Events During Biomass Burning Period at an Upwind Site of Delhi. Journal of Geophysical Research: Atmospheres, 130(7), e2024JD042347. https://doi.org/10.1029/2024JD042347

5. Malik, T. G., **Gupta, M.**, Tripathi, N., & Sahu, L. K. (2025). Change in monoterpene concentrations during winter-to-summer transition period and impact of COVID-19 lockdown at an urban site in India. Atmospheric Environment, 350, 121141. https://doi.org/10.1016/j.atmosenv.2025.121141

6. Goel, V., Tripathi, N., **Gupta, M.**, Sahu, L. K., Singh, V., & Kumar,

M. (2024). Study of secondary organic aerosol formation and aging using ambient air in an oxidation flow reactor during high pollution events over Delhi. Environmental Research, 251, 118542. https://doi.org/10.1016/j.envres.2024.118542

7. Malik, T. G., **Gupta, M.**, Shukla, G., Kumar, A., & Sahu, L. K. (2024). Detection of biogenic volatile organic compounds emitted from common tropical plant species in the Western Ghats region of India: Chamber-based experiments. CURRENT SCIENCE, 126(1), 59–66. doi:10.18520/cs/v126/i1/59-66.

8. Ambade, B., Sankar, T. K., **Gupta, M.**, Sahu, L. K., & Gautam, S. (2023). A Comparative Study in Black Carbon Concentration and its Emission Sources in Tribal Area. Water, Air, & Soil Pollution, 234(3), 173. https://doi.org/10.1007/s11270-023-06197-9

9. Malik, T. G., Sahu, L. K., **Gupta, M.**, Mir, B. A., Gajbhiye, T., Dubey, R., Clavijo McCormick, A., & Pandey, S. K. (2023). Environmental Factors Affecting Monoterpene Emissions from Terrestrial Vegetation. Plants, 12(17). https://doi.org/10.3390/plants12173146

10. Jain, V., Tripathi, N., Tripathi, S. N., **Gupta, M.**, Sahu, L. K., Murari, V., Gaddamidi, S., Shukla, A. K., & Prevot, A. S. H. (2023). Real-time measurements of non-methane volatile organic compounds in the central Indo-Gangetic basin, Lucknow, India: Source characterisation and their role in O_3 and secondary organic aerosol formation. Atmospheric Chemistry and Physics, 23(5), 3383–3408. https://doi.org/10.5194/acp-23-3383-2023

11. Sahu, L. K., Tripathi, N., **Gupta, M.**, Singh, V., Yadav, R., & Patel, K. (2022). Impact of COVID-19 Pandemic Lockdown in Ambient Concentrations of Aromatic Volatile Organic Compounds in a Metropolitan City of Western India. Journal of Geophysical Research: Atmospheres, 127(6), e2022JD036628. https://doi.org/10.1029/2022JD036628

12. Yadav, R., Vyas, P., Kumar, P., Sahu, L.K., Kumar, U., Pandeya, V., Tripathi, N., **Gupta, M.**, et al. (2022). Particulate-matter pollution in urban cities of India during unusually restricted anthropogenic activities. Frontiers in Sustainable Cities, section Climate Change and Cities. https://doi.org/10.3389/frsc.2022.792507

Communicated

1. **Gupta, M.**, Sahu, L. K., Tripathi, N., Nazirahmed, S., Singh, A. (under review, *Global Biogeochemical Cycles*; manuscript ID: 2025GB008718). Atmospheric DMS in the northeast Indian Ocean and impact of oceanic emissions and transport processes.

2. **Gupta, M.** and Sahu, L. K. (under review *Geophysical Research Letters*; manuscript ID: 2025GL118388). Effects of oceanic sources and terrestrial outflow on the atmospheric DMS variability over the southern coastal waters of the Indian subcontinent.

Under Preparation

1. **Gupta et al.** Impact of terrestrial outflow and air–sea exchange in the longitudinal variation of isoprene in the marine boundary layer of the Bay of Bengal.

2. **Gupta et al.** Emissions of dimethylsulfide from coral reefs in the Andaman Sea.